Reliability-based Environmental Impact Assessment in Geotechnical Engineering

by

Mina Lee

A thesis

presented to the University of Waterloo

in fulfillment of the

thesis requirement for the degree of

Doctor of Philosophy

in

Civil Engineering

Waterloo, Ontario, Canada, 2023

EXAMINING COMMITTEE MEMBERSHIP

The following served on the Examining Committee for this thesis. The decision of the Examining Committee is by majority vote.

External Examiner	Tim Newson Associate Professor
Supervisor(s)	Dipanjan Basu Professor
Internal Member	Giovanni Cascante Professor
Internal Member	Rebecca Saari Associate Professor
Internal-external Member	Kumaraswamy Ponnambalam Professor

AUTHOR'S DECLARATION

I hereby declare that I am the sole author of this thesis. This is a true copy of the thesis, including any required final revisions, as accepted by my examiners.

I understand that my thesis may be made electronically available to the public.

ABSTRACT

A sustainable design is achieved by balancing the four aspects, so called the four Es, of sustainability – environment, economy, equity, and engineering. Given that geotechnical constructions involve land transformations through earthworks and construction of large-scale concrete and/or steel structures (e.g., bridge abutments, retaining structures, and tunnels), geotechnical engineering can play a vital role in sustainable development by ensuring that the resources are consumed responsibly with minimal emissions to the environment. In this thesis, methodology frameworks, developed based on (i) environmental impact assessment, (ii) reliability-based design, and (iii) multi-objective optimization, are proposed to facilitate the process of sustainable design in geotechnical engineering. The frameworks are applied to common geotechnical structures such as drilled shaft foundation, pile group, and mechanically stabilized earth (MSE) wall. To quantify the environmental sustainability of geo-structures, life cycle assessment (LCA) is used. LCA utilizes inventory of energy and materials to calculate the emissions from the life cycle stages and characterize the emissions into environmental impacts. In this thesis, the procedures of LCA, which have been tailored to geotechnical applications, are demonstrated meticulously with detailed sample calculations to encourage the use of LCA in standard design practices and to demonstrate the usefulness of information obtained from LCA. In fact, for example, it was found, based on this research study, that the global warming impact and human toxicity of a typical drilled shaft are 39 and 486% of annual world impact per person, respectively. The use of reliability-based design (RBD) methods has been strongly promoted in the last two decades to better tackle the uncertainties involved in design and soil parameters; hence, the connection between important factors in RBD and environmental impacts is investigated in

this thesis. A comprehensive analysis is conducted on the relationship between reliability and global warming impact of geotechnical designs (i.e., drilled shaft and MSE wall) considering uncertainties in soil properties, material properties, applied load, model, and design dimension. Parametric and sensitivity studies are systematically conducted using reliability analyses, like first-order reliability method (FORM) and Monte Carlo simulations, and LCA. To balance the multiple aspects of sustainability, a multi-objective optimization framework is proposed using which designers can determine design dimensions that aim for minimizations of cost and global warming impact and maximization of reliability of a geotechnical structure. The framework utilizes several methodologies including LCA, FORM, response surface methodology, and non-dominated sorting genetic algorithm (NSGA-II). To encourage sustainability considerations in geotechnical engineering design, charts are developed which are useful for determining (i) global warming impact of the geo-structures designed with working stress design (WSD) and RBD approaches and (ii) design dimensions optimized with respect to cost, engineering reliability, and environmental impact, without the use of and knowledge in the sophisticated methodologies incorporated in the proposed frameworks.

ACKNOWLEDGEMENTS

I would like to express my sincere gratitude to my supervisor, Dr. Dipanjan Basu, for his unwavering support throughout my entire graduate studies at the University of Waterloo. It was indeed a long journey with many challenges and obstacles along the way, but his encouragement served as a driving force that kept me going throughout this journey. His technical expertise and philosophies were pivotal in broadening the knowledge and perspectives on my research studies. I am deeply grateful to have had the opportunity to work with Dr. Basu, who has been a remarkable mentor, offering guidance that has not only enriched my academic life but also had a significant positive influence on my personal development.

I am also thankful to my examining committee members, Dr. Giovanni Cascante, Dr. Rebecca Saari, and Dr. Kumaraswamy Ponnambalam, and the external reviewer, Dr. Tim Newson, for their invaluable feedback which was helpful for refining and improving the quality of my research and thesis.

I would like to extend my appreciation to my dearest friends, Hannah Jin, Jennifer Yoo, and Jessica Yoo for their support.

Lastly, I thank my beloved parents and brother for their constant support, patience, and understanding throughout this long journey.

TABLE OF CONTENTS

LIST OF FIGURES

LIST OF TABLES

CHAPTER 1: SUSTAINABILITY IN GEOTECHNICAL ENGINEERING

1.1 Need of Sustainable Practices in Geotechnical Engineering

In a broad context, sustainability advocates the well-being of human and other life forms that is maintained over generations within the carrying capacity of the earth. In civil engineering, sustainability can be achieved by balancing the four E's of sustainability – environment, economy, equity, and engineering, as illustrated in Figure 1.1 (Basu *et al*., 2015). Geotechnical engineering involves all the four E's of sustainability and plays an important role in developing "quality, reliable, sustainable and resilient infrastructure, including regional and transborder infrastructure, to support economic development and human well-being", and in making "cities and human settlements inclusive, safe, resilient and sustainable", which are some of the goals of the *2030 Agenda for Sustainable Development* of the United Nations (UN, 2015).

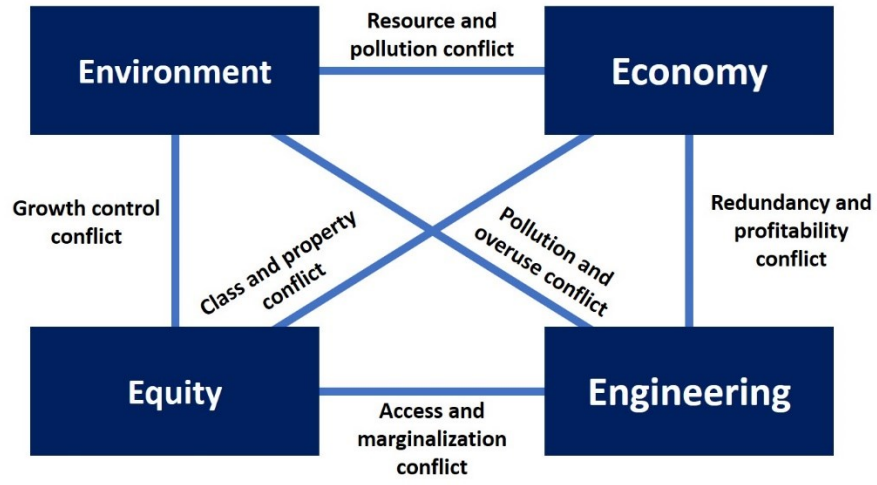

Figure 1.1. The four E's of sustainable development (adapted from Basu *et al*., 2015)

There has been a rising awareness on the importance of employing sustainability principles in civil and geotechnical engineering because the construction sector is responsible for nearly 40% of carbon emissions and energy use in the world. Globally, the building and construction sector emitted 6.9 billion tonnes of direct-energy related carbon dioxide (CO_2) in 2019, which is equal to

19% of the global carbon dioxide emissions (UNEP, 2020). Manufacturing and use of construction materials for buildings such as steel, cement, and glass, resulted in 3.5 billion tonnes of carbon dioxide emissions in 2019, which is 10% of all energy sector emissions. The main sources of direct carbon dioxide emissions in the construction sector are the gasoline and diesel used for on-site construction operations (Huang *et al*., 2018). Other significant contributors to global carbon dioxide emissions in the construction sector include the use of fossil fuels (e.g., hard coal and natural gas) in processing sand and gravel, and in manufacturing energy- and carbon-intensive materials like cement and steel. The construction sector is also the largest generator of waste resulting in 1.1 tonnes of waste (equivalent to 36% of the global waste) every year (UNEP, 2015). Construction of buildings accounts for 40% of annual stone, sand and gravel use, 25% of annual timber use, and 16% of annual water consumption globally (Arena and de Rosa, 2003). Thus, the construction sector is responsible for a significant portion of emissions and resource consumption in the world.

Global population growth and expanding economic activities are the major drivers of natural resource use (UNEP, 2016). To accommodate higher living standards and human wellbeing, the demand for civil infrastructure systems has been growing and the global extraction of materials has tripled since the 1970s (IRP, 2019). Many geo-structures are important components of the physical infrastructure belonging to transportation, power and energy, and defense sectors, and it is likely that the demand for geotechnical construction will keep rising as investments in infrastructure increase. Hence, ensuring responsible consumption of non-renewable resources and reduction of pollutants in construction are important for achieving sustainable development. However, addressing these impacts has not been an integral part of geotechnical designs, and the current practice has focused primarily on optimizing designs based on cost and

safety. Use of recycled materials has often been blindly accepted as an approach to reduce cost, energy, and carbon footprint; however, quantitative environmental impact assessments are necessary to verify the merits of using recycled materials. An absence of tailored guidelines of environmental impact assessment for geo-structures and a lack of general awareness, experience, and expertise among the geotechnical engineers are possibly some of the reasons why geotechnical designs are not optimized with respect to the four E's of sustainability (Abreu *et al*., 2008; Damians *et al*., 2017; Holt *et al*., 2010; Jefferis, 2008).

Geotechnical constructions are directly connected with issues like depletion of non-renewable resources and environmental pollution. For example, earthwork constructions for embankments and subgrades consume substantial amounts of natural aggregates (e.g., stone, sand, and gravel) while geo-structures such as foundations, retaining structures, and tunnels are made of energy- and carbon- intensive materials like cement, concrete, and steel. The production processes of these construction materials consume significant amount of fossil fuels (e.g., hard coal and natural gas), natural aggregates, and metal ores, and generate carbon emissions that significantly contribute to global warming impact. According to *Global Resource Outlook 2019* (IRP, 2019), the global iron and steel production chain causes the largest climate change impacts among metal resources. Cement, one of the primary materials for concrete production, is responsible for 1.5% of global anthropogenic carbon emissions because of calcination of limestone (Spaulding *et al*., 2008). The carbon emissions from the use of gasoline, diesel, and compressed natural gas for on-site construction operations are also concerning (Shillaber *et al*., 2014). Hence, the environmental impacts of geotechnical structures cannot be overlooked. Efforts toward minimization of the environmental impacts of geotechnical structures should be made as early as possible in the design phase (Basu *et al*., 2015). In order to consider the environmental sustainability as a criterion in

geotechnical design, a proper estimation of the environmental impacts of geo-structures is, undeniably, necessary.

Geotechnical projects involve earth works, ground improvement, building geotechnical structures, and practice of geo-environmental engineering, which require consumption and transportation of both natural resources (e.g., aggregates and soil) and man-made materials (e.g., concrete and steel) over the life cycle of the projects. Although geotechnical engineers cannot solve global sustainability problems, they can contribute significantly toward sustainable development, as illustrated in Figure 1.2. In geotechnical engineering, the sustainability objectives (i.e., desirable outcomes) can be considered as the followings: (i) energy efficiency and carbon reduction, (ii) materials and waste reduction, (iii) maintaining natural water cycle and enhancing natural watershed, (iv) climate change adaptation and resilience, (v) effective land use and management, (vi) economic viability and whole life cost, and (vii) positive contribution to society (Pantelidou *et al*., 2012). Basu *et al*. (2015) considered the following to be part of sustainable geotechnical engineering practice: (i) use of alternate, environment friendly materials and reuse of waste materials in geotechnical construction (e.g., use of construction and demolition wastes in pavement subgrade, and appropriate use of geosynthetics), (ii) innovative, environment friendly and energy efficient geotechnical techniques for site investigation, construction, monitoring, retrofitting, ground improvement, and deconstruction (e.g., bioslope engineering and use of natural fiber in soil reinforcement), (iii) retrofitting and reuse of foundations and other geotechnical structures, (iv) use and reuse of underground space for beneficial purposes like pedestrian pathways, public transit and water distribution system, and for storage of energy, carbon dioxide and waste products, (v) characterization, analysis, design, monitoring, repairing and retrofitting techniques in geotechnical engineering that ensure safety, serviceability, and resilience, (vi)

geotechnical techniques involved in the discovery and recovery of geologic resources like minerals and hydrocarbons, (vii) geotechnical techniques for pollution control and redevelopment of brownfields and other marginal sites, (viii) mitigation of geohazards (e.g., landslides, earthquakes, heavy rainfall, and blast) that also include the effects of global climate change, (ix) practice of energy geotechnics (e.g., geo-facilities for storage and extraction of renewable energy sources like solar, wind, and geothermal energies), (x) environmental and socio-economic impacts from geo-activities, for example from mining and petroleum extraction, dam construction and landfill/waste disposal, (xi) practice of geoethics and geodiversity, and (xii) development of sustainability indicators and assessment tools in geotechnical engineering.

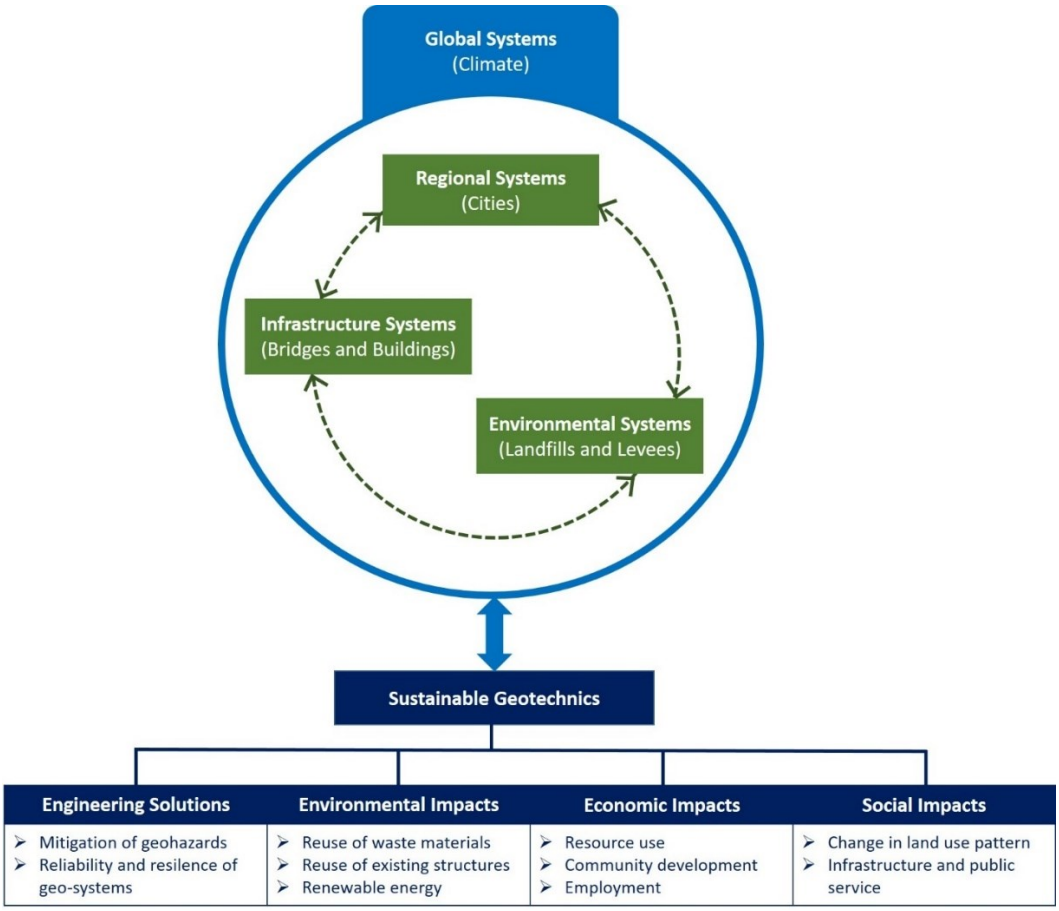

Figure 1.2. Scope of sustainable geotechnics

Over the last two decades, geotechnical engineering designs have undergone a paradigm shift in North America and Europe from the traditional working/allowable stress design (WSD/ASD) method to the limit state design method (LSD) or load and resistance factor design (LRFD) method (Fenton *et al*., 2016). The factor of safety in ASD, determined from ad hoc assumptions and experience, is replaced by rationally and/or mathematically determined load and resistance factors in LSD and LRFD. In North American practice, the load and resistance factors are determined probabilistically with different target values of reliability index (or probability of failure) so that the uncertainties associated with the designs can be approximately accounted for (FHWA, 2010b). Reliability based design (RBD) method is a more rigorous approach in which the probability of failure is explicitly quantified on a case-specific basis based on actual loads, geologic site interpretations, geotechnical properties, and calculation models (Wang *et al*., 2011). LRFD and RBD both help reduce overdesign and ensure safety and serviceability with a quantified level of probability of failure.

Restricting overdesign is necessary to not only minimize the construction cost but also reduce the environmental impact. There is a growing awareness that the Earth has limited natural resources, and geotechnical engineering has an important role in avoiding overuse of non-renewable materials and energy sources like natural aggregates, minerals, and fossil fuels (Abreu *et al*., 2008; Basu *et al*., 2015; Pantelidou *et al*., 2012). The quantities of construction materials differ based on how much risk the designer decides to accept. For example, a pile foundation designed with 0.1% chance of failure will need larger dimensions to attain the desired level of reliability than that designed with 1% chance of failure. Higher quantities of construction materials increase energy consumption, emissions, and the embodied carbon considering the life cycle (Purnell, 2012). For a geotechnical structure, emissions are typically generated during extraction

and refining of raw materials, production of construction materials like concrete and steel, transportation of construction materials to the site, operation of construction machineries, and decommissioning at its end-of-life span. Therefore, there is a direct relationship between reliability of a geotechnical structure and its environmental impacts. It is necessary to understand and quantify the relationship and trade-offs between safety and environmental impacts of geotechnical structures so that optimal design outcomes can be achieved.

From the foregoing discussion, it is clear that sustainability problems require multidimensional and lifecycle views in a systematic manner to unravel their complexities. A balanced geotechnical design that not only ensures the safety and serviceability but also uses less resources are considered sustainable. Therefore, sustainable design entails considering and evaluating multiple criteria that include environmental impact, cost, and reliability over the life cycle of the structure.

1.2 Methodologies for Sustainability Assessment in Geotechnical Engineering

In geotechnical engineering, a large number of studies are based on the common notions of sustainability like recycling, reuse and use of alternative materials, technologies, and resources; but, without a life cycle view, it is difficult to understand if these practices are truly sustainable. For example, use of recycled materials may seem a sustainable solution at all times; however, there are cases in which the benefits of recycling are largely offset by the environmental impact of transporting back the recycled materials and may be unsustainable when looked upon with a life cycle point of view. Thus, development and use of a proper sustainability assessment framework is necessary to assess whether sustainable choices are indeed made for a project. Sustainability assessment tools available in geotechnical engineering can be categorized into (i) single criterion

based methods (quantitative), (ii) multiple criteria based methods (qualitative or quantitative or combined), and (iii) point based rating systems (quantitative), as shown in Figure 1.3.

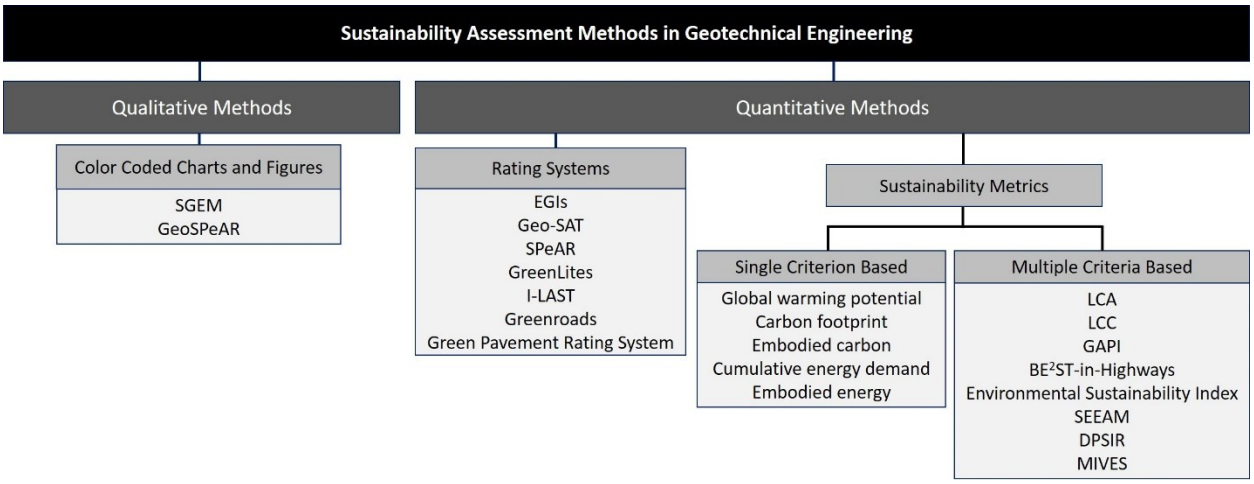

Figure 1.3. Existing sustainability assessment frameworks in geotechnical engineering

Quantitative environmental metrics like global warming potential, carbon, embodied carbon, cumulative energy demand, embodied energy and a combination of embodied energy and emissions (carbon dioxide, methane, nitrous oxide, sulfur oxides and nitrogen oxides) have been used to compare competing alternatives in geotechnical engineering. However, assessment of sustainability on the basis of a single metric like embodied carbon or global warming potential involves ad hoc assumptions, puts excess emphasis on the environmental aspects, and neglects the technical, financial and social aspects (Jefferson *et al*., 2007). According to Carpenter *et al*. (2007), a combination of life cycle analysis and site and material specific factors is more contextual for any decision-making framework than a singular metric. The multidimensional aspect of sustainability has been addressed in geotechnical engineering through qualitative and quantitative methods. Qualitative models are comprised of indicators that are evaluated based on color coded rose diagrams. Life cycle-based tools have been widely used for quantifying environmental impacts or costs that are expected over the life cycle of geotechnical projects. Life cycle assessment

(LCA) and life cycle costing (LCC) have been particularly used. LCA focuses on quantifying the environmental impacts and LCC is used to quantify the costs associated with the life cycle of a system. The third approach to sustainability assessment comprises point-based rating systems in which points scored in different relevant categories are used as measures of sustainability of geotechnical projects. Table 1.1 summarizes the past studies that developed or utilized sustainability assessment methods for various geotechnical applications. It is important to note that sustainability assessment frameworks in geotechnical engineering should (i) have a life cycle view of the geotechnical processes and products (Dam and Taylor, 2011), (ii) incorporate all the 4 E's of sustainability (Holt *et al*., 2010; Steedman 2011), (iii) enforce sound engineering design and maintenance, (iv) assess the reliability and resilience of the geo-system and offer flexibility to the user to identify site specific needs, and (v) account for uncertainties in geotechnical works. Many studies, especially the single criterion based methods, focused on assessing sustainability solely based on environmental impacts and did not incorporate multidimensional perspective by capturing the four E's of sustainability. Further, most studies outlined in Table 1.1 did not consider the impact of engineering design (e.g., reliability) on sustainability.

Table 1.1. Sustainability assessment methods used in geotechnical engineering

Sustainability assessment method	Application	Indicator, metric, rating, or model	References
Single criterion based methods	Concrete retaining walls and bioengineered slopes	Global warming potential	Storesund *et al*. (2008)
	Ground improvement methods	Carbon footprint	Spaulding *et al*. (2008)
	Retaining wall systems	Embodied carbon	Inui *et al*. (2011)
	Ground improvement methods	Embodied carbon	Egan and Slocombe (2010)
	Geosynthetics	Cumulative energy demand	Heerten (2012)

Table 1.1 (continued).

Sustainability assessment method	Application	Indicator, metric, rating, or model	References
Single criterion based methods	Retaining wall systems	Embodied energy	Chau *et al*. (2006) Inui *et al*. (2011)
	Tunnel	Embodied energy	Chau *et al*. (2012)
Multiple criteria based methods (qualitative)	Slope stabilization	The Sustainable Geotechnical Evaluation Model (SGEM)	Jimenez (2004)
	Geotechnical projects	Geotechnical Sustainable Project Appraisal Routine (GeoSPeAR)	Holt (2011) Holt *et al*. (2010)
Multiple criteria based methods (quantitative)	Pavement design	Life cycle costing (LCC)	Reigle *et al*. (2002) Praticò *et al*. (2011) Zhang *et al*. (2008)
	Airport pavement treatments	Green Airport Pavement Index (GAPI)	Pittenger (2011)
	Recycled materials in pavement	Life cycle assessment (LCA) and LCC	Lee *et al*. (2010b)
	Highway construction	Building Environmentally and Economically Sustainable Transportation – Infrastructure – Highways (BE^2ST-in-Highways)	Lee *et al*. (2010a)
	Underground mining	Environmental Sustainability Index	Torres and Gama (2006)
	Geotechnical projects	LCA	Misra (2010) Misra and Basu (2012)
	Ground improvement projects	Streamlines Energy and Emissions Assessment Model (SEEAM)	Shillaber *et al*. (2016a; 2016b)
	Geotechnical projects	Driver-Pressure-State-Impact-Response (DPSIR)	Lee and Basu (2018)
	Treatments for surficial slope	LCA	Das *et al*. (2018)
	Geotechnical projects	Integrated Value Model for Sustainable Assessment (MIVES)	da S Trentin *et al*. (2019)

Table 1.1 (continued).

Sustainability assessment method	Application	Indicator, metric, rating, or model	References
Multiple criteria based methods (quantitative)	Retaining walls	LCA and MIVES	Damians *et al*. (2017; 2018)
Point based rating systems	Ground improvement projects	Environmental Geotechnics Indicators (EGIs)	Jefferson *et al*. (2007)
	Geotechnical projects	Geotechnical Sustainability Assessment Tool (Geo-SAT)	Raza *et al*. (2020; 2021)
	Foundation reuse	Sustainable Project Appraisal Routine (SPeAR)	Laefer (2011)
	Highway construction	GreenLites	McVoy *et al*. (2010)
	Highway construction	Illinois – Livable and Sustainable Transportation (I-LAST)	Knuth and Fortman (2010)
	Highway construction	Greenroads	Muench and Anderson (2009)
	Pavement construction	Green Pavement Rating System	Chan and Tighe (2010)

Understanding the flows of energy, raw materials, and emissions in a geotechnical project can be complex because of the involvement of a wide range of construction materials and activities. Life cycle thinking systematically breaks down these flows with respect to the different stages a product goes through over its life span — from the extraction of raw materials from the Earth, through the production and distribution of primary materials and energy, to the use, reuse, and final disposal (Curran, 2008). The term 'product' here refers to a geo-structure (an assembled system like a pile foundation) and sub-products are components such as concrete shaft and steel reinforcing bars. LCA is a method for quantifying environmental impacts of a product using life cycle thinking. It can quantify various environmental impacts, including global warming, ozone depletion, ionizing radiation, acidification, eutrophication, particulate matter formation,

photochemical oxidant formation, toxicity to human health, toxicity to ecosystems, depletion of natural resources (e.g., water, metal, and fossil fuel), and land use (Huijbregts *et al*., 2017; Matthews *et al*., 2014). LCA can help decision makers determine the most environment-friendly option among design alternatives. For example, two different pile foundation designs can be compared in terms of their impacts to global warming after performing their LCAs. In geotechnical engineering, LCA has been applied to pile foundations (Ay-Eldeen and Negm, 2011; Giri and Reddy, 2014; Luo *et al*., 2019; Misra, 2010; Sandanayake *et al*., 2015; Sandanayake *et al*., 2017), retaining structures (Damians *et al*., 2017; Djadouni *et al*., 2019; Inui *et al*., 2011), embankments (Das *et al*., 2018; Lee and Basu, 2018), earthen dams (Robbins and Chittoori, 2021), ground improvement methods (Raymond *et al*., 2021; Shillaber *et al*., 2016b), site investigation methods (Purdy *et al*., 2022), environmental remediation (da S Trentin *et al*., 2019), and underground utility infrastructure (Hojjati *et al*., 2017). However, a rigorous description of the LCA procedure in the context of geo-structures (e.g., foundations, retaining structures, and embankments) with detailed demonstration of LCA calculations is not readily available in the literature.

1.3 Reliability and Sustainability

The paradigm of geotechnical design has evolved from being simply conservative to optimizing several design criteria like the reliability of geotechnical structures and cost of project. Foundations have been designed using traditional methods developed since the early twentieth century in which the capacities are checked against demands with sufficient safety margins (Bowles, 1997; Coduto, 2001; Tomlinson and Woodward, 2008). Capacity calculations of foundations are usually performed using empirical equations that are developed based on numerical analysis, experimental observations, precedence, rules of thumb, or local experience (Kulhawy *et al*., 2012; Salgado, 2008). Historically, the working stress design (WSD) or allowable

stress design (ASD) method has been used for geotechnical engineering design and is still used in several parts of the world. In ASD, a factor of safety (FS) is used to capture all the uncertainties into a single arbitrary number that the designer feels comfortable with. More recently, the load and resistance factor design (LRFD) has been used for geotechnical engineering design, particularly in North America, and is gaining popularity. For example, in LRFD, resistance and load factors are used to separately capture the uncertainties associated with the foundation capacity and applied load, respectively. Recent developments in LRFD include rigorous probabilistic analysis at the background, which is used to determine the resistance and load factors. Reliability based design (RBD) is more rigorous than LRFD in that the probability of failure is explicitly quantified in this approach, and it is directly used in determining the design dimensions. In fact, RBD has been useful in reducing overdesign through informed decision based on quantification of risk.

The importance of reliability-based design and its superiority over conventional, factor of safety-based deterministic design can be illustrated with an example of a pile foundation. A jacket pile installed in 1976 for an offshore structure in Norway was reanalyzed 13 years later (Lacasse and Nadim, 1998) after a new soil investigation and new calculations of the environmental and gravity loads were completed. Initially, the factor of safety of the pile was calculated to be 1.78, and the new deterministic analysis resulted in a lower factor of safety of 1.40. However, the new information reduced the uncertainties in both the soil and load parameters, which resulted in a safety margin greater than that perceived at the time of first design. The lower uncertainties, illustrated in Figure 1.4 as a 'narrow' probability distribution, led to a reduction in the probability of failure by a factor of 2. This shows that the factor of safety is not a sufficient indicator of safety margin because the uncertainties are not explicitly considered in deterministic calculations. Thus, probabilistic methods like the reliability-based design methods may help reduce excess safety

margins that are often used in traditional design methods or in factors of safety prescribed in codes. (Lacasse and Nadim, 1996). Naturally, overdesigning is reduced in reliability-based approaches and satisfactory performance of the geotechnical structure is ensured with a quantified probability of failure, which promotes the sustainability goals.

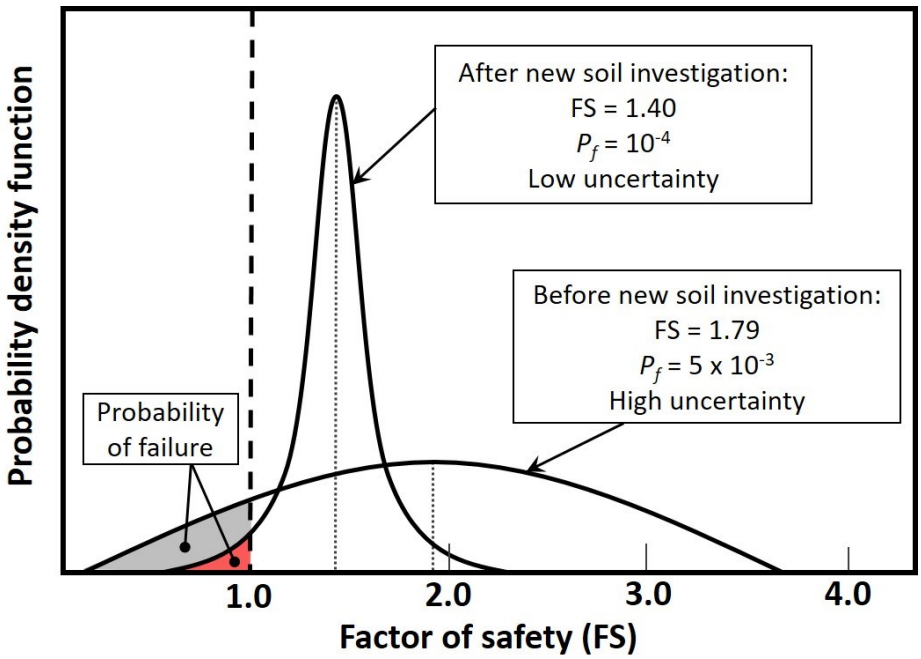

Figure 1.4. Probability of failure versus factor of safety (adapted from Lacasse and Nadim, 1996)

1.3.1 Methodologies for Reliability Analysis and RBD of Geotechnical Structures

There is a plethora of studies available on probabilistic analysis, LRFD, and RBD of geo-systems and geo-structures (Basu and Salgado, 2012; Bathurst *et al*., 2019; Fenton *et al*., 2008; Kim and Salgado, 2012a; 2012b; Low 2005; Phoon, 2008). In the past studies on reliability analysis or RBD of pile foundations, different methods, different assumed uncertainties, and different failure criteria have been considered. Phoon *et al*. (1995) used the first-order reliability method (FORM) to conduct RBD of drilled shafts for transmission line structure considering uplift, compression, and lateral loads. Wang *et al*. (2011) used Monte Carlo simulations (MCS)

and considered both ultimate limit state (ULS) and serviceability limit state (SLS) criteria in their RBD of drilled shafts. Fenton and Griffiths (2007) used MCS to estimate the distribution of the serviceability and ultimate limit state loads of pile foundations. Roberts and Misra (2009) developed a framework for RBD of pile foundations considering a differential settlement criterion using MCS. Basu and Salgado (2012) and Haldar and Basu (2013) used MCS and FORM to determine the load and resistance factors of pile foundations in sand and clay, respectively. Basu *et al*. (2020) performed fragility analysis of drilled shafts to establish an analytical correlation between FS and reliability index values of drilled shaft considering five different subsurface profiles consisting sand layers. Chalermyanont and Benson (2004) and (2005) conducted RBD for external and internal stabilities of mechanically stabilized earth (MSE) walls using MCS. Kim and Salgado (2012a) and (2012b) used FORM to develop resistance factor values for different limit states of MSE walls and for different target probabilities of failure. Low and Tang (1997) analyzed the reliability of reinforced embankments using an efficient form of FORM. Low (2005) performed RBD of gravity and anchored walls using FORM. Sayed *et al*. (2008) used FORM to analyze the reliability of retaining wall reinforced by geosynthetics and subjected to seismic forces. However, there is no study available in the literature that investigates the relationship between reliability and sustainability of geotechnical structures.

1.4 Design Optimization of Geotechnical Structures

Optimization techniques have been used in geotechnical engineering to find appropriate dimensions of retaining structures, foundations, and slopes satisfying the safety requirements and loading conditions (Juang and Wang, 2013; Saribaş and Erbatur, 1996; Wang and Kulhawy, 2008). In the optimization, the common approach was to find the design dimensions of geotechnical structures (e.g., width and length of spread footing) that will result in the minimum cost of

materials and construction works (e.g., concrete, reinforcing steel, formwork, excavation, and compaction) while making sure the geotechnical structure is safe (e.g., factor of safety and probability of failure pertaining to ultimate and serviceability limit states that meet a specified requirement). Evolutionary algorithms have been used for conducting multi-objective optimization (MOO) of different geotechnical applications such as design of mechanically stabilized earth (MSE) walls (Kashani *et al*., 2022a) and reinforced concrete cantilever retaining walls (Kashani *et al*., 2022b) in which a balance between factor of safety (FS) and cost was sought. Sensitivity analyses were conducted to study the effects of significant parameters such as friction angle of soil, surcharge load, and slope of the backfill, on the FS and cost. Dodigović *et al*. (2021) used non-dominated sorting genetic algorithm (NSGA-II), an evolutionary algorithm, to maximize the FS and minimize the cost of a reinforced concrete retaining wall. The study highlighted the difficulties of converging to optimal solutions as the number of objective functions increased in the MOO. Tang *et al*. (2019) used NSGA-II to design stabilizing piles in earth slopes for maximizing the reinforcement effectiveness of stabilizing piles and cost efficiency. NSGA-II was also applied to spread foundations (Juang and Wang, 2013), drilled shafts (Juang *et al*., 2013; Khoshnevisan *et al*., 2014), raft foundations, and pile groups (Ravichandran and Shrestha, 2020) to perform reliability-, robust-, and cost-based MOO. Khajehzadeh *et al*. (2014) combined two objectives related to cost and carbon dioxide emissions of a spread foundation by applying a weight factor to each objective and transformed a multi-objective optimization problem into a single objective optimization problem. Constraints related to the ultimate and serviceability limit states of the spread foundation were added to the single objective function as a penalty term, and the optimization problem was solved using a modified gravitational search algorithm. Kayabekir *et al*. (2020) used a heuristic harmony search algorithm to optimize a reinforced concrete retaining wall

based on cost, carbon dioxide emissions, and stability considerations. Guo *et al*. (2023) performed MOO for designing geosynthetic-reinforced and pile-supported embankments using a direct multi-search algorithm to minimize the cost, differential settlement, and factor of safety for tension failure of geosynthetics. It is clear from the foregoing literature review, MOO has been used mostly for minimizing cost and maximizing the FS, reliability, or robustness of a geotechnical structure. There is no study available in which MOO is performed with simultaneous considerations of reliability, cost, and environmental impact of geotechnical structures. It is important that environmental impacts are not considered secondary in design hierarchy but taken into account simultaneously along with reliability (safety), and cost (Basu *et al*., 2015; Seager *et al*., 2012).

1.5 Research Objectives

The main objectives of this research study are (i) to quantify the environmental impacts of geotechnical structures, such as pile foundations and retaining structures, (ii) to understand the impacts of design decisions in working stress design and reliability-based design methods to the environmental impacts of the geotechnical structures, and (iii) to develop a unified framework for optimizing geotechnical engineering designs considering sustainability criteria such as environmental impact, cost, and engineering reliability.

1.6 Structure of Thesis

This thesis is presented in three parts to discuss the followings: (I) life cycle assessment in geotechnical engineering, (II) relationship between reliability and sustainability in geotechnical engineering, and (III) optimization for sustainable geotechnical design. In each part, illustrative examples of pile foundations and retaining structures, specifically drilled shafts and mechanically stabilized earth (MSE) walls, are used to demonstrate the methodologies. Both drilled shafts and

MSE walls are commonly used geotechnical structures in North America and are used for different applications in civil infrastructure systems. It is important that sustainability of pile foundations and retaining structures are thoroughly studied individually because, from a sustainability point of view, the two structures are different in terms of materials used and construction activities which are directly connected with environmental impacts. The unique aspects of drilled shaft and MSE walls in terms of environmental sustainability are discussed in relevant sections.

In Part I, Chapter 2 discusses the principles and framework of LCA with detailed demonstration of LCA calculations for geotechnical structures. In Chapter 3, LCA is applied to drilled shafts and the usefulness of LCA results is discussed with respect to achieving environmental sustainability in drilled shaft design. In Chapter 4, the application of LCA to MSE walls and interpretation of the LCA results are presented.

Part II of this thesis is presented with Chapter 5 and Chapter 6 in which the relationship between the reliability and sustainability of drilled shafts and MSE walls are investigated and discussed, respectively.

In Part III, Chapter 7 proposes a multi-objective optimization framework which determines optimized design dimensions of geotechnical structures based on multiple criteria related to sustainability. In Chapter 8, the optimization framework is demonstrated through an example of MSE wall reinforced by steel strips and geogrids. Chapter 9 presents the application of the optimization framework to single drilled shafts and pile group consisting of multiple drilled shafts.

PART I: LIFE CYCLE ASSESSMENT (LCA) IN GEOTECHNICAL ENGINEERING

CHAPTER 2: LCA METHODOLOGY

Life cycle assessment (LCA) is a standardized method for quantifying environmental impacts of a product caused throughout its life cycle (ISO, 2006a). In the context of geotechnical engineering, a product can be an assembled geotechnical structure such as a reinforced concrete pile foundation. Life cycle refers to the consecutive stages of life of a product from raw material extraction to material processing, manufacture, transportation, operation, maintenance and repair, as well as disposal or recycling (ISO, 2006a). Defining the life cycle of a product and its system boundaries are important in LCA because the defined life cycle helps to outline a process flow diagram based on which the flows of raw materials, energy, and emissions are determined. Figure 2.1 shows an example of the complete life cycle of a drilled shaft. The life cycle comprises several stages and within each stage there may be several processes.

The life cycle starts with the stage of *raw material extraction and refining* followed by the *manufacturing* stage for the production of primary materials like concrete and steel. For example, to manufacture steel, raw materials such as iron ore and limestone and energy sources like coal are extracted from the Earth and refined (e.g., grinding, screening, and separation process of iron ore). The refined materials then undergo processes such as steelmaking, casting, shaping, and treating at a steel mill to manufacture steel. The *transportation* stage in the life cycle involves hauling construction materials and equipment to the site. The *construction* stage is a unique stage for building structures and considers the fuel usage of equipment for performing construction activities. The newly constructed geo-structure may require *maintenance and repair* if it undergoes premature deterioration or if it becomes damaged from extreme events such as earthquakes, flooding, and landslides. The geo-structure may have a *structure reuse* stage (e.g., foundation reuse)

and this stage should be considered prior to the *demolition and disposal* stage. Once the built structure reaches its end-of-life span, it is demolished and the construction wastes (e.g., concrete debris) are processed for disposal or recycling. The demolished concrete structures can be crushed into rubbles and used as subgrade materials for pavement or recycled as raw material for new concrete. Thus, the *material reuse and recycling stage* marks the end of the life cycle for drilled shafts. The *operation* stage is not considered in the life cycle of conventional geo-structures (e.g., drilled shafts) because energies or resources are not consumed for 'operating' the conventional geo-structures. The operation stage is relevant for a few specific geo-structures like geothermal piles.

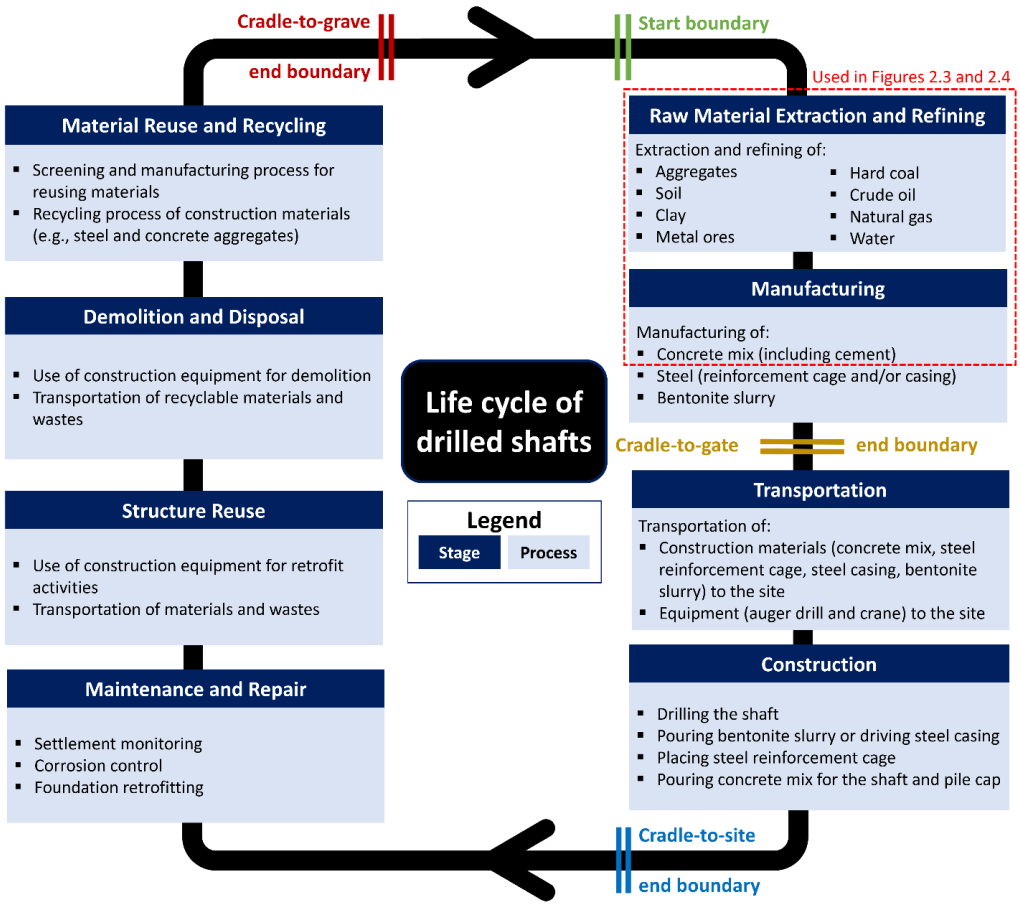

Figure 2.1. Typical life cycle of drilled shafts

LCA comprises four parts: (i) definition of goal and scope, (ii) life cycle inventory analysis (LCI), (iii) life cycle impact assessment (LCIA), and (iv) interpretation of results (ISO, 2006a). Figure 2.2 shows the framework of LCA for a typical geotechnical structure. The quantitative parts of LCA are completed in the LCI (calculation of the flows of materials, energy, and chemical substances) and LCIA (characterization of the emissions into environmental impacts). The details of each part are explained and demonstrated with a drilled shaft example in the subsequent sections.

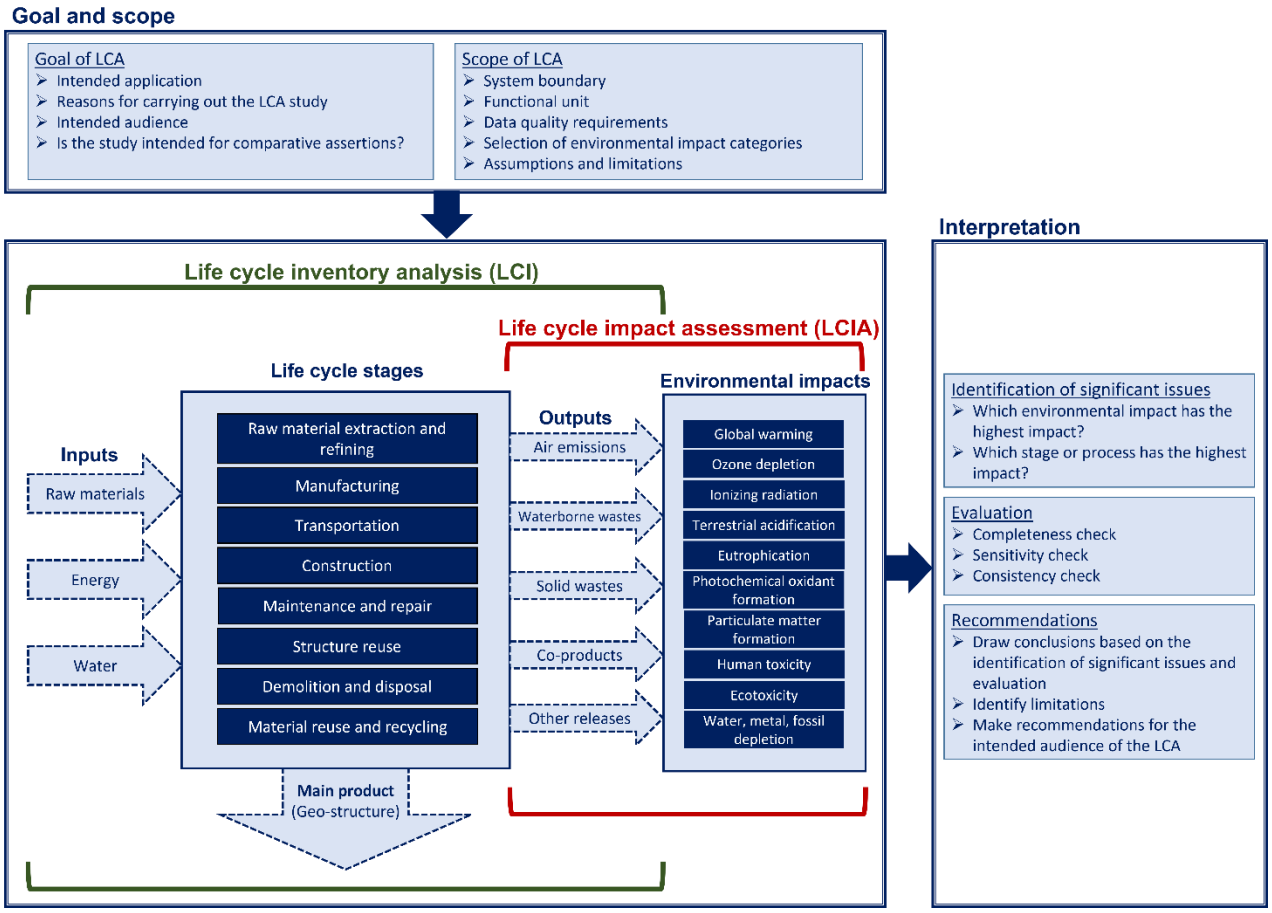

Figure 2.2. Life cycle assessment of geo-structures

2.1 Goal and Scope

According to the ISO 14044:2006 standards (ISO, 2006b), the following items should be discussed to define the goal of the LCA study: (i) the intended application, (ii) the reasons for

carrying out the study, (iii) the intended audience, and (iv) whether the results are intended to be used in comparative assertions or intended to be disclosed to the public. The scope of LCA includes defining the system (e.g., type of geo-structure) to be studied, the system boundary, the functional unit of the system (discussed in the previous section), data quality requirements, the categories of environmental impacts, assumptions, and limitations.

The typical system boundaries of life cycle include the *raw material extraction and refining* stage on the start boundary and (i) the end of *manufacturing* stage (also known as 'cradle-to-gate' or modules A1-A3 according to EN 15978:2011 standards), (ii) the end of *construction* stage ('cradle-to-site' or modules A1-A5), or (iii) the end of whole lifespan ('cradle-to-grave' or modules A1-C4) on the end boundary (Figure 2.1) (CEN, 2011; Song *et al*., 2020). Within the defined system boundaries, different processes are identified corresponding to each stage. For example, the processes during the *construction* stage of a drilled shaft include drilling the shaft, placement of steel reinforcement cage, and pouring concrete mix (see Figure 2.1). The selection of system boundaries and processes within each life cycle stage should be done based on the defined goal of LCA study and the degree of confidence in the LCA results. Life cycle stages or processes that will not significantly change the overall conclusions of the LCA study can be excluded (ISO, 2006a).

The functional unit is a quantified description of the performance characteristics of a product to fulfill its primary purpose. Simply put, the functional unit of a product describes its intended purpose. For example, the functional unit of a pile foundation can be 'the mass of pile foundation without bearing capacity failure for a factor of safety (FS) of 2'. The mass of pile foundation differs based on the applied load, soil properties, and specified FS. Defining the functional unit is important because it provides a reference point based on which the inputs (e.g.,

raw materials and energy) and outputs (e.g., product and emissions) are related. An increase in the quantity of functional unit will result in an equivalent increase in the associated inputs, outputs, and environmental impacts (Crawford, 2011). For example, if the factor of safety of the pile foundation, defined in the above example, is increased to 3, it is likely that piles with larger diameter and/or length will be required, and the consumption of raw materials and energy (for concrete, steel, and fuel) will increase resulting in a corresponding increase in the environmental impacts. It is also important to clearly define the functional unit when comparing two or more products because the comparison should be made based on equivalent performances described by quantitative indicators (Curran, 2017). For example, comparing the environmental impacts of two different pile foundations that have different requirements of factor of safety (e.g., FS = 2 versus FS = 3) is not reasonable.

The quantification phases of LCA – LCI and LCIA – require the use of databases that provide (i) inventory of raw material, energy, and emissions associated with a life cycle process and (ii) factors for the characterization of emissions into environmental impacts. Table 2.1 lists examples of databases for LCI and LCIA. Data quality requirements specify the characteristics of the data needed for the study. It is important to properly describe the quality of data in order to gauge the reliability of the results and to properly interpret the outcome of the study (Crawford, 2011). The quality of data depends on the (i) geographical coverage (geographical area from which data for the processes should be collected to satisfy the goal of the study), (ii) time-related coverage (the desired age of data and the period of time over which the data is collected), and (iii) technology coverage, such as the nature of the technology mix – combinations of different energy sources (Jensen *et al*., 1997). The impacts of a particular manufacturing process and energy production can vary significantly between factories (companies) or locations (e.g., between local areas, regional

areas, nations, and continents). For example, databases developed in European countries may not be suitable for products/systems made in North America or Australia. Old data may no longer be relevant if new techniques are being used for the manufacturing process and energy production to meet stricter environmental regulations (e.g., reducing carbon emissions) or to improve the efficiency of production (e.g., replacing human labor with machines). The length of time can affect the representativeness of data; for example, data collected over a month may not be adequate and annual data may be more appropriate to reflect the true population of data. The technology mix of energy sources can be different from one another depending on how energy (electricity, thermal energy, and steam) is supplied to operate the processing activities (e.g., using electricity for mixing materials for concrete manufacturing). Data can be developed based on technology mix that is heavily dependent on non-renewable resources (e.g., coal, crude oil, and natural gas), or utilizes renewable energy resources (e.g., solar, wind, hydropower, and geothermal energy), or uses both (Lewis and Demmers, 1996; Matthews *et al*., 2014).

Table 2.1. LCI and LCIA databases

Name	Type	Reference
Life cycle inventory analysis (LCI)		
GaBi	Commercial	GaBi (2021)
Ecoinvent	Commercial	Wernet *et al*. (2016)
US Life cycle inventory	Open	National Renewable Energy Laboratory (2012)
Inventory of carbon and energy (ICE)	Open	Hammond and Jones (2018)
European reference Life Cycle Database (ELCD)	Open	European Commission (2018)
Life cycle impact assessment (LCIA)		
CML 2001	Open	Leiden University (2016)
Impact 2002+	Open	Humbert *et al*. (2012)
ReCiPe	Open	Goedkoop *et al*. (2013)
TRACI	Open	EPA (2012)
EFFC/DFI Carbon Calculator Tool (for global warming impact)	Open	Wilmotte and Borie (2020)

Based on the defined goal of LCA, the categories of environmental impacts are selected. For example, the goal of an LCA study may be focused only on the carbon footprint (which is equivalent to the global warming impact category in LCA) or may include different types of environmental impacts. Further, any assumptions and limitations pertaining to the LCA are stated in the scope to evaluate the reliability of LCA study and to ensure that comparative assertions are properly made. Table 2.2 lists the categories of environmental impacts.

The GaBi software program, a commercial LCA tool, is used to conduct the LCA in this study; however, this LCA study can be replicated using other open or commercial databases in open-source LCA software programs (e.g., openLCA 1.11.0) or in spreadsheet software program (e.g., Microsoft Excel). LCA is capable of quantifying various environmental impacts; however, if one is interested in quantifying only the global warming impact, then the EFFC/DFI Carbon Calculator Tool (Wilmotte and Borie, 2010) may be used as an alternative computation program. It should be noted that the results will not be exactly the same if different LCI and LCIA databases are used.

Table 2.2. Environmental impact categories (adapted from Huijbregts *et al*., 2017)

Impact Category	Indicator	Characterization Factor	Equivalent Measurement Unit
Global warming (GW)	Infra-red radiative forcing increase	Global Warming Potential (GWP)	[1]kg of CO_2
Ionizing radiation (IR)	Absorbed dose increase	Ionizing radiation potential (IRP)	[2]kBq Co-60
Ozone depletion (OD)	Stratospheric ozone decrease	Ozone depletion potential (ODP)	[3]kg CFC-11
Terrestrial acidification (TA)	Proton increase in natural soils	Acidification Potential (TAP)	[4]kg of SO_2
Freshwater eutrophication (FE)	Phosphorus increase in freshwater	Freshwater eutrophication potential (FEP)	[5]kg P

Table 2.2 (continued).

Impact Category	Indicator	Characterization Factor	Equivalent Measurement Unit
Marine eutrophication (ME)	Nitrogen increase in marine water	Marine eutrophication potential (MEP)	[6]kg N
Photochemical oxidant formation (POF)	Tropospheric ozone increase	Photochemical Oxidant Formation Potential (POFP)	[7]kg of NMVOC
Particulate matter formation (PMF)	Intake of fine particulate matter	Particulate Matter Formation Potential (PMFP)	[8]kg of PM_{10}
Human toxicity (HT)	Risk increase of cancer and non-cancer disease incidence	Human Toxicity Potential (HTP)	[9]kg of 1,4-DB
Terrestrial ecotoxicity (TET)	Emission of organic substances and chemicals to natural soils	Terrestrial ecotoxicity potential (TETP)	kg of 1,4-DB
Marine ecotoxicity (MET)	Emission of organic substances and chemicals to marine water	Marine Ecotoxicity Potential (METP)	kg of 1,4-DB
Freshwater ecotoxicity (FET)	Emission of organic substances and chemicals to fresh waters	Freshwater Ecotoxicity Potential (FETP)	kg of 1,4-DB

[1]CO_2: Carbon dioxide, [3] Co-60: Cobalt-60, [3]CFC-11: Tricholorofluoromethane, [4]SO2: Sulfur dioxide, [5]P: Phosphorus, [6]N: Nitrogen [7]NMVOC: Non-methane volatile organic carbon compound, [8]PM_{10}: fine particulate matter [9]1,4-DB: 1,4 dichlorobenzene

2.2 Life Cycle Inventory Analysis

The LCI quantifies the inputs (e.g., raw materials and energy) and outputs (e.g., emissions) for all the processes in the life cycle of a product (system) defined in the *goal and scope* (ISO, 2006b). The steps followed in the LCI for each of the life cycle processes are: (i) determination of the quantity of products (e.g., concrete, steel, and diesel) for the selected process, (ii) finding the inventory database that best represents the selected process, and (iii) calculation of the total inputs and outputs based on steps (i) and (ii). The stages and processes within the system boundary of the life cycle (shown in Figure 2.1), as defined in the *goal and scope*, are considered in the LCI.

Specifically, the stages considered within the cradle-to-site boundary include (i) *raw material extraction and refining*, (ii) *manufacturing*, (iii) *transportation*, and (iv) *construction*.

2.2.1 Raw Material Extraction and Refining, and Manufacturing

Examples of raw materials required for the construction of drilled shafts are natural aggregate, quartz, limestone, clay, iron ore, water, crude oil, natural gas, and hard coal. These raw materials are extracted from the environment and refined (e.g., producing iron from a blast furnace) for manufacturing the primary materials of drilled shafts (i.e., cement, concrete, steel, and diesel). For every process (shown in Figure 2.1), inputs (e.g., raw materials and energy) are required to operate the processing activities, and outputs (i.e., emissions to the air, water and land) are released as environmental consequences (see Figure 2.2). For example, to manufacture concrete, raw materials like natural aggregates and limestone are consumed and air emissions like carbon dioxide and sulfur dioxide are generated from the manufacturing plant.

In the LCI, the processes included within the stages of *raw material extraction and refining* and *manufacturing* are considered together because most LCA inventory databases provide the inputs and outputs for these two stages in a combined way (i.e., the databases cover processes between the start and the cradle-to-gate boundaries). Table 2.3 shows sample calculations in LCI for a single drilled shaft (L_p = 15m and B_p = 0.8m) and for the following selected emissions: carbon dioxide, methane, and nitrous oxide (calculations for other emissions such as nitrate, nitrogen oxides, and sulfur dioxide are not shown in Table 2.3 to simplify the demonstration). The calculation steps are discussed in detail for the processes related to the *raw material extraction and refining* and *manufacturing* stages of concrete, which includes the processes of manufacturing of cement (these processes are referred as cradle-to-gate processes in this paper – see the box with red dashed lines in Figure 2.1) for demonstration purpose. In other words, the calculation steps in

the second row in Table 2.3 are explained here. Further details on the calculation procedures of the masses of products, shown in Table 2.3, will be discussed in Chapter 3.

Table 2.3. Sample calculations for life cycle inventory analysis (LCI) of a single drilled shaft (L_p = 15 m and B_p = 0.8 m)

Process	Mass of product[1], m (kg)	Emission factor[2], $(EF)_x$ (kg/kg)			Total emission, E_x [using Equation (2.1)] (kg)		
		CO_2	CH_4	N_2O	CO_2	CH_4	N_2O
(1)	(2)	(3)	(4)	(5)	(6) = (2)×(3)	(7) = (2)×(4)	(8) = (2)×(5)
Raw material extraction and refining, and manufacturing of concrete	18096	1.24×10^{-1}	7.17×10^{-5}	8.15×10^{-7}	2244	1.30	1.47×10^{-2}
Raw material extraction and refining, and manufacturing of steel	1480	1.16	3.02×10^{-3}	9.61×10^{-5}	1717	4.47	1.42×10^{-1}
Transportation of concrete	18096	6.59×10^{-4}	4.53×10^{-10}	4.19×10^{-8}	11.93	8.20×10^{-6}	7.58×10^{-4}
Transportation of steel	1480	3.3×10^{-3}	2.27×10^{-9}	2.09×10^{-7}	4.88	3.35×10^{-6}	3.10×10^{-4}
Transportation of equipment	55340	3.3×10^{-3}	2.27×10^{-9}	2.07×10^{-7}	182.62	1.26×10^{-4}	1.15×10^{-2}
Operation of construction equipment	9.65	3.23	1.6×10^{-4}	0	31.17	1.54×10^{-3}	0

[1]Mass of concrete = 18096kg, and Mass of steel = 1480kg (obtained from design calculations); Mass of auger drilling machine = 43000kg and Mass of hydraulic crane = 12340kg so that Mass of construction equipment = 43000 + 12340 = 55340kg (obtained from specification sheet of the equipment); Mass of diesel = 9.65kg (obtained from fuel calculation)
[2]Obtained from LCI databases

First, it is important to understand the flows of inputs and outputs for the cradle-to-gate processes of concrete, and these flows are shown in Figure 2.3. For manufacturing a unit mass of concrete, raw materials like natural aggregate, limestone, and crude oil are consumed and air emissions like carbon dioxide and methane are generated. Calculation of total inputs and outputs

are completed in relation to the functional unit defined in the *goal and scope*; therefore, the masses of primary materials needed to satisfy the defined functional unit are used in the LCI (step (i)). These masses are obtained from the design stage and shown in column (2) of Table 2.3. To determine the total amount of inputs and outputs for constructing a single drilled shaft, the values of inputs and outputs shown in Figure 2.3 are scaled up (multiplied) by the total mass of concrete (e.g., 18096 kg for a single drilled shaft with L_p = 15 m and B_p = 0.8 m). For example, the total amount of natural aggregate needed to construct the designed drilled shaft is 13988 kg (= 0.773 kg/kg × 18096 kg), and the total mass of carbon dioxide generated is 2244 kg (= 0.124 kg/kg × 18096 kg). Thus, the emission of a specific substance (e.g., carbon dioxide [CO_2], sulfur dioxide [SO_2], nitrous oxide [N_2O] and other chemical substances) is calculated (step (iii)) as follows:

$$E_x = m \times (EF)_x \tag{2.1}$$

where E_x is the total emission of substance (pollutant) x (kg), m is the mass of sub-product (e.g., concrete, steel, and diesel) (kg), and $(EF)_x$ is the emission factor of substance x, obtained from the inventory databases (kg/kg). The values of outputs shown in Figure 2.3 are called emission factors, which are the specific emissions per unit (mass) of sub-products (concrete in this case). Emission factors are used to calculate the total quantity of emissions corresponding to a particular process or sub-product. For example, 0.124 kg of carbon dioxide [CO_2] is released per 1 kg of concrete within the cradle-to-gate boundary; therefore, 0.124 kg/kg is the emission factor $(EF)_{CO_2}$ of carbon dioxide. Some of the calculated emission factors (for CO_2, SO_2 and N_2O) corresponding to *raw material extraction and refining* and *manufacturing* stages of concrete together are shown in the second row and columns (3)-(5) in Table 2.3, and the corresponding calculated values of E_x, using Equation (2.1), are shown in columns (6)-(8) of the second row.

Figure 2.3 and Table 2.3 show the selected inputs and outputs and sample calculations for demonstration purpose. For the complete LCI, a complete inventory of inputs and outputs (emissions) is used in the calculations for all the life cycle processes, and these are obtained from the inventory databases. To find inventory databases that best represent the life cycle processes (step (ii)), it is important to define the characteristics of sub-products or assumptions in the *goal and scope*. For example, the inventory of inputs and outputs differ depending on the strength class of concrete and type of steel. A sample of inventory database for cradle-to-gate processes of concrete is shown in Table 2.4.

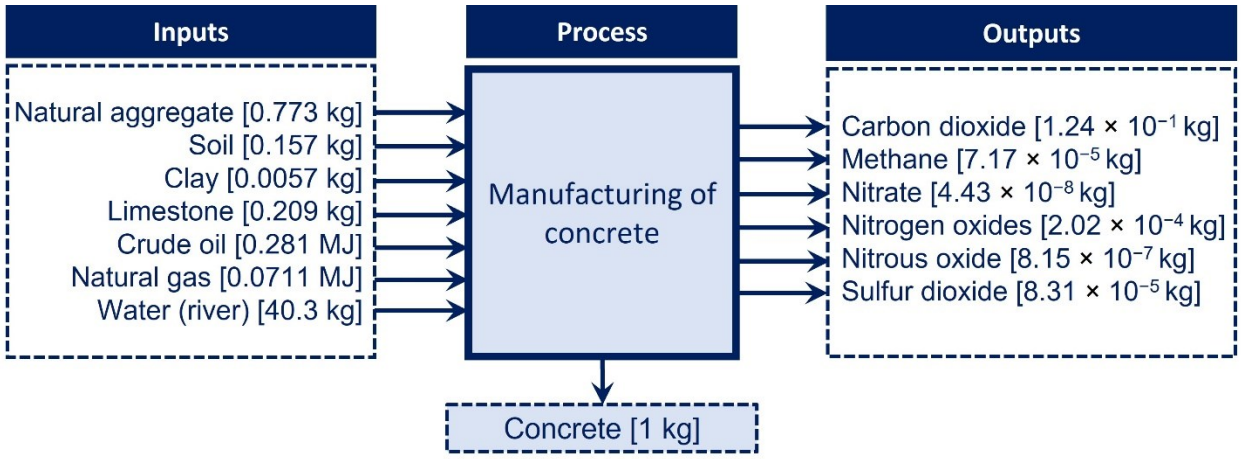

Figure 2.3. Sample calculation of life cycle inventory analysis (LCI) for concrete

Table 2.4. Example of life cycle inventory analysis (LCI) data for manufacturing 1 kg of concrete[1]

Input (per 1 kg of concrete)	Value	Unit	Output (per 1kg of concrete)		Value	Unit
Air	9.53×10^{-2}	kg	Air emissions	Beryllium	1.54×10^{-9}	kg
Clay	5.68×10^{-3}	kg		Carbon dioxide (CO_2)	1.24×10^{-1}	kg
Crude oil	2.81×10^{-1}	MJ		Cobalt (Co-60)	4.24×10^{-6}	Bq
Gypsum	5.49×10^{-3}	kg		Mercury	8.47×10^{-9}	kg

Table 2.4 (continued).

Input (per 1 kg of concrete)	Value	Unit	Output (per 1kg of concrete)		Value	Unit
Hard coal	1.40×10^{-1}	MJ		Methane (CH_4)	7.17×10^{-5}	Kg
Iron	1.24×10^{-3}	kg		Nitrogen oxides (NO_x)	2.02×10^{-4}	kg
Lignite	4.52×10^{-2}	MJ		Nitrous oxide (N_2O)	8.15×10^{-7}	kg
Limestone	2.09×10^{-1}	kg		[2]NMVOC	7.87×10^{-6}	kg
Natural aggregate	7.73×10^{-1}	kg		Sulfur dioxide (SO_2)	8.31×10^{-5}	kg
Natural gas	7.11×10^{-2}	MJ	Water emissions	Ammonia (NH_3) to sea water	5.54×10^{-16}	kg
Oil sand (10% bitumen)	6.10×10^{-5}	MJ		Arsenic (As) to fresh water	1.64×10^{-8}	kg
Oil sand (100% bitumen)	5.32×10^{-5}	MJ		Copper (Cu) to fresh water	6.72×10^{-9}	kg
Quartz (silica sand)	9.19×10^{-4}	kg		Lead (Pb) to fresh water	9.24×10^{-9}	kg
Shale	1.25×10^{-3}	kg		Mercury (Hg) to fresh water	7.95×10^{-11}	kg
Soil	1.57×10^{-1}	kg		Nitrate (NO_3-) to sea water	4.43×10^{-8}	kg
Stone from mountains	7.49×10^{-7}	kg		Nitrogen (N) to sea water	2.95×10^{-16}	kg
Water (river water)	40.3	kg		Zinc (Zn) to fresh water	3.73×10^{-9}	kg

[1]The complete list of inputs and outputs can be obtained from the Thinkstep database or from any other life cycle inventory database on concrete manufacturing. The data shown here includes the extraction and refining of raw materials for manufacturing concrete.
[2]NMVOC: non-methane volatile organic carbon compound

2.2.2 Transportation

The total emissions from truck *transportation* are dependent on factors like travel distance, cargo weight, utilization ratio, and type of road (i.e., motorway, urban, and rural). These factors are considered in the calculation of the emission factors $(EF)_x$ for transportation using Equations (2.2)-(2.4) given below (Thinkstep, 2022). The emission factors for transportation (in kg/kg-km) for 1 kg of cargo and 1 km of travel distance are given by:

$$(EF)_{x,\text{road}} = \frac{(EF)_{x,\text{empty}} + \left[(EF)_{x,\text{loaded}} - (EF)_{x,\text{empty}}\right] \cdot u}{p \cdot 1000 \cdot u} \tag{2.2}$$

in which

$$u = Q/p \tag{2.3}$$

where the subscript x represents a specific pollutant (e.g., carbon dioxide, sulfur dioxide, phosphorus, etc.), $(EF)_{x,\text{road}}$ is the emission factor for driving on a certain type of road (e.g., motorway, rural road, or urban road) (kg/kg-km), $(EF)_{x,\text{empty}}$ is the emission factor for empty runs (kg/kg-km), $(EF)_{x,\text{loaded}}$ is the emission factor for loaded runs (kg/kg-km), u is the utilization ratio, Q is the weight of cargo (tonne), and p is the maximum payload capacity of the truck (tonne). $(EF)_{x,\text{empty}}$ and $(EF)_{x,\text{loaded}}$ are obtained from the database by HBEFA (2010).

For the construction of a drilled shaft, construction materials (e.g., ready-mix concrete and steel reinforcement cage) and equipment (e.g., auger drilling machine and hydraulic crane) are transported to the site. Hence, the cargo weights in Equation (2.3) are the mass of ready-mix concrete, mass of steel reinforcement cage (obtained from design calculations) and mass of construction equipment. The utilization ratio is used to account for materials that are low in density but bulky in size (e.g., expanded polystyrene foam materials). For standard practices, typical values of utilization ratio for different sizes of truck are provided in Thinkstep (2019). In this study, a utilization ratio of 0.45 is used for all transportation activities, following Thinkstep (2019), to account for the travel of trucks with empty trailer after hauling construction materials and equipment to the site. Considering the travel distance and proportion of the type of road the truck has driven on, the total transportation emission factors are then calculated as follows:

$$(EF)_{x,\text{transportation}} = \left[\left\{s_M \cdot (EF)_{x,M}\right\} + \left\{s_R \cdot (EF)_{x,R}\right\} + \left\{s_U \cdot (EF)_{x,U}\right\}\right] \cdot d_t \tag{2.4}$$

where $(EF)_{x,\text{transportation}}$ is the total emission factor of emission x (kg/kg); s_M, s_R, and s_U are the driving share factors on motorway, rural road, and urban road (ranging from 0 to 1), respectively; $(EF)_{x,M}$, $(EF)_{x,R}$, and $(EF)_{x,U}$ are respectively the emission factors for driving on motorway, rural road, and urban road (kg/kg-km) calculated from Equation (2.2); and d_t is the transportation distance (km). Default values, defined in Thinkstep (2019), are assumed for the driving share factors (i.e., $s_M = 0.7$, $s_R = 0.23$, and $s_U = 0.07$).

Some of the calculated emission factors (for CO_2, SO_2, and N_2O) corresponding to the transportation stage are shown in columns (3)-(5) of the 4th, 5th and 6th rows in Table 2.3. Sample calculations of emission factor for CO_2, using Equations (2.2) and (2.4), for transporting concrete are shown in Table 2.5. This procedure is repeated for other relevant emissions (SO_2, N_2O, etc.) and for other transportation processes. Note that the emission factors for transportation of steel and equipment are the same (see Table 2.3) because the type and payload capacity of trucks and the travel distances are the same.

Table 2.5. Sample calculation of transportation emission for carbon dioxide (for transporting concrete mix using a 27-tonne capacity truck)

Road type	$(EF)_{CO_2,\text{empty}}$[1] **(kg/kg-km)**	$(EF)_{CO_2,\text{loaded}}$[1] **(kg/kg-km)**	$(EF)_{CO_2,\text{road}}$ **(kg/kg-km) [using Equation (2.2)[2]]**	$(EF)_{CO_2,\text{total}}$ **(kg/kg) [using Equation (2.4)[3]]**	E_{CO_2} **(kg) [using Equation (2.1)[4]]**
Motorway	0.607	0.983	6.39×10^{-5}	6.59×10^{-4}	11.93
Rural road	0.594	0.1044	6.56×10^{-5}		
Urban road	0.771	0.1416	8.73×10^{-5}		

[1]obtained from HBEFA (2010)
[2]utilization ratio $u = 0.45$
[3]travel distance $d_t = 10$ km (one-way) with driving share factors $s_M = 0.7$, $s_R = 0.23$, and $s_U = 0.07$
[4]total mass of cargo (ready-mix concrete) $m = Q = 18096$ kg

Finally, the total emission of a specific pollutant is calculated using Equation (2.1) with the assumption that m is equivalent to the cargo weight Q (see the last column in Table 2.5 for sample calculation). The values of selected total emission E_x are given in columns (6)-(8) of the 4th, 5th and 6th rows in Table 2.3. This procedure is repeated for all the other emissions from the transportation processes.

2.2.3 Construction

The fuel consumption of construction equipment is the key parameter in determining the emissions generated during the construction stage. In this study, it is assumed that diesel is used for operating construction equipment. The volume of diesel $V_{\text{diesel,total}}$ used for operating the construction machinery is estimated by the product of fuel consumption rate q_d and operation time t:

$$V_{\text{diesel,total}} = q_d \cdot t \tag{2.5}$$

with

$$q_d = \frac{P \cdot k_o \cdot s_d}{\rho_{\text{diesel}}} \tag{2.6}$$

where q_d is in L/hr, t is in hr, P_e is the rated engine power (kW), k_o is the engine load factor, s_d is the specific fuel consumption (kg/kWh), and ρ_{diesel} is the density of diesel (kg/L). P_e, k_o, and s_d can be obtained from specification sheet of construction equipment which will be further discussed in Chapters 3 and 4 for drilled shafts and MSE walls, respectively. The volume of diesel calculated using Equation (2.5) is converted into mass m, assuming $\rho_{\text{diesel}} = 0.832$ kg/L, and the mass is used in Equation (2.1) to compute the emissions from operating a construction machine. For example, the total volume of diesel needed to construct a drilled shaft with L_p = 15 m and B_p = 0.8 m using the dry method is 11.60 L. This volume is equivalent to 9.65 kg of diesel and this mass is used in

LCI (see column (2) and last row of Table 2.3). The inventory database related to construction equipment are not available; therefore, the diesel combustion processes are assumed to be equivalent to the diesel combustion of a generator or portable well-drilling equipment. However, it should be noted that LCA data developed for the specific construction equipment of interest will result in better accuracy because the emission and fuel-use rates may depend on the activities performed by the equipment. While the engines of generators, pumps, and well-drilling equipment typically maintain constant engine speed (measured in revolutions per minute or RPM), the engines of construction equipment such as, excavators, bulldozers, and loaders, run at different engine speeds for different activity modes, which correspondingly result in variable emission and fuel-use rates (Abolhasani *et al*., 2008; Abolhasani and Frey, 2013; Hong and Lu, 2022; Lewis *et al*., 2011). For example, it is likely that the engine speed of auger drilling machine is very high when drilling the shaft and pulling a loaded auger out of the hole, and the engine speed is lower when emptying the loaded auger and placing the auger back into the hole. These series of tasks represent one typical duty cycle of a drilling machine, and variability in fuel use and emissions depending on the tasks mentioned above should be accounted for obtaining more accurate LCI results for the construction stage. The emission factors for the operation of construction equipment (see columns (3)-(5) and last row of Table 2.3) are obtained from the inventory database by NREL (2012). For example, 3.23 kg of CO_2 is emitted per unit mass of diesel consumed for operating construction equipment. The total emission is calculated using Equation (2.1) as demonstrated in columns (6)-(8) and the last row of Table 2.3. It should be noted that the calculation for fuel consumption of construction equipment is conducted based on limited data; therefore, the fuel volumes estimated in this study are approximate.

2.3 Life Cycle Impact Assessment

The LCIA characterizes the emissions, calculated in the LCI, in terms of their environmental impacts selected in the *goal and scope*. The steps to complete the LCIA are: (i) *compilation* of the emissions calculated in the LCI, (ii) *classification* of the emissions to contributing environmental impact categories, (iii) finding the *characterization* factors from LCIA databases (i.e., selection of characterization models) and calculation of the environmental impacts in equivalent measurements, and (iv) *normalization* of the calculated environmental impacts. Table 2.6 shows sample calculations for LCIA of a drilled shaft (L_p = 15m and B_p = 0.8m) for global warming impact based on selected emissions – CO_2, CH_4, and N_2O. Other relevant emissions are not included in Table 2.6 to simplify the demonstration. The calculation steps (i)-(iv) of LCIA for the cradle-to-gate processes of concrete are discussed here in relation to the sample calculations shown in Table 2.6 (specifically the second row in Table 2.6).

Table 2.6. Sample calculations for life cycle impact assessment (LCIA) of a drilled shaft (L_p = 15 m and B_p = 0.8 m) for global warming

Process	Total emission[1], E_x (kg)			Characterization factor[2], $(GWP)_x$			Mass of CO_2e (kg) [3] [using Equation (2.8)]			Total mass of CO_2e (kg)
	CO_2	CH_4	N_2O	CO_2	CH_4	N_2O	CO_2	CH_4	N_2O	
(1)	(2)	(3)	(4)	(5)	(6)	(7)	(8) = (2)× (5)	(9) = (3)× (6)	(10) = (4)× (7)	(11) = (8)+(9)+(10)
Raw material extraction, refining, and manufacturing of concrete	2244	1.30	1.47×10^{-2}	1	25	298	2244	32.5	4.38	2281

Table 2.6 (continued).

Process	Total emission[1], E_x (kg)			Characterization factor[2], $(GWP)_x$			Mass of CO_2e (kg) [3] [using Equation (2.8)]			Total mass of CO_2e (kg)
	CO_2	CH_4	N_2O	CO_2	CH_4	N_2O	CO_2	CH_4	N_2O	
(1)	(2)	(3)	(4)	(5)	(6)	(7)	(8) = (2)× (5)	(9) = (3)× (6)	(10) = (4)× (7)	(11) = (8)+(9)+(10)
Raw material extraction, refining, and manufacturing of steel	1717	4.47	1.42×10^{-1}	1	25	298	1717	111.75	42.32	1871.07
Transportation of concrete	11.93	8.20×10^{-6}	7.58×10^{-4}				11.93	2.05×10^{-4}	2.26×10^{-1}	12.16
Transportation of steel	4.88	3.35×10^{-6}	3.10×10^{-4}				4.88	8.38×10^{-5}	9.23×10^{-2}	4.97
Transportation of equipment	182.62	1.26×10^{-4}	1.15×10^{-2}				182.62	3.15×10^{-3}	3.43	186.05
Operation of construction equipment	31.17	1.54×10^{-3}	0				31.17	3.84×10^{-2}	0	31.21

[1]Obtained from the results of life cycle inventory analysis (LCI) as shown in Table 2.3
[2]Obtained from the ReCiPe database by Goedkoop *et al*. (2014) and assumed 100-year time period
[3]CO_2e: carbon dioxide equivalent

2.3.1 Compilation

The first step of LCIA is to compile the mass of emissions calculated in LCI for every life cycle process. The columns (2)-(4) in Table 2.6 show the data compiled from LCI (see columns (6)-(8) in Table 2.3).

2.3.2 Classification

Different emissions contribute to different environmental impacts. For example, carbon dioxide is one of the main contributors to global warming while sulfur dioxide causes acidification and excessive potassium results in eutrophication. Therefore, the emissions calculated in the LCI are classified into the contributing environmental impacts. Figure 2.4 shows an example of classification of the emissions arising from the cradle-to-gate processes for concrete into different categories of environmental impact. For example, carbon dioxide contributes only to global warming while methane contributes to both global warming and photochemical oxidant formation, and nitrogen oxides contribute to terrestrial acidification, photochemical oxidant formation, and particulate matter formation. These emissions are classified accordingly into the categories of impact they contribute to (e.g., methane is classified into global warming and photochemical oxidant formation). The complete list of emissions that contribute to different environmental impacts can be found in LCIA databases such as the ReCiPe database by Goedkoop *et al*. (2014).

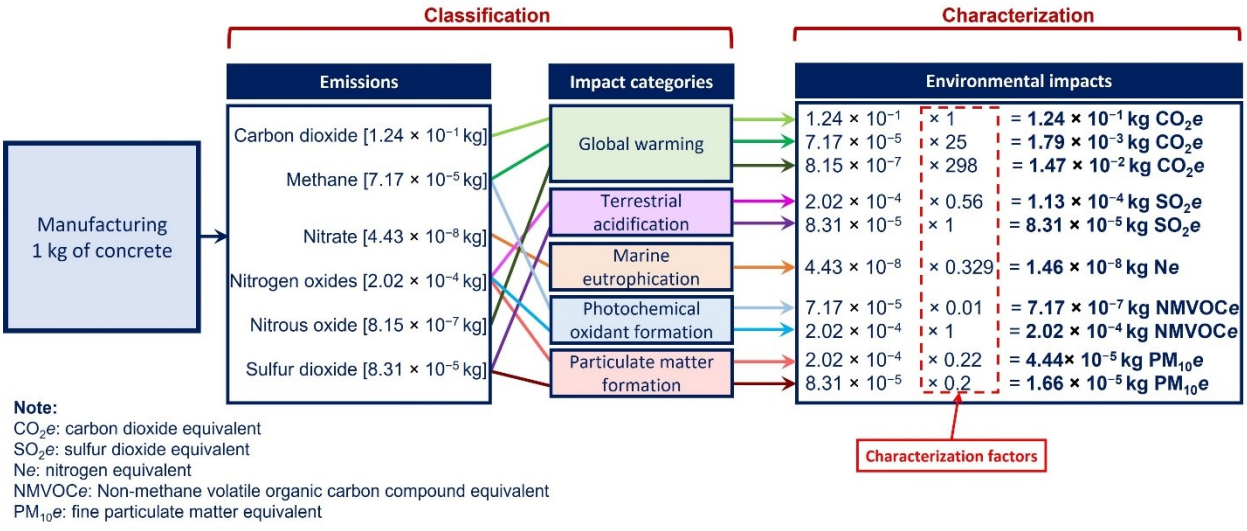

Figure 2.4. Sample calculation of life cycle impact assessment (LCIA) for concrete

2.3.3 Characterization

The classified emissions are characterized as environmental impacts, but the degree of influence of each emission to the environmental impact differs. For example, greenhouse gases (GHGs), such as carbon dioxide (CO_2), methane (CH_4), and nitrous oxides (N_2O), contribute to global warming; however, their degrees of influence to the global warming are not the same because they remain in the atmosphere for different amounts of time and have different potencies to absorb Sun's energy or the heat radiated by Earth (IPCC, 1990). For a 100-year time period, methane and nitrous oxides have 25 and 298 times higher impacts, respectively, to trap heat in the atmosphere when compared to that of carbon dioxide, which is the reference gas for global warming. Such difference in potencies is quantified in terms of characterization factors. Table 2.2 lists the names of characterization factors used for the selected categories of environmental impact. For example, the characterization factor of *global warming* impact category is called global warming potential (GWP) and it is measured in relation to the mass of carbon dioxide, which is the reference gas for quantifying *global warming*. Because methane and nitrous oxides have 25 and 298 times higher impacts than carbon dioxide, GWP of these gases are 25 and 298 times that of carbon dioxide (GWP of carbon dioxide is 1 because it is the reference gas).

The calculation of characterization factors is explained here using the GWP. GWP of a gas is a measure of how much infrared radiation (Sun's energy or heat radiated by Earth) an emission of 1 kg of the gas will absorb over a given period of time (e.g., 100 years) relative to the instantaneous emissions of 1 kg of CO_2. In other words, it is a measurement for comparing the gases that have different abilities of absorbing energy and the different time periods these gases remain in the atmosphere. The GWP of an emission with respect to carbon dioxide is calculated as:

$$(\mathrm{GWP})_x = \frac{\int_0^{TH} a_x \cdot C_x(t)dt}{\int_0^{TH} a_{\mathrm{CO}_2} \cdot C_{\mathrm{CO}_2}(t)dt} \tag{2.7}$$

where x is the emission of interest, TH is the time horizon (e.g., 20, 100, or 500 years), a_x is the radiative efficiency of the emission x (W/m^{2}kg), $C_x(t)$ is the time-dependent abundance of x (the atmospheric mass of emission x over time starting with a pulse at time $t = 0$ with the assumption of instantaneous release of all the emissions), and a_{CO_2} and $C_{\mathrm{CO}_2}(t)$ are the radiative efficiencies and time-dependent abundance of carbon dioxide (reference gas), respectively. In this study, 100 years of time horizon is chosen because it is commonly considered in most environmental policies. The GWPs of selected emissions (i.e., CO_2, CH_4, and N_2O) are shown in columns (5)-(7) in Table 2.6. The GWPs are calculated using Equation (2.7) or are readily obtained from LCIA databases like the ReCiPe by Goedkoop *et al*. (2014). Table 2.7 shows sample LCIA database of GWPs of different emissions for different time horizons *TH*.

Table 2.7. Sample characterization factors of emissions in GWP

Emission	**Time horizon *TH* (years)**		
	20	100	500
Carbon dioxide [CO_2]	1	1	1
Methane [CH_4]	72	25	7.6
Nitrous oxide [N_2O]	289	298	153
Chloroform [$CHCl_3$]	108	31	9.3
Carbon tetrachloride [CCl_4]	2700	1400	435
Chlorodifluoromethane (HCFC-22) [$CHClF_2$]	5160	1810	549
Trichlorofluoromethane (CFC-11) [CCl_3F]	6730	4750	1620
Bromotrifluoromethane (Halon-1301) [$CBrF_3$]	8480	7140	2760
Nitrogen trifluoride [NF_3]	12300	17200	20700
Sulphur hexafluoride [SF_6]	16300	22800	32600

In order to account for the higher potency of an emission (e.g., CH_4) to global warming with respect to CO_2, the mass of that emission is converted into an equivalent mass of CO_2

(reference gas for *global warming*) by multiplying with the respective characterization factor (i.e., $(\text{GWP})_{\text{CH}_4} = 25$). The equivalent mass of CO_2 is calculated as follows:

$$\text{CO}_2e = E_x \times (\text{GWP})_x \tag{2.8}$$

where CO_2e is the equivalent mass of CO_2 of emissions x, E_x is the emission of climate forcer x (i.e., air emissions such as CO_2, CH_4, and N_2O that change the temperature of atmosphere), and $(\text{GWP})_x$ is the characterization factor of climate forcer x relative to carbon dioxide. The calculation of equivalent masses of CO_2 for the selected emissions are shown in columns (8)-(10) in Table 2.6. For example, the CO_2e of CH_4, emitted from the cradle-to-gate process of concrete is 32.5kg (= 1.30kg × 25) given $(\text{GWP})_{\text{CH}_4}$ is 25 for a 100-year time period. The total mass of CO_2e can be calculated by the summation of all CO_2e values obtained for different greenhouse gases. This calculation step is shown in column (11) in Table 2.6. It should be noted that the values of GWPs may change over time because of the evolved science in estimating the radiative efficiency and lifetime of the greenhouse gases; therefore, it is advised that comparisons in terms of mass of CO_2 equivalent or GWP are conducted with caution (Myhre *et al*., 2013).

The calculations shown in Table 2.6 are repeated for other environmental impacts using (i) equations (analogous to Equation (2.7)) to calculate the corresponding characterization factor (refer to Goedkoop *et al*. (2013) for the equations or other characterization models for the LCIA databases listed in Table 2.1) and (ii) conversion into equivalent measurements of reference substances using equations analogous to Equation (2.8). For example, the characterization factor for the impact category of *terrestrial acidification* is terrestrial acidification potential (TAP) and it is calculated in relation to sulfur dioxide (which is the reference gas). TAP is calculated as:

$$\text{TAP} = \frac{(FF)_x}{(FF)_{\text{SO}_2}} \tag{2.9}$$

in which $(FF)_x$ is the fate factor of emission x (m^2·year/kg), and $(FF)_{SO_2}$ is the fate factor of sulfur dioxide and

$$(FF)_x = \frac{\sum_j [\Delta(BS)_j \times A_j]}{\Delta M_x} \tag{2.10}$$

where $\Delta(BS)_j$ is the change in base saturation of forest area j, A_j is the size of forest area j (m^2), and ΔM_x is the change in emitted mass of acidifying substance x (kg/year). Similar to Equation (2.8), emissions related to terrestrial acidification (e.g., sulfur oxides, nitrogen oxides, and ammonia) are converted into the equivalent mass of sulfur dioxide SO_2e using TAP as:

$$SO_2e = E_x \times (\text{TAP})_x \tag{2.11}$$

For example, as shown in Figure 2.4, manufacturing 1 kg of concrete generates 2.02×10^{-4} kg of nitrogen oxides and the TAP of nitrogen oxides is 0.56 (see the box with dashed lines in Figure 2.4). Therefore, the contribution of nitrogen oxides towards terrestrial acidification, calculated using Equation (2.11), is 1.13×10^{-4} kg (= 2.02×10^{-4} kg× 0.56).

2.3.4 Normalization

The results of LCIA (see, for example, Table 2.6) may not be completely perceivable in terms of what the global impact of the emissions are. Therefore, the total equivalent masses of emissions (e.g., CO_2e, SO_2e, etc.) are normalized with respect to the annual world impact per person. Table 2.8 summarizes the world impact per person in 2010 (a reference year), according to ReCiPe (National Institute for Public Health and Environment (RIVM), 2016). The values in Table 2.8 indicate the annual impact caused worldwide divided by the world population in 2010. For example, the annual world impact per person in the category of global warming is 10757 kg of CO_2e. Given the global warming impact of a drilled shaft is 5000 kg of CO_2e, it is equivalent to

46.5% of the annual global warming impact per person (i.e., annual global warming impact of one person).

Table 2.8. World impact per person in 2010 (normalization factors in LCIA) (adapted from RIVM, 2016)

Impact category	Value	Unit
Global warming	10757	kg CO2*e* per person
Ionizing radiation	480	kBq Co-60*e* per person
Ozone depletion	0.065	kg CFC-11*e* per person
Terrestrial acidification	41	kg SO_2*e* per person
Marine eutrophication	4.6	kg N*e* per person
Freshwater eutrophication	0.65	kg P*e* per person
Photochemical oxidant formation	21	kg NMVOC*e* per person
Particulate matter formation	26	kg PM_{10}*e* per person
Human toxicity	31262	kg 1,4-DB*e* per person
Marine ecotoxicity	43	kg 1,4-DB*e* per person
Freshwater ecotoxicity	25	kg 1,4-DB*e* per person

2.4 Interpretation

The interpretation phase involves reporting the findings from the LCI and LCIA. Conclusions are drawn through an iterative process that follows these sequences: (i) identification of significant issues, (ii) evaluation of the methodology and results for completeness, sensitivity, and consistency, (iii) drawing preliminary conclusions and checking that these are consistent with the goal and scope of the study, data quality requirements, predefined assumptions and values, and limitations, and (iv) reporting the conclusions if they are found to be consistent; otherwise, reiteration from steps (i), (ii), and (iii) as appropriate (ISO, 2006b). Examples of significant issues are the significant contributions of the different stages or processes to the environmental impacts

or to specific emissions of interest, and implications of the assumptions made, selection of impact categories, characterization methods (models) used to the LCI and LCIA results. Significant issues (e.g., contributions or anomalies) can be identified by structuring the LCI and LCIA results with respect to the variable of interest (e.g., life cycle stages, life cycle processes, impact categories, emissions, and any other variables related to assumptions made in LCA). The completeness check ensures that all relevant information and data needed for the interpretation are available and complete. The sensitivity check involves evaluating the influence of variations in assumptions, methods and data on the results. Lastly, the consistency check is completed to determine whether the assumptions, calculation methods, and data are consistent with the goal and scope. Recommendations are given based on the final conclusions and according to the goal of LCA. For example, if the goal of LCA is to compare the global warming impacts of two alternative designs for a drilled shaft, the design with the least mass of CO_2e is recommended.

2.5 Summary

In this chapter, the procedures of life cycle assessment (LCA) in the context of geotechnical engineering are explained. LCA is a standardized environmental impact assessment for the quantification of various environmental impacts of a system, such as global warming impact, acidification, eutrophication, particulate matter formation, and other environmental impacts, caused throughout the life cycle of the system. Typical stages considered in the life cycle of geotechnical structure are extraction and refining of raw materials, manufacturing, transportation, construction, maintenance and repair, structure reuse, demolition and disposal, and material reuse and recycling. Following the standards specified in ISO 14044:2006, LCA is conducted in four stages: (i) defining goal and scope of LCA, (ii) life cycle inventory analysis (LCI), (iii) life cycle impact assessment (LCIA), and (iv) interpretation of LCA results. In the goal and scope of LCA,

essential inputs, such as the functional unit of geotechnical structure being studied, system boundary of the life cycle, and database requirements, are defined. The purpose of LCI is to quantify the emissions, such as carbon dioxide, particulate matter, and sulfur dioxide, generated during the defined system boundary of the life cycle. The emissions are then interpreted as global environmental impacts in the LCIA. In the interpretation stage of LCA, the results of LCA are analyzed to determine the significant life cycle processes and environmental impacts that need the most attention when designing the geotechnical structure with environmental considerations. In this study, the quantified environmental impacts are normalized with respect to reference values (i.e., annual world impact per person and environmental impact of a typical passenger car) to provide perspectives on the relative impact of geotechnical structures compared to commonly perceived polluters.

2.6 List of Symbols

Notation	Description
$\Delta(BS)_j$	Change in base saturation of forest area j
ρ_{diesel}	Density of diesel
$(EF)_x$	Emission factor of substance x
$(EF)_{x,\text{empty}}$	Emission factor for empty runs of transportation
$(EF)_{x,\text{loaded}}$	Emission factor for loaded runs of transportation
$(EF)_{x,M}$, $(EF)_{x,R}$, and $(EF)_{x,U}$	The emission factors for driving on motorway, rural road, and urban road, respectively
$(EF)_{x,\text{road}}$	Emission factor for driving on a certain type of road (e.g., motorway, rural road, or urban road)
$(EF)_{x,\text{transportation}}$	Total emission factor of emission x for transportation
$(FF)_{SO_2}$	Fate factor of sulfur dioxide
$(FF)_x$	Fate factor of emission x
$(\text{GWP})_x$	Characterization factor of climate forcer x relative to carbon dioxide
ΔM_x	Change in emitted mass of acidifying substance x
$(\text{TAP})_x$	Characterization factor of acidifying substance x relative to sulfur dioxide
a_{CO_2}	Radiative efficiency of carbon dioxide
A_j	Size of forest area j
a_x	Radiative efficiency of the emission x
$C_{CO_2}(t)$	Time-dependent abundance of carbon dioxide

List of Symbols (continued).

Notation	Description
CO_2e	Equivalent mass of CO_2 of emissions x
$C_x(t)$	Time-dependent abundance of x (the atmospheric mass of emission x over time starting with a pulse at time $t = 0$ with the assumption of instantaneous release of all the emissions)
d_t	Transportation distance
E_x	Total emission of substance (pollutant) x
k_o	Engine load factor
m	Mass of sub-product (e.g., concrete, steel, and diesel)
p	Maximum payload capacity of the transportation truck
P_e	Rated engine power
Q	Weight of cargo loaded in the transportation truck
q_d	Fuel consumption rate
s_d	Specific fuel consumption
s_M, s_R, and s_U	Driving share factors on motorway, rural road, and urban road (ranging from 0 to 1), respectively
SO_2e	Equivalent mass of sulfur dioxide
t	Time
TH	Time horizon (e.g., 20, 100, or 500 years)
u	Utilization ratio of transportation trucks
$V_{\text{diesel,total}}$	Total volume of diesel

CHAPTER 3: ENVIRONMENTAL IMPACTS OF PILE FOUNDATIONS

Drilled shafts are pile foundations widely used in North America for providing support to bridges, high-rise buildings, excavations, retaining structures, and slopes (FHWA, 2010a). These are widely used in different geologic settings (Kulhawy, 1991) and usually have extremely high axial resistances. Further, drilled shafts can have excellent strength against flexure in resisting overturning and seismic forces. Large diameter drilled shafts are also used as alternatives to group piles for eliminating the use of pile caps and reducing the footprint area (FHWA, 2010a; Salgado, 2008). Although drilled shafts have been widely used for various applications, there is a lack of knowledge regarding their environmental impacts. The procedure and details of LCA calculations for drilled shafts are not available. At the same time, there is no easy-to-use guideline available using which a designer can relate a particular design to its environmental impact without the use of specialized LCA software packages.

3.1 Problem Description and Scope

Single drilled shafts and pile groups (consisting drilled shafts) embedded in sandy soils are considered in this study for which life cycle assessments are performed. Table 3.1 provides a summary of the parameters considered in the design of single drilled shafts and groups in this study. The pile length L_p is varied from 5 m to 30 m, and pile diameter B_p is varied from 0.3 m to 1.5 m. Three different group configurations with 2×3, 3×3, and 3×4 drilled shafts are considered. The applied vertical load P ranges from 1000 kN to 3000 kN.

Table 3.1. Range of parameters considered in drilled shaft design

Variable	Values
Pile length, L_p (m) – for fixed length designs	5, 10, 15, 20, 25, and 30
Pile diameter, B_p (m) – for fixed diameter designs	0.3. 0.6. 0.9, 1.2, and 1.5
Concrete density (kg/m^3)	2400 (Vieira, 2015)
Cylinder compressive strength of concrete (MPa)	35 (CEN, 2004)
Elastic modulus of concrete (MPa)	34077 (CEN, 2004)
Steel density (kg/m^3)	7850 (CEN, 2002)
Percentage volume of steel with respect to concrete volume (%)	1, 2, 3, and 4 (FHWA, 2010a)
Factor of safety	2, 2.5, and 3
Applied load, P (kN)	1000, 2000, and 3000
Pile group design	
Pile configuration	2 × 3, 3 × 3, and 3 × 4
Pile diameter, B_p (m)	0.9
Pile cap thickness, T_c (m)	0.5, 1, 2, and 3
Center-to-center pile spacing, s_p (m)	$2B_p$, $3B_p$, $4B_p$, and $5B_p$ (Salgado, 2008)
Clear edge distance, d_{ce} (m)	Minimum of (⅔)B_p or 0.1 m (ACI, 2011; Magade and Ingle, 2020)
Minimum area of steel reinforcement in pile cap	0.2% of cross-sectional area of concrete pile cap in each direction (CAC, 2006)
Soil properties for parametric study (Profiles 1 and 4 – See Figure 3.2)	
Relative density, D_R (%)	30, 50, 65, and 80 (Basu and Salgado, 2012)
Critical state friction angle, ϕ_c (°)	28, 31, 34, and 37 (Basu and Salgado, 2012)
Coefficient of lateral earth pressure at rest, K_0	0.4, 0.5, and 0.6 (Basu and Salgado, 2012)

3.1.1 Design of Single and Group Drilled Shafts

The drilled shafts in this study are designed by satisfying the ultimate limit state criterion of ultimate pile capacity corresponding to 10% relative settlement and the serviceability limit state criterion of allowable pile settlement. The ultimate axial pile capacity is calculated following a property-based capacity calculation method (Salgado, 2008). The ultimate capacity of pile foundations is calculated as the summation of capacities developed at the base and along the shaft:

$$Q_{ult} = q_{b,ult} A_b + \sum_i q_{sL,i} A_{s,i} \tag{3.1}$$

where Q_{ult} is the total ultimate capacity (kN), $q_{b,ult}$ is the ultimate unit base resistance (kPa), A_b is the cross-sectional area of the pile base (m^2), $q_{sL,i}$ is the limit unit shaft resistance of the i^{th} soil layer (kPa), and $A_{s,i}$ is the surface area of the pile in contact with the i^{th} layer (m^2). The allowable pile capacity Q_{all} is obtained by reducing Q_{ult} with a factor of safety (FS) — $Q_{all} = Q_{ult}$/FS.

According to Salgado (2008), the ultimate unit base capacity of drilled shafts in sand is given by

$$q_{b,ult} = \left[0.23 \exp(-0.0066 D_R)\right] q_{bL} \tag{3.2}$$

in which

$$\frac{q_{bL}}{p_A} = 1.64 \exp\left[0.1041 \phi_c + (0.0264 - 0.0002 \phi_c) D_R\right] \left(\frac{\sigma'_h}{p_A}\right)^{0.841 - 0.0047 D_R} \tag{3.3}$$

where q_{bL} is the limit base resistance (kPa), D_R is the relative density of sand (%), p_A is the atmospheric pressure (= 100 kPa), ϕ_c is the angle of friction at the critical state, and σ'_h is the effective horizontal stress (kPa) at the pile base.

The limit unit shaft capacity of drilled shafts in sand is given by (Salgado 2008)

$$q_{sL} = \sigma'_v K \tan\delta \tag{3.4}$$

in which

$$\frac{K}{K_0} = 0.7 \exp\left\{\left[0.0114 - 0.0022 \ln\left(\frac{\sigma'_v}{p_A}\right)\right] D_R\right\} \tag{3.5}$$

$$\delta = \phi_c \tag{3.6}$$

where σ_v' is the effective vertical stress (kPa) at a depth where q_{sL} is determined, K_0 is the coefficient of lateral earth pressure at rest, and δ is the friction angle at the interface of the pile and soil.

Settlement calculations are completed following the method by Bowles (1997) to ensure that the designed pile dimensions, determined based on the bearing capacity calculations, do not result in exceeding the allowable settlement of 30 mm, as recommended by Salgado (2008). The total settlement is the summation of the axial and point settlements:

$$\Delta H_p = \Delta H_a + \Delta H_{pt} \tag{3.7}$$

where ΔH_p is the total settlement of drilled shaft (m), ΔH_a is the axial settlement (m), and ΔH_{pt} is the point settlement (m). The axial settlement is computed as:

$$\Delta H_a = \frac{PL_p}{A_p E_p} \tag{3.8}$$

where P is the axial force (kN), L_p is the length of pile (m), A_p is the cross-section area of pile (m^2), and E_p is the Young's modulus of pile (kPa). The point settlement is calculated as:

$$\Delta H_{pt} = \Delta q_p B_p \frac{1-\mu_s^2}{E_s} m I_s I_F F_1 \tag{3.9}$$

where Δq_p is the bearing pressure at the pile base (kN/m^2), B_p is the drilled shaft diameter (m), μ_s is the Poisson's ratio of soil (= 0.35), E_s is the Young's modulus of soil below the pile base (kPa), mI_s is the shape factor (= 1.0), I_F is the Fox embedment factor (= 0.55 if $L_p/B_p \leq 5$ and = 0.50 if $L_p/B_p > 5$), and F_1 is reduction factor (= 0.25 if the axial load is fully resisted by the shaft (floating pile), = 0.50 if the shaft capacity is fully mobilized and the excess applied load is resisted by the base, and = 0.75 if the entire axial load is resisted by the base (end bearing pile)).

The distribution of applied (structure or column) load for the drilled shafts in groups is calculated as (Salgado, 2008):

$$Q_j = \frac{P}{n_p} + \frac{M_y x_j}{\sum_{j=1}^{n_p} x_j^{\,2}} + \frac{M_x y_j}{\sum_{j=1}^{n_p} y_j^{\,2}} \tag{3.10}$$

where Q_j is the applied axial load acting on the i^{th} pile of the group (kN), P is the total applied load (kN), n_p is the total number of piles, M_y is the applied moment with respect to the y-axis (kN m), M_x is the applied moment with respect to the x-axis (kN m), and x_j and y_j are the x- and y-coordinates of the center of pile j from the centroid of the pile cap in plan (m).

The working (allowable) stress design method is used to obtain the drilled shaft dimensions with a FS ranging over 2-3. The allowable settlement of drilled shaft is assumed to be 30 mm, as recommended by Salgado (2008). The pile dimensions obtained after satisfying the ultimate capacity (with a factor of safety) are checked against the allowable pile settlement. The volume of steel reinforcement in the drilled shaft is assumed to vary between 1% and 4% of the volume of concrete shaft (FHWA, 2010a). Pile caps are not considered for single drilled shafts based on the recommendations of FHWA (2010a) and CAC (2006).

The pile (drilled shaft) groups are designed following the working stress design method with FS = 2.5 to ensure that (i) the total applied load does not exceed the group capacity and (ii) the distributed loads on individual piles do not exceed the individual pile capacity. Block and row failures in pile groups are unlikely in sand and neglected in the calculations. The distribution of axial loads into different piles in a group are calculated using Equation (3.10). For determining the pile cap dimensions, the clear edge distance is assumed to be the minimum of ⅔ of the pile diameter or 100 mm (Table 3.1), following the recommendations of ACI (2011) and Magade and Ingle

(2020). The pile cap thickness T_c is varied from 0.5 m to 3 m and center-to-center pile spacing s_p is varied from $2B_p$ to $5B_p$ (Salgado, 2008). The minimum area of steel reinforcement in the pile cap in each direction is assumed to be 0.2% of cross-sectional area of the pile cap, based on CAC (2006). Figure 3.1 shows the top and section views of a pile group with 2 by 2 configuration.

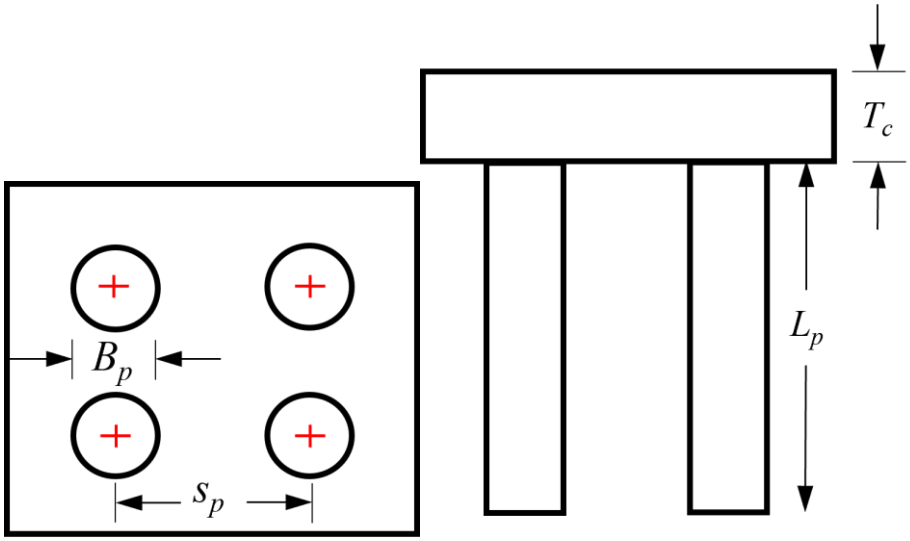

Figure 3.1. Top and section views of a pile group

Five different sandy soil profiles, denoted as Profiles 1 to 5, are considered in this study, as described in Figure 3.2(a)-(e). Profile 1 is a completely dry homogeneous sand profile with a relative density D_R = 70%, critical-state friction angle ϕ_c = 33°, and a coefficient of lateral earth pressure at rest K_0 = 0.45. Profile 2 is the same as Profile 1 but with a water table located at the ground surface. Profile 3 consists of a completely dry sand deposit with D_R = 50% overlying a strong bearing layer with D_R = 80%. Both sand layers have mean ϕ_c = 33° and K_0 = 0.45. Profile 4 is the same as Profile 3 but with a water table located at a depth of 2 m below the ground surface. Profile 5 consists of an extremely loose sand layer with D_R = 20% overlying a dense sand layer with D_R = 80%.

The soil properties of Profiles 1 and 4 are varied, as specified in Table 3.1. Range of parameters considered in drilled shaft design, to perform a parametric study and to investigate the effect of soil properties on the environmental impacts. For an applied load, the drilled shafts are designed assuming either (i) a fixed diameter or (ii) a fixed length. For example, if a fixed diameter of, say, 600 mm is assumed, the pile length that satisfies the ultimate limit capacity with a factor of safety is determined, and if a fixed length of, say, 10 m is assumed, the pile diameter is determined. The serviceability limit state criterion is also satisfied in both cases. This procedure is followed to investigate if fixing a certain pile dimension plays a role in increasing the environmental impacts.

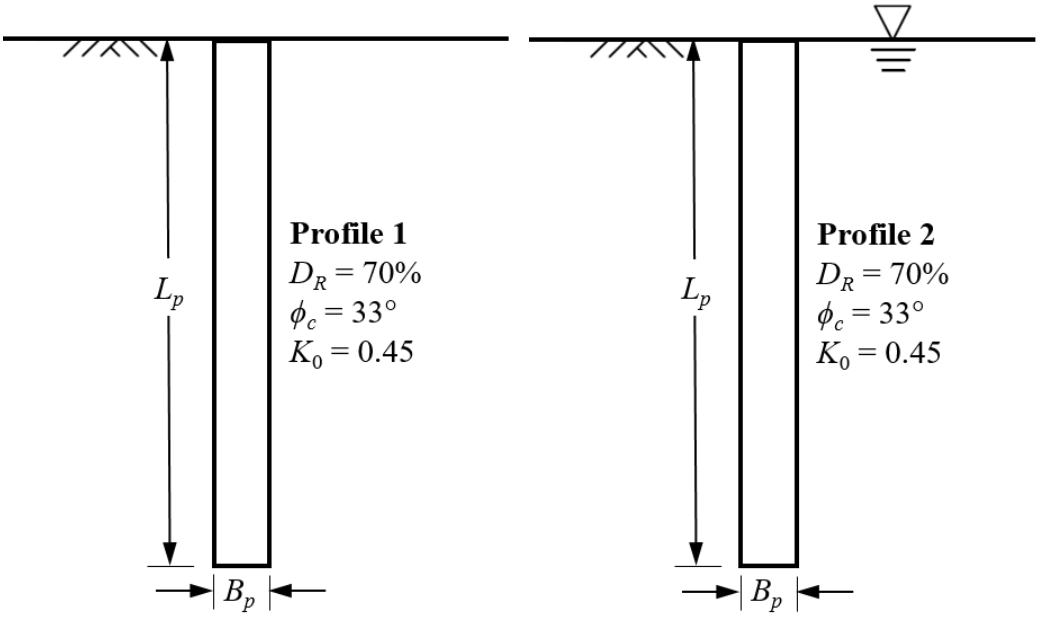

(a) (b)

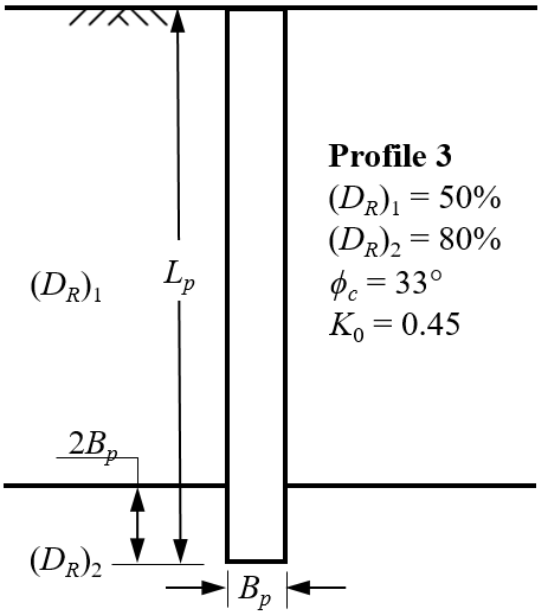

(c)

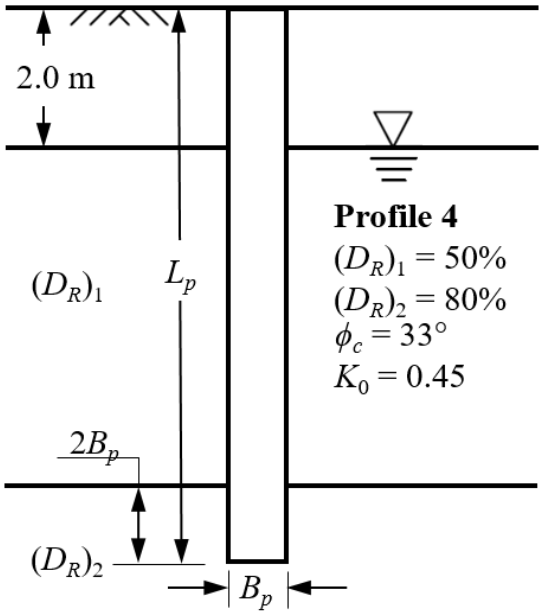

(d)

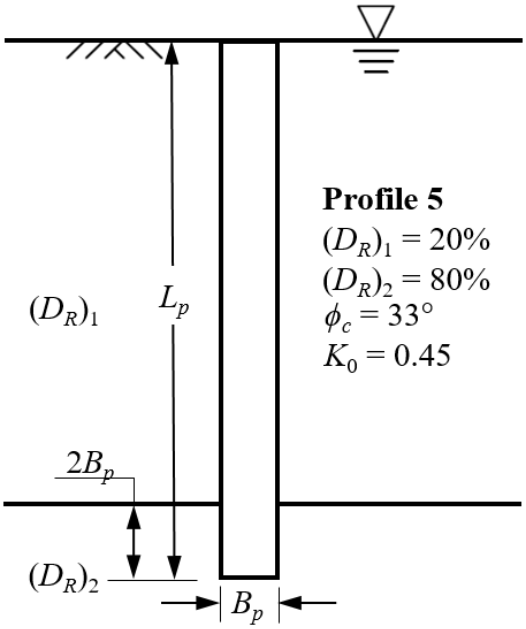

(e)

Figure 3.2. Sand profiles considered in this study: (a) Profile 1, (b) Profile 2, (c) Profile 3, (d) Profile 4, and (e) Profile 5

For a given profile and applied load, the drilled shaft dimensions are determined as part of design. After the dimensions of the drilled shafts and pile cap are finalized, the total volumes of concrete and steel are computed and converted into their corresponding masses using the respective densities of 2400 kg/m^3 (Vieira, 2015) and 7850 kg/m^3 (CEN, 2002), respectively (Table 3.1). Table 3.2 summarizes the design dimensions, and volumes and masses of materials for sample drilled shaft designs. For example, for a single drilled shaft with 0.8 m diameter, 15 m length, and 2.5% steel reinforcement, the total masses of concrete and steel are 18096 kg and 1480 kg, respectively. These values are used as inputs to the LCA. The LCA is performed following the standards by ISO (2006a; 2006b) and using the GaBi software (version 6.115).

Table 3.2. Samples of drilled shaft designs

	Profile 1		Profile 2	
Parameter	**Fixed length**	**Fixed diameter**	**Fixed length**	**Fixed diameter**
Length (m)	15	9	15	16
Diameter (m)	0.8	0.9	1.0	0.9
Volume of concrete (m^3)	7.54	5.73	11.78	10.18
Volume of steel (m^3)	0.19	0.14	0.29	0.25
Mass of concrete (kg)	18096	13741	28274	24429
Mass of steel (kg)	1480	1124	2312	1998

3.2 LCA of Drilled Shafts

3.2.1 Goal and scope

In this study, LCA is carried out to investigate and quantify the environmental impacts of single drilled shafts and pile groups in sandy soil profiles. The results can be used in comparative assertions; however, the loading conditions, subsurface profiles, soil properties, construction processes, and any design or LCA related factors should be similar for such comparisons. The system boundaries of LCA considered in this study includes the *raw material extraction and refining* stage on the start boundary and the *construction* stage on the end boundary (i.e., 'cradle-

to-site' system boundaries are considered as shown in Figure 2.1). Stages beyond the end of construction are omitted in this study because drilled shafts typically have a long service life and require minimum or no maintenance. The life cycle stages of structure reuse, demolition and disposal, and material reuse and recycling are also excluded in this study because it is usually not decided during the design and construction stages whether a drilled shaft will be abandoned, reused or deconstructed (with material recycling) at the end of designed lifespan. Further, it is assumed in this study that little or no construction waste is generated during the construction stage. LCA data related to bentonite slurry is not available; therefore, the impacts of bentonite slurry are quantified based on generic data of materials that are used to prepare bentonite slurry. If the impacts of bentonite slurry are found to be insignificant, then the processes related to bentonite slurry can be excluded from the system boundaries, as recommended in ISO (2006a). Further, the processes related to steel casing are omitted because steel casing is used if caving soil (e.g., sandy or gravelly soil under the water table) is underlain by a clayey and impervious soil, which is not the case in this study (Figure 3.2) (Reese *et al*., 2006; Salgado, 2008). For single drilled shafts, the processes related to concrete pouring for pile cap are also omitted because pile cap is not required (CAC, 2006; FHWA, 2010a).

The functional unit considered in the LCA study is the mass (in kg) of a drilled shaft required to support the applied load in a given subsurface profile without (i) a bearing capacity failure (corresponding to FS = 2-3) and (ii) the settlement exceeding 30 mm. LCI and LCIA databases for the Canadian and American practices are used if available; otherwise, European or global databases are used. It is assumed that the life cycle processes of drilled shaft are not significantly sensitive to the time-related coverage; therefore, data collected in the 21st century should be adequate as they are the most recent data available at the time this LCA is conducted.

To obtain more accurate LCA results, it is recommended that databases updated to date are used because the energy efficiency in manufacturing processes and construction technologies continue to improve. The technology coverage of data for this LCA study is not a concern because the primary materials for drilled shafts (e.g., concrete and steel) are widely used construction materials for which the energy sources used in the manufacturing process are assumed to not vary significantly both over time and across locations.

The following environmental impact categories are considered in the study: global warming, ionizing radiation, terrestrial acidification, marine eutrophication, photochemical oxidant formation, particulate matter formation, human toxicity, marine ecotoxicity, and freshwater ecotoxicity. Additional environmental impacts like ozone depletion, freshwater eutrophication, terrestrial ecotoxicity, water and metal depletion can be quantified if these have important impacts to the geo-structure being studied; however, these have relatively low impacts for drilled shafts and are not considered in this study. Other assumptions made in this LCA study are discussed when describing the LCI and LCIA in details.

3.2.2 Assumptions in LCI and LCIA

Based on the defined goal and scope of LCA for drilled shafts, the LCI databases are selected accordingly. Table 3.3 summarizes the information of selected databases for conducting LCI of drilled shafts. All databases are in compliance with the ISO standards (ISO 2006a; 2006b). Alternative databases that best represent the processes listed in Table 3.3 may be used if necessary. Table 3.4 summarizes the characteristics of sub-products (i.e., concrete and steel) and assumptions used in LCI and LCIA calculations.

Table 3.3. Summary of LCI databases used for drilled shafts

Process	Data source	Reference year[1]	Geography	Technology description
From extraction and refining of raw materials to manufacturing of concrete	Thinkstep – from GaBi (2021)	2015	Europe	Manufacturing of ready-mix concrete with strength class of C35/45 according to Eurocode 2 (CEN, 2004). Manufacturing of cement is included in the data.
From extraction and refining of raw materials to manufacturing of steel reinforcement cage	World Steel Association – from GaBi (2021)	2007	Global	Manufacturing of steel reinforcing bar used to strengthen concrete in highway and building construction
Road transportation	Thinkstep – from GaBi (2021)	2015	Global	Use of diesel-driven heavy-duty trucks (27-tonne payload capacity). Emission factors obtained from the Handbook Emissions Factors for Road Transport (HBEFA, 2010)
Concrete pumping	Thinkstep – from GaBi (2021)	2015	Global	Pumping process of 1 m^3 of concrete assuming 2365 kg/m^3 density
Diesel combustion	NREL (2012)	2005	United States	Diesel combustion in industrial applications such as mobile refrigeration units, generators, pumps, and portable well-drilling equipment.

[1]Start year of the time period for which the data set is valid.

Table 3.4. Characteristics of sub-product or assumptions used in LCA of drilled shaft

Life cycle stage	Characteristics of sub-product or assumptions	
From raw material extraction to manufacturing	Strength class of concrete (e.g., 20/25, 35/45, 50/60)	C35/45 strength according to Eurocode 2 (CEN, 2004)
	Type of steel	Steel reinforcing bar rolled on a hot rolling mill

Table 3.4 (continued).

Life cycle stage	Characteristics of sub-product or assumptions	
Transportation	Type of construction machinery to be transported	Auger drilling machine and hydraulic cane
	Weight of the construction machinery	Mass of auger drilling machine = 43000kg (Bauer Maschinen GmbH, 2021) Mass of hydraulic cane = 12340kg (Tadano, 2018)
	Hauling distance from machinery rental location/material manufacturing plant to construction site	Distance from concrete manufacturing plant to construction site = 10km Distance from steel manufacturing plant to construction site = 50km Distance from machinery rental location to construction site = 50km
	Type and payload capacity of hauling trucks	Concrete mixer truck represented as a diesel-driven 27-tonne capacity truck (p = 27) Machineries hauled by diesel-driven 27-tonne capacity trucks (p = 27)
Construction	Productivity rate of the construction machinery	See Table 3.5
	Fuel consumption rate of the construction machinery	Concrete mixer truck: 11.1L/hr (Zagula *et al*., 2012) Hydraulic crane: 11.6L/hr (calculated based on engine specifications – Tadano, 2018; EPA, 2004; EPA, 2010) Auger drilling machine: 21.4L/hr (calculated based on engine specifications – Bauer Maschinen GmbH, 2021; EPA, 2004; EPA, 2010)

In this study, it is assumed that auger drilling machine and hydraulic crane are used in the construction stage, and their masses are obtained from Bauer Maschinen GmbH (2021) and Tadano (2018), respectively (see Table 3.4). The steel reinforcement cage, auger drilling machine, and hydraulic crane are assumed to be hauled by 27-tonne capacity trucks (p = 27 in Equations (2.2) and (2.3)). The concrete mix is delivered to the construction site by a mixer truck; however,

because of lack of data available, the concrete mixer is represented as a 27-tonne capacity truck in this study. It is assumed that the one-way transportation distances to the construction site for hauling the ready-mix concrete and steel reinforcement cage are 10 km and 50 km, respectively. The one-way transportation distance from the rental location of the construction machinery to the construction site is 50 km. Note that these distances are site-specific.

Three installation activities are involved in the *construction* stage of drilled shafts: (i) drilling the shaft, (ii) placement of steel reinforcement cage, and (iii) erection of funnel or tremie depending on the construction method, and pouring of concrete mix for the shaft. Auger drilling machine is used for drilling the shaft, and hydraulic crane is used for placing the steel reinforcement cage into the drilled shaft.

Two construction methods of drilled shafts, the dry and wet methods, are available (Reese *et al*., 2006). Depending on the location of the water table and the type of soil, the construction method differs. If the soils are dry down to the depth of drilling and the water table is located far below the pile base, then the dry method is practiced. If it is expected that the water table is encountered during the drilling process, then drilled shafts are installed by the wet method. The difference between the two construction methods lies in the method of concrete pouring and the use of bentonite slurry. The dry method uses a funnel to pour the concrete into the shaft, whereas the wet method utilizes a tremie system to prevent water flow into the concrete mix. In the LCA calculations, the difference between the two concrete pouring method is reflected in the difference in time required for the erection of the funnel or tremie system. Another commonly used construction method is the casing method, in which a steel casing is driven prior to concrete pouring to control the caving soil that usually occurs in layered profiles comprising a loose layer between competent soil layers. The casing method is not applicable in this study because the caving

soil in layered profiles 3-5 is not underlain by or in between cohesive impermeable soil. In this study, the dry method of construction is assumed for drilled shafts in soil profiles 1 and 3 and the wet method is assumed for soil profiles 2, 4, and 5 (see Figure 3.2).

Bentonite slurry is typically used for the wet method to stabilize the excavation; however, the use of bentonite slurry is not considered in this LCA study because relevant LCA data is not available. It is expected that the impacts caused by the bentonite slurry are not significant for this study based on approximate surrogate calculation considering the three main ingredients of bentonite slurry – bentonite powder, sand, and water – to replicate the impact of bentonite slurry. Based on the recommendations by FHWA (2010a), the density of bentonite slurry is 1046 kg/m^3 and the concentrations of bentonite powder and sand are both 40 kg/m^3 of water. The $(EF)_{CO_2}$ for bentonite powder ranges from 0.101 (Shillaber *et al*., 2016b) to 0.157 kg CO_2/kg (European Commission, 2018), and the $(EF)_{CO_2}$ for sand and water are 0.00234 kg CO_2/kg and 0.00619 kg CO_2/kg, respectively (European Commission, 2018). The $(EF)_{CO_2}$ for bentonite powder, mentioned above, is not a fixed number because of different assumptions on energy mix and technology used for manufacturing bentonite powder. For a drilled shaft with L_p = 15 m and B_p = 0.8 m, for example, the volume of bentonite slurry is equivalent to the volume of shaft (= 7.54 m^3); hence, the total mass of bentonite slurry is 7887 kg (= 7.54 m^3 × 1046 kg/m^3). Given the density of bentonite powder, concentrations of bentonite powder and sand, and the volume of shaft, the masses of bentonite powder (= 297 kg), sand (= 297 kg), and water (= 7430 kg) are back calculated using the method by Lam (2016). Hence, the total mass of CO_2 from the cradle-to-gate processes of bentonite slurry is estimated to be in the range 77 to 93 kg depending on the emission factor used for bentonite powder. The mass of CO_2 from the transportation of bentonite slurry from the factory to the site is calculated using the same parameters and assumptions used for the

transportation of concrete mix. Hence, the $(EF)_{CO_2}$ for transportation of bentonite slurry is 6.59 × 10^{-4} kg CO_2/kg (see 4th row and 3rd column of Table 2.3), and the mass of CO_2 from the transportation of bentonite slurry is equal to 5.2 kg (= 7887 kg × 6.59×10^{-4} kg CO_2/kg). The CO_2 emission caused by the pouring of bentonite slurry in the construction stage is also assumed to be equivalent to pouring of concrete mix, and calculation of the mass of CO_2 generated from this construction activity will be discussed in the next paragraph. The validity of excluding bentonite slurry from the defined system boundaries will be discussed after the complete LCA results are obtained.

In this study, it is assumed that diesel is used for operating the construction equipment. The diesel consumption rates and operation times of construction equipment for different activities are summarized in Table 3.5. According to Zagula *et al*. (2012), the diesel consumption rate q_d of concrete mixer truck is 11.1 L/hr; however, it is unclear if the engine idling time is accounted in the specified consumption rate. The diesel consumption rates of hydraulic crane and drilling auger machine are calculated assuming that the rated engine powers P_e are 101 kW (Tadano, 2018) and 186kW (Bauer Maschinen GmbH, 2021), respectively. For both hydraulic crane and drilling auger machine, the specific fuel consumption rate q_d is 0.223 kg/kWh (EPA, 2004); the load factor k_o is 0.43 (EPA, 2010); and the density of diesel ρ_{diesel} is 0.832 kg/L (Measurement Canada, 2018). Because of lack of data, the diesel consumption rates for the erection of tremie and funnel are assumed to be identical to that of operating the hydraulic crane. The operation times for drilling, placement of steel cage, erection of tremie and funnel, and pouring of ready-mix concrete are estimated based on the regression models (equations in Table 3.5) provided by Zayed and Halpin (2005). For pouring bentonite slurry, 1.52 kg of diesel is consumed (= 1.83 L × 0.832 kg/L, see

Table 3.5); hence, 4.92 kg CO_2 (= 1.52 kg × 3.23 kg CO_2/kg, see 7th row and 3rd column of Table 2.3 for $(EF)_{CO_2}$) is emitted.

Table 3.5. Parameters for fuel calculation

Construction activity	Diesel consumption rate (L/hr)	Regression models for operation time[1, 2] t (min)	Operation time for drilled shaft (hr) (L_p = 15 m, B_p = 0.8 m)	Diesel consumption (L)
Drilling hole	21.4	$t_{\text{drilling}} = 15.5 + 1.522z_d - 13.189h$	0.337	7.21
Installing steel cage reinforcement using a crane	11.6	$t_{\text{cage}} = -3.6 + 0.787z_d$	0.137	1.59
Erection of funnel	11.6	$t_{\text{funnel}} = 2.873 + 0.141z_d$	0.083	0.963
Erection of tremie	11.6	$t_{\text{tremie}} = 6.6041 + 0.4603z_d$	0.225	2.61
Pouring concrete	11.1	$t_{\text{pouring}} = -0.843 + 0.715z_d$	0.165	1.83
$V_{\text{diesel,total}}$ (dry method)[3]				11.60 (9.65 kg)[5]
$V_{\text{diesel,total}}$ (wet method)[4]				13.24 (11.02 kg)[5]

[1]The regression models for calculating the operation time are obtained from Zayed and Halpin (2005) and developed based on 0.45m of pile diameter, 15.24 m of pile length, and 1.37 m of auger height
[2]z_d = drilling depth in m (= L_p) and h = height of auger in m (= 1.37 m)
[3]Total diesel consumption for dry method = 7.21 + 1.59 + 0.963 + 1.83 = 11.60 L
[4]Total diesel consumption for wet method = 7.21 + 1.59 + 2.61 + 1.83 = 13.24 L
[5]density of diesel ρ_{diesel} = 0.832 kg/L

3.3 Results

The results of LCA conducted for single and group drilled shafts are provided in this section. The environmental impacts of drilled shafts, selected according to the scope of LCA, are reported in normalized figures to provide perspectives on the relative impacts of drilled shafts compared to commonly perceived polluters. Based on the results of LCA, the significant life cycle

processes and environmental impacts are determined. The results of parametric study are provided in which the effects of soil properties, design parameters, and hauling distances of transportation trucks are investigated. To make the results of LCA more accessible to practitioners, charts are developed using which practitioners can estimate global warming impact of drilled shafts solely based on the design dimensions.

3.3.1 Environmental Impacts of Single Drilled Shafts

Table 3.6 summarizes a sample result of LCA for a drilled shaft (L_p = 15 m, B_p = 0.8 m, P = 1000 kN, and Profile 1) for the selected environmental impact categories. The actual values of the environmental impacts are compared with the annual impact per person in year 2010, obtained from Huijbregts *et al*. (2016), to determine their relative impacts. The human toxicity of drilled shaft construction exceeds the annual impact per person by a significant amount. The environmental impacts of drilled shafts are also compared with the environmental impacts of a complete life cycle of a typical passenger vehicle in Table 3.6. According to the European Commission (2008), 56.2 tonnes of greenhouse gases are emitted by a typical passenger car over its life span. A typical drilled shaft with L_p = 15 m and B_p = 0.8 m, for example, generates 4.2 tonnes of global warming potential (GWP), which is 7.6% of the GWP of a typical passenger car. Noting that the results shown in Table 3.6 are based only on one drilled shaft, the total environmental impact from the construction of drilled shafts (or, for that matter, other bored reinforced concrete piles) all over the world is enormous. The comparisons with the annual impact per person and with the environmental impacts of a typical passenger are made to put the environmental impacts of drilled shaft construction in perspective with respect to the commonly perceived polluters. Clearly, quantification of the environmental impacts of foundations and other

geo-structures is very important and worth a detailed investigation, and designs must take into consideration the environmental aspect so that overdesign is avoided.

Table 3.6. Environmental impacts of a drilled shaft (L_p = 15 m and B_p = 0.8 m)

Impact category (equivalent measurement unit)	Drilled shaft impacts[1]	Typical passenger vehicle impacts[1,2]	Proportional drilled shaft impact with respect to passenger vehicle (%)	Annual world impact per person[1,2]	Proportional drilled shaft impact with respect to annual world impact (%)
Global warming (kg of CO_2)	4244	56200	7.6	10757	39
Ionising radiation (kBq of Co-60)	79	-	-	470	17
Terrestrial acidification (kg of SO_2)	8.2	164	5	41	20
Marine eutrophication (kg of P)	2.6	-	-	4.6	57
Photochemical oxidant formation (kg of NMVOC)	8.6	48	18	20.5	42
Particulate matter formation (kg of PM_{10})	3.2	3.9	82	16	20
Human toxicity (kg of 1,4-DB)	252	-	-	51.9	486
Marine ecotoxicity (kg of 1,4-DB)	0.17	-	-	8.8	1.9
Freshwater ecotoxicity (kg of 1,4-DB)	0.39	-	-	12.6	3.1

[1]In equivalent measurement units given in the first column

[2]Data from European Commission (2008)

[2]Data from Huijbregts *et al*. (2016)

Figure 3.3 shows the normalized environmental impacts (with respect to the annual world impact per person listed in Table 3.6) of two drilled shaft designs assuming (i) fixed length of 15

m and (ii) fixed diameter of 0.9 m. It is evident that marine eutrophication (ME), global warming (GW), and photochemical oxidant formation (POF) are the most concerning environmental impacts for drilled shaft, accounting for 40-87% of the world impact per person. It is also evident that the environmental impacts of drilled shaft are dependent on site conditions because the environmental impacts of drilled shaft in Profile 2, shown in Figure 3.3(b), are higher than those in Profile 1 (Figure 3.3(a)). Based on Figure 3.3, the fixed-diameter approach resulted in lower environmental impacts. To investigate the effect of selection of fixed-diameter of drilled shaft to the environmental impacts, the LCA results are also normalized to a base design assuming a fixed-diameter of B_p = 0.9 m. Figure 3.4 shows the change in the most significant environmental impacts (i.e., GW, ME, and POF) of drilled shaft with respect to the fixed diameters of B_p = 0.3, 0.6, 0.9, 1.2, and 1.5 m. As the pile diameter is increased, the selected environmental impacts, shown in Figure 3.4, increased for most cases. Minimal changes in the environmental impacts were observed despite an increase in the pile diameter because the volume of concrete and steel remained constant.

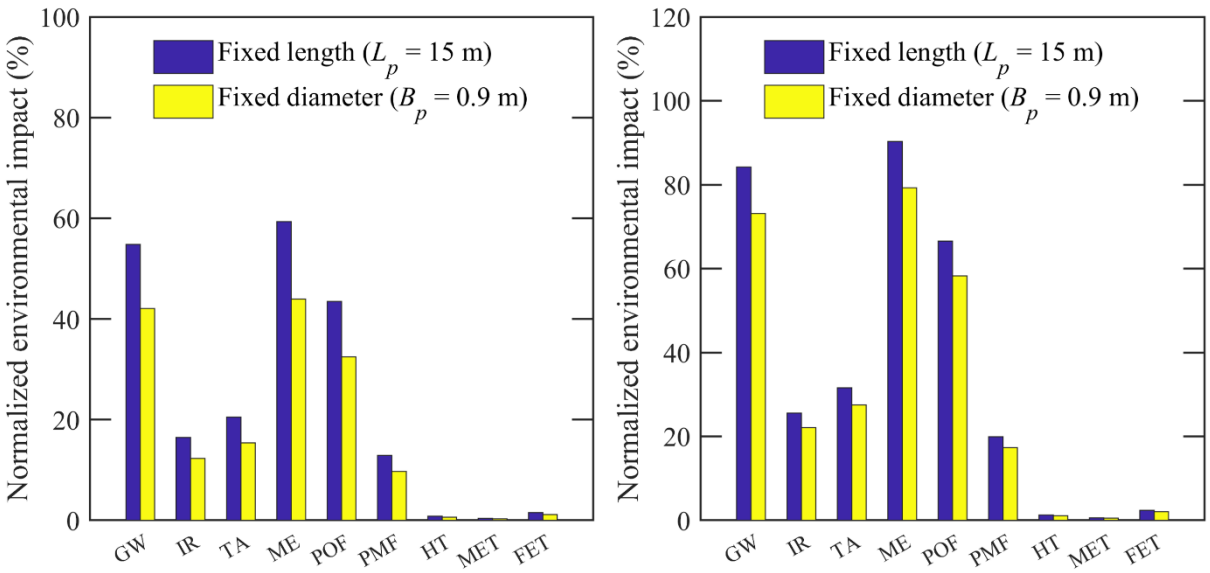

Figure 3.3. Environmental impacts of a drilled shaft with fixed length and fixed diameter in (a) soil profile 1 and (b) soil profile 2. Environmental impacts normalized to the annual world

impact per person in 2010. [GW: global warming; IR: ionizing radiation; TA: terrestrial acidification; ME: marine eutrophication; POF: photochemical oxidant formation; PMF: particulate matter formation; HT: human toxicity; MET: marine ecotoxicity; FET: freshwater ecotoxicity]

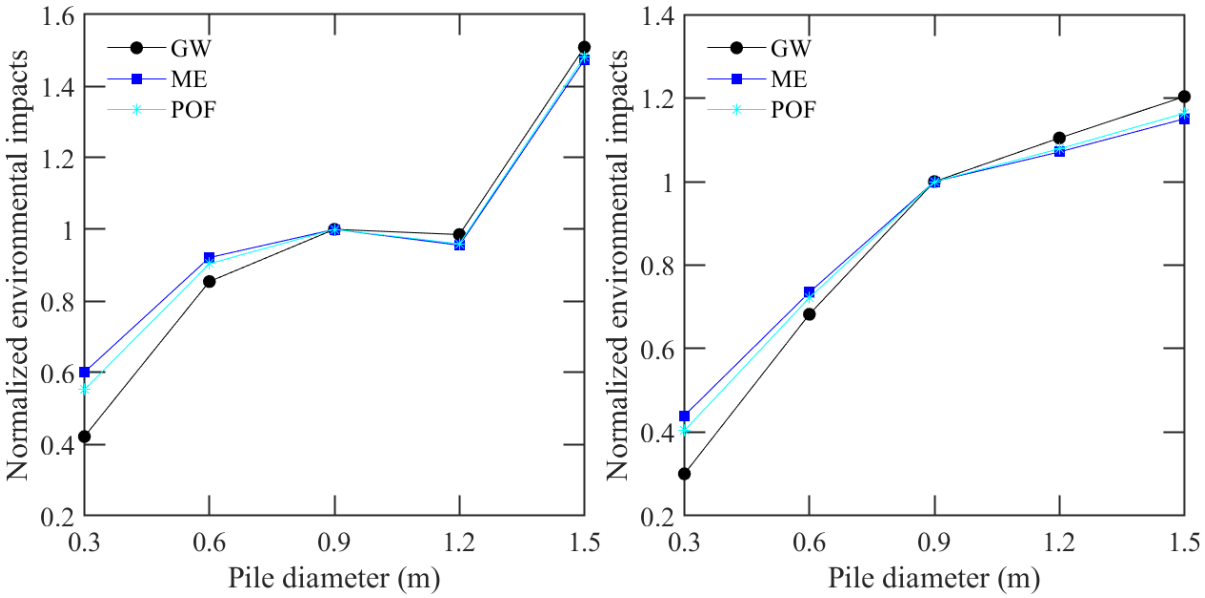

Figure 3.4. Change in environmental impacts of drilled shaft designs with different pile diameters in (a) soil profile 1 and (b) soil profile 2. Environmental impacts normalized to the drilled shaft design with fixed diameter of B_p = 0.9 m

The significant contributions of different processes to the environmental impacts, considering 22 drilled shaft designs in soil profiles 1 and 2, are computed and plotted in Figure 3.5. Using the fixed length approach, six designs were completed assuming different lengths L_p = 5, 10, 15, 20, 25, and 30 m (see Table 3.1) for soil profiles 1 and 2 each (12 designs in total). Similarly, using the fixed diameter approach, five designs were completed assuming different diameters B_p = 0.3, 0.6, 0.9, 1.2, and 1.5 m (see Table 3.1) for soil profiles 1 and 2 each (10 designs in total). The environmental impacts are largely influenced by the processes related to the manufacturing of concrete and steel (including the extraction and refining of raw materials), and there are relatively small contributions from the transportation and construction stages. The

ionizing radiation is mostly affected by the manufacturing of concrete, accounting over 90% of the impact. The carbon dioxide emissions caused by the cradle-to-gate processes of bentonite powder were compared with the total mass of CO2*e* to verify the assumption on excluding processes related to bentonite slurry from the system boundary is valid. The carbon dioxide emissions from bentonite powder are equivalent to a very small percentage of the total CO_2e, ranging from 0.7 to 1.1%, depending on which emission factor is used.

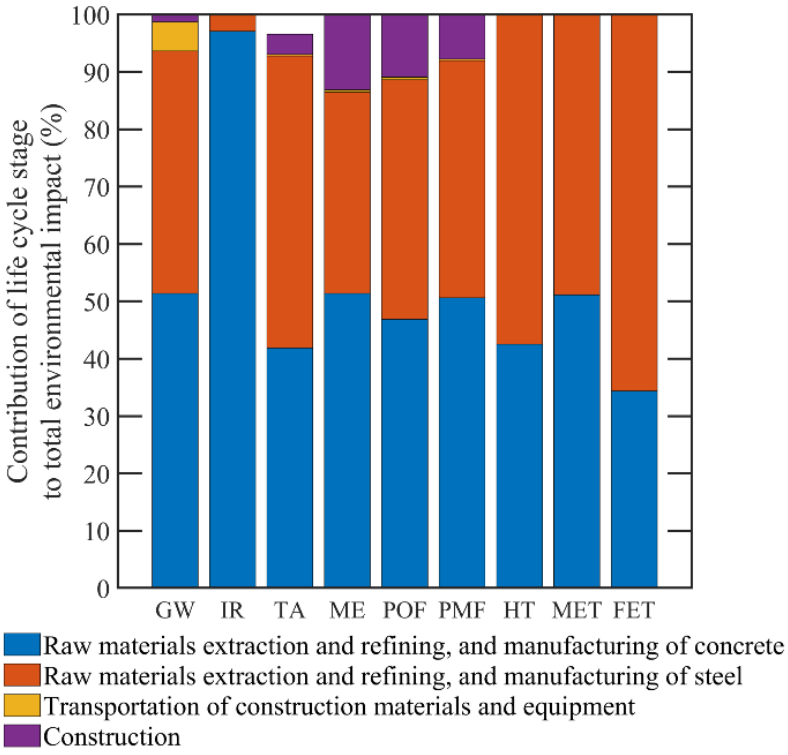

Figure 3.5. Breakdown of environmental impacts per life cycle stage of drilled shafts

Sensitivity analyses are completed by varying some of the assumptions made in this LCA study – pile dimensions, volume of concrete, and volume of steel. Figure 3.6(a)-(b) show the relationship of the environmental impacts with the dimensions of drilled shaft. According to Figure 3.6(a)-(b), the environmental impacts increase as the pile diameter increases, while the opposite is observed when the pile length increases for both the fixed length and fixed diameter design approaches. The decrease in impacts with an increase in the pile length occurs because of

the trade-off between the pile length and diameter in design. Longer piles usually require smaller pile diameters, which result in lower volumes of concrete (and steel) when compared with shorter piles that require larger pile diameters. For example, for the same soil and loading conditions (Profile 1 with applied axial load P = 1000kN), a drilled shaft with 30 m of fixed length is designed with diameter B_p = 0.4 m (volume of concrete = 3.77 m^3), and a drilled shaft with 5 m of fixed length is designed with B_p = 1.6 m which has higher volume of concrete (= 10.05 m^3). The environmental impacts are mostly influenced by the manufacturing of concrete and steel (evident from Figure 3.5); therefore, an increase in the pile diameter increases the volume of concrete and steel substantially because of which there is a sharp increase in the environmental impacts. The difference in results between Figure 3.6(a)-(b) are caused by the design increments of pile diameter (200 mm increment) and pile length (1 m increment) for fixed length and fixed diameter design approaches, respectively. If the design increments were extremely small (which is impractical), it is likely that Figure 3.6(a)-(b) would become identical. The impacts under different categories shown in Figure 3.6(a)-(b) are consistent with Figure 3.3 indicating that ME, GW, and POF are the most significant environmental impacts for drilled shaft.

To investigate the relationship between the volume of concrete and steel with the environmental impacts, the normalized environmental impacts are plotted as functions of volumes of concrete and steel in Figure 3.7 and Figure 3.8 for both the soil profiles 1 and 2. Linear increases of normalized environmental impacts are observed in both Figure 3.7 and Figure 3.8. The rate of change in the environmental impact with respect to the volume of concrete is the highest for global warming (= 0.078), which indicates that global warming impact is the most affected by a change of volume of concrete. Marine eutrophication is also highly influenced by the change in volume of concrete with 0.066 as the rate of change. Marine ecotoxicity has the least rate of change (=

0.0005). Similarly, the change in the volume of steel reinforcement influences global warming impact (= 0.121) and marine eutrophication (= 0.112) the most and marine ecotoxicity the least (= 0.0009).

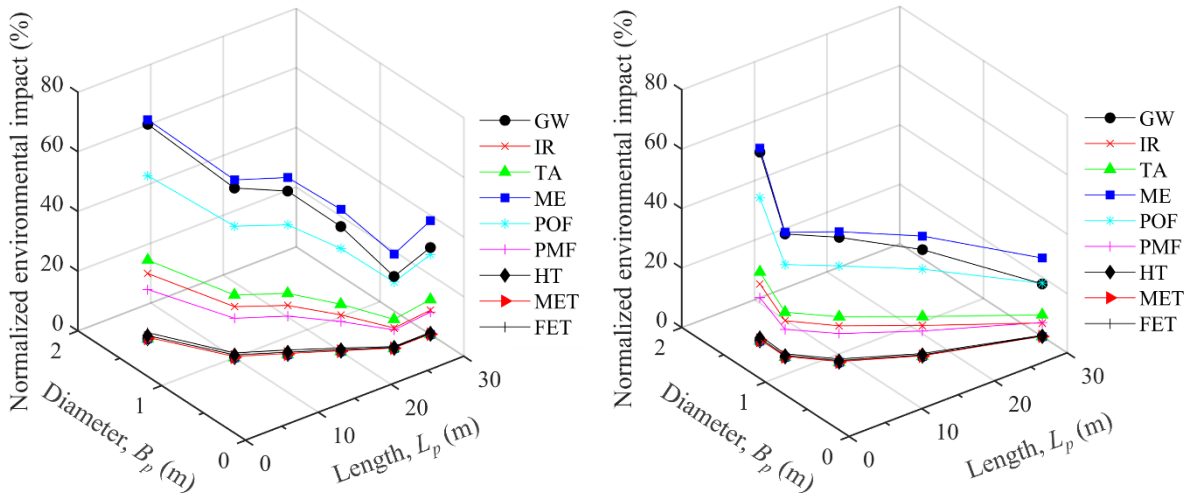

Figure 3.6. Relationship of normalized environmental impacts with drilled shaft dimensions: (a) fixed length design approach and (b) fixed diameter design approach

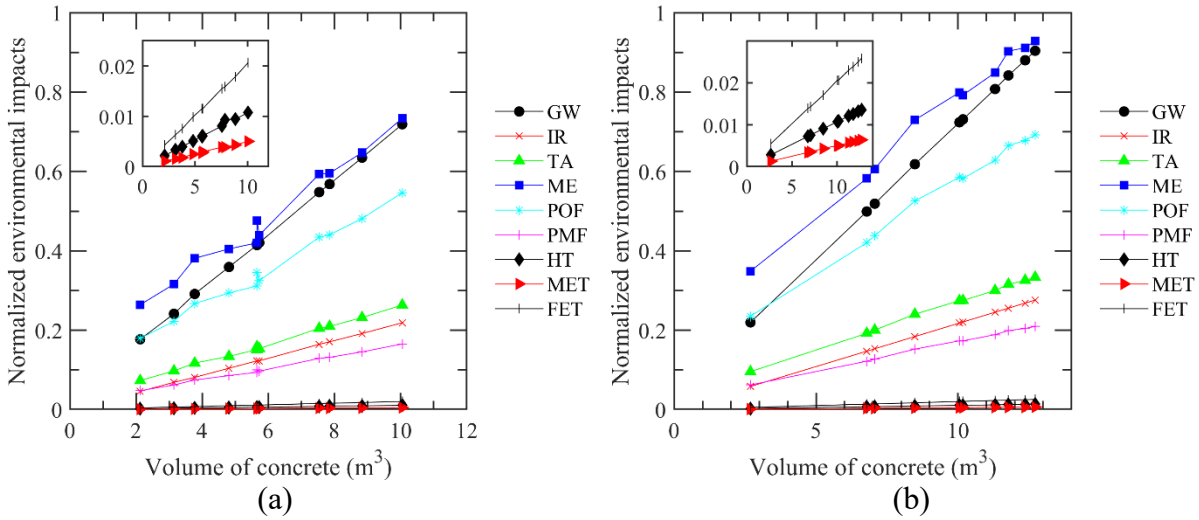

Figure 3.7. Environmental impacts as a function of volume of concrete for (a) Profile 1 and (b) Profile 2

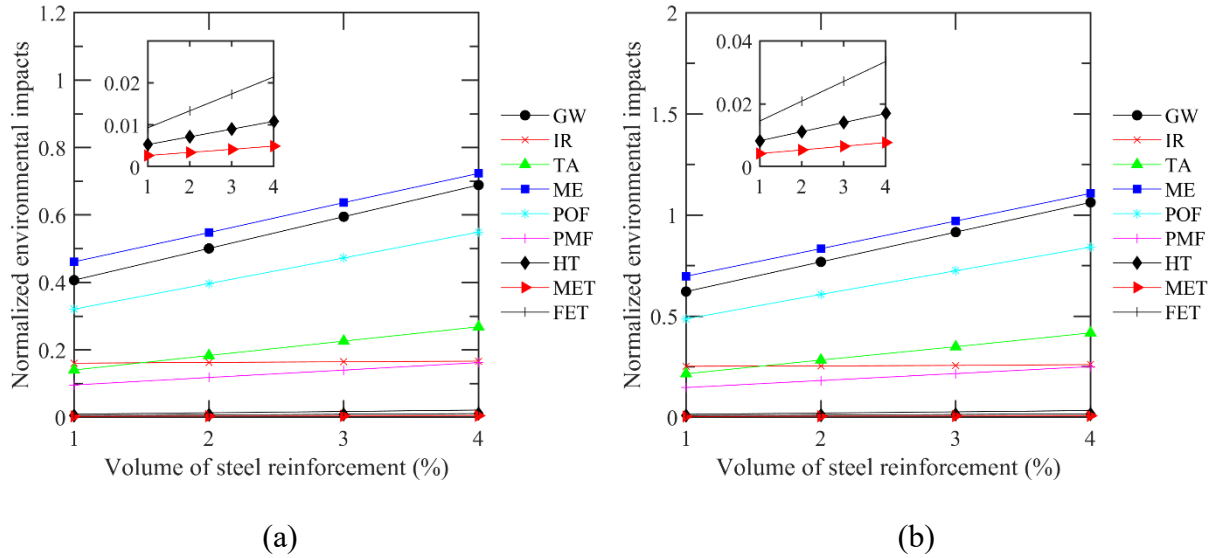

Figure 3.8. Environmental impacts as a function of volume of steel reinforcement for (a) Profile 1 and (b) Profile 2

The LCA results were also compared with the results obtained from the EFFC/DFI Carbon Calculator Tool (v4.0), as summarized in Table 3.7. The difference between the two results is observed for the life cycle processes related to steel, especially for the raw material extraction, refining, and manufacturing processes. The values of emission factors for carbon dioxide are 1.16 kg CO_2/kg and 1.608 kg CO_2/kg (assuming 30% recycled content) in GaBi and EFFC/DFI Carbon Calculator Tool, respectively; thereby, approximately 500 kg CO_2 of difference between the two results are caused.

Table 3.7. Comparison with the results obtained from the EFFC/DFI Carbon Calculator Tool

Process	**GaBi (kg CO_2e)**	**EFFC/DFI Carbon Calculator Tool (kg CO_2e)**
Raw material extraction, refining, and manufacturing of concrete	2283	2506
Raw material extraction, refining, and manufacturing of steel	1876	2380

Table 3.7 (continued).

Process	GaBi (kg CO_2e)	EFFC/DFI Carbon Calculator Tool (kg CO_2e)
Transportation of concrete	12	16
Transportation of steel	5	79
Transportation of equipment	186	104
Operation of construction equipment	32	39

3.3.2 Parametric Study of LCA of Drilled Shafts

The environmental impacts (global warming, terrestrial acidification, human toxicity, etc.) of drilled shafts are more or less proportional to the total concrete volume of drilled shaft (the volume of steel is also proportional to the concrete volume). Thus, for a construction, doubling the concrete volume would nearly double all the environmental impacts. In other words, if GWP is doubled, then it is likely that acidification is also doubled (i.e., all the categories portray the same trend). Therefore, in this study, the parametric results are focused only on global warming (with the understanding that the other environmental impacts would convey a similar story) because it is the most accessible information to engineers and it is considered to be one of the most important environmental impacts. In problems where tradeoffs between different environmental impacts exist, multiple environmental impacts may have to be considered and quantified.

3.3.2.1 Effect of Soil Properties

Parametric studies are conducted to investigate the effect of soil properties on the global warming impacts of drilled shaft design. Figure 3.9 shows the GWPs of single drilled shafts in different soil profiles 1-5 (Figure 3.2) designed against an applied load of 1000 kN with FS = 2.5. The pile length and diameter are fixed at 15 m and 0.9 m for fixed length and fixed diameter

designs, respectively, and a 2.5% steel reinforcement is assumed. The maximum difference in GWP across the soil profiles is 67%, which shows that site selection can have a significant influence on the environmental impacts arising from foundations.

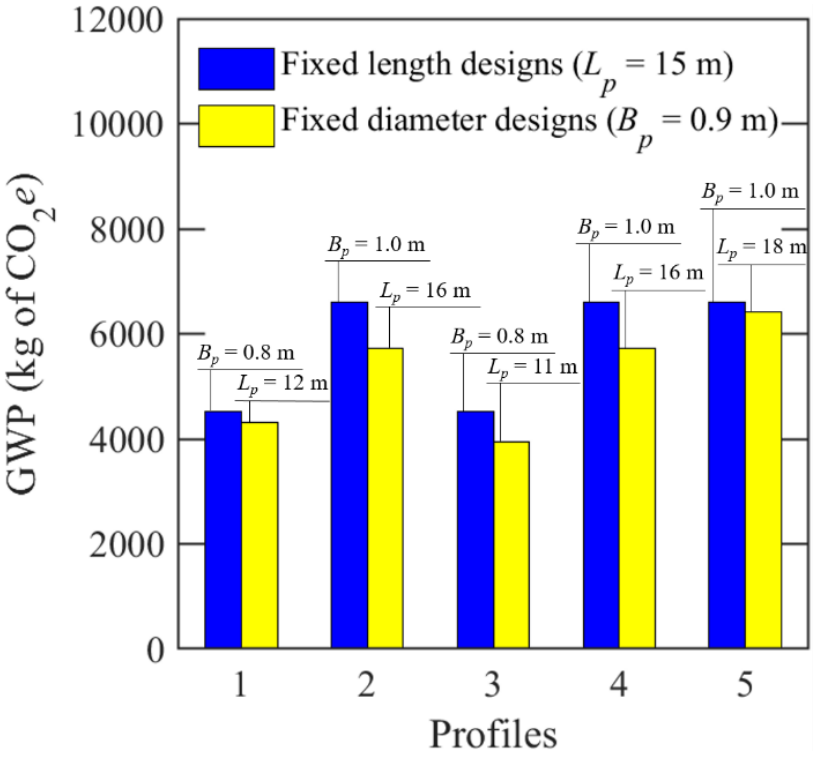

Figure 3.9. GWPs of drilled shafts in different soil profiles under an applied load P = 1000 kN

The effects of soil properties D_R, ϕ_c, and K_0 on GWP are next investigated for Profiles 1 and 4 in which the drilled shafts are designed against P = 1000 kN with FS = 2.5. For fixed length designs, the drilled shaft length is fixed at 15 m and the diameter is varied in increments of 200 mm following Coduto (2001) to simulate the practical cases where the dimensions of the available augers would restrict the choice of the pile diameters. For fixed diameter designs, the drilled shaft diameter is fixed at 0.9 m and the length is varied in intervals of 1 m. For all the cases, the reinforcement volume is assumed to be 2.5% of the concrete volume. The values of the soil properties used in the calculations are given in Table 3.1.

Figure 3.10(a) shows how relative density D_R of sand influences the GWP. D_R is varied over 30-80% for Profile 1 and the top layer of Profile 4. D_R in the strong bearing layer of Profile 4 is kept constant at 80% (see Figure 3.10(a) and Table 3.1 for the soil properties used in the calculations). Figure 5(a) also shows, on the secondary vertical axis, the GWP normalized with respect to the annual world impact per person. As D_R increases, the unit load carrying capacity of the drilled shaft increases because of which less quantities of concrete and steel are required to resist a given applied load. Thus, the GWP decreases (more or less linearly) with an increase in D_R for the homogeneous Profile 1. Such a (linear) decrease in GWP with an increase in D_R is not always observed for Profile 4 because the bearing layer with a constant D_R often controls the design (i.e., the pile dimensions). The maximum difference in GWP observed across the range of D_R considered in this study is 66.9%.

Figure 3.10(b) shows the effect of critical state friction angle ϕ_c on GWP (the soil properties used in the study are given in Figure 3.10(b) and in Table 3.1). An increase in ϕ_c results in an increased capacity because of which GWP reduces. The change in GWP can be as high as 66.9% or as low as 33.0% depending on the design methodology followed (fixed length versus fixed diameter) and the soil profile.

Figure 3.10(c) shows the variation of GWP with the coefficient of earth pressure at rest K_0. As K_0 increases, pile capacity increases because of which GWP decreases (see Figure 3.10(c) and Table 3.1 for the soil properties used). The maximum difference in GWP across the range of K_0 is found to be 49.3%. However, depending on the soil profile and design approach, K_0 may or may not have any impact on the GWP.

Figure 3.9 and Figure 3.10 show that, for a construction project, soil profiles and properties have a significant impact on the GWP arising from foundations. Thus, judicious choices in terms

of site selection, and considerations of ground improvement for improving the soil properties must be made for an optimized design that minimizes the environmental impacts while keeping the project cost within the budget. Figure 3.10(a)-(c) show that fixed diameter designs have lower GWP than fixed length designs for most cases. Fixed diameter designs usually involve lower volumes of concrete and steel because volume increase depends linearly on the increase of pile length. In contrast, volume increase in fixed length designs depends on the square of pile diameter, which results in greater concrete and steel volumes. Fixed diameter designs are usually chosen when augers with one (or two) diameter(s) are available at a site. Fixed length piles are usually chosen when a bearing stratum is present at a certain depth or when there are restrictions in the rig size that limit the length of the reinforcement cage. Therefore, design approaches should be judiciously chosen based on the availability of construction equipment and other constraints such that the GWP is minimized.

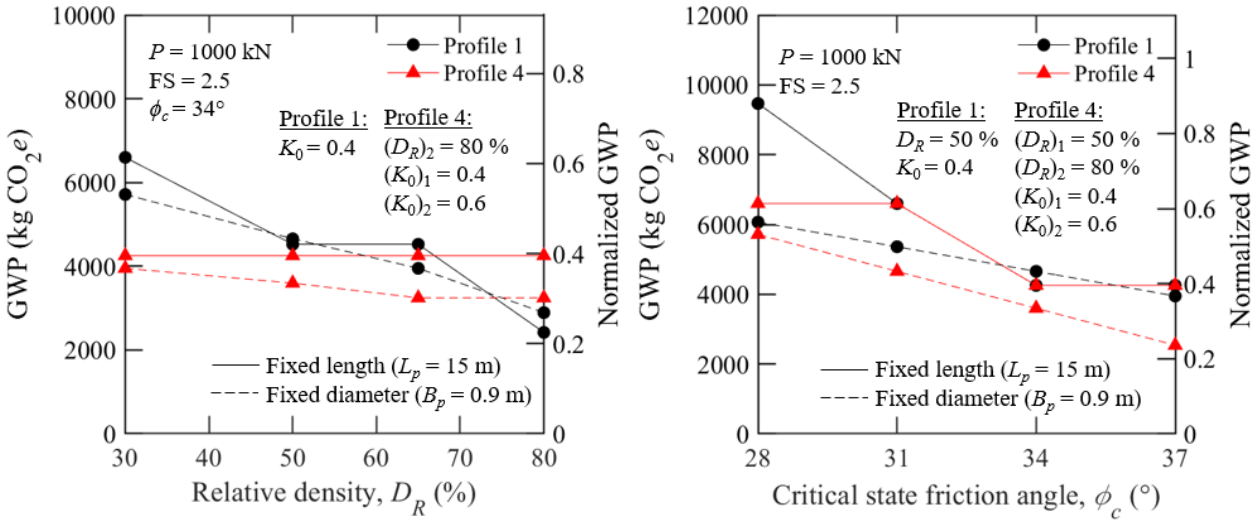

(a) (b)

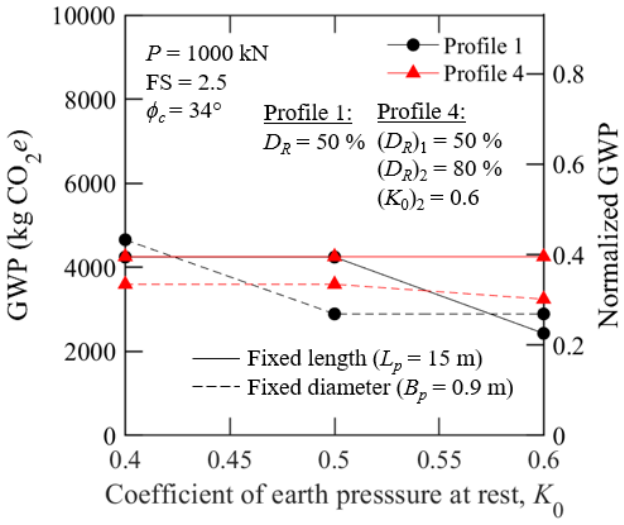

(c)

Figure 3.10. Variation of GWP with soil properties: (a) relative density, (b) critical state friction angle, and (c) coefficient of earth pressure at rest (normalization of GWP in the secondary vertical axis is done with respect to the annual world impact per person, which is 10757 kg of CO_2e)

3.3.2.2 Effect of Design Parameters

The parameters related to design, such as applied load, factor of safety, and volume of steel reinforcement are varied in this study to investigate their impacts on GWP. For fixed length designs, the drilled shaft length is assumed to be 15 m and the diameter is varied in increments of 200 mm. For fixed diameter designs, the drilled shaft diameter is fixed at 0.9 m. The steel reinforcement is assumed to be 2.5% of concrete volume unless otherwise mentioned. The factor of safety assumed is 2.5 unless mentioned otherwise.

Figure 3.11(a) shows the increase in GWP as the applied load increases from 1000 kN to 3000 kN for drilled shafts in Profiles 1 and 4 (see Figure 3.11(a) for the details of soil parameters used in the calculations). The change in GWP with applied load depends on the soil profile and the design approach. Figure 3.11(b) shows the variation of GWP with factor of safety. While the GWP increases with an increase in the factor of safety as expected, in certain cases a flat curve is

observed for a certain range of factor of safety for the fixed length designs because the diameter is increased in increments of 200 mm. For example, for fixed length designs corresponding to factors of safety of 2.5 and 3, the required diameters are 1.237 m and 1.399 m, respectively. But because the diameters are selected in increments of 200 mm, the chosen design diameter for both the cases is 1.4 m, resulting in the same GWP.

The volume of steel reinforcement in drilled shafts can vary between 1% and 4% of the concrete volume in drilled shafts according to FHWA (2010a). Therefore, the effect of variation of the percentage of steel on the GWP is investigated. Figure 3.11(c) shows that GWP increases linearly with an increase in the percentage of reinforcement.

In order to further investigate the relationship between GWP and pile dimensions for different applied loads, GWPs of drilled shaft designs with fixed pile length with L_p = 5-30 m and correspondingly B_p = 0.4-2.2 m are calculated for P = 1000, 2000, and 3000 kN in Profile 1. Figure 3.12 shows the plots of the designed pile length and diameter on the horizontal and vertical axes, respectively, corresponding to the different applied loads. The GWP for each design is calculated and plotted on the same figure, and curves joining these points generate the GWP contours. Clearly, for a particular applied load, pile length and diameter are inversely related, as expected, and the diameter has a greater impact on the GWP. For a site, these plots can be generated as part of design charts and then used by designers for a quick estimate of GWP corresponding to a particular design.

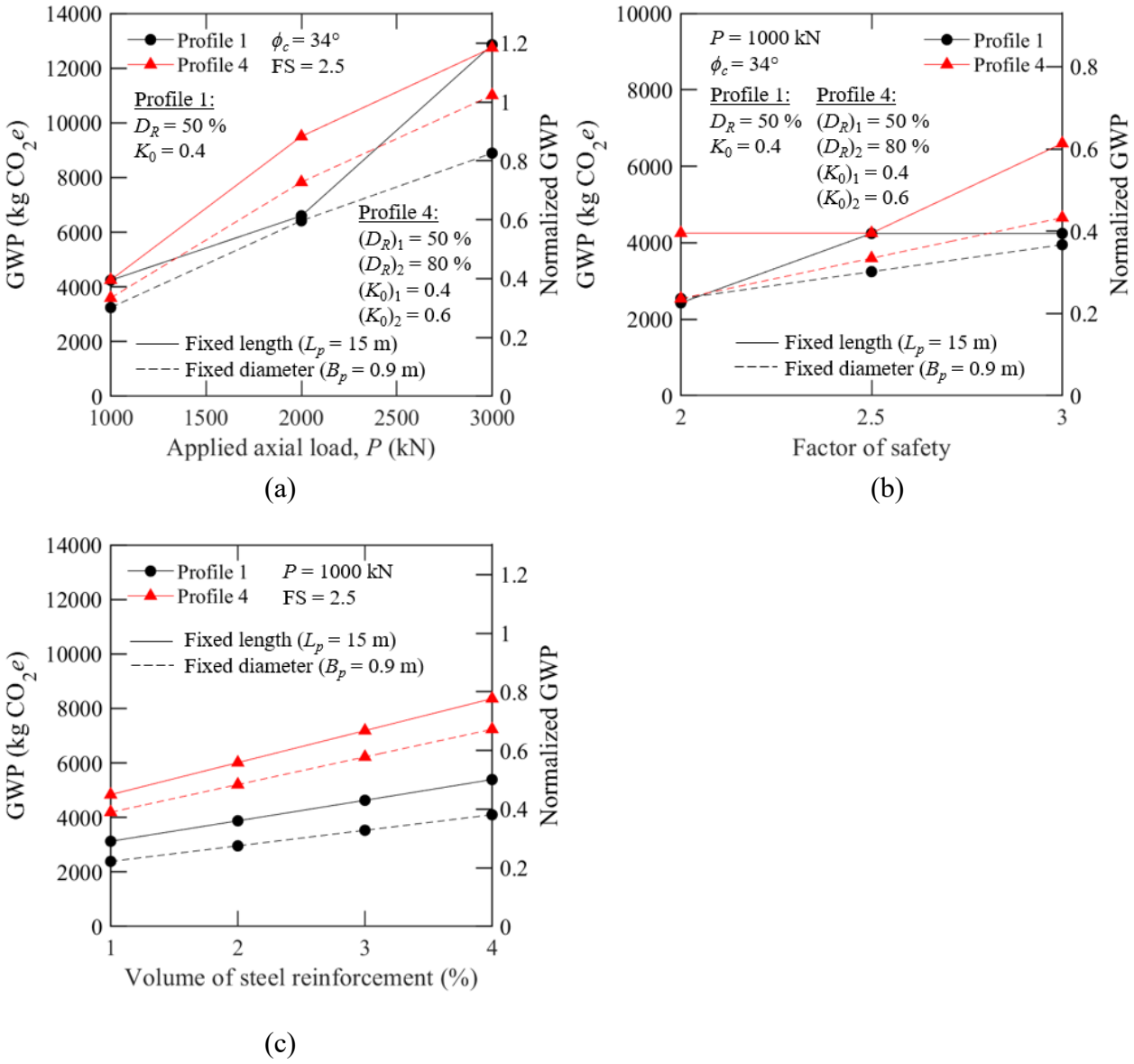

Figure 3.11. Variation of GWP with (a) applied load, (b) factor of safety, and (c) volume of steel reinforcement (normalization of GWP in the secondary vertical axis is done with respect to the annual world impact per person, which is 10757 kg of CO_2e)

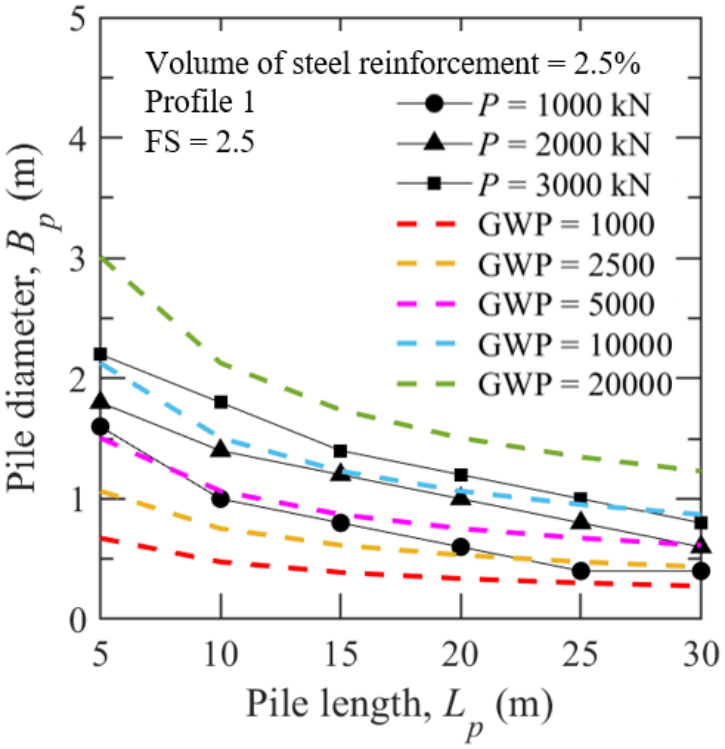

Figure 3.12. Relationship between designed length and diameter of drilled shafts for different applied loads along with GWP contours (GWP in kg CO_2e)

3.3.2.3 *Effect of Hauling Distance*

Three main transportation activities are involved prior to or during the construction phase of drilled shafts. Concrete mix and steel reinforcement cage are transported by trucks from the supplier to the construction site, and construction equipment like auger drill and crane are transported from rental locations. According to Zagula *et al*. (2012), the average, minimum, and maximum one-way travel distances of a concrete mixer truck are 22 km, 8 km, and 48 km, respectively. Therefore, the travel distance of concrete mixer truck is varied from 5 to 50 km. For hauling the reinforcement cage and construction machineries, one-way travel distances of 10, 50, and 100 km are considered. Figure 3.13 shows the variation of GWP with different one-way transportation distances for drilled shafts designed against P = 1000 kN in Profile 1 with 2.5% steel reinforcement and FS = 2.5. The hauling distance has a rather modest impact on GWP.

Hauling distance has practically no impact on the transportation of reinforcement cage because the mass of steel reinforcement is much smaller compared to the masses of concrete mix and construction equipment. However, it should be noted that Figure 3.13 shows the results for a single drilled shaft construction, and the impacts can be potentially significant for large-scale construction of several drilled shafts.

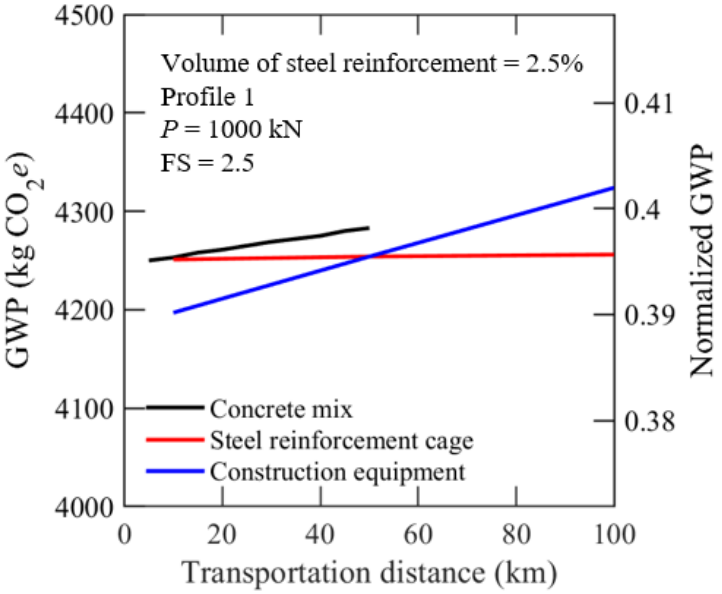

Figure 3.13. GWP versus one-way hauling distance (normalization of GWP in the secondary vertical axis is done with respect to the annual world impact per person, which is 10757 kg of CO2e)

3.3.3 Environmental Impacts of Pile Groups

For the three pile group configurations considered in this study, the variations of GWP with applied vertical load P, center-to-center pile spacing s_p, and pile cap thickness T_c are shown in Figure 3.14(a), (b), and (c), respectively, for Profile 1. The pile groups are designed considering a fixed diameter B_p = 0.9 m and FS = 2.5. GWP increases with an increase in the applied load, pile spacing, and pile cap thickness, as expected. The lengths of the piles were reduced in the designs as the number of piles underneath the pile cap increased. However, the volume of the pile caps impacted the GWP because of which the GWP increased as the number of piles increased.

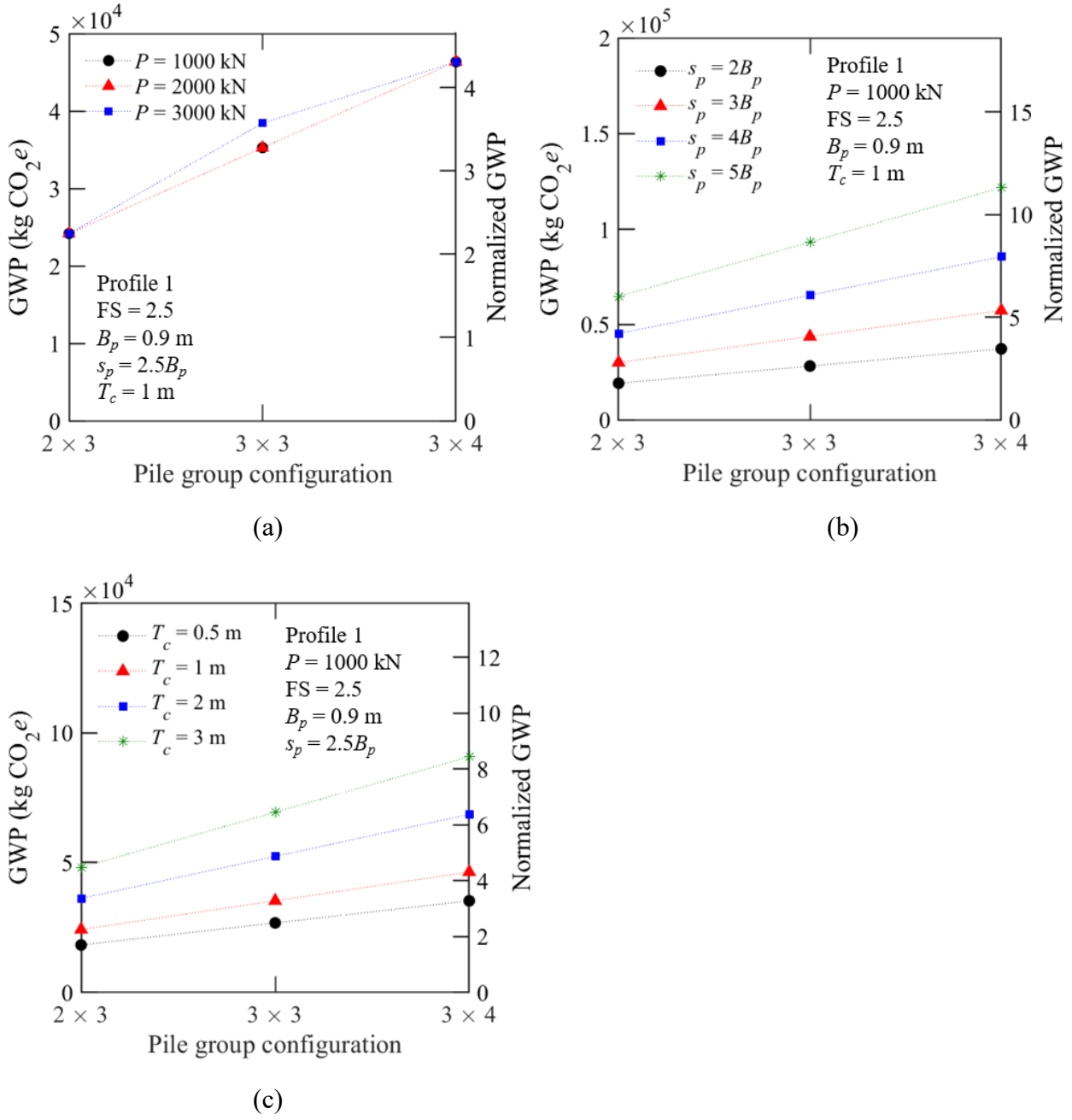

Figure 3.14. GWP of pile groups for (a) different applied loads, (b) different center-to-center pile spacings, and (c) different thicknesses of pile cap (normalization of GWP in the secondary vertical axis is done with respect to the annual world impact per person which is 10757 kg of CO_2e)

3.3.4 GWP per Unit Volume and Length

Table 3.8 shows the different values of GWP per unit concrete volume obtained from the different cases of single drilled shaft designs described in Figure 3.9 and Figure 3.14. It is found that the average GWP per 1 m^3 of drilled shaft is 564 kg of CO_2e. The manufacturing of concrete and steel reinforcement cage (including the extraction and refining of raw materials) account for about 52-55% and 42-45% of the total GWP, respectively, and the transportation and construction phases account for about 0.4-7% of the total GWP. Thus, the environmental impacts of drilled shafts are largely influenced by the quantity of concrete and steel used, and the impacts of transportation and construction phases are relatively small.

The GWP per unit volume of the pile groups considered in Figure 3.14(a)-(c) are given in Table 3.8. GWP per unit volume of drilled shaft. As evident, the average GWP per unit volume for these pile groups is 404 kg of CO_2e which is less than that of single piles.

The GWP per 1 m length of drilled shafts is calculated for different drilled shaft diameters ranging from 0.3 to 1.6 m for 1-4% steel reinforcement. For these calculations, 10 km of one-way transportation distance of concrete, 50 km of one-way transportation distance of steel, and 50 km of one-way transportation distance of construction equipment are assumed. Figure 3.15 shows that GWP per 1 m length increases significantly as the pile diameter increases. Thus, for a drilled shaft with 0.8 m diameter and 2.5% reinforcement, the GWP per unit length is 289 kg CO_2e/m and the total GWP for a 15 m-long drilled shaft can be estimated as approximately 4335 kg CO_2e, which is very close to the GWP reported in Table 3.6. Project specific plots similar to Figure 3.15 can be generated that can aid the designers in quick estimation of GWP from the designed dimensions of drilled shafts.

Table 3.8. GWP per unit volume of drilled shaft

Figure	GWP per unit volume (kg of CO_2e/m^3)
Single drilled shafts	
Figure 3.9	562
Figure 3.10 (a)	565
Figure 3.10 (b)	563
Figure 3.10(c)	566
Figure 3.11 (a)	562
Figure 3.11 (b)	562
Figure 3.11(c)	563
Figure 3.13	566
Average	**564**
Pile groups	
Figure 3.14(a)	421
Figure 3.14 (b)	392
Figure 3.14 (c)	398
Average	**404**

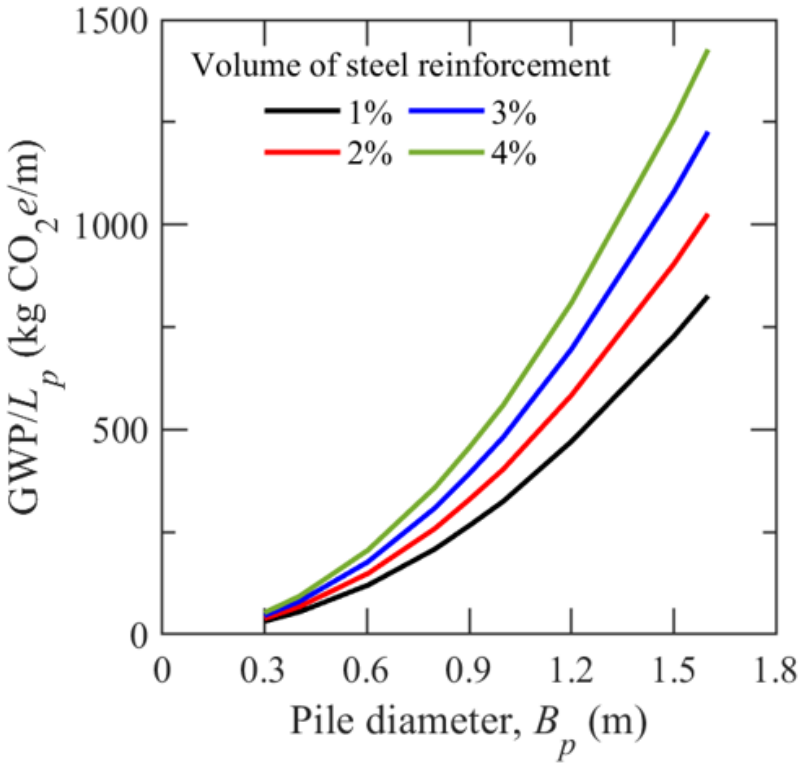

Figure 3.15. GWP per meter length of drilled shaft

3.4 Summary

In this chapter, the environmental impacts of single and group drilled shafts were quantified using LCA. Five different soil profiles were considered out of which two are homogeneous and three are layered sand profiles. The drilled shafts were designed considering both ultimate and serviceability limit states using the working stress design method. Based on the pile dimensions (i.e., pile diameter and length) obtained from the design, the quantities of materials (i.e., concrete and steel) were estimated which were then used as inputs in the LCA calculations. The functional unit defined in this study is the mass of a drilled shaft that can support the applied load without (i) bearing capacity failure assuming a factor of safety of 2 and (ii) excessive settlement exceeding 30 mm. The selected system boundary for the life cycle of drilled shaft is from the extraction of raw materials to the completion of construction stages. The following environmental impacts were quantified using LCA: global warming, ionizing radiation, terrestrial acidification, marine eutrophication, photochemical oxidant formation, particulate matter formation, human toxicity, marine ecotoxicity, and freshwater ecotoxicity. The quantified environmental impacts were normalized with respect to two reference values – annual world impact per person and environmental impacts caused by a typical passenger vehicle.

Based on the LCA results, it was found that global warming impact, marine eutrophication, and photochemical oxidant formation are the most significant environmental impacts of drilled shaft. Further, the environmental impacts of drilled shaft were highly influenced by the impacts caused by the cradle-to-gate processes (i.e., from raw material extraction to the end of manufacturing stage) of concrete and steel. Parametric study was conducted to investigate the effects of (i) soil properties (i.e., relative density of soil, critical-state friction angle of soil, and coefficient of lateral earth pressure at rest), (ii) design parameters (i.e., applied load, factor of

safety, and volume of steel reinforcement), and (iii) hauling distances of transportation activities. Decreasing global warming potentials (GWPs) of drilled shafts were observed as stronger soil properties were assumed in the parametric study. As the design requirements increased (e.g., higher factor of safety assumed), increasing GWPs were observed. The effect of hauling distances to the GWPs of drilled shafts was minimal. Several charts for quick estimation of global warming impact of drilled shafts were developed. Using these charts, the GWP of drilled shafts can be estimated solely based on different combinations of (i) pile length, (ii) diameter, and (iii) volume of steel reinforcement. The main purpose of these charts is to facilitate the process of drilled shaft designs with environmental considerations for practitioners without the need for specialized LCA software packages.

3.5 List of Symbols

Notation	Description
ϕ_c	Critical state friction angle
ρ_{diesel}	Density of diesel
$(EF)_{CO_2}$	Emission factor of carbon dioxide
$(EF)_x$	Emission factor of substance x
$(\text{GWP})_x$	Characterization factor of climate forcer x relative to carbon dioxide
ΔH_a	Axial settlement of drilled shaft
ΔH_p	Total settlement of drilled shaft
ΔH_{pt}	Point settlement of drilled shaft
Δq_p	Bearing pressure at the pile base
A_b	Cross-sectional area of the pile base
A_p	Cross-section area of pile
$A_{s,i}$	Surface area of the pile in contact with the i^{th} layer
B_p	Pile diameter
CO_2e	Equivalent mass of CO_2 of emissions x
d_{ce}	Clear edge distance of pile cap
D_R	Relative density of soil
E_p	Young's modulus of pile
E_s	Young's modulus of soil below the pile base
E_x	Total emission of substance (pollutant) x
F_1	Reduction factor
h	Height of auger

List of Symbols (continued).

Notation	Description
I_F	Fox embedment factor
K_0	Coefficient of earth pressure at rest
k_o	Engine load factor
L_p	Pile length
m	Mass of sub-product (e.g., concrete, steel, and diesel)
mI_s	Shape factor
M_x	Applied moment with respect to the x-axis
M_y	Applied moment with respect to the y-axis
n_p	Total number of piles
P	Applied load
p	Maximum payload capacity of the transportation truck
p_A	Atmospheric pressure (= 100 kpa)
P_e	Rated engine power
Q_{all}	Allowable pile capacity
$q_{b,ult}$	Ultimate unit base resistance of pile
q_{bL}	Limit base resistance of pile
q_d	Fuel consumption rate
Q_j	Applied axial load acting on the i^{th} pile of the group
q_{sL}	Limit unit shaft capacity of pile
$q_{sL,i}$	Limit unit shaft resistance of the i^{th} soil layer
Q_{ult}	Total ultimate capacity of pile
s_p	Center-to-center pile spacing in group piles
T_c	Pile cap thickness
t_{drilling}, t_{cage}, t_{funnel}, t_{tremie}, and $t_{pouring}$	Regression models for estimating the operation times for drilling, installing cage, installing funnel, installing tremie, and concrete pouring, respectively
$V_{\text{diesel,total}}$	Total volume of diesel
x_j and y_j	X- and y-coordinates of the center of pile j from the centroid of the pile cap in plan
z_d	Drilling depth
δ	Friction angle at the interface of the pile and soil
μ_s	Poisson's ratio of soil
σ'_h	effective horizontal stress
σ'_z	effective vertical stress

CHAPTER 4: ENVIRONMENTAL IMPACTS OF MECHANICALLY STABILIZIED EARTH (MSE) WALLS

Mechanically stabilized earth (MSE) wall is a type of retaining structure that develops resistance to earth pressures from retained soil using soil-reinforcement techniques. Conventional retaining structures include gravity and cantilever walls; however, the use of MSE walls has risen because of their cost-effectiveness and ability to tolerate larger settlements than concrete retaining walls (FHWA, 2009b; Salgado, 2008). The cost-effectiveness of MSE walls becomes apparent as the cost of concrete retaining walls increases rapidly as the height of wall increases. MSE walls are used extensively in North America and are particularly used for transportation systems such as for bridge abutments, wing walls, slope stabilization, and minimizing right-of-way for embankments (FHWA, 2009b). For reinforcing the backfill in an MSE wall, steel strips have been widely used since the 1970s, and the use of geogrids for reinforcement has increased significantly since the 1980s. In this chapter, the environmental impacts of MSE walls, reinforced by steel strips and geogrids, are quantified and compared.

4.1 Problem Description and Scope

An MSE wall with a required backfill height H = 7 m is considered as the design problem (Figure 4.1). The wall is placed on a foundation soil with a critical-state friction angle ϕ_f = 30° and a unit weight γ_f = 16 kN/m^3. The retained soil has a critical-state friction angle ϕ_r = 32° and a unit weight γ_r = 19 kN/m^3. The backfill soil has a critical-state friction angle ϕ_b = 36° and a unit weight γ_b = 19 kN/m^3. A live load surcharge q, caused by traffic, is applied on top of the MSE wall. According to AASHTO (2017), the live load surcharge can be estimated as:

$$q = \gamma_b h_{eq} \tag{4.1}$$

where h_{eq} is the equivalent height of soil for vehicular load (m). For a wall with $H \geq 6.0$ m and assuming the distance from wall back face to the edge of traffic load to be greater or equal to 0.3 m, $h_{eq} = 0.60$ m (AASHTO, 2017). Hence, the live load surcharge is assumed to be 11.4 kN/m^2 in this study.

Both inextensible and extensible materials are considered for the reinforcement of the MSE wall. For inextensible reinforcement, steel strips are used and, for extensible reinforcement, geogrids are considered. For the geogrid, a tensile strength $T = 30$ kN/m and a thickness of 2.5 mm are assumed (Strata, 2014). For the steel reinforcement, 65-grade steel strips with yield strength f_y = 448 MPa are considered with a width $b = 50$ mm and thickness $t_n = 4$ mm (FHWA, 2009b). A ribbed surface is assumed for the steel strips to enhance the friction between reinforcement and soil; thus, higher pullout resistance is developed. It is assumed that the steel strip will gradually corrode, which will result in reduced thickness over time. The corrosion rate of steel $c_r = 12\times10^{-6}$ m per year for each side (FHWA, 2009a). The service life SL_c of Zinc coating on the strips is assumed to be 16 years, and the service life of retaining wall SL_{MSE} is assumed to be 75 years (Kim and Salgado, 2012b). Therefore, the sacrificial thickness of steel strip t_c expected to be lost by corrosion during the design life of the wall is calculated as below:

$$t_c = 2c_r(SL_{MSE} - SL_c) \tag{4.2}$$

Table 4.1 summarizes the parameters used in designing the MSE walls in this study.

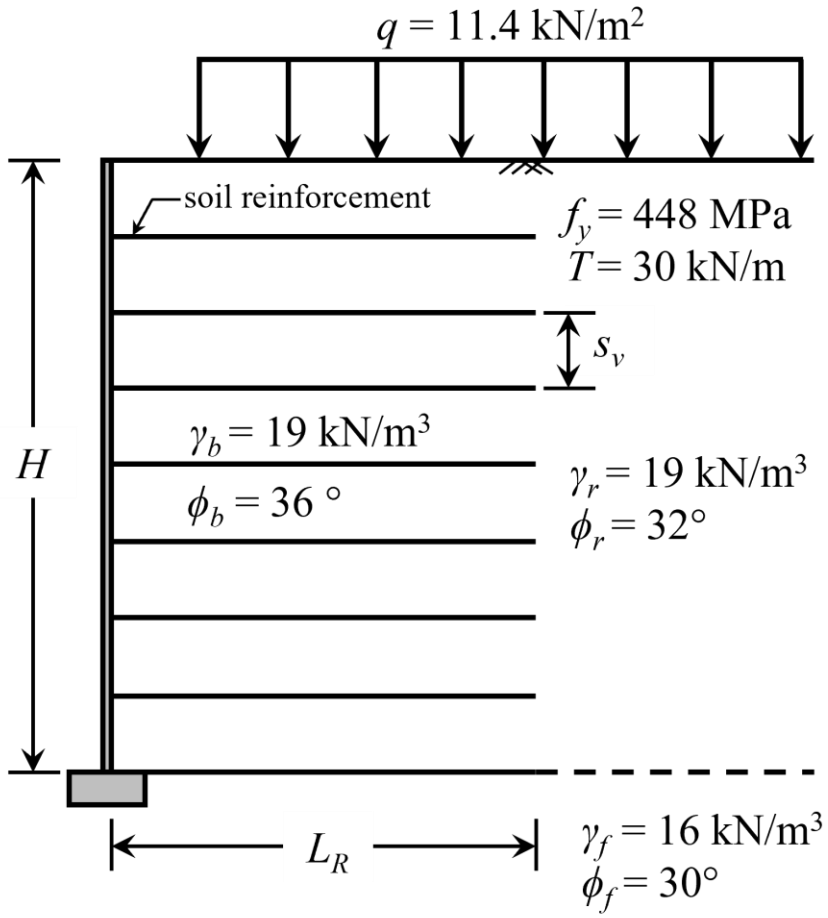

Figure 4.1. Schematic diagram of MSE wall

Table 4.1. Values of parameters considered in MSE wall designs

Parameter	Values
Unit weights of backfill, retained, and foundation soil, γ_b, γ_r, γ_f (kN/m^3)	16, 18, 20, 22 (Salgado, 2008)
Friction angles of backfill, retained, and foundation soil, ϕ_b, ϕ_r, ϕ_f (°)	28, 31, 34, 37 (Salgado, 2008)
Yield strength of steel, f_y (MPa)	450, 500, 550, 600 (Kim and Salgado, 2012b)
Tensile strength of geogrid, T (kN/m)	20, 80, 140, 200 (Strata, 2014)
Live load surcharge, q (kN/m^2)	0, 7, 14, 21 (Chalermyanont and Benson, 2004)
Factor of safety, FS	2, 2.5, 3
Height of wall, H (m)	5, 7, 9, 11, 13, 15

4.1.1 Design of MSE walls

In the design of MSE wall, the goal is to determine the length of reinforcement L_R and spacings of reinforcement in both vertical and horizontal directions (s_v and s_h) such that the wall is stable both externally and internally, for a given height of wall H. External failure modes considered in this study are outward sliding, overturning, and bearing capacity failures of the reinforced backfill soil. For internal failure modes, the tension and pullout failures of individual reinforcement layers are checked. A factor of safety of 2 is assumed for designing the MSE walls against external and internal failure modes. The design procedures specified in Clayton *et al*. (1993), Salgado (2008), Kim and Salgado (2012a; 2012b), and Chalermyanont and Benson (2004; 2005) are followed here.

External stability calculations treat the wall as a unit and consider its equilibrium with respect to moment, horizontal force, and vertical force. Internal stability calculations consider the design of reinforcement elements in the wall. In general, the factor of safety for external and internal stabilities are calculated as the ratio of resisting forces (or moments) to the driving forces (or moments):

$$\mathrm{FS} = \frac{R}{D} \tag{4.3}$$

where R is the summation of all resisting forces or moments and D is the summation of all driving forces or moments in an MSE wall. Table 4.2 summarizes the resistance R and driving D components for each failure mode. To be conservative, the contribution of live load surcharge q to the resistance forces are neglected for all stability limit states (AASHTO, 2017). Critical-state friction angles are used to calculate the coefficient of lateral earth pressure at active state K_A

because the use of peak friction angle leads to lower K_A values and underestimate driving forces (Kim and Salgado 2012a; Salgado 2008).

For internal stabilities, different slip surfaces are assumed for extensible and inextensible reinforcements. For the case of inextensible reinforcement (i.e., steel strip in this study), the slip surface resembles a trapezoid shape, as shown in Figure 4.2(a), and for the case of extensible reinforcement (i.e., geogrid), a Rankine failure surface is assumed, as illustrated in Figure 4.2(b) (FHWA, 2009b). Based on the slip surfaces shown in Figure 4.2, the effective length of reinforcement L_e, where the resistance against pullout is developed, is estimated accordingly, as specified in Table 4.2. The FSs for tension and pullout failures are calculated for individual reinforcement layers and the minimum FS for each internal failure mode is determined.

Table 4.2. Resistance and driving forces/moments for external and internal stabilities of MSE wall

Stability	Limit state equation	Parameter
Sliding	$R = \mu_f L_R \gamma_b H$	$K_A = \tan^2\left(45 - \frac{\phi_r}{2}\right)$ for external stabilities
	$D = HK_A\left(\frac{1}{2}\gamma_r H + q\right)$	$\mu_f = \tan\phi_f$
Overturning	$R = \frac{1}{2}\left(\gamma_b H L_R{}^2\right)$	
	$D = \frac{1}{2}H^2 K_A\left(\frac{1}{3}\gamma_r H + q\right)$	
Bearing capacity	$R = \frac{1}{2}\left(L_R - 2e\right)\gamma_f N_\gamma$	$N_\gamma = \left(N_q - 1\right)\tan\left(1.32\phi_f\right)$
	$D = \frac{L_R\left(\gamma_b H + q\right)}{L_R - 2e}$	$N_q = \tan^2\left(45 + \frac{\phi_f}{2}\right)e^{\pi\tan\phi_f}$
		$e_c = \frac{\sum M}{W_t} = \frac{\frac{1}{2}H^2 K_A\left(\frac{1}{3}\gamma_b H + q\right)}{L_R\left(\gamma_b H + q\right)}$

Table 4.2 (continued).

Stability	Limit state equation	Parameter
Tension	$R = T$ $D = K_r\left(\gamma_b z + q\right)s_v s_h$	$K_A = \tan^2\left(45 - \frac{\phi_b}{2}\right)$ for internal stabilities For steel strip: $T = \frac{0.55 f_y A_c R_c}{b}$ $R_c = \frac{b}{s_h}$ $\frac{K_r}{K_A} = \left\{\begin{array}{c} 1.7 - \frac{z}{12} \text{ for } z \le 0 < 6 \text{ m} \\ 1.2 \text{ for } z \ge 6 \text{ m} \end{array}\right\}$ For geogrid: $K_r = K_A$ $s_h = 1$
Pullout	$R = C_P C_R C_S\left(\gamma_b z\right)L_e R_c$ $D = K_r\left(\gamma_b z + q\right)s_v s_h$	$L_e = L_R - L_a$ $C_P = 2$ For steel strip: $C_R = \left\{\begin{array}{c} z\left(\frac{\tan\phi_b - 1.8}{6}\right) + 1.8 \text{ for } 0 \le z < 6 \text{ m} \\ \tan\phi_b \text{ for } z \ge 6 \text{ m} \end{array}\right\}$ $C_S = 1$ $L_a = \left\{\begin{array}{c} 0.3H \text{ for } z \le \frac{H}{2} \\ 0.6(H - z) \text{ for } z > \frac{H}{2} \end{array}\right\}$

Table 4.2 (continued).

Stability	Limit state equation	Parameter
Pullout		For geogrid: $C_R = \tan\phi_b$ for all z $C_S = 0.8$ $L_a = (H - z)\tan\left(45 - \frac{\phi_b}{2}\right)$ $R_C = 1$

H : height of wall
s_v : vertical spacing of reinforcement; s_h : horizontal spacing of reinforcement
γ_b, γ_r, γ_f : unit weight of backfill, retained, and foundation soils, respectively
ϕ_b, ϕ_r, ϕ_f : critical-state friction angle of backfill, retained, and foundation soil, respectively
K_A : coefficient of lateral earth-pressure at active state; K_r/K_A : lateral stress ratio
L_R : length of reinforcement
T : tensile strength of reinforcement
fy : yield strength of steel strip
q : live load surcharge
μ_f: friction between reinforced soil and foundation soil
e : eccentricity of load; M : moment; W_t : weight
N_γ and N_q : bearing capacity factors
z : depth below top of the wall
A_c : cross-sectional area of steel strip (= $b(t_n\text{-}t_c)$); b : width of steel strip; t_n : thickness of steel strip; t_c : sacrificial thickness of steel strip; R_c : coverage ratio;
L_e : effective length of reinforcement; L_a : length of reinforcement within failure wedge
C_P : coefficient of reinforcement effective perimeter; C_R : coefficient of pullout resistance; C_S : scale-effect coefficient

The steel strips are spaced both vertically and horizontally, while the geogrids are assumed to be continuous in the horizontal direction (i.e., throughout the length of wall) spaced vertically with a spacing s_v. According to FHWA (2009b), the length of reinforcement can vary from 0.7H to 1.1H. The vertical spacing of reinforcement is dependent on the thickness of compaction layers; therefore, it typically ranges between 300 mm and 600 mm with an increment of 150 mm (Fratta and Kim, 2015; Salgado, 2008). Hence, discrete values of s_v = {300, 450, 600} mm are used when designing the MSE walls in this study. A typical horizontal spacing for steel strip is 30 inches according to FHWA (2009b); hence s_h = 750 mm is assumed in this study, and s_h = 1000 mm is

assumed for geogrids. At a selected s_v, the length of reinforcement L_R is increased until the safety requirements for all external and internal stabilities are satisfied. In other words, the minimum FS calculated for external and internal stabilities governs the design of MSE wall and needs to be at least greater than 2. The MSE wall is designed per 1 m length of the wall (into the plane of paper). Table 4.3 shows sample design results for MSE walls with steel strips and geogrids. Based on the design dimensions, masses of (i) excavated soil, (ii) backfill soil, and (iii) reinforcement are estimated which are important inputs in LCA. Table 4.4 demonstrates the calculation procedures for estimating the masses mentioned above.

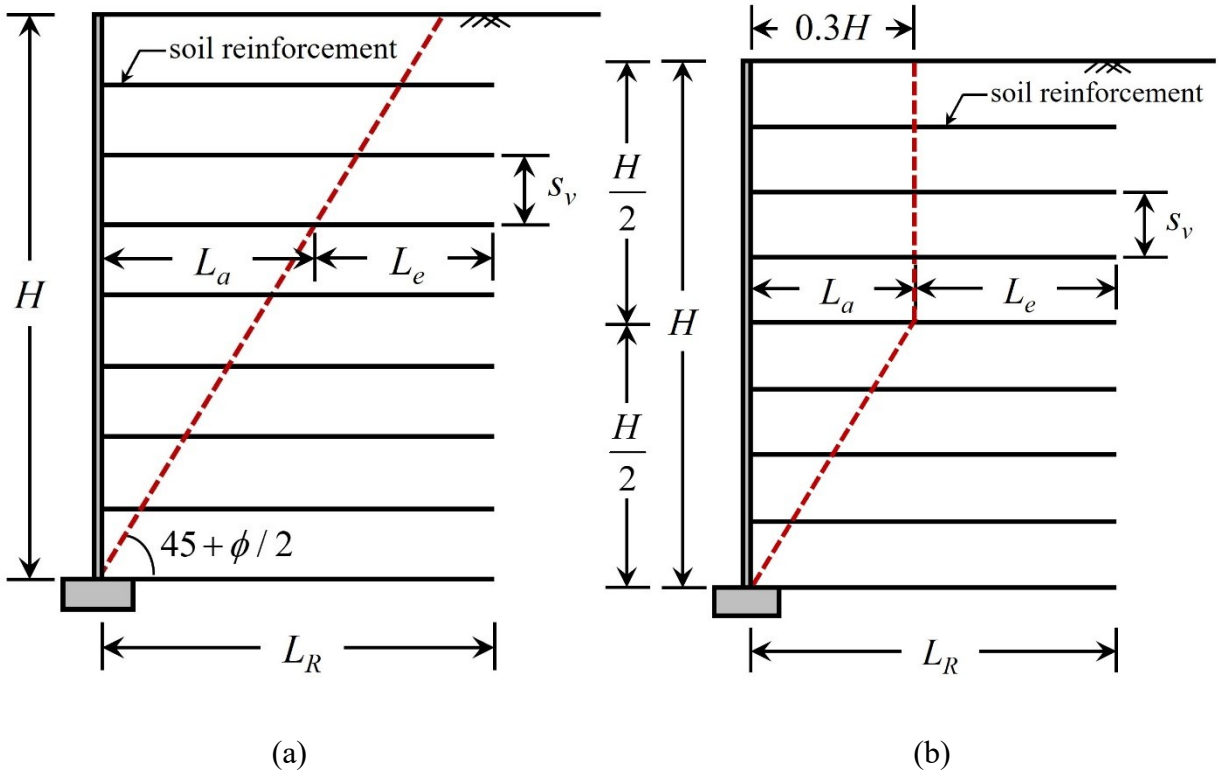

Figure 4.2. Failure surface for internal stability design of MSE walls with (a) inextensible reinforcements and (b) extensible reinforcements (adapted from FHWA, 2009b)

Table 4.3. Samples of MSE wall designs

Design variable	Reinforcement	
	Steel strip	Geogrid
L_R/H	0.9	0.7
s_v (m)	0.45	0.3
s_h (m)	0.75	1.0

Table 4.4. Estimation of masses for excavation, backfill, and reinforcement for H = 7 m, L_R/H = 0.9, and s_v = 0.45 m

	Volume (m^3) (1)	Density (kg/m^3) (2)	Mass (kg) = (1)×(2)
Excavation[1]	$V_b = \left(\frac{L_R}{H}\right) H^2 (1)$ $= (0.9)7^2(1)$ $= 44.1$	1937 (based on γ_b = 19 kN/m^3)	85413
Backfill[2]	$V_l = V_b(1+b_f)$ $= 44.1(1+0.25)$ $= 55.1$	1937	106766
Steel strip[3] (assuming s_h = 0.75 m)	$= \left(\frac{L_R}{H}\right)(H)(b)(t_n)(N_{rf})$ $= (0.9)(7)(0.05)(0.004)(30)$ $= 0.0378$ in which $N_{rf} = \left\lfloor \frac{H}{s_v} \right\rfloor \left\lceil \frac{1}{s_h} \right\rceil = 30$	7850 (CEN, 2002)	297
Geogrid[3] (assuming s_h = 1 m)	$= \left(\frac{L_R}{H}\right)(H)(1)(t)(N_{rf})$ $= (0.9)(7)(1)(0.0025)(15)$ $= 0.23625$ in which $N_{rf} = 15$	950 (Thinkstep, 2022)	224

[1]Volume of excavated soil is measured in bank volume V_b
[2]Volume of backfill soil is measured in loose volume V_l with a bulk factor b_f = 0.25
[3]N_{rf} is the number of reinforcement layers

4.2 LCA of MSE Walls

4.2.1 Goal and scope

The goal of this LCA is to quantify the environmental impacts associated with the life cycle of MSE walls reinforced by steel strips and geogrids. The functional unit defined in this LCA is an assembled MSE wall that is safely designed against external and internal stabilities with at least FS > 2.0. In this study, LCA is conducted following the procedures and requirements specified in the ISO standards (ISO, 2006a; 2006b), and GaBi software is used to complete the LCA calculations. Databases, parameters, and assumptions used in the LCA of MSE walls are described.

A cradle-to-site approach is used in which the emissions generated from the extraction and refining of raw materials, manufacturing of materials, transportation of materials, and construction activities are considered, as shown in Figure 4.3. The processes considered in the life cycle of MSE walls are summarized in Table 4.5 with the sources of database used for conducting the life cycle inventory analysis (LCI). For selecting the LCI databases, North American databases are preferred, otherwise European or global databases are used if not available. It is assumed that the databases for construction materials and are not highly sensitive to time and technology related coverage; hence, the databases in Table 4.5 are considered adequate for conducting LCA in this study. The cradle-to-gate processes (i.e., from the extraction of raw materials to manufacturing) for steel strip and geogrid are represented by the cradle-to-gate processes of galvanized steel sheet and high-density polyethylene (HDPE) granulate, respectively. Diesel-driven heavy-duty trucks are considered for transporting the construction materials. The combustion of diesel during the operation of construction equipment is assumed to be equivalent to the diesel combustion of industrial equipment such as mobile refrigeration units, generators, pumps, and portable well-drilling equipment. Processes related to the facing panels of MSE walls are omitted in this study

because the environmental impacts associated with these processes are assumed to be the same for MSE walls with the same height.

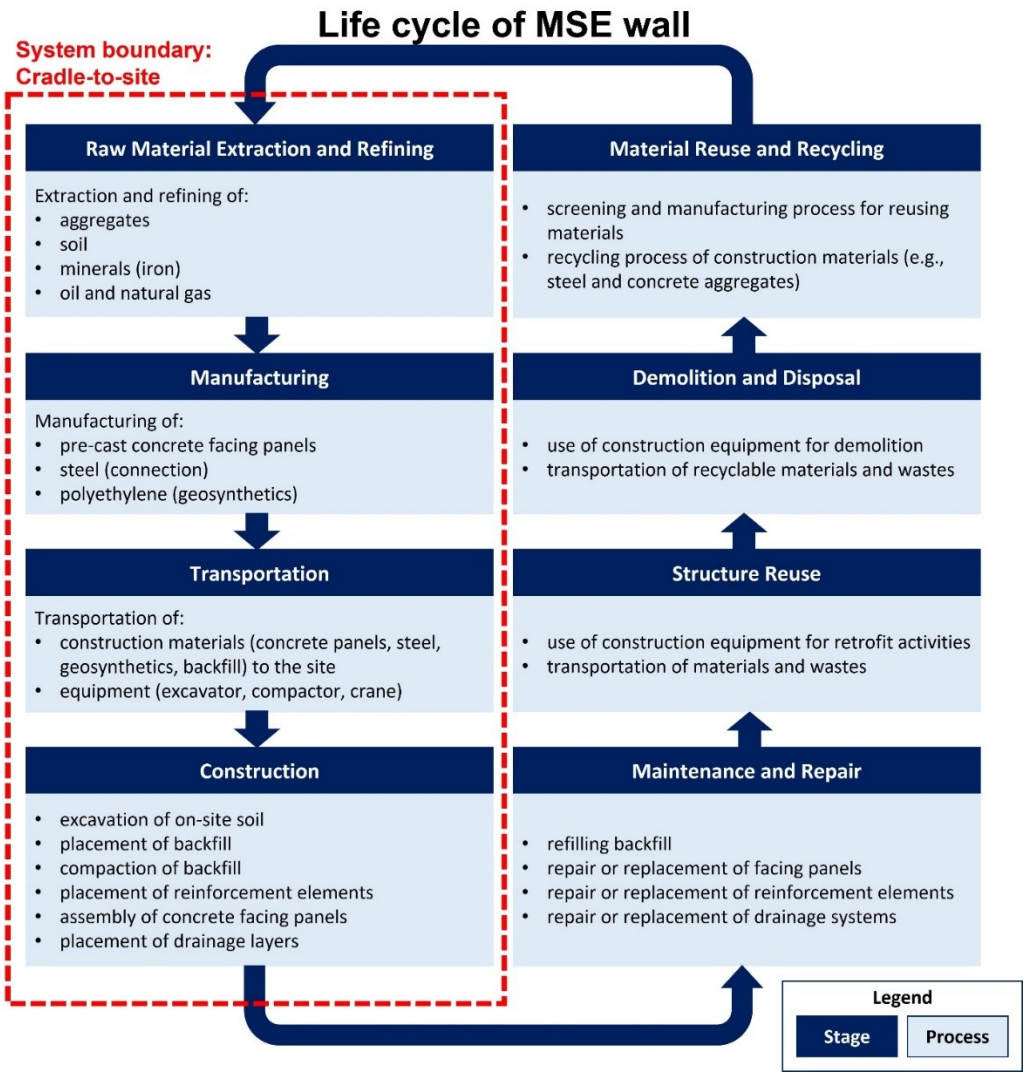

Figure 4.3. Typical life cycle of a mechanically stabilized earth (MSE) wall

In this LCA study, the following environmental impact categories are selected: climate change (global warming), terrestrial acidification, marine eutrophication, particulate matter formation, photochemical oxidant formation, and freshwater ecotoxicity. These environmental impacts provide adequate information for evaluating the environmental sustainability of the designed MSE wall. The details of the selected environmental impact categories are summarized

in Table 2.2. Additional environmental impacts like ozone depletion, ionizing radiation, human toxicity, terrestrial ecotoxicity, land occupation, and water depletion can be quantified if these have important impacts to the system being studied (not important for MSE walls). For conducting the life cycle impact assessment (LCIA), the characterization factors (i.e., GWP values) are obtained from Goedkoop *et al*. (2014). Table 4.5 also summarizes the parameters used in this LCA.

Table 4.5. Life cycle processes, databases, parameters, and assumptions used in LCA of MSE walls

Life cycle phase	Product	LCI database	Parameter and assumption
From extraction of raw material to manufacturing	Steel strip (galvanized steel sheet)	NREL (2012)	Density: 7850 kg/m^3 (CEN, 2002)
	Geogrid (HDPE granulate)	Thinkstep (2022)	Density: 950 kg/m^3 (Thinkstep, 2022)
Transportation	Reinforcement material (from the manufacturing plant to the construction site)	Thinkstep (2022)	Capacity: 27 t Travel distance (one-way): 50 km Utilization ratio: 0.1
	Excavated soil (from the construction site to the disposal site)	Thinkstep (2022)	Capacity: 22 t One-way travel distance: 15 km Utilization ratio: 0.45
	Backfill soil (from the borrow pit to the construction site)	Thinkstep (2022)	Capacity: 22 t One-way travel distance: 15 km Utilization ratio: 0.45
Construction	Excavation of existing soil	NREL (2012)	See Table 4.8 and Table 4.9
	Loading and spreading backfill soil	NREL (2012)	See Table 4.8 and Table 4.9
	Compaction of backfill soil	NREL (2012)	See Table 4.8 and Table 4.9

4.2.2 Assumptions in LCI and LCIA

The LCI for MSE walls is conducted following the procedures specified in Section 2.2. Table 4.6 shows examples of inputs and outputs (for HDPE) that can be obtained from typical LCI databases. The calculations in the LCI are demonstrated here using an example of manufacturing of high-density polyethylene (HDPE) which is the primary material for the geogrid reinforcement.

Based on the LCI database (see Table 4.6, for example), the quantity of material and energy (inputs) required for manufacturing 1 kg of HDPE are determined, and the quantity of emissions (outputs) generated during the manufacturing process are also determined.

Table 4.6. Example of life cycle inventory analysis (LCI) data for HDPE (adapted from NREL, 2012)

Input (per 1 kg of HDPE)	Value	Unit	Output (per 1 kg of HDPE)		Value	Unit
Coal (lignite)	1.03×10^{-2}	kg	Air emissions	Carbon dioxide (CO_2)	1.32	kg
Coal (unprocessed bituminous)	1.07×10^{-1}	kg		Carbon monoxide (CO)	3.06×10^{-4}	kg
Natural gas	8.57×10^{-1}	kg		Methane (CH_4)	7.69×10^{-3}	kg
Crude oil	5.59×10^{-2}	kg		Nitrogen oxides (NO_x)	2.34×10^{-3}	kg
Uranium oxide (UO_2)	2.61×10^{-6}	kg		Nitrous oxide (N_2O)	3.04×10^{-5}	kg
Water	9.22×10^{-3}	m^3		NMVOC[1]	6.77×10^{-4}	kg
Energy from biomass	2.17×10^{-3}	kg		Particulate matter (< 2.5μm)	8.14×10^{-5}	kg
Energy (hydro power)	1.00×10^{-1}	MJ		Sulfur dioxide (SO_2)	3.82×10^{-3}	kg
Energy (geothermal)	5.27×10^{-3}	MJ		Sulfur oxides (SO_x)	5.49×10^{-4}	kg
Energy (kinetic)	5.22×10^{-3}	MJ	Water emissions	Ammonia (NH_3)	7.29×10^{-6}	kg
Energy (solar)	2.21×10^{-4}	MJ		Arsenic (As)	6.92×10^{-8}	kg
Energy (unspecified)	7.06×10^{-3}	MJ		Copper (Cu)	4.31×10^{-8}	kg
				Lead (Pb)	1.86×10^{-7}	kg
				Mercury (Hg)	4.17×10^{-10}	kg
				Nitrogen (N)	7.38×10^{-8}	kg
				Phosphorus (P)	1.00×10^{-7}	kg
				Zinc (Zn)	8.86×10^{-7}	kg

[1]NMVOC: non-methane volatile organic carbon compound

Figure 4.4 illustrates the flow of inputs and outputs for the manufacturing of HDPE. The inputs in Figure 4.4 are the energy and raw materials required for manufacturing 1 kg of HDPE, and outputs are the emissions caused during the manufacturing process of the 1 kg HDPE. The complete list of inventory is not provided in Figure 4.4 for the sake of brevity, but the details

provided are sufficient for describing the calculation procedure. Table 4.7 shows sample calculations of LCI in which selected emissions are quantified. The masses in Table 4.7 are obtained from the design phase of MSE wall (see Table 4.4). The details related to the LCI calculations for the transportation and construction stages are discussed in the subsequent paragraphs. Note that Equation (2.1) is used for calculating the emissions for all the life cycle stages (manufacturing, transportation, and construction).

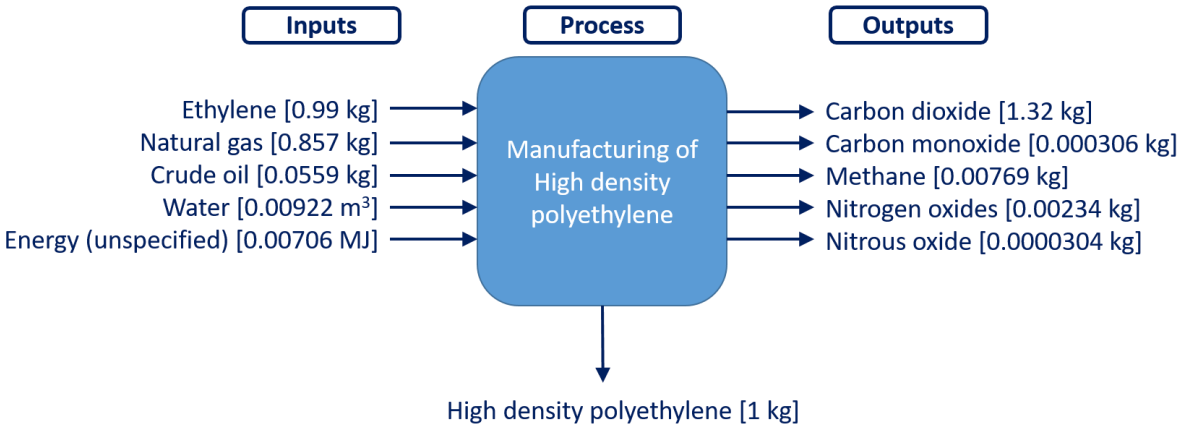

Figure 4.4. Life cycle inventory analysis (LCI) example for HDPE

It is assumed that the reinforcement materials are hauled by a diesel-driven 27-tonne capacity truck and that the one-way transportation distance to the construction site is 50 km. The excavated soil and backfill material is assumed to be transported by a 22-tonne transfer dump truck and the one-way travel distance is 15 km. Trucks with 22- to 27-tonne capacities are selected because these are the typical sizes used for transporting construction materials, and the haul distance is a site-specific parameter that can change across projects (FHWA, 2000; Thinkstep, 2019). The trucks for transporting the soil, from the borrow pit to the construction site, are assumed to be loaded to 90% of their load capacity (i.e., the utilization ratio is 0.9). Emissions from transporting the excavated and backfill soils are adjusted for considering empty runs (e.g., trucks

going back to material provider after unloading backfill soil at the construction site) by using a utilization ratio of 0.45 (= 90% ÷ 2 = 45%) (Thinkstep, 2022). Emissions generated during the mobilization of construction equipment are omitted in this study because they are assumed to be the same irrespective of the design dimensions of MSE wall.

Table 4.7. Sample calculations for LCI of an MSE wall with geogrid reinforcement

Process	Mass[1], m (kg)	Emission factor[2], $(EF)_x$ (kg/kg)			Total emission, E_x [using Equation (2.1)] (kg)		
		CO_2	CH_4	N_2O	CO_2	CH_4	N_2O
	(1)	(2)	(3)	(4)	(5) = (1)×(2)	(6) = (1)×(3)	(7) = (1)×(4)
Cradle-to-gate processes of HDPE	224	1.32	7.69×10^{-3}	3.04×10^{-5}	296	1.72	6.81×10^{-3}
Transportation of geogrid	224	2.1×10^{-4}	2.69×10^{-9}	2.22×10^{-7}	4.70×10^{-2}	6.03×10^{-7}	4.97×10^{-5}
Transportation of excavated soil	85413	1.09×10^{-3}	7.44×10^{-10}	7.15×10^{-8}	93.1	6.35×10^{-5}	6.11×10^{-3}
Transportation of backfill	106766	1.09×10^{-3}	7.44×10^{-10}	7.15×10^{-8}	116.4	7.94×10^{-5}	7.63×10^{-3}
Operation of construction equipment	134.8	2.3	1.14×10^{-4}	0	310	1.54×10^{-2}	0

[1]Obtained from design calculations as shown in Table 4.4
[2]Obtained from LCI databases listed in Table 4.5

The environmental impact caused during the construction phase is estimated based on the fuel use for operating construction equipment. The following construction activities are considered in this LCA: (i) excavation of existing soil using a hydraulic excavator, (ii) loading and spreading backfill soil using a front-end wheel loader, and (iii) compaction of backfill soil using a vibratory plate compactor. To estimate the volume of diesel used for an equipment, the fuel consumption rate and operation time of the equipment should be determined. The fuel consumption rate is available from the specification sheets of the equipment, and the operation time can be estimated

based on the workload and production rate of the equipment. Table 4.8 and Table 4.9 summarize the parameters and assumptions used in computing the total volume of diesel. Subsequently, the fuel volume is computed using Equation (2.5).

It is assumed that the volume of soil expands or shrinks depending on the state of soil; thus, appropriate volume needs to be used when calculating the workload for the construction activities. For example, the workload for excavation is calculated in terms of bank volume V_b because the soil is in the in-situ state. Loose volume V_l is used for calculating the workload of loading and spreading of backfill soil using the front-end wheel loader because the backfill soil is already in the disturbed state when transported from the borrow pit (e.g., soil expands by 25% in volume – captured by the bulking factor b_f in Table 4.8). The workload of compaction is calculated with respect to the compacted volume of soil V_c (e.g., compaction reduces the volume of soil by 10% - captured by the shrinkage factor s_f in Table 4.8 (Crooks, 2013; Entwisle *et al.*, 2015). The calculation of the volumes for different states of soil, mentioned above, are shown in Table 4.8 (see 3rd column of Table 4.8).

The number of cycles per unit time is useful information for estimating the production of construction equipment. For example, it is assumed that the hydraulic excavator for excavating the existing soil at the site performs 200 cycles per hour (Caterpillar, 2014). In each cycle, the hydraulic excavator performs excavation using the bucket and unloading the excavated soil. In this study, the bucket capacity of the hydraulic excavator is assumed to be 0.764 m^3, and its full capacity is used in each cycle (i.e., 0.764 m^3 of soil is loaded in each cycle and this is captured by the bucket fill factor BFF = 1). The 200 cycles per hour are adjusted to account for the operational efficiency (e_o = 50 min/hr), operator skill efficiency (e_{os} = 90%), and machine availability (a_m = 0.95). RSMeans (2015) also provides an estimation of production rate for a hydraulic excavator;

hence, the average of bank volumes per hour (V_b/hr) calculated using the Caterpillar (2014) and RSMeans (2015) methods is used in this study (see 1st row and 3rd column in Table 4.8). For operating a front-end wheel loader for loading and spreading the backfill soil, the one-way travel distance d_1 (between the loading and unloading locations at the site) and travel speed of wheel loader $v_{s,w}$ are assumed to be 500 m and 20 km/hr, respectively (Caterpillar, 2014). It is further assumed that the time for operating one cycle (i.e., loading, unloading, spreading but not including the travel time) takes approximately 0.5 min. Subsequently, the total time per one cycle (including travel time) can be estimated (see 2nd row and 3rd column in Table 4.8). For compacting the backfill soil, it is assumed three passes $N_p = 3$ are needed to reach the optimum dry unit weight of soil (i.e., compaction requirement) (Lewis, 1961). Based on the specifications provided by Mikasa Sangyo (2019), the travel speed of the compactor $v_{s,c}$ is 9 m/min and the width of the compactor is 350 mm. Based on the specifications of the compactor, mentioned above, the compacted volume per hour (V_c/hr) is calculated (see 3rd row and 3rd column in Table 4.8).

Table 4.8. Estimation of workload and production rate of the construction equipment for MSE wall

Construction activity (equipment)	Specifications	Workload	Production rate
Excavation of existing soil (hydraulic excavator)	Bucket capacity (BC) = 0.764 m^3 (Caterpillar, 2014) Bucket fill factor (BFF) = 1 (Caterpillar, 2014) Cycles per hour = 200 (Caterpillar, 2014) [1]Adjusted cycles per hour (ACHP) $= (\text{Cycles per hour})(e_o)(e_{os})(m_a)$	[2]$V_b = L_R H(1\text{ m})$	V_b per hour $= (\text{ACPH})(\text{BC})(\text{BFF})$ (Caterpillar, 2014) = 61.1 m^3/hr (RSMeans, 2015) Average of the two values is used

Table 4.8 (continued).

Construction activity (equipment)	Specifications	Workload	Production rate
Loading and spreading backfill soil (front-end wheel loader)	BC = 0.764 m^3 BFF = 1 One-way travel distance, d_1 = 500 m Travel speed, $v_{s,w}$ = 20 km/hr (Caterpillar, 2014) Cycles per hour = 120 (Caterpillar, 2014) Time for one cycle, t_1 = 0.5 min (Caterpillar, 2014)	[2,3] $V_l = V_b(1+b_f)$ Total number of cycles $= \frac{V_l}{(\text{BC})(\text{BFF})}$	Total time per cycle $= t_1 + 2\frac{(d_1)}{(v_{s,w})(16.67)}$
Compaction of backfill soil (vibratory plate compactor)	Plate width, w_p = 350 mm (Mikasa Sangyo, 2019) Travel speed, $v_{s,c}$ = 9 m/min (Mikasa Sangyo, 2019) Number of passes, N_p = 3 (Lewis, 1961)	[2,3] $V_c = \frac{V_l}{(1-s_f)}$	V_c per hour $= \frac{w_p v_{s,c} e_o s_v}{N_p}$ (RSMeans, 2015)

[1]Operational efficiency, e_o = 50 min/hr = 0.833; Operator skill efficiency, e_{os} = 0.9; Machine availability, a_m = 0.95 (Caterpillar, 2014)
[2]V_b = bank volume; V_l = loose volume; V_c = compacted volume
[3]Shrinkage factor, s_f = 0.1; Bulking (swelling) factor, b_f = 0.25

Table 4.9. Calculation of fuel volume used by the construction equipment for MSE wall

Construction activity (equipment)	Fuel consumption rate	Operation time (See Table 4.8 for workload and production rate)
Excavation of existing soil (hydraulic excavator)	18 L/hr (Caterpillar, 2022)	= Workload ÷ Production rate $= V_b \div \text{average}\left((\text{ACPH})(\text{BC})(\text{BFF}), \frac{61.1\ m^3}{hr}\right)$
Loading and spreading backfill soil (front-end wheel loader)	34 L/hr (NCHRP, 2013)	= Workload × Production rate $= \frac{V_l}{(\text{BC})(\text{BFF})} \times \left(t_1 + 2\frac{(d_1)}{(v_{s,w})(16.67)}\right)$
Compaction of backfill soil (vibratory plate compactor)	1.4 L/hr (Mikasa Sangyo, 2019; Honda, 2020)	= Workload ÷ Production rate $= V_c \div \frac{w_p v_{s,c} e_o s_v}{N_p}$

Fuel volume = fuel consumption rate × operation time (Equation (2.5))

Table 4.10 shows a sample calculation of life cycle impact assessment for calculating GWP of MSE wall with geogrids, considering selected emissions. The total emissions in Table 4.10 are the results of the LCI (see Table 4.7).

Table 4.10. Sample calculations for LCIA of an MSE wall with geogrid reinforcement

Process	Total emission[1], E_x (kg)			Characterization factor[2], $(GWP)_x$			Mass of CO_2e (kg) [using Equation (2.8)]			Total mass of CO_2e (kg)
	CO_2	CH_4	N_2O	CO_2	CH_4	N_2O	CO_2	CH_4	N_2O	
	(1)	(2)	(3)	(4)	(5)	(6)	(7) = (1)×(4)	(8) = (2)×(5)	(9) = (3)×(6)	(10) = (7)+(8)+(9)
Cradle-to-gate processes of HDPE	296	1.72	6.81×10^{-3}	1	25	298	296	43	2.03	341
Transportation of geogrid	4.70×10^{-2}	6.03×10^{-7}	4.97×10^{-5}				4.70×10^{-2}	1.51×10^{-5}	1.48×10^{-2}	1.48×10^{-2}
Transportation of excavated soil	93.1	6.35×10^{-5}	6.11×10^{-3}				93.1	1.59×10^{-5}	1.82	94.9
Transportation of backfill	116.4	7.94×10^{-5}	7.63×10^{-3}				116.4	1.99×10^{-3}	2.27	118.7
Operation of vibrating plate compactor	310	1.54×10^{-2}	0				310	3.85×10^{-1}	0	310.4

[1]obtained from the LCI as shown in Table 4.7
[2]obtained from the ReCiPe database by Goedkoop *et al*. (2014)

4.3 Results

In this section, the LCA results of MSE walls reinforced by (i) steel strips and (ii) geogrids are provided. The quantified environmental impacts are normalized with respect to two values, (i)

annual world impact per person and (ii) environmental impact by typical passenger vehicle, to understand the impacts of MSE walls compared to the reference values. The most significant life cycle processes and environmental impacts of MSE walls are identified. The results of parametric study are provided which help understanding the effects of (i) soil properties, (ii) material properties of reinforcement, (iii) design parameters, and (iv) hauling distances of transportation trucks to the global warming impact of MSE walls. Ultimately, GWP estimation charts are provided using which the GWP of MSE walls can be estimated based on different configurations of design dimensions (i.e., length and spacings of reinforcement) for different live load surcharges.

4.3.1 Environmental Impacts of MSE walls

In this section, conclusions are drawn based on the results of LCA of MSE walls and significant issues are identified. Table 4.11 shows sample results of LCA for MSE walls with geogrids (with L_R/H = 0.7, s_v = 0.45 m, and H = 7 m). The total environmental impacts reported in Table 4.11 are in actual measurements which are difficult to understand their significance; hence, these values are interpreted by comparing with two reference values in Table 4.12 – (i) the annual world impact per person and (ii) the environmental impacts caused by a typical life cycle of a passenger car. Based on the normalized environmental impacts, calculated in Table 4.12, the most important environmental impacts are marine eutrophication (58% of annual world impact) and photochemical oxidant formation (33.3% of annual world impact) which are mostly caused by the operation of equipment for constructing the MSE walls.

Figure 4.5 compares the normalized environmental impacts of MSE walls with steel strips and geogrids. The use of steel strips results in higher environmental impacts except for marine eutrophication. Figure 4.6 illustrates how much each life cycle stage of MSE walls contributes to the total environmental impacts. The operation of construction equipment has the highest influence

especially on marine eutrophication and photochemical oxidant formation. Freshwater ecotoxicity is not caused by the construction activities but solely by the cradle-to-gate processes of reinforcement materials. Transportation activities in the life cycle of MSE walls only contribute to global warming impact.

Table 4.11. Environmental impacts of an MSE wall with geogrids (L_R/H = 0.7 and s_v = 0.45 m)

Life cycle process	GWP[1] (kg CO_2e)	TAP[2] (kg of SO_2e)	MEP[3] (kg of Ne)	POFP[4] (kg of NMVOCe)	PMFP[5] (kg of PM)	FETP[6] (kg of 1,4-DBe)
Cradle-to gate processes of geogrid	175	2.73×10^{-1}	7.44×10^{-2}	3.56×10^{-2}	8.46×10^{-2}	5.83×10^{-2}
Transportation of materials	157	0	0	0	0	0
Construction	341	3.81	2.6	6.78	1.69	0
Total	673	4.1	2.67	6.82	1.77	5.83×10^{-2}

[1]GWP: global warming potential, [2]TAP: terrestrial acidification potential, [3]ME: marine eutrophication potential, [4]POFP: photochemical oxidant formation potential, [5]PMFP: particulate matter formation potential, [6]FETP: freshwater ecotoxicity potential

Table 4.12. Normalized environmental impacts of MSE walls with geogrids (L_R/H = 0.7 and s_v = 0.45 m)

Impact category (equivalent measurement unit)	MSE wall impacts[1]	Typical passenger vehicle impacts[1,2]	Proportional MSE wall impact with respect to passenger vehicle (%)	Annual world impact per person[1,2]	Proportional MSE wall impact with respect to annual world impact (%)
Global warming (kg of CO_2)	673	56200	1.2	10757	6.3
Terrestrial acidification (kg of SO_2)	4.1	164	2.5	41	10
Marine eutrophication (kg of P)	2.67	-	-	4.6	58

Table 4.12 (continued).

Impact category (equivalent measurement unit)	MSE wall impacts[1]	Typical passenger vehicle impacts[1,2]	Proportional MSE wall impact with respect to passenger vehicle (%)	Annual world impact per person[1,2]	Proportional MSE wall impact with respect to annual world impact (%)
Photochemical oxidant formation (kg of NMVOC)	6.82	48	14.2	20.5	33.3
Particulate matter formation (kg of PM_{10})	1.77	3.9	45.4	25.6	6.9
Freshwater ecotoxicity (kg of 1,4-DB)	0.0583	-	-	25.2	0.23

[1]In equivalent measurement units given in the first column

[2]Data from European Commission (2008) and Huijbregts *et al*. (2016)

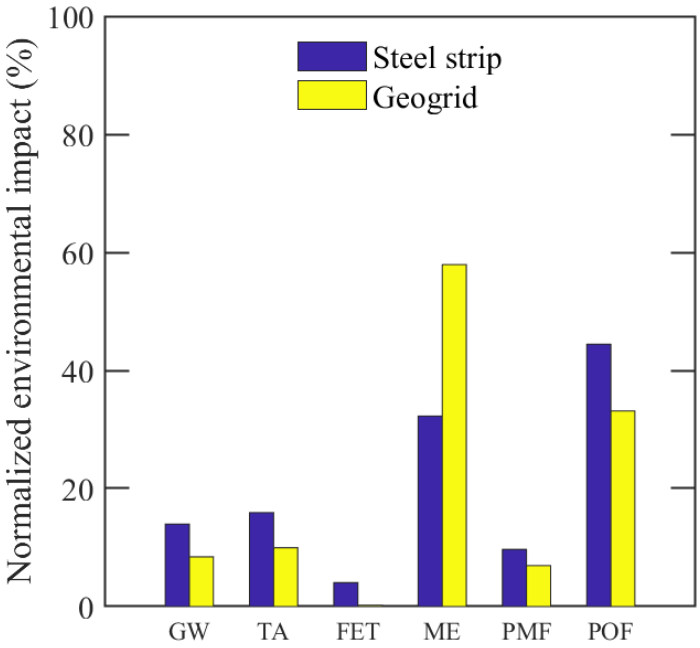

Figure 4.5. Environmental impacts of MSE walls. Environmental impacts normalized to the annual world impact per person in 2010. [GW: global warming; TA: terrestrial acidification; ME: marine eutrophication; POF: photochemical oxidant formation; PMF: particulate matter formation; FET: freshwater ecotoxicity]

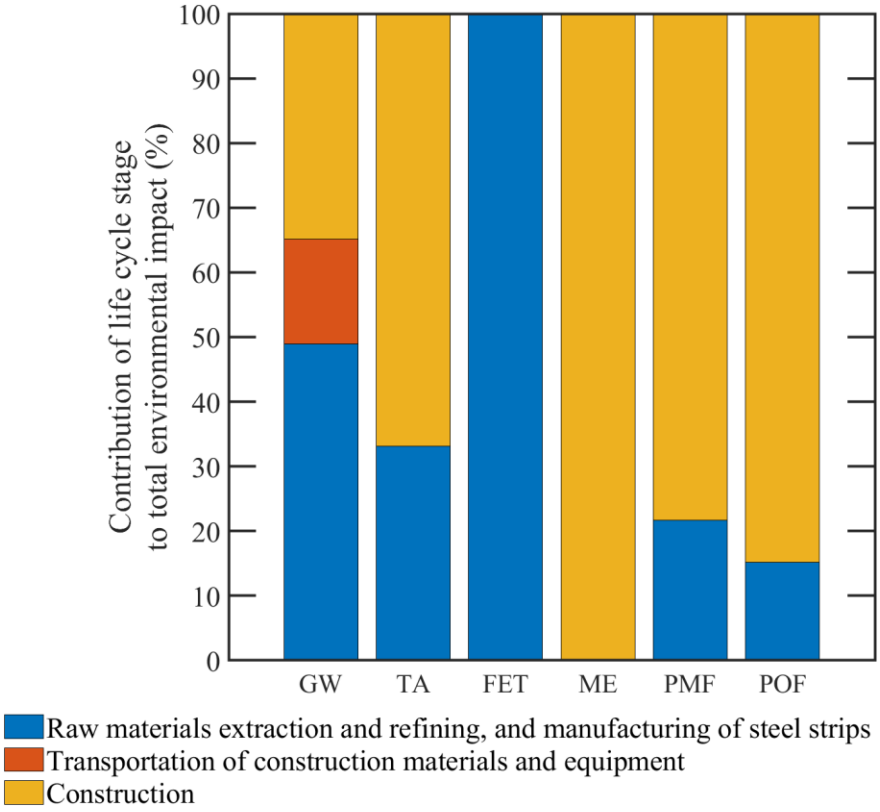

Figure 4.6. Breakdown of environmental impacts per life cycle stage of MSE walls with steel strips

4.3.2 Parametric study of LCA of MSE walls

Parametric study of MSE walls is conducted to understand the effects of (i) soil properties, (ii) material properties of reinforcement, (iii) design parameters, and (iv) hauling distances to the global warming impact of MSE walls. The parameter of interest is varied according to the values specified in Table 4.1 and the rest of parameters is fixed to the default values shown in Figure 4.1, otherwise mentioned. The discussion will focus on the results for global warming potential as it is the most accessible environmental impact to engineers.

4.3.2.1 Effect of Soil Properties

Figure 4.7 shows the variations of GWP with respect to the soil properties of MSE walls with steel strips for different s_v. According to Figure 4.7(a), the GWPs of MSE walls are constant

with the change in the unit weights of backfill, retained, and foundation soil. Similar results are observed when friction angles of retained and foundation soils, ϕ_r and ϕ_f, are varied; however, a decrease in GWP is observed when the friction angle of backfill soil ϕ_b is varied from 28 to 37°. Although ϕ_r and ϕ_f are used in the calculation of the coefficient of active earth pressure K_A for external stabilities and bearing capacity factors N_q and N_γ, the designs of MSE walls in this study generally have high FS for external stabilities and are governed by the internal stabilities. Therefore, increasing ϕ_b results in decreased K_A (for internal stabilities) which lead to decreased GWP. MSE walls with geogrids showed no change in GWP with respect to soil properties.

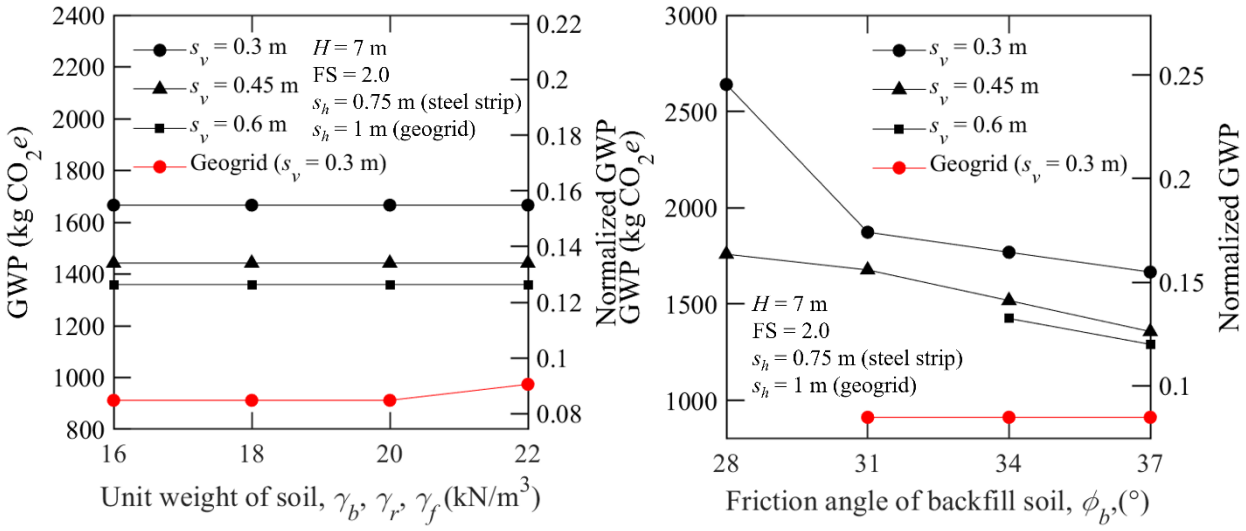

(a) (b)

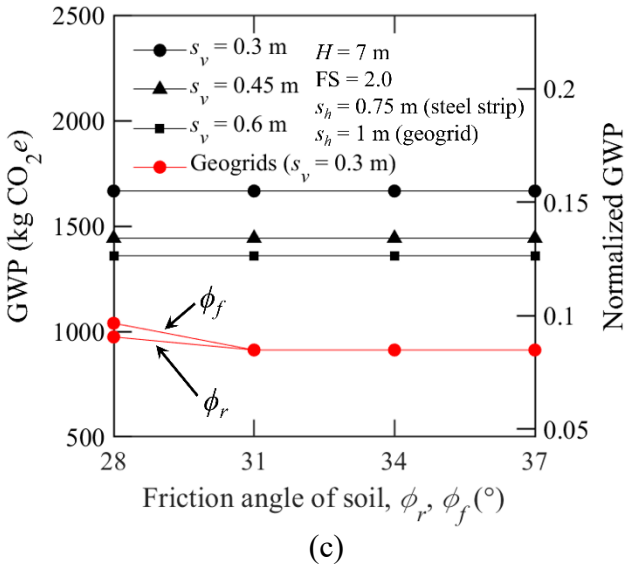

(c)

Figure 4.7. Variation of GWP with soil properties (a) unit weights of backfill, retained, and foundation soil (b) friction angle of backfill soil, and (c) friction angles of retained and foundation soil (normalization of GWP in the secondary vertical axis is done with respect to the annual world impact per person, which is 10757 kg of CO_2e)

4.3.2.2 Effect of Material Properties

Figure 4.8 shows the effects of yield strength of steel f_y and tensile strength of geogrid T to the GWP of MSE walls. The GWPs remained constant with increasing strengths of materials, and it appears these strengths need to be significantly increased (beyond the ranges used in this study) to observe a change in the GWPs. For geogrids with T = 20 kN/m, design results that satisfy the safety requirements (i.e., FS > 2) could not be obtained.

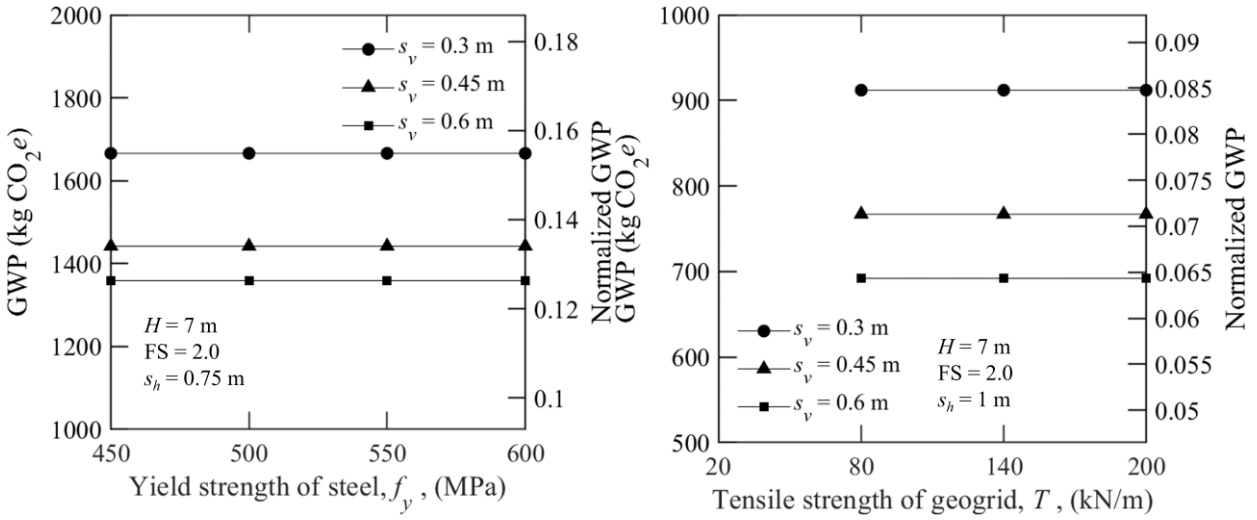

(a) (b)

Figure 4.8. Variation of GWP with material properties of reinforcement (a) yield strength of steel and (b) tensile strength of geogrid (normalization of GWP in the secondary vertical axis is done with respect to the annual world impact per person, which is 10757 kg of CO_2e)

4.3.2.3 Effect of Design Parameters

The changes in GWP with respect to design parameters (i.e., live load surcharge, factor of safety, and height of wall) are investigated, as shown in Figure 4.9. For most cases, increase in the GWPs is observed as q, FS, and H are increased. Minimal changes in GWP are observed for MSE walls with geogrids with varied q. Some designs are not possible (e.g., FS = 3 or $H > 9$ m) because the FS for tension failure cannot be satisfied without reducing the vertical or horizontal spacings of reinforcement.

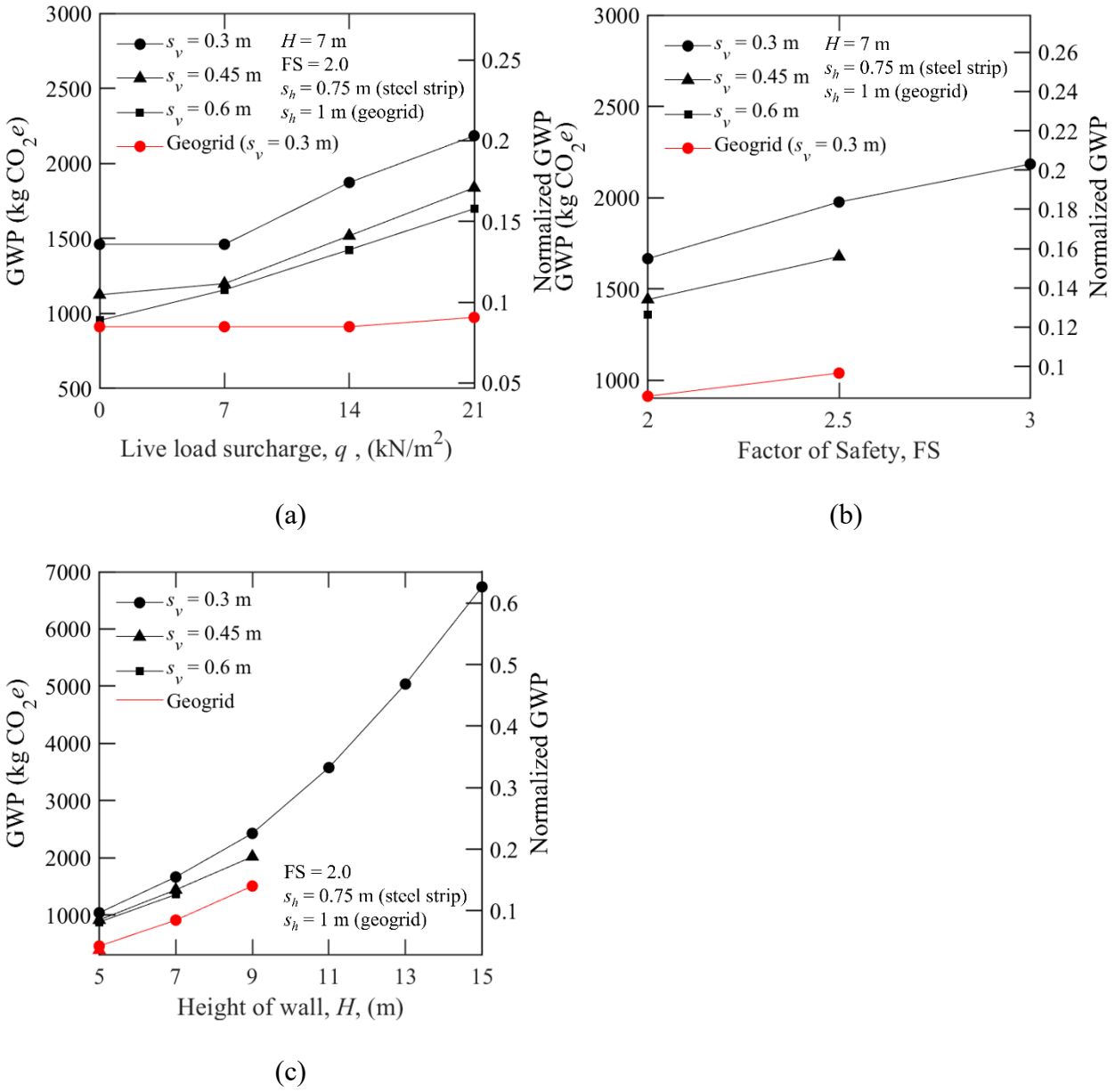

Figure 4.9. Variation of GWP with design parameters (a) live load surcharge, (b) factor of safety, and (c) height of wall (normalization of GWP in the secondary vertical axis is done with respect to the annual world impact per person, which is 10757 kg of CO_2e)

4.3.2.4 *Effect of Hauling Distance*

The effects of hauling distances for transporting (i) the reinforcement materials (i.e., steel strips and geogrids) and (ii) soils for excavation and backfilling, to the GWP of MSE walls are examined and illustrated in Figure 4.10. In this study, the distance for transporting the

reinforcement materials from the manufacturing plant to the construction site is varied to 10, 50, and 100 km, and the distance for transporting excavated and backfill soils is varied to 5, 15, and 30 km. Increasing the transportation distance for the reinforcement materials shows very minimal changes in GWP because the associated workload is relatively low (e.g., required only one trip and low cargo weight). On the contrary, an increase in the GWP is observed for varied transportation distances for soils. Although the one-way distance for transporting the soils is significantly lower compared to that for transporting the reinforcement materials, the dump trucks need to make multiple trips with much higher cargo weights (i.e., 90% of 22 t capacity). Hence, the high workload for transporting the soils results in increased GWP. L_R and H are important design parameters in determining the volumes of excavated and backfill soils; therefore, these parameters need to be adjusted if the GWP from transportation activities is to be reduced.

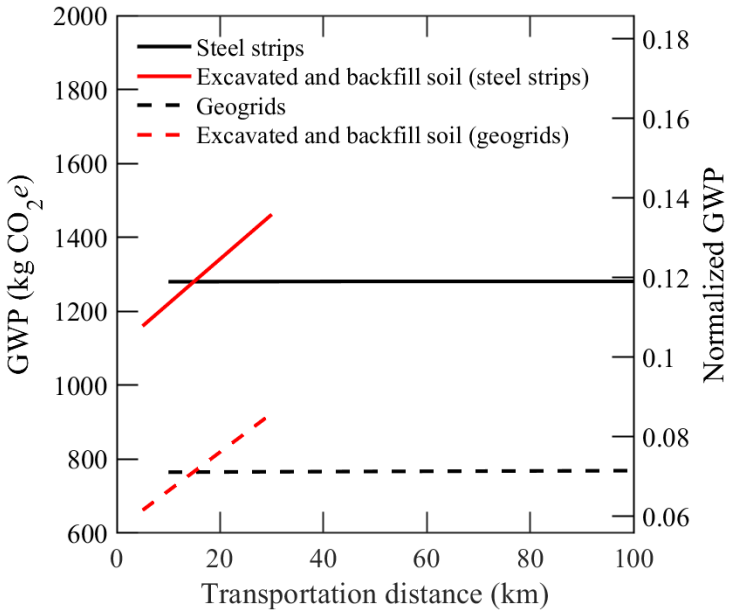

Figure 4.10. Variation of GWP with transportation distances of reinforcement materials and soils

4.3.3 GWP Estimation Charts

Figure 4.11 shows an example of design chart that can be used for approximate estimation of GWP based on the design dimensions of MSE wall with steel strips. The main advantage of using Figure 4.11 is the ease of incorporating environmental impact considerations in the process of MSE wall design without conducting LCA calculations. The coloured and dashed lines in Figure 4.11 indicate the different values of GWP. Various possible designs with different combinations of L_R/H and s_v (see Figure 4.11(a)) and L_R/H and H (see Figure 4.11(b)) are considered. Different surcharge loads ranging from 0 to 21 kN/m^2 are considered and parameters related to soil properties, material properties, and design requirement are fixed to the values shown in Figure 4.1. For example, given q = 14 kN/m^3, three MSE wall designs, with varied s_v of steel strips, are possible (see triangle markers in Figure 4.11). According to Figure 4.11(a), the GWP for the design with L_R/H = 0.95 and s_v = 0.45 m is estimated to be approximately 1600 kg of CO_2e. The GWP contours in Figure 4.11 are expected to change as the dimensions of steel strip (e.g., width and thickness) and specifications of construction equipment change. Figure 4.12 shows the GWP estimation charts for MSE walls with geogrids. The designs in Figure 4.12 are not variant to the change in the live load surcharge q and have L_R/H = 0.7. In this study, the MSE walls with geogrids are governed by the tension failure of reinforcement which can be alleviated by reducing the vertical spacing of geogrids or increasing the tensile strength of geogrids, and increasing the length of reinforcement L_R does not improve the tensile resistance of geogrids. Hence, the designs in Figure 4.12 have L_R/H =0.7 given the geogrids have T = 30 kN/m. Most MSE wall designs with geogrids that have s_v > 0.3 m are not considered safe (i.e., designs that result in FS < 2) in this study.

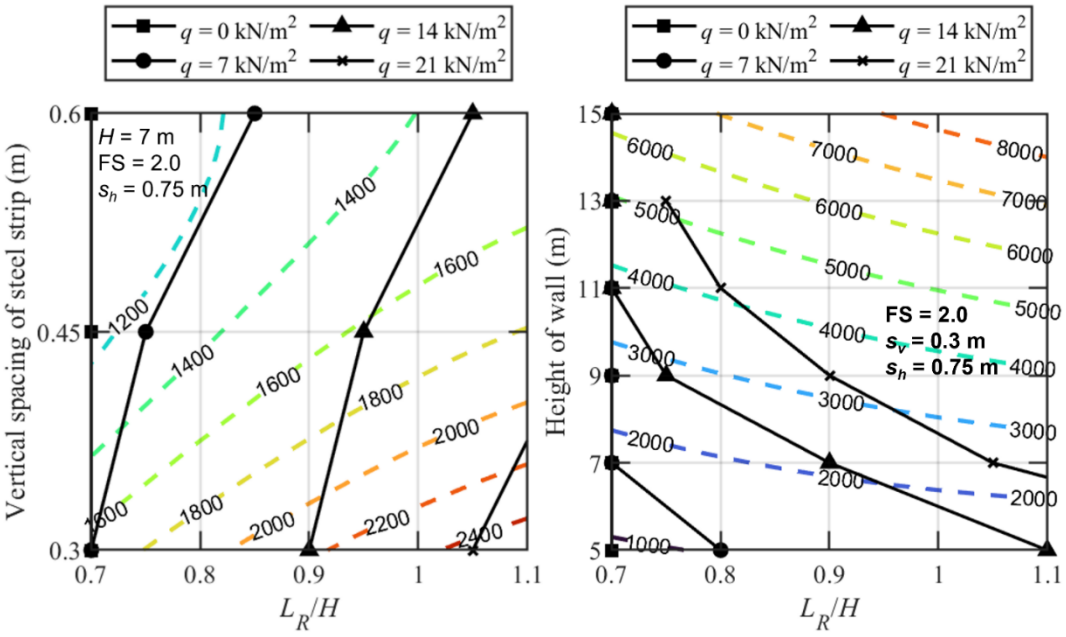

Figure 4.11. Estimation of GWP based on design dimensions of MSE wall with steel strips: (a) vertical spacing of steel strip and (b) height of wall [Soil properties: γ_b = 19 kN/m^3, γ_r = 19 kN/m^3, γ_f = 16 kN/m^3, ϕ_b = 36°, ϕ_r = 32°, ϕ_f = 30°]

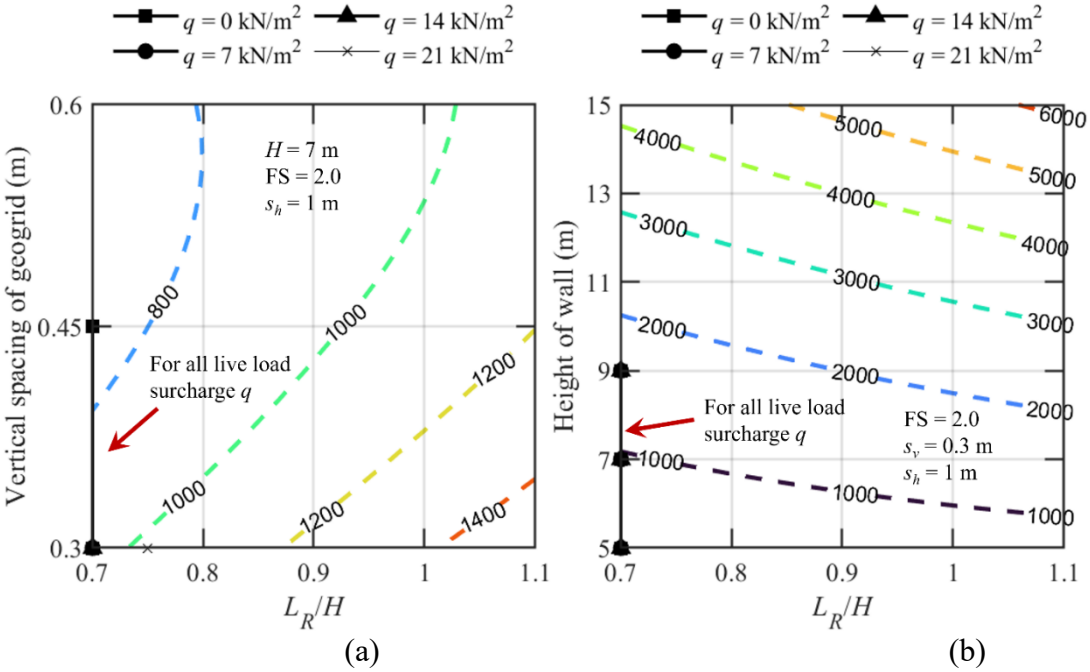

Figure 4.12. Estimation of GWP based on design dimensions of MSE wall with geogrids: (a) vertical spacing of steel strip and (b) height of wall [Soil properties: γ_b = 19 kN/m^3, γ_r = 19 kN/m^3, γ_f = 16 kN/m^3, ϕ_b = 36°, ϕ_r = 32°, ϕ_f = 30°]

4.4 Summary

LCA was applied to mechanically stabilized earth (MSE) walls reinforced by two types of soil reinforcement – steel strips or geogrids. The MSE walls were designed such that the factors of safety are at least 2 considering both external (i.e., sliding, overturning, and bearing capacity failures) and internal stabilities (i.e., tension and pullout failures). Given a soil profile, live load surcharge (applied at the ground surface of reinforced soil), and height of wall, the length of reinforcement and spacings of reinforcement, both in vertical and horizontal directions, are determined in the design of MSE walls. Subsequently, the masses of excavated soil, backfill soil, and reinforcement materials are determined. These masses are then used as inputs in the LCA calculations.

In this study, the following environmental impacts of MSE walls are quantified: global warming, terrestrial acidification, marine eutrophication, particulate matter formation, photochemical oxidant formation, and freshwater ecotoxicity. The quantified environmental impacts were normalized with respect to (i) annual world impact per person and (ii) environmental impact by a typical passenger car. For MSE walls, marine eutrophication and photochemical oxidant formation were found to be the most important environmental impacts. In comparison between the two types of reinforcement, MSE walls with geogrids are considered more environmentally friendly for most environmental impacts except for marine eutrophication. Parametric study was conducted to study the effects of (i) soil properties (i.e., unit weight and critical-state friction angle of soil), (ii) properties of reinforcement material (i.e., tensile strength), (iii) design parameters (i.e., factor of safety, live load surcharge, and height of wall), and (iv) hauling distances of transportation activities, to global warming impact of MSE walls. Based on the parametric study, some variations in the GWPs of MSE walls with steel strips were observed

as the parameters were varied; however, constant GWPs were observed for MSE walls with geogrids. Further, the GWPs of MSE walls (with steel strips) were most sensitive to the changes in the critical-state friction angle of backfill soil among the soil properties considered in the parametric study. The tensile strength of reinforcement materials was found to be a trivial factor in changing the GWPs of MSE walls, at least for the ranges of tensile strength considered in this study. For hauling distances, increased GWPs of MSE walls were observed as the distances for transporting excavated and backfill soils increased. For the ease of estimating the GWPs of MSE walls without conducting LCA calculations, GWP estimation charts were developed. The charts consider different combinations of design dimensions (i.e., length of reinforcement, vertical and horizontal spacings of reinforcement, and height of wall) for different loads of surcharge.

4.5 List of Symbols

Notation	Description
$(EF)_x$	Emission factor of substance x
$(\text{GWP})_x$	Characterization factor of climate forcer x relative to carbon dioxide
A_c	Cross-sectional area of steel strip
a_m	Machine availability
b	Width of steel strip
b_f	Bulk factor
CO_2e	Equivalent mass of CO_2 of emissions x
C_P	Coefficient of reinforcement effective perimeter
c_r	Corrosion rate of steel
C_R	Coefficient of pullout resistance
C_S	Scale-effect coefficient
D	Summation of all driving forces or moments in an MSE wall
d_1	One-way travel distance (between the loading and unloading locations at the site) of front-end wheeal loader
e_c	Eccentricity of load
e_o	Operational efficiency of machine
e_{os}	Operator skill efficiency
E_x	Total emission of substance (pollutant) x
fy	Yield strength of steel strip
H	Height of wall
h_{eq}	Equivalent height of soil for vehicular load

List of Symbols (continued).

Notation	Description
K_A	Coefficient of lateral earth-pressure at active state
K_r/K_A	Lateral stress ratio
L_a	Length of reinforcement within failure wedge
L_e	Effective length of reinforcement
L_R	Length of reinforcement
M	Moment
m	Mass of sub-product (e.g., concrete, steel, and diesel)
N_p	Number of passes for compaction
N_{rf}	Number of reinforcement layers
N_γ and N_q	Bearing capacity factors
q	Live load surcharge
R	Summation of all resisting forces in an MSE wall
R_c	Coverage ratio
s_f	Shrinkage factor
s_h	Horizontal spacing of reinforcement
SL_c	Service life of Zinc coating on the strips
SL_{MSE}	Service life of retaining wall
s_v	Vertical spacing of reinforcement
T	Tensile strength of reinforcement
t_1	Time for one cycle of front-end wheel loader
t_c	Sacrificial thickness of steel strip
t_n	Thickness of steel strip
V_b	Bank volume of soil
V_c	Compacted volume of soil
V_l	Loose volume of soil
$v_{s,c}$	Travel speed of compactor
$v_{s,w}$	Travel speed of wheel loader
w_p	Plate width
W_t	Weight
z	Depth below top of the wall
γ_b, γ_r, γ_f	Unit weight of backfill, retained, and foundation soils, respectively
μ_f	Friction between reinforced soil and foundation soil
ϕ_b, ϕ_r, ϕ_f	Critical-state friction angle of backfill, retained, and foundation soil, respectively

PART II: THE RELATIONSHIP BETWEEN RELIABILITY AND SUSTAINABILITY IN GEOTECHNICAL ENGINEERING

CHAPTER 5: RELIABILITY AND SUSTAINABILITY OF PILE FOUNDATIONS

In this chapter, the relationship between reliability and environmental impacts is investigated for drilled shafts. Single drilled shafts are considered embedded in different sandy soil profiles, and these are designed using a soil property-based design method within a probabilistic framework. Monte Carlo Simulations (MCS) and first order reliability method (FORM) are used to perform reliability analysis and reliability-based design (RBD) of drilled shafts in which uncertainties related to soil properties, design equations, applied loads, and pile dimensions are considered. Given a soil profile (with associated soil properties) and applied loads, RBD of drilled shafts is performed to determine the pile dimensions that meet a specified target probability of failure. Based on the pile dimensions determined in RBD, the total volume (or mass) of construction materials like concrete and steel, and fuel required to complete the drilled shaft construction are quantified. These volumes of construction material and fuel are then used as inputs in LCA to estimate the environmental impact associated with a particular design. The global warming impact is used in the quantification of environmental impact because it is the most accessible and important impact in the civil engineering field. It is expected that this study will make geotechnical engineers aware of the impact of design on sustainability and help them make informed decisions balancing the technical and environmental aspects of geotechnical practice.

5.1 Reliability-based Design

Reliability analysis is related to solving supply-demand problems, in which the supply and demand are considered random variables. For geotechnical engineering problems, the supply is

usually the resistance (capacity) of a system and the demand comprises the applied loads on the system. The difference between the resistance and load is defined as the safety margin:

$$S = R - Q \tag{5.1}$$

where S is the safety margin, R is the resistance (capacity) of the system, and Q is the load applied to the system. If R and Q are random variables (characterized by probability distribution functions, means, and variances), then S is also a random variable characterized by a probability distribution function, mean and variance. The probability of failure p_f of the system is estimated as:

$$p_f = \int_{-\infty}^{0} f_S(s)ds \tag{5.2}$$

where p_f is the probability of failure, and $f_S(s)$ is the probability distribution function of S (Figure 5.1), and s is a realization of the random variable S. Graphically, the probability of failure is the area under $f_S(s)$ for $s < 0$, as indicated by the shaded area in Figure 5.1. The mean μ_S of the safety margin S is calculated as:

$$\mu_S = \mu_R - \mu_Q \tag{5.3}$$

where μ_R and μ_Q are the means of R and Q, respectively. For statistically independent R and Q, the variance of S is given by:

$$\sigma_S^2 = \sigma_R^2 + \sigma_Q^2 \tag{5.4}$$

where σ_S, σ_R, and σ_Q are the standard deviations of S, R, and Q, respectively. Assuming that the resistance R and load Q follow normal distributions, the probability of failure p_f estimated based on Equation (5.2) is given by

$$p_f = 1 - \Phi\left(\frac{\mu_S}{\sigma_S}\right) \tag{5.5}$$

where Φ is the standard normal distribution function. The reliability index β is defined as:

$$\beta = \frac{\mu_S}{\sigma_S} \tag{5.6}$$

and it is related to p_f. Graphically, the reliability index is related to the horizontal shift of the mean of safety margin from $s = 0$, as shown in Figure 5.1.

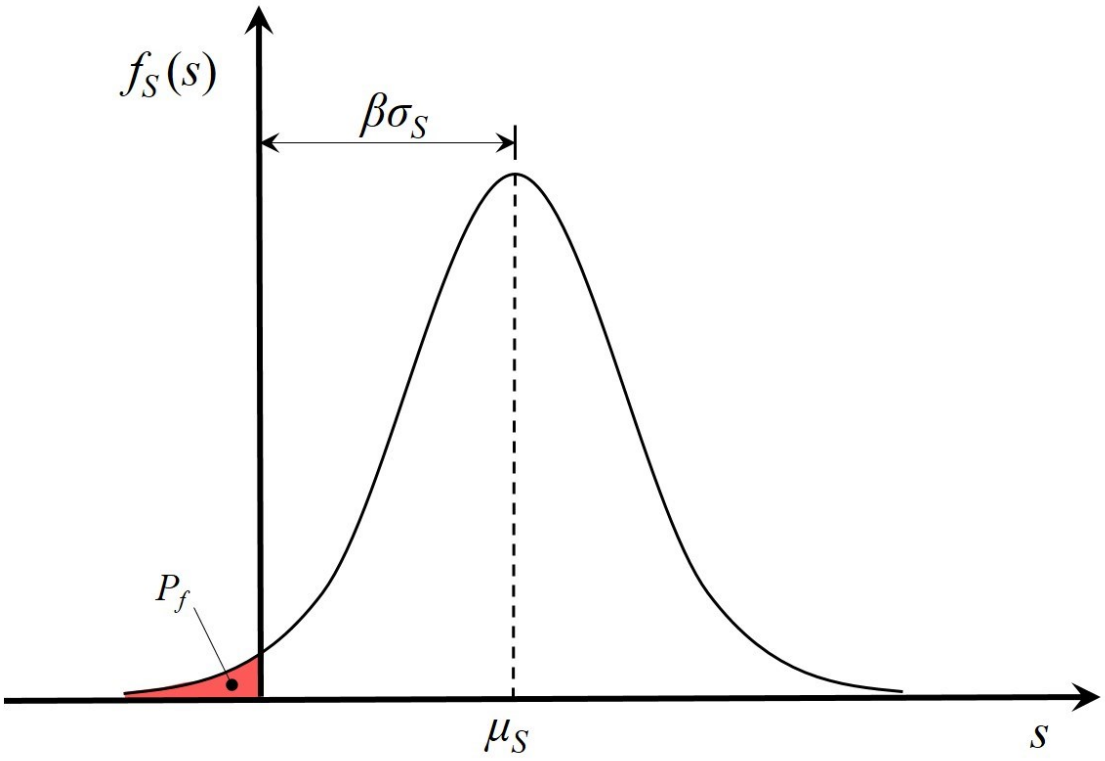

Figure 5.1. Probability distribution of safety margin

The objectives of reliability-based design are to quantify the performance of a system with uncertain information and to minimize the probability of failure (or maximize the reliability index) by adjusting the design parameters or by updating additional information on uncertain variables (e.g., soil properties, loads, and limit state function). Different reliability analysis methods are available such as the first-order second moment (FOSM) method, first-order reliability method (FORM), point estimate method (PEM), and Monte Carlo simulation (MCS) method. The

integrated framework described in the next section uses FORM because of which it is briefly described in the following paragraphs.

FORM, also known as the Hasofer-Lind approach, is an optimization method involving the loads and resistances (Q and R) which are the random variables (there can be multiple loads and resistances) such that the minimum distance D_β between the design state O (corresponding to a particular combination of loads and resistances) and the limit state function $G(R_1, R_2, \ldots, Q_1, Q_2 \ldots)$ is determined. In the probability space of the loads and resistances, the limit state function is a surface that separates the feasible design space (within which the design state has to lie) from the unfeasible (unsafe) space. For example, $G(R, Q) = R - Q$ is a possible limit state function and the unsafe (or unfeasible) space consists of all possible combinations of R and Q for which $G < 0$. The minimum distance between O and $G(R_1, \ldots, Q_1, \ldots)$ is related to the probability of failure or the reliability index. In the actual calculations, the original probability space of the loads and resistances is mapped to the standard normal space expressed in terms of reduced variables Y_i defined as

$$Y_i = \frac{X_i - \mu_i}{\sigma_i} \tag{5.7}$$

where Y_i is the reduced variable for a set of random variables X_i (with $i = 1, 2, \ldots, n$) in the original space ($R_1, R_2, \ldots, Q_1, Q_{2, \ldots}$ are the x_i-s), and μ_i and σ_i are the means and standard deviations of x_i, respectively. The problem of finding the minimum distance between O and $G(X)$ in the original space translates into finding the minimum distance in the standard normal space between the point of origin and the limit state function (surface) $G(Y) = 0$ expressed in terms of reduced variables, as shown in Figure 5.2.

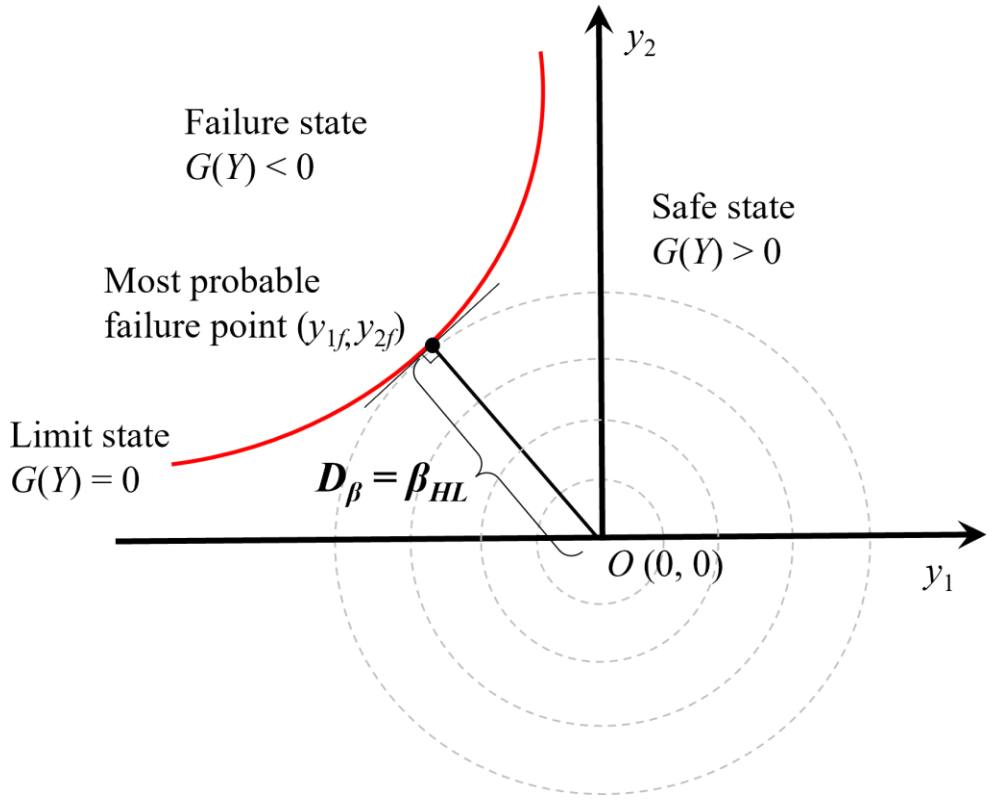

Figure 5.2. Illustration of the first-order reliability method (FORM)

If all the random variables follow normal distribution and are uncorrelated, the reduced variables have a mean of 0 and a unit standard deviation. In the standard normal space (in which the random variables are reduced to standard normal variables), the probability is rotationally symmetric around the origin, illustrated as the grey dashed circles (joint distribution surface of the reduced variables Y_1 and Y_2) in Figure 5.2.

The minimum distance from the origin (which indicates the mean values of the reduced variables) to the limit state function $G(Y) = 0$ is defined as the reliability index. The objective of FORM is to find this minimum distance. As the limit state surface (or failure surface) $G(Y) = 0$ moves further or closer to the origin, the safe region, $G(Y) > 0$ increases or decreases, respectively. Therefore, the position of the failure surface relative to the origin of the reduced variates should

determine the reliability of the system. The point on the failure surface with minimum distance to the origin is the most probable failure point, as indicated by (y_{1f}, y_{2f}) in Figure 5.2 (Ang and Tang, 1984). Simply put, FORM is a constrained optimization problem with the following formulation:

$$\begin{aligned} &\text{Minimize } D_\beta (= \beta_{HL}) \\ &\text{Subject to } G(X) \;=\; G(Y) \;=\; 0 \end{aligned} \tag{5.8}$$

where D_β is the minimum distance between the origin and most probable failure point in the standard normal space and β_{HL} is the Hasofer-Lind reliability index.

For multi-dimensional problems with a number of random variables x_i, the distance from a point $Y = (Y_1, Y_2, \ldots, Y_n)$ on the failure surface $G(Y) = 0$ to the origin is calculated as:

$$D_\beta = \beta_{HL} = \sqrt{(Y_1)^2 + (Y_2)^2 + \cdots + (Y_n)^2} \tag{5.9}$$

5.2 Drilled Shaft Cases Considered

Drilled shafts of length L_p and diameter B_p embedded in five different sandy profiles are considered in this study, as shown in Figure 3.2. Profile 1 comprises a completely dry homogeneous sand deposit with a mean relative density D_R = 70%. Profile 2 is the same as Profile 1 but with a water table located at the ground surface. Profile 3 consists of a completely dry sand deposit with mean D_R = 50% overlying a strong bearing layer with mean D_R = 80%. Profile 4 is the same as Profile 3 but with a water table located at a depth of 2 m below the ground surface. Profile 5 consists of an extremely loose sand layer with mean D_R = 20% overlying a dense sand layer with mean D_R = 80%. For all the profiles and sand layers, it is assumed that the mean critical-state friction angle ϕ_c = 33° and the coefficient of lateral earth pressure at rest K_0 = 0.45. The mean values of D_R, ϕ_c, and K_0 are kept unaltered except in cases parametric studies with respect to these

parameters are performed. When there are multiple layers, the drilled shafts are assumed to be embedded in the bearing layer with an embedment depth of $2B_p$.

5.3 Probabilistic Characterization and Quantification

5.3.1 Soil Variables

The soil variables required in this study are D_R, ϕ_c, K_0, and soil unit weight γ. Following Basu and Salgado (2012) and Baecher and Christian (2003), D_R, ϕ_c, and γ are treated as random variables with their mean values, coefficients of variation (COVs), and probability distributions given in Table 5.1. K_0 and the maximum and minimum void ratios e_{max} and e_{min} are treated as deterministic variables because information about their randomness is rather limited. The effect of variation of K_0 is indirectly taken into account by considering multiple values of K_0.

Table 5.1 summarizes the characteristics of variables used in reliability analysis and RBD of drilled shaft. In this study, the uncertainties in soil properties are accounted by representing ϕ_c, D_R, and unit weight of soil γ_{soil} as random variables. Kim and Salgado (2012a) reported that the highest COV value of ϕ_c for sand is 0.012 based on the studies of Baecher and Christian (2003), Foye *et al*. (2006), and Negussey *et al*. (1998). Therefore, in this study, it is assumed that ϕ_c follows a normal distribution with a COV of 0.02 to be conservative. For D_R, Phoon and Kulhawy (1999) reported that the COV ranges from 0.1 to 0.4 for D_R ranging from 30 to 70%; however, Kim (2008) and Basu and Salgado (2012) report that variability changes depending on the value of D_R (i.e., high variability as D_R decreases and low variability as D_R increases). Therefore, in this study, it is assumed that D_R follows a normal distribution with varying COV as summarized in Table 5.1. Baecher and Christian (2003) reported that the COV of γ_{soil} ranges from 0.05 to 0.1; therefore, it is assumed that γ_{soil} follows a normal distribution with COV of 0.1 to be conservative.

Table 5.1. Characteristics of deterministic and random variables used in drilled shaft design

Deterministic variables	**Value or range**		
Coefficient of lateral earth pressure at rest, K_0	0.4, 0.45, 0.5, 0.65 (Basu and Salgado, 2012)		
Maximum void ratio, e_{max}	0.9 (Basu and Salgado, 2012)		
Minimum void ratio, e_{min}	0.45 (Basu and Salgado, 2012)		
Deterministic bias in the model, M_{qb}^{bias}	0.97 for $D_R \leq 50\%$ (Basu and Salgado, 2012) 1.16 for $D_R \geq 90\%$ linearly interpolated between 0.97 and 1.16 for $50\% < D_R < 90\%$		
Pile length, L_p	5 – 30 m		
Ratio of live load to dead load, LL/DL	0.25 – 2 (Basu and Salgado, 2012)		
Random variable	**Type of probability distribution**	**Mean Range**	**COV**
Critical-state friction angle of soil, ϕ_c	Normal	28 - 37° (Basu and Salgado, 2012)	0.02 (Baecher and Christian, 2003; Foye *et al*., 2006; Kim and Salgado, 2012a; Negussey *et al*., 1998)
Relative density of soil, D_R	Normal	20 - 80 % (Basu and Salgado, 2012)	0.35 for D_R = 20% 0.23 for D_R = 30% 0.18 for D_R = 40% 0.14 for D_R = 50% 0.12 for D_R = 60% 0.10 for D_R = 70% 0.09 for D_R = 80% (Basu and Salgado, 2012; Kim, 2008; Phoon and Kulhawy, 1999)
Unit weight of soil, γ_{soil}	Normal	Calculated based on mean D_R , e_{max}, and e_{min}	0.1 (Baecher and Christian, 2003)
Model uncertainty associated with shaft resistance of drilled shaft, M_β	Normal	0.5 – 1.5	0.2 (Basu and Salgado, 2012)
Model uncertainty associated with base resistance of drilled shaft, M_{qb}	Normal	0.5 – 1.5	0.1 (Basu and Salgado, 2012)

Table 5.1 (continued).

Random variable	Type of probability distribution	Mean Range	COV
Dead load, *DL*	Normal	500 – 3000 kN	0.1 (Ellingwood and Tekie, 1999)
Live load, *LL*	Lognormal	500 – 3000 kN	0.25 (Ellingwood and Tekie, 1999; Foye *et al*., 2006)
Pile diameter, B_p	Normal	0.3 – 2.0 m	0.02 (Basu and Salgado, 2012)

5.3.2 Design Equations

Deterministically, $Q_{b,ult}$ and Q_{sL} for drilled shafts are given by (Salgado 2008):

$$Q_{ult} = Q_{b,ult} + Q_{sL} = q_{b,ult} A_b + \sum_i q_{sL,i} A_{s,i} \tag{5.10}$$

where Q_{ult} is the total ultimate capacity, $Q_{b,ult}$ is the ultimate base resistance, Q_{sL} is the limit shaft resistance, $q_{b,ult}$ is the ultimate unit base resistance, A_b is the cross-sectional area of the pile base, $q_{sL,i}$ is the limit unit shaft resistance of the i^{th} soil layer, and $A_{s,i}$ is the surface area of the pile in contact with the i^{th} layer. Considering model uncertainty, the ultimate unit base resistance for 10% relative settlement and the limit unit shaft resistance are given by (Basu and Salgado, 2012):

$$q_{b,ult} = q_{b,10\%} = M_{qb}^{\text{bias}} M_{qb} 0.38 p_A e^{-0.0066 D_R} e^{0.1041\phi_c + (0.0264 - 0.0002\phi_c) D_R} \times \left(\frac{\sigma_h^{'}}{p_A} \right)^{0.841 - 0.0047 D_R} \tag{5.11}$$

$$q_{sL} = M_\beta \left(K \tan\delta \right) \sigma_v^{'} = M_\beta \beta \sigma_v^{'} \tag{5.12}$$

in which

$$K = \frac{0.7 K_0}{e^{0.2\sqrt{K_0 - 0.4}}} e^{\frac{D_R}{100}\left[1.3 - 0.2 \ln\left(\frac{\sigma_v^{'}}{p_A}\right)\right]} \tag{5.13}$$

where p_A is the atmospheric pressure (=100 kPa), σ'_v and σ'_h are the corresponding effective vertical and lateral stresses, respectively, acting at the depths where q_{sL} and $q_{b,ult}$ are calculated, δ is the friction angle mobilized along pile-soil interface (= ϕ_c according to Loukidis and Salgado (2008)) M_{qb}^{bias} is the deterministic bias in the $q_{b,ult}$ model expressed in Equation (5.11), M_{qb} is the random part of the model uncertainty in $q_{b,ult}$, and M_β is the random error of the uncertainty in modeling β in Equations (5.12) and (5.13) (the deterministic bias of β model M_β^{bias} is assumed to be 1 according to Basu and Salgado (2012)).

The parameters in Equations (5.11)-(5.13) are represented as random variables characterized by their probability distributions, means, and coefficients of variation (COVs). The uncertainties in model are considered by including bias factor M^{bias} and random factor M in the equations for calculating the unit base resistance and unit shaft resistance shown in Equations (5.11) and (5.12), respectively. Basu and Salgado (2012) determined the M^{bias} associated with $q_{b,10\%}$ equation by comparing with the results of plate load tests by Lee and Salgado (1999). In this study, the M_{qb}^{bias} is 0.97 for $D_R \leq 50\%$, 1.16 for $D_R \geq 90\%$, and linearly interpolated between 0.97 and 1.16 for $50\% < D_R < 90\%$. The random variable M_{qb} in Equation (5.11) is assumed to follow normal distribution with a COV of 0.1. Basu and Salgado (2012) estimated the model uncertainty in q_{sL} equation based on the results of centrifuge tests by Fioravante (2002) and Colombi (2005). However, the M^{bias} associated with q_{sL} equation is omitted because there is lack of data available from the centrifuge tests. M_β in equation (5.12) is assumed to be normally distributed with COV of 0.2.

5.3.3 Applied Loads

The uncertainties in applied loads are considered by representing *DL* and *LL* as random variables. In this study, it is assumed *DL* follows a normal distribution and COV of 0.1 based on

the study by Ellingwood and Tekie (1999). *LL* is assumed to follow lognormal distribution with a COV of 0.25 based on the studies by Ellingwood and Tekie (1999) and Foye *et al*. (2006).

5.3.4 Pile Dimensions

The uncertainties in pile dimensions are accounted by considering the pile diameter B_p as random variable that follows normal distribution with a COV of 0.02 (Basu and Salgado, 2012). L_p are considered deterministic in this study because they do not vary significantly in practical cases.

5.4 Reliability Analysis of Drilled Shaft

For the reliability analysis performed in this study, the uncertainties considered are those associated with soil properties, design equations, applied loads, and pile dimensions. The FORM (Ang and Tang, 1984) is followed, and the limit state function for drilled shafts is defined as:

$$Q_{b,ult} + Q_{sL} = DL + LL \tag{5.14}$$

where *DL* is the applied dead load and *LL* is the applied live load . Note that, in Equation (5.14), $Q_{b,ult}$, Q_{sL}, *DL*, and *LL*, are treated as random variables with associated probability distributions. Therefore, in FORM, the performance function is expressed as follows:

$$g(X) = X_1 + X_2 - X_3 - X_4 = 0 \tag{5.15}$$

where $X = \{X_1, X_2, X_3, X_4\}$ is the vector of the random variables representing Q_{sL}, $Q_{b,ult}$, *DL*, and *LL*, respectively. Because the soil properties, uncertainties in design equations, and uncertainties in pile dimensions are assumed to be normally distributed random variables, X_1, and X_2 also follow normal distributions. Figure 5.3 shows the distributions of X_1 and X_2 obtained using MCS for soil profile 1 (as described later). It is assumed that X_3 (dead load) follows a normal distribution

(Ellingwood and Tekie, 1999) and X_4 (live load) follows a lognormal distribution (Ellingwood and Tekie, 1999; Foye *et al*., 2006).

Assuming the random variables X_i to be uncorrelated, X_i is transformed into standard normal variate using Equation (5.7). As the live load X_4 follows a lognormal distribution, the equivalent normal distribution is obtained using Rosenblatt transformation assuming the random variables are statistically independent. The equivalent normal distribution of X_4 is characterized by the equivalent mean and standard deviation as expressed below:

$$\mu_4^N = x_4^* - \sigma_4^N \Phi^{-1}[F_{X_4}(x_4^*)] = x_4^*(1 - \ln x_4^* + \lambda_4) \tag{5.16}$$

$$\sigma_4^N = \frac{\phi\left\{\Phi^{-1}[F_{X_4}(x_4^*)]\right\}}{f_{X_4}(x_4^*)} = x_4^* \zeta_4 \tag{5.17}$$

where $\mu_4{}^N$ and $\sigma_4{}^N$ are the mean and standard deviation, respectively, of the equivalent normal distribution for X_4; $F_{X_4}(x_4{}^*)$ and $f_{X_4}(x_4{}^*)$ are the lognormal cumulative distribution function and lognormal probability density function, respectively, of X_4 evaluated at the failure point $x_4{}^*$; $\Phi(.)$ and $\phi(.)$ are the cumulative distribution function and probability density function, respectively, of the standard normal distribution; and λ and ζ are the scale parameter and shape parameter, respectively, of lognormal distribution. By inputting Equations (5.16) and (5.17) into Equation (5.7), the standard normal variate of lognormal X_4 is obtained:

$$Y_4 = \frac{\ln X_4 - \lambda_4}{\zeta_4} \tag{5.18}$$

Therefore, the performance function in terms of standard normal variates is obtained by inputting Equations (5.7) and (5.18) into Equation (5.15):

$$g(Y) = (Y_1\sigma_1 + \mu_1) + (Y_2\sigma_2 + \mu_2) - (Y_3\sigma_3 + \mu_3) - e^{(Y_4\zeta_4 + \lambda_4)} = 0 \tag{5.19}$$

In the standard normal space, the distance from a point on the failure surface $g(Y) = 0$ to the origin of the standard normal variates Y_i and is calculated using Equation (5.9). The minimum distance represents the reliability of the system which is also called the Hasofer-Lind reliability index β_{HL}. FORM is essentially solving a constrained optimization problem by minimizing the distance from a point on the limit state function to the origin of standard normal space, subject to the constraint $g(Y) = 0$ (which represents the limit state surface). Therefore, using the method of Lagrange's multiplier the optimization problem can be formulated as follows:

$$L_L = D_\beta + \lambda_L g(Y) \tag{5.20}$$

where λ_L is the Lagrange's multiplier. By minimizing the function L_L, the minimum distance (or reliability index) can be calculated:

$$\beta_{HL} = \frac{-\sum_i y_i^* \left(\frac{\partial g}{\partial Y_i} \right)_*}{\sqrt{\sum_i \left(\frac{\partial g}{\partial Y_i} \right)_*^2}} \tag{5.21}$$

where the derivatives $(\partial g/\partial Y_i)_*$ are evaluated at the most probable failure points y_i^*. The probability of failure p_f is then calculated as:

$$p_f = 1 - \Phi(\beta_{HL}) \tag{5.22}$$

The FORM is performed using a MATLAB program in which an iterative approach is taken to determine the most probable failure point that results in $g(Y) \approx 0$.

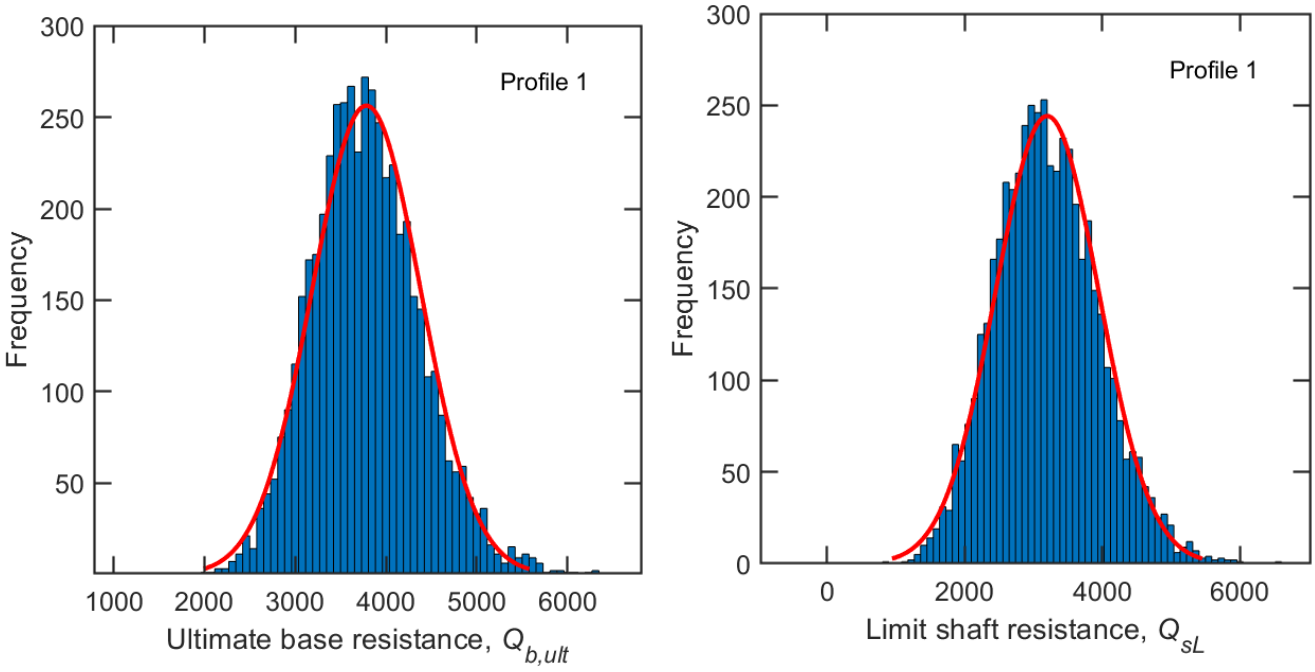

(a) (b)

Figure 5.3. Distributions of (a) ultimate base resistance $Q_{b,ult}$ and (b) limit shaft resistance Q_{sL}

5.5 Reliability-based Drilled Shaft Design

Given a soil profile and loading condition, and given the characteristics of random variables for soil properties, model uncertainties, applied load and pile dimensions, as summarized in Table 5.1, the base and shaft resistances of drilled shaft are calculated using Equations (5.11) and (5.12). Subsequently, the pile dimensions are adjusted to increase the base and shaft resistances until a target reliability index (or probability of failure) is achieved. The pile dimensions are selected based on either of the two following approaches: (i) fixed diameter approach and (ii) fixed length approach. In the fixed diameter approach, a fixed diameter of, say, 0.9 m, is assumed and the pile length is increased in increments of 1 m until the design requirements are satisfied. Similarly, in the fixed length approach, a fixed length of, say, 15 m is assumed and the pile diameter is determined in increments of 0.1 m until the design requirements

are satisfied. In this study, pile diameter is selected within a range of 0.3 to 2.0 m, and pile length is selected within a range of 5 to 30 m.

According to U.S. Army Corps of Engineers (1997), drilled shafts are designed such that they have at least "above average" expected performance level. Table 5.2 shows the expected performance level for different values of reliability index β_{HL} or probability of failure p_f. In practical cases, it is assumed that drilled shafts are designed aiming for "above average" or "good" expected performance levels. Therefore, the drilled shafts are designed for five different target reliability indices corresponding to probabilities of failure $p_f = \{10^{-3}, 5.5 \times 10^{-4}, 10^{-4}, 5.5 \times 10^{-5}, 10^{-5}\}$.

Table 5.2. Expected performance level (adapted from U.S. Army Corps of Engineers, 1997)

Reliability index, β_{HL}	Probability of Failure, p_f	Expected performance level
1.0	1.6×10^{-1}	Hazardous
1.5	7.0×10^{-2}	Unsatisfactory
2.0	2.3×10^{-2}	Poor
2.5	6.0×10^{-3}	Below average
3.0	1.0×10^{-3}	Above average
4.0	3.0×10^{-5}	Good
5.0	3.0×10^{-7}	High

The design dimensions calculated from RBD of drilled shaft are used to calculate the volume of construction materials (e.g., concrete and steel). The total volumes of concrete and steel are converted into their corresponding masses using the respective densities of 2400 kg/m^3 (Vieira, 2015) and 7850 kg/m^3 (CEN, 2004), respectively. The drilled shafts are assumed to be reinforced with a steel cage comprising 2.5% volume of the concrete shaft, as recommended by FHWA (2010a). Pile caps are not considered for single drilled shafts because it is not required if the bearing capacity and the interface reinforcement/connection meet the code criteria (CAC 2006;

FHWA 2010). For example, for a single drilled shaft with 1.2 m diameter, 15 m length, and 2.5% steel reinforcement, the total masses of concrete and steel are 40,715 kg and 3,329 kg, respectively. These values are used as inputs to the LCA to estimate the environmental impacts of drilled shaft.

5.6 Environmental Impact Assessment

The scope and goal of LCA performed in this study are to quantify the environmental impacts of drilled shafts designed for different target reliability indices (or probabilities of failure) so that the impact of target reliability index on the environmental impact can be quantified. The functional unit of the drilled shafts considered in this study is 'the mass of a single drilled shaft that supports the applied load without bearing capacity failure and that meets the reliability requirements specified by the designer'. Details of assumptions and parameters used in LCA are provided in Section 3.2.

5.7 Multiple Regression Analysis

The required number of realizations N in MCS depends on the target probability of failure $p_{f,\text{target}}$ and is computed as (Fenton and Griffiths, 2008):

$$N = p_{f,\text{target}}(1 - p_{f,\text{target}})\left(\frac{z_{\alpha/2}}{\varepsilon_{\max}}\right)^2 \tag{5.23}$$

where $z_{\alpha/2}$ is the point on the standard normal distribution satisfying $p[Z > z_{\alpha/2}]$ (p = probability), α_s is the significance level, and $\varepsilon_{\max}$ is the maximum error on p_f at confidence $(1 - \alpha_s)$. For example, assuming 90% confidence level ($\alpha_s = 0.1$), $\varepsilon_{\max}$ is 10^{-4} and $p_{f,\text{target}}$ is 10^{-3}, the required number of realizations in MCS is 270,332 ≈ 271,000. For each MCS run, an LCA should be performed and the prohibitively large number of LCA calculations is avoided by performing multiple regression

analyses to create a surrogate regression model using which the global warming impact of drilled shafts can be estimated faster than by performing a large number of LCA calculations.

In general, a response y_r that depends on the controllable input variables ξ_1, ξ_2, …, ξ_k is expressed as:

$$y_r = f(\xi_1, \xi_2, ..., \xi_k) + \varepsilon \tag{5.24}$$

where y_r is the response surface that represents a performance measure or quality characteristic (e.g., GWP in this study), $f(.)$ is a mathematical function that surrogates the true response (e.g., GWP as a function of pile dimensions, in this study), ε is the error that represents the discrepancy between the true and observed responses, and k is the total number of input variables ξs ($k = 2$ because ξs are pile diameter and length in this study). The error results from failure of regression models to fit data exactly, sources of variation that are inherent in the system, measurement error, and effect of other variables (possibly unknown) to the response. It is assumed that ε is a random variable that follows a normal distribution with a zero mean and variance σ^2 (Montgomery *et al*., 2012; Myers *et al*., 2009). Therefore, the expected response of y_r is obtained as:

$$E(y_r) = E[f(\xi_1, \xi_2, ..., \xi_k)] + E(\varepsilon) = f(\xi_1, \xi_2, ..., \xi_k) \tag{5.25}$$

where $E(.)$ is the expectation.

Developing a suitable approximation for $f(.)$ is critical. Usually, a low-order polynomial model over a relatively small region of the independent variable space is considered appropriate (Myers *et al*., 2009). Therefore, in many cases, a first-order or a second-order model is used. For convenience, the natural variables ξ_1, ξ_2, …, ξ_k (variables expressed in natural units of measurement such as kilograms and meters) are transformed into dimensionless coded variables c_1 c_2, … c_k in regression analysis using:

$$c_i = \frac{\xi_i - \left(\xi_{\max} + \xi_{\min}\right)/2}{\left(\xi_{\max} - \xi_{\min}\right)/2} \tag{5.26}$$

where $\xi_{\max}$ and $\xi_{\min}$ are the upper and lower bounds of the natural variable ξ_i.

In terms of coded variables, the first-order and second-order regression models are expressed as:

$$y_r = \beta_0 + \sum_{j=1}^{k} \beta_j c_j + \sum \sum_{i<j=2}^{k} \beta_{ij} c_i c_j + \sum_{j}^{k} \beta_{jj} c_j^2 + \varepsilon \quad (\beta_{jj} = 0 \text{ for first-order model}) \tag{5.27}$$

In case $k = 2$,

$$y_r = \beta_0 + \beta_1 c_1 + \beta_2 c_2 + \beta_{11} c_1^2 + \beta_{22} c_1^2 + \beta_{12} c_1 c_2 + \varepsilon \tag{5.28}$$

where β_i are the regression coefficients and c_i are the independent coded variables. In this study, c_1 (or ξ_1) represents the pile diameter and c_2 (or ξ_2) represents the pile length. Other independent variables such as transportation distance, and operation times of construction equipment can be considered; however, the global warming impact caused by transporting materials and equipment, and during construction phase account for only 1.2 and 0.3% of the total global warming impact, respectively. Therefore, it is assumed that these effects are negligible and omitted in the regression analysis.

Equation (5.27) with $\beta_{jj} = 0$ is a first-order model which indicates that response y_r has a bilinear relationship with the variables c_i. The first-order model is appropriate for approximating the true response surface over a relatively small region of the independent variable space in a location where there is little curvature. The second term in Equation (5.27) models the main effects of the two variables c_1 and c_2. The third term in Equation (5.27) models the interaction between the variables. If the curvature in the response surface is strong enough; then a second-order model (Equation (5.27) with $\beta_{jj} \neq 0$) is appropriate. It is useful as an approximation to the true response

surface in a relatively small region around the optimum of the surface. Equation (5.27) with $\beta_{jj} \neq 0$ is able to model the response with curvature. The advantages of using second-order model are (a) the flexibility in taking a wide variety of functional forms, (b) the ease with estimation of the regression coefficients because the second-order model can be expressed in a linear regression model (for example, by assuming $\beta_{11} = \beta_3$, $c_1^2 = c_3$, $\beta_{22} = \beta_4$, $c_2^2 = c_4$, $\beta_{12} = \beta_5$, and $c_1 c_2 = c_5$ in Equation (5.28)) based on which the method of least squares can be used to estimate the regression coefficients, and (c) the considerable practical experience indicating that second-order models work well in solving real response surface problems (Myers *et al*., 2009).

The method of least squares is used to estimate the regression coefficients β_i in Equation (5.27) (Myers *et al*., 2009). The method of least squares chooses the regression coefficients so that the sum of the squares of the error are minimized. The Equation (5.27) is generalized as the following:

$$\begin{aligned} y_{r,i} &= \beta_0 + \beta_1 c_{i1} + \beta_2 c_{i2} + \cdots + \beta_k c_{ik} + \varepsilon_i \\ &= \beta_0 + \sum_{j=1}^{k} c_{ij} + \varepsilon_i \text{ for } i = 1, 2, \ldots, n \end{aligned} \tag{5.29}$$

The least squares function is defined as below:

$$\begin{aligned} L_s &= \sum_{i}^{n} \varepsilon_i^2 \\ &= \sum_{i}^{n} \left(y_i - \beta_0 - \sum_{j=1}^{k} \beta_j c_{ij}^2 \right)^2 \end{aligned} \tag{5.30}$$

where n is the total number of observations, and k is the number of variables (i.e., $k = 2$ in this study).

The function L_s is to be minimized with respect to regression coefficients, and the least-squares estimators of regression coefficients must satisfy the following conditions:

$$\left.\frac{\partial L_s}{\partial \beta_0}\right|_{\hat{\beta}_0,\hat{\beta}_1,\ldots\hat{\beta}_k} = -2\sum_{i=1}^{n}\left(y_i - \hat{\beta}_0 - \sum_{j=1}^{k}\hat{\beta}_j c_{ij}\right) = 0 \tag{5.31}$$

$$\left.\frac{\partial L_s}{\partial \beta_i}\right|_{\hat{\beta}_0,\hat{\beta}_1,\ldots\hat{\beta}_k} = -2\sum_{i=1}^{n}\left(y_i - \hat{\beta}_0 - \sum_{j=1}^{k}\hat{\beta}_j c_{ij}\right)c_{ij} = 0 \tag{5.32}$$

where $\hat{\beta}_0, \hat{\beta}_1, \ldots, \hat{\beta}_k$ are the least-squares estimators.

To determine the regression coefficients in Equation (5.27), data that shows the correlation between the response surface y_r (e.g., GWP in this study) and variables ξ (e.g., pile diameter and length in this study) need to be collected. Data collection (i.e., GWP in relation to pile diameter and length) is conducted using the experimental design because it is the most appropriate method and other data collection methods such as retrospective study (i.e., using historic data) and observational study are not applicable in this study (Montgomery *et al*., 2012). In an experimental design, trials of experiments are conducted in which the variables ξ (i.e., pile diameter and length in this study) are controlled to certain values (e.g., minimum and/or maximum of the ranges shown in Table 5.1) and the corresponding responses y_r (i.e., GWP in this study) are obtained. There are multiple experimental designs available, such as two-level factorial design (2^k) and central composite design (CCD) and they differ in terms of information they collect useful for estimating the regression coefficients (Myers *et al*., 2009). Since it is unclear if the response surface of global warming impact follows a first-order or second-order polynomial functions, CCD is used because it also collects sufficient information to conduct a two-level factorial design. CCD is widely used for fitting second-order models (Myers *et al*., 2009).

Figure 5.4 illustrates the experimental design of central composite designs at different levels of the two variables (i.e., pile diameter and length in this case). Each colored point in Figure 5.4 indicates the different levels of the variables (e.g., minimum, average, and maximum of B_p and

L_p). As shown in Figure 5.4, the design consists of four runs at the corners of a square (yellow dots in Figure 5.4), plus four runs at the center of the square (red dot), plus four axial runs (blue dots). The corner (also called factorial) points explore the combination of minimum and maximum levels of B_p and L_p, and they provide information related to the first-order and interaction terms in Equation (5.27). The axial points isolate each variable (e.g., $B_p = -\sqrt{2}$ and $L_p = 0$) to examine the effect of each variable towards curvature in the response surface; therefore, the axial points are used to estimate the second-order terms in Equation (5.27). The center points are used to find if curvature exists in the response surface. For example, a 2^k factorial design assumes that the response surface is a plane or a hyperplane; however, if the data at the center point indicates there exists a minima or maxima, a second-order model may be more appropriate. Hence, the center points are often used to test if second-order models are better choice than first-order models. Total of 12 observations ($n = 12$), in which different combinations of B_p and L_p are considered as shown in Figure 5.4, are collected in this study, and they are used for estimating the regression coefficients βs in Equation (5.27). LCA is used to quantify the global warming impact of the 9 observations. In this study, the global warming impacts obtained for the 12 observations are not replicated because it is assumed that there are no sources of uncertainty that leads to the variation in the quantification of global warming impact. In other words, it is assumed that given the pile dimensions are the same (and other conditions related to subsurface profile, loading, construction, and etc.), the global warming impact (measured in GWP) obtained from LCA will be consistent. The regression models, estimated using the least squares method and the central composite design method, are summarized in Table 5.3.

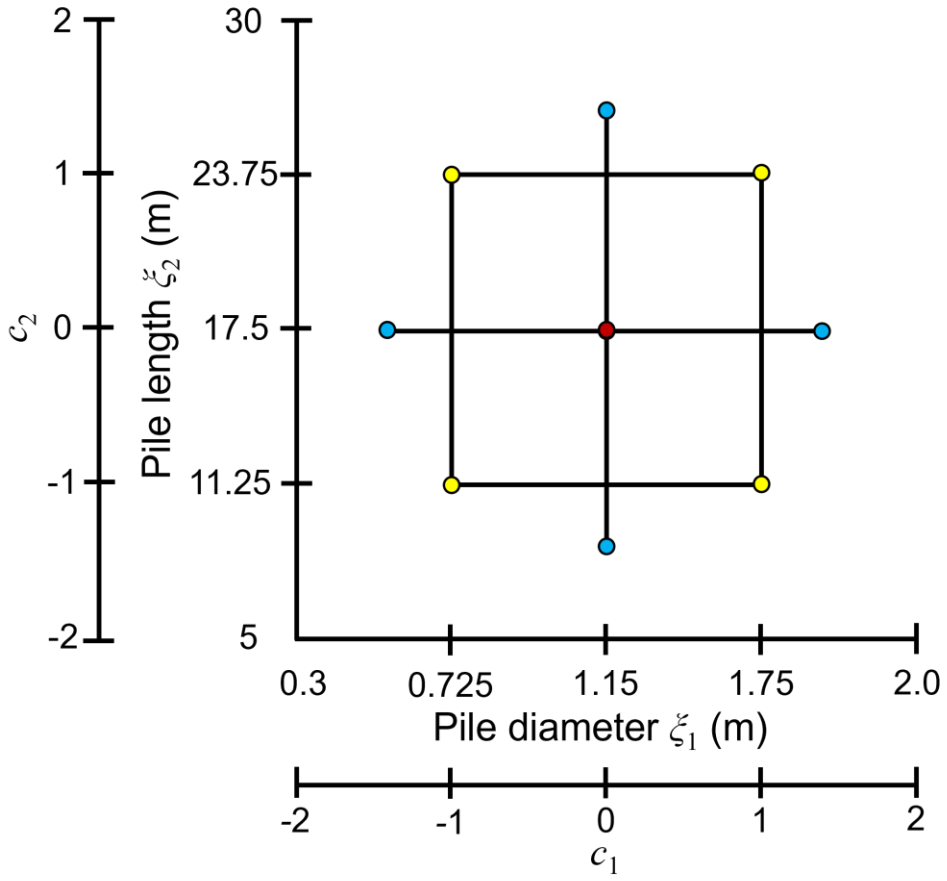

Figure 5.4. Central composite design for 2 design variables

Table 5.3. Regression models for global warming impact of drilled shafts

Regression Model	Equation[1]
Linear (without interaction effect)	$y_r = -19804.46 + 17480.84\xi_1 + 614.60\xi_2$
Linear (with interaction effect)	$y_r = 299.71 - 1.04\xi_1 - 534.21\xi_2 + 998.96\xi_1\xi_2$
Second-order (without interaction effect)	$y_r = -10670.42 + 0.84\xi_1 + 614.82\xi_2 + 7600\xi_1^2 - 0.01\xi_2^2$
Second-order (with interaction effect)	$y_r = 9433.75 - 17481.04\xi_1 - 533.99\xi_2 + 7600\xi_1^2 - 0.01\xi_2^2 + 998.86\xi_1\xi_2$

[1] ξ_1: pile diameter (m); ξ_2: pile length (m);

The regression models in Table 5.3 are developed based on several assumptions: (i) the relationship between the GWP (response y_r) and the pile diameter and length (regressors x_i) is

linear, (ii) the error ε in Equation (5.27) has zero mean, constant variance, and (iii) the errors are uncorrelated and normally distributed (Montgomery *et al*., 2012). Several diagnostics are performed to check if the models in Table 5.3 are adequate (i.e., the assumptions stated above are valid) using (i) analysis of variance (ANOVA), (ii) normal probability plot of residuals, (iii) coefficient of multiple determination, (iv) prediction error sum of squares (PRESS), and (v) multicolinearity test (Myers *et al*., 2009; Montgomery *et al*., 2012). The ANOVA is performed to test for the significance of regression (i.e., if βs in Equation (5.27) are significant or not). Equation (5.27) can be expressed differently by assuming $c_3 = c_1^2$, $c_4 = c_2^2$, $c_5 = c_1c_2$, $\beta_3 = \beta_{11}$, $\beta_4 = \beta_{22}$, and $\beta_5 = \beta_{12}$:

$$y_r = \beta_0 + \beta_1 c_1 + \beta_2 c_2 + \beta_3 c_3 + \beta_4 c_4 + \beta_5 c_5 + \varepsilon \tag{5.33}$$

Hence, both first-order and second-order models are linear in the β values, regardless of the shape of the response surface. In other words, ANOVA tests if there is a linear relationship between the response and any of the regressor variables (or regression coefficient). This procedure is often thought of as a global test of model adequacy. To conduct ANOVA, the following hypotheses are set:

$$\begin{aligned} &H_0 : \beta_1 = \beta_2 = \cdots = \beta_i = 0 \\ &H_1 : \beta_i \neq 0 \text{ for at least one } i \end{aligned} \tag{5.34}$$

Rejection of the null hypothesis H_0 implies that at least one of the regressor variables contributes significantly to the model. The null hypothesis is rejected if the following condition is met in the F-test:

$$F_0 > F_{\alpha,k,n-k-1} \tag{5.35}$$

in which

$$F_0 = \frac{SS_R / k}{SS_E / (n-k-1)} = \frac{MS_R}{MS_E} \tag{5.36}$$

Where F_0 is the F statistic value that follows the $F_{k,\, n-k-1}$ distribution and calculated as the ratios of mean squares by regression and error, $F_{\alpha,k,n-k-1}$ is the F critical value at preselected significance level α_s (= 0.05 in this study) and degrees of freedom k and $n-k-1$, SS_R is the sum of squares of regression (model), SS_E is the sum of squares of error (residual), MS_R is the mean square (variance) caused by regression, and MS_E mean square caused by error. Table 5.4 summarizes the results of ANOVA for the regression models considered in this study. As shown in Table 5.4, F_0 values of all regression models exceed the corresponding F critical value; therefore, all regression models considered in this study are adequate in terms of significance of regression. In other words, at least one of the regression coefficients for each model in Table 5.3 is proven to be significant in defining the relationship between GWP and pile dimensions. For example, if the regression coefficients for the second term and third term in the linear model (without interaction effect) are all close to zero, it is likely that the model is not adequate.

Table 5.4. Analysis of variance (ANOVA) for the GWP regression models

Regression Model	SS_R	SS_E	SS_T	MS_R	MS_E	F_0	$F_{\alpha,k,n-k-1}$
Linear (without interaction effect)	5.60×10^8	4.12×10^7	6.01×10^8	1.87×10^8	5.15×10^6	36.21	4.07
Linear (full)	5.88×10^8	1.30×10^7	6.01×10^8	1.47×10^8	1.86×10^6	78.85	4.12
Second-order (without interaction effect)	5.72×10^8	2.86×10^7	6.01×10^8	1.14×10^8	4.77×10^6	23.97	4.39
Second-order (full)	6.00×10^8	4.81×10^5	6.01×10^8	1.00×10^8	9.62×10^4	1039.65	4.95

Graphical analysis of residuals is also a very effective way to investigate the adequacy of the fit of a regression model and to check the underlying assumptions (e.g., normality assumption of residuals) (Montgomery *et al*., 2012). The residuals are scaled to observe if there are outliers or extreme values. In this study, the residuals are scaled into standardized residuals *d*, studentized residuals *r*, and externally studentized residuals *t* using the equations shown in Table 5.5.

Table 5.5. Residual diagnostics

Scaled residual	Equation
Standardized residual	$d_i = \frac{e_i}{\hat{\sigma}} = \frac{e_i}{\sqrt{MS_E}}$ for $i = 1, 2, \ldots, n$
Studentized residual	$r_i = \frac{e_i}{\sqrt{\hat{\sigma}^2(1-h_{ii})}}$ for $i = 1, 2, \ldots, n$
Externally studentized residual	$t_{s,i} = \frac{e_i}{\sqrt{S^2_{(i)}(1-h_{ii})}}$ for $i = 1, 2, \ldots, n$
	in which
	$S^2_{(i)} = \frac{(n-k-1)MS_E - e_i^2/(1-h_{ii})}{n-k-2}$

d: studentized residual; *r*: studentized residual; t_s: externally studentized residual
n: total number of observations; *k*: number of variables
e: residual
MS_E: mean square caused by error
$\hat{\sigma}$: estimate of standard deviation
$S^2_{(i)}$: estimate of variance (σ^2) based on a data set with the ith observation removed
h_{ii}: diagonal element of H matrix which maps the vector of observed values into a vector of fitted values

The standardized residuals should lie within the interval of $-3 \leq d_i \leq 3$, variance of studentized residuals should be 1, and externally studentized residuals are often used for outlier detection. To validate the normality assumption of residuals (i.e., to check if ε follows a standard normal distribution), the normal probability plot of residuals is constructed, as shown in Figure 5.5. The red line in Figure 5.5 indicates the normality of residuals. The residuals appear to more or less follow the red line and slight deviations are observed. Given the limited number of observations (n = 12), it is assumed the residuals are normally distributed based on Figure 5.5. The externally

studentized residuals are plotted against the predicted values to observe if there is a particular pattern (e.g., funnel, double bow, and nonlinear patterns) which indicate model deficiencies. Figure 5.6 shows the plot of residuals versus the corresponding fitted values. The residuals do not portray any particular pattern and are contained in a horizontal band; hence, no model deficiency is assumed.

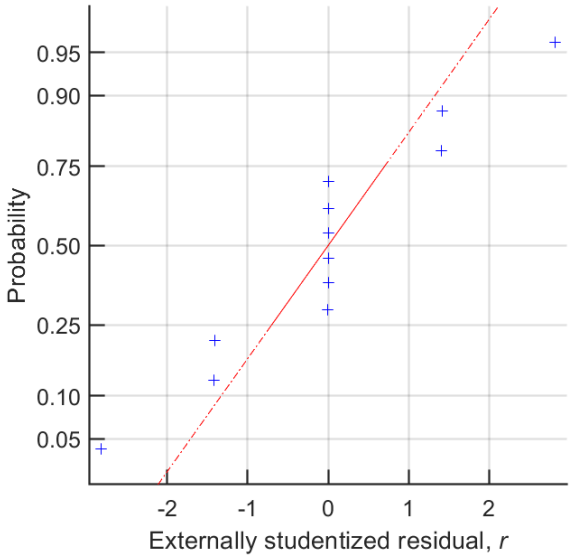

Figure 5.5. Normal probability plot of residuals for the full second-order model of GWP

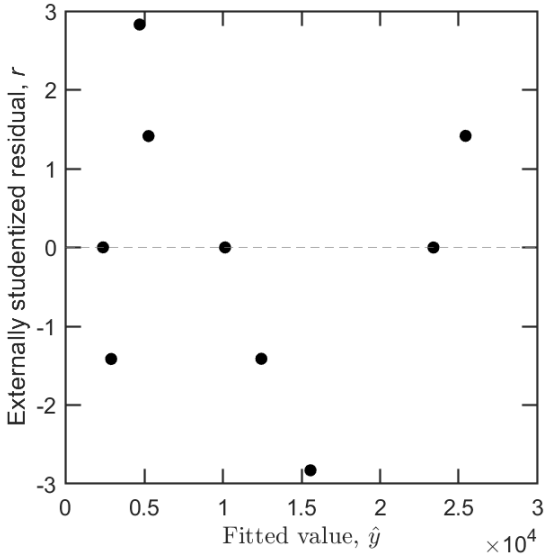

Figure 5.6. Residual plot for the full second-order model of GWP

The coefficient of multiple determination R^2 is computed which is a measure of the amount of reduction in the variability of y obtained by using the regressor variables in the model.

$$R^2 = \frac{SS_R}{SS_T} \tag{5.37}$$

where R^2 is the coefficient of multiple determination, and SS_T is the total sum of squares (=SS_R + SS_E).

In other words, a value of R^2 = 0.9992 indicates that the model explains about 99.92% of the variability observed in the response. Adjusted R^2 statistic is used to evaluate if unnecessary terms are included in the model.

$$R^2_{adj} = 1 - \frac{SS_E / (n-k-1)}{SS_T / (n-1)} \tag{5.38}$$

In this case, the adjusted R^2 is increased as the order of model is increased and as the interaction term is included, indicating that the second-order model (with interaction effect) is the most adequate.

The ability of the model prediction is also examined. PRESS is generally regarded as a measure of how well a regression model will perform in predicting new data. A model with a small value of PRESS is desired.

$$\begin{aligned} PRESS &= \sum_{i=1}^{n} (y_i - \hat{y}_{(i)})^2 \\ &= \sum_{i=1}^{n} \left(\frac{e_i}{1-h_{ii}} \right)^2 \end{aligned} \tag{5.39}$$

where $\hat{y}_{(i)}$ is predicted value of the i^{th} observed response based on a model fit to the remaining n-1 sample points. e_i is the residual, h_{ii} is the diagonal element of H matrix which maps the vector of observed values into a vector of fitted values. In this study, the second-order model with interaction

effect has the lowest PRESS value; therefore, it is the most adequate model. The coefficient of multiple determination for prediction is also computed which gives some indication of the predictive capability of the regression model.

$$R^2_{pred} = 1 - \frac{PRESS}{SS_T} \tag{5.40}$$

For example, the second-order model with interaction effect has $R^2_{pred} = 0.9943$, which implies that this model explains about 99.43% of the variability in predicting new observations. The second-order model with interaction effect has the highest predictive capability. Table 5.6 summarizes the results of diagnostics calculated using Equations (5.37)–(5.40). The coefficients of multiple determination (including the adjusted and for measuring the prediction capability) are the highest and the *PRESS* value is the lowest for the full second-order model. Therefore, based on the results of ANOVA and other diagnostics, shown in Table 5.6, the second order model with interaction effect is used to estimate the global warming impact of drilled shaft, given the pile dimensions obtained from RBD, when LCA is not the efficient method. Figure 5.7(a) shows the second-order response surface (with interaction effect) of global warming impact, and Figure 5.7(b) shows the contour plot of the response surface. For example, a drilled shaft with L_p = 30 m and B_p = 2.0 m is estimated to cause nearly 50,000 kg of CO_2e.

Table 5.6. Results of regression diagnostics

Regression Model	R^2	R^2_{adj}	***PRESS***	R^2_{pred}
Linear (without interaction effect)	0.9314	0.9057	8.92×10^7	0.8516
Linear (with interaction effect)	0.9783	0.9659	2.96×10^7	0.9508
Second-order (without interaction effect)	0.9523	0.9126	7.44×10^7	0.8761
Second-order (with interaction effect)	0.9992	0.9982	3.42×10^6	0.9943

Problems related to multicolinearity arises when the variables have near-linear relationship. Regression models fit to data by the method of least squares when strong multicolinearity is present are notoriously poor prediction equations, and the values of the regression coefficients are often very sensitive to the data in the particular sample collected. Orthogonality relationship between the variables provides more stable results. Since central composite design (method of designed experiment) is used in this study, near-linear relationship between variables are not observed (Montgomery *et al*., 2012).

Lack-of-fit test is a formal test to see whether or not the regression model is fitting the data well. For example, a second-order model may have better fit than a linear model because of the curvature terms. Replicate observations are necessary when testing for the lack of fit because they convey information related to pure error (e.g., measurement error). In this study, however, meaningful replicate observations cannot be obtained for this problem because it is assumed that the results of LCA will be consistent. Hence, the lack-of-fit test is not performed.

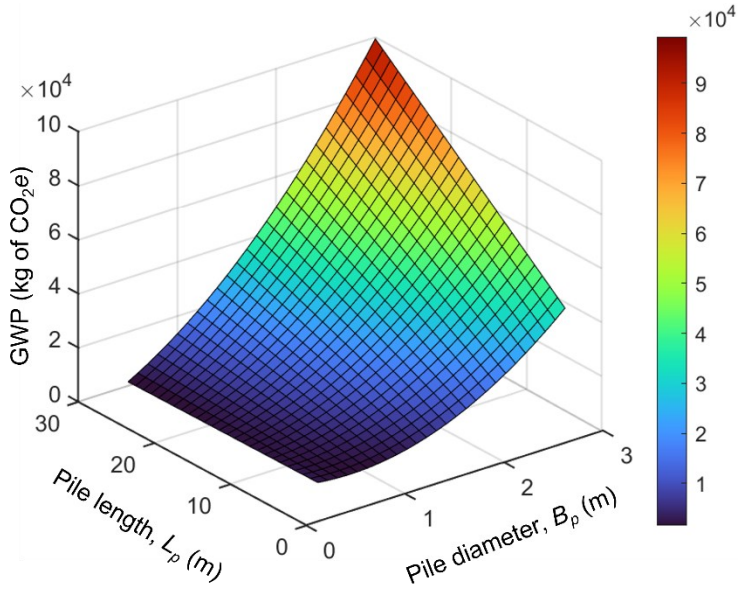

(a)

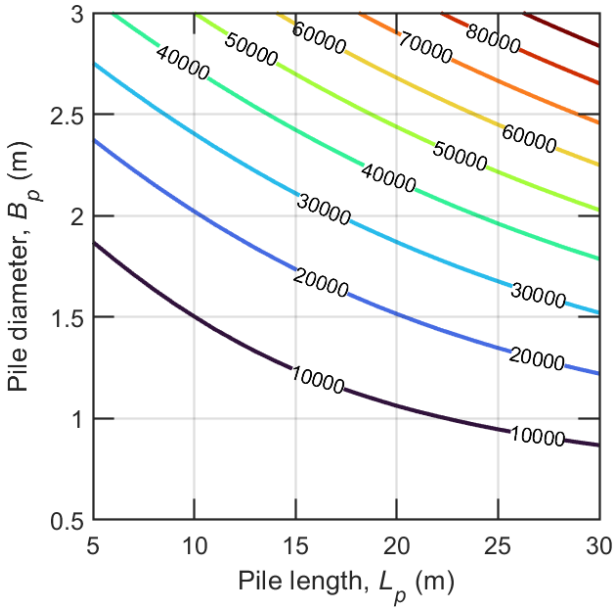

(b)

Figure 5.7. (a) Response surface and (b) contour plot of global warming impact as a function of pile dimensions

5.8 Connecting Reliability and Global Warming Impact of Drilled Shaft

Given a soil profile, load condition, random soil properties (see Figure 3.2 and Table 5.1), and other random variables related to pile dimensions and modeling, the pile dimensions are calculated N times in MCS. The corresponding global warming impact is then estimated using the second-order regression model with interaction effect (see Table 5.3) to obtain the mean and standard deviation of GWP. Parametric studies are performed by varying the means of the random variables within practical ranges as summarized in Table 5.1. The parametric studies are conducted to understand the sensitivity of global warming impact with respect to the random variables. MCS is used to perform simulations in which the random variables are defined with corresponding mean, COV, and distribution, and the pile dimensions are adjusted until the specified target probability of failure is reached. Parametric studies are conducted, for all profiles, to investigate the change in the means and standard deviations of GWP with respect to change in the means of (i) ϕ_c, (ii) D_R,

(iii) γ_{soil}, (iv) K_0, (v) M_β, (vi) M_{qb}, and (vii) ratio of *LL* to *DL* (*LL*/*DL*). The mean values of soil properties were fixed to the values shown in Figure 3.2, the mean values of model uncertainties are fixed to the values shown in Table 1, and *LL*/*DL* is fixed to 1, except the variable of interest. For example, given a drilled shaft is to be designed for Profile 1 and the following conditions are assumed in MCS: (i) *DL* = 2000 kN and *LL* = 2000 kN or *LL*/*DL* = 1, (ii) fixed-length approach (L_p = 15 m), (iii) fixed mean D_R = 70%, K_0 = 0.45, (iv) fixed mean M_β =1 and M_{qb} =1, (v) target p_f = 10^{-3}, and (vi) ϕ_c varied from 28 to 37°, the pile diameter is calculated. Other variables in (i) – (v) are varied to study their effects. The global warming impact of the simulated designs are then estimated using the second-order regression model with interaction effect (Table 5.3) to understand the connection between reliability and environmental sustainability of drilled shaft.

The direct relationship between selection of target probability of failure and global warming impact is studied through the use of FORM. The mean values of soil properties are taken from the values shown in Figure 3.2, and the mean values of other random variables are assumed to be equal to the values shown in Table 5.3, otherwise mentioned. To understand the role of LRFD in reducing global warming impact of drilled shaft, the direct relationship between resistance factors and global warming impact are also examined. The LRFD is performed by solving the pile diameter (assuming fixed L_p = 15 m) from the expression below:

$$(\mathrm{RF})_s Q_{sL}^{(n)} + (\mathrm{RF})_b Q_{b,ult}^{(n)} = (\mathrm{LF})_{DL}(\mathrm{DL})^{(n)} + (\mathrm{LF})_{LL}(\mathrm{LL})^{(n)} \tag{5.41}$$

where $(\mathrm{RF})_s$ and $(\mathrm{RF})_b$ are the resistance factors for shaft resistance and base resistance, respectively, $(\mathrm{LF})_{DL}$ and $(\mathrm{LF})_{LL}$ are the load factors for dead load and live load, respectively, and $Q_{b,ult}^{(n)}$ and $Q_{sL}^{(n)}$ are the ultimate base resistance and limit shaft resistance, respectively, computed deterministically, and *DL* and *LL* are the deterministic dead load and live load, respectively. The resistance factors are obtained from Basu and Salgado (2012) as the exact same subsurface profiles

are considered in this study. Table 5.7 summarizes the resistance factors for different probabilities of failure and soil profiles (Figure 3.2). LF_{DL} = 1.25 and LF_{LL} = 1.75 are assumed as recommended by AASHTO (2007). The deterministic ultimate base and limit shaft resistances are calculated using Equations (5.11) and (5.12) assuming M^{bias} and M are equal to 1. The pile diameter calculated using LRFD is then used to compute the total volume concrete and steel, and the volumes are inputted in the LCA to estimate the corresponding global warming impact.

Table 5.7. Resistance factors for LRFD of drilled shafts (adapted from Basu and Salgado, 2012)

		Probability of failure, p_f			
		10^{-3}		10^{-4}	
Soil profile	**Statistics**	**$(RF)_s$**	**$(RF)_b$**	**$(RF)_s$**	**$(RF)_b$**
1	Mean	0.805	0.916	0.704	0.809
	Maximum	0.851	0.984	0.760	0.947
	Minimum	0.745	0.789	0.663	0.708
2	Mean	0.801	0.970	0.715	0.831
	Maximum	0.852	1.067	0.808	1.036
	Minimum	0.774	0.890	0.657	0.706
3	Mean	0.823	0.959	0.723	0.851
	Maximum	0.861	1.091	0.814	1.062
	Minimum	0.789	0.867	0.667	0.734
4	Mean	0.821	0.955	0.721	0.848
	Maximum	0.856	1.088	0.807	0.807
	Minimum	0.789	0.862	0.667	0.667
5	Mean	0.815	0.956	0.713	0.847
	Maximum	0.851	1.088	0.799	1.057
	Minimum	0.766	0.856	0.654	0.730

5.9 Results

The results of RBD and LCA of drilled shaft are connected such that the relationship between the reliability (or target probability of failure) and global warming impact of drilled shaft is studied. The results of parametric are provided which illustrate the effects of (i) soil properties, (ii) model uncertainties, and (iii) ratio of live load to dead load, to the global warming impact of drilled shafts. The global warming impact of drilled shafts, designed using LRFD method, are

quantified to understand the effects of resistance factors to the global warming impact. Lastly, charts for estimating the GWP of drilled shafts for different target probabilities of failure and ratios of live load to dead load are developed.

5.9.1 Parametric Study

Figure 5.8 show the means and standard deviations of global warming impact (measured in GWP or kg of CO_2e) with respect to the means of input random variables considered in the study. It is observed that increasing the means of ϕ_c, D_R, M_β, and M_{qb} results in reducing the means of GWP. This reduction is expected because higher values ϕ_c and D_R imply stronger soils which require less pile capacity resulting in lower use of construction materials. However, varying the relative density of the upper layer in profiles 3-5 has minimum impact on GWP because the base resistance controls the total capacity of drilled shaft for these profiles. A similar trend is observed with the model uncertainty variables M_{qb} and M_β, are increased. Mathematically, if the values of M_{qb} and M_β are less than 1, reduced capacities of drilled shaft are calculated; hence, the mean GWPs are increased accordingly. Increasing the ratio of *LL* to *DL* while *DL* = 2000 kN increases the means of GWP because the total applied load (*LL* + *DL*) is increased as *LL*/*DL* increases. The standard deviations of GWP are increased or decreased proportionally to the means of GWP because COV of GWP is more or less constant to approximately 0.041 (ranging from 0.039 to 0.042) for all soil profiles and parametric studies conducted. Table 5.8 summarizes the sensitivities of GWP with respect to the random variables considering all soil profiles. The sensitivities were computed by dividing the percent changes in GWP by the percent changes in the input variables. GWP is most sensitive to unit weight of soil with a sensitivity value of -4.11 for homogeneous soil profiles. In contrast, GWP appears to be less sensitive to the unit weight of soil for layered profiles because relatively lower variation in GWP was observed when increasing the D_R of upper layer

(unit weight of soil is estimated as a function of D_R). GWP appears to be quite sensitive to ϕ_c and appears to be relatively less sensitive to model uncertainties and applied load.

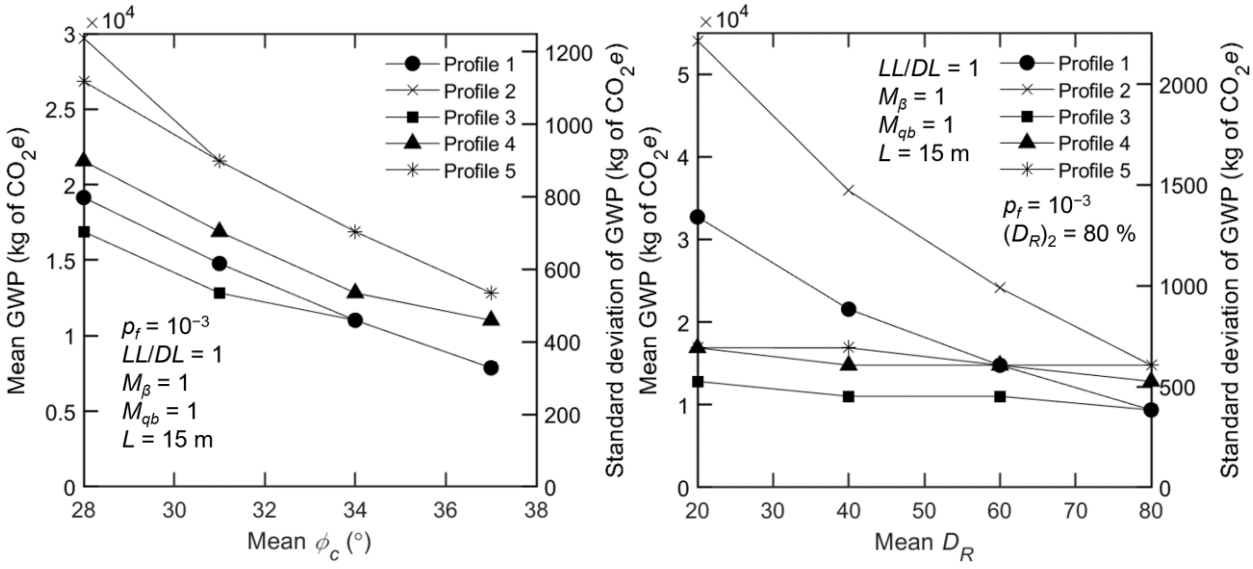

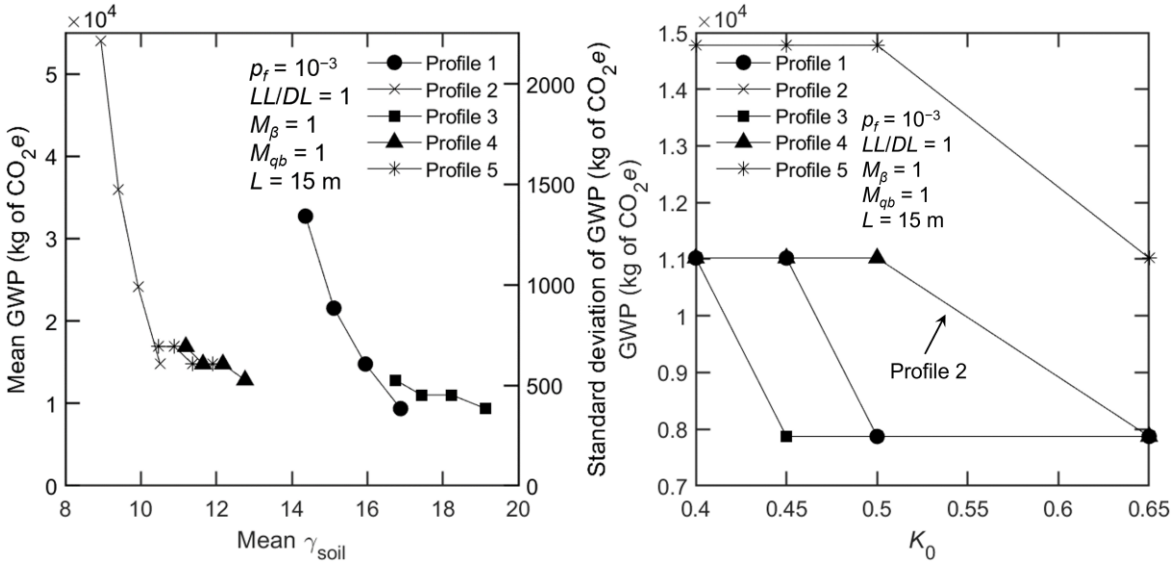

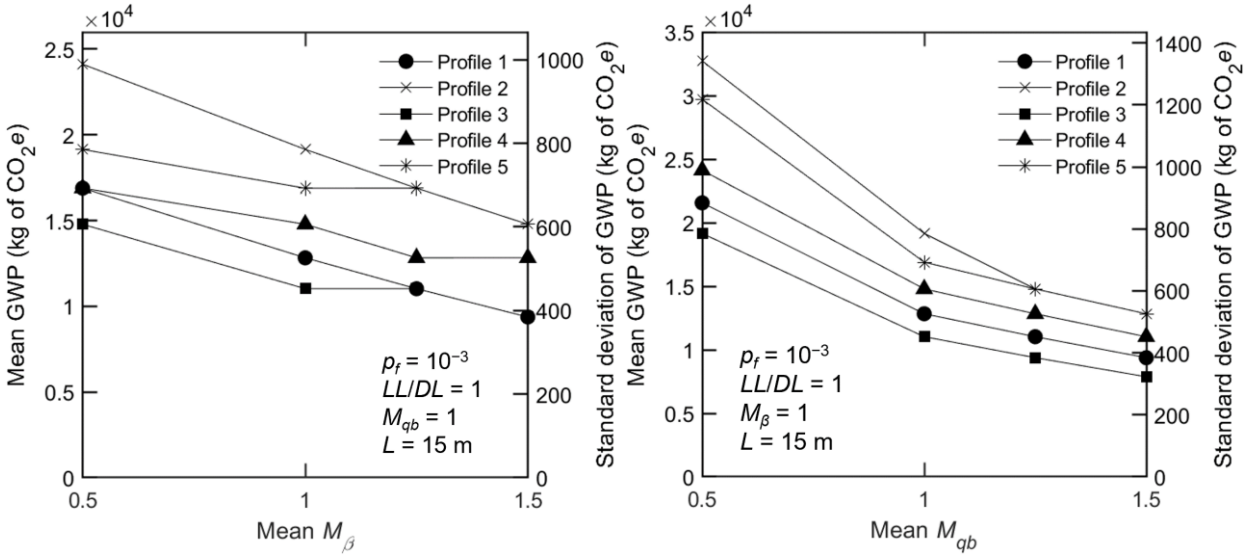

(e)

(f)

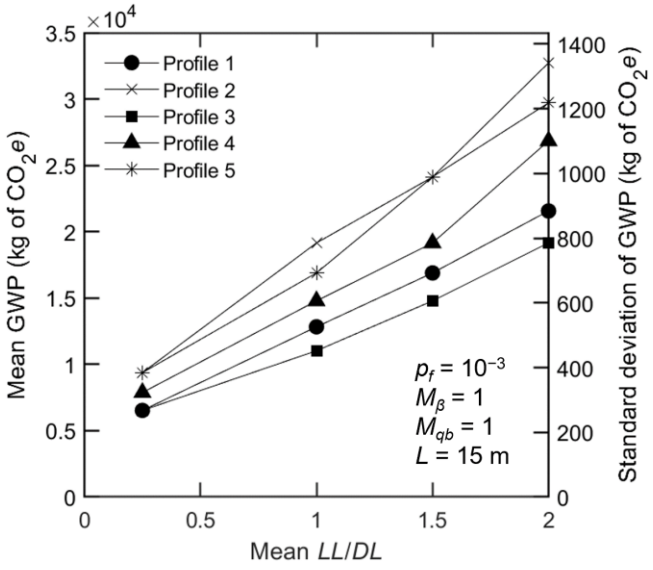

(g)

Figure 5.8. Variation of mean global warming impact for different means of (a) critical state friction angle, (b) relative density of soil, (c) unit weight of soil, (d) coefficient of lateral earth pressure at rest, (e) model uncertainty associated with unit base resistance, (f) model uncertainty associated with unit shaft resistance, and (g) ratio of live load to dead load

Table 5.8. Sensitivity of GWP with respect to input variables

Input variable	Sensitivity for homogeneous profiles (Figure 3.2(a) – (b))	Sensitivity of layered profiles (Figure 3.2(c) – (e))
Critical-state friction angle, ϕ_c	-1.80	-1.60
Relative density, D_R	-0.24	-0.07
Unit weight of soil, γ_{soil}	-4.11	-1.50
Model uncertainty associated with $q_{b,10\%}$, M_{qb}	-0.21	-0.14
Model uncertainty associated with q_{sL}, M_{β}	-0.29	-0.28
Ratio of live load to dead load, LL/DL	0.34	0.31

5.9.2 Relationship Between Reliability and Global Warming Impact

The direct relationship between the reliability (or probability of failure) of drilled shaft and their corresponding global warming impact is illustrated in Figure 5.9. Two soil profiles were considered – one homogeneous (Profile 1) and one layered (Profile 4) with the mean values of soil properties shown in Figure 3.2. The drilled shafts were designed using FORM for different target probability of failures assuming the means of the random variables are equal to the values shown in Figure 3.2 and Table 5.1. Both fixed length approach assuming L_p = 15 m, and fixed diameter design approach with B_p = 0.9 m were considered. The global warming impacts of the drilled shafts were directly computed from LCA. According to Figure 5.9, the GWP appears to decrease following a step-like function as the target probability of failure is increased. For example, there is a significant reduction in GWP as the target probability of failure approaches 5.0×10^{-5} and 2.0×10^{-4}. Identifying the points, at which the global warming impact start to show drastic changes, can be useful information when optimizing pile designs with respect to reliability and environmental sustainability. For example, for the particular designs shown in Figure 5.9, the designer is informed that designs with target p_f ranging $5.0\times10^{-5} \leq p_f \leq 2.0\times10^{-4}$ will result in the

same GWP for drilled shaft (in Profile 4 designed with fixed-length approach). Fixed-diameter designs resulted in lower GWPs compared to the fixed-length designs because the effect of pile diameter to the total volume of construction materials (i.e., concrete and steel) is greater than that of pile length; hence, higher GWPs are observed accordingly. It is desirable that the fixed-diameter approach is used in designing drilled shaft unless the pile needs to reach a certain depth to the bearing stratum.

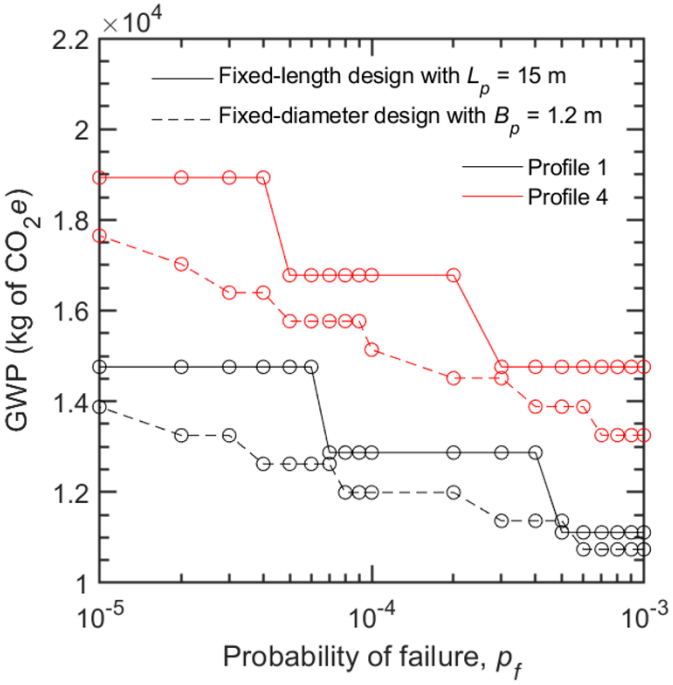

Figure 5.9. Relationship between global warming impact and probability of failure of drilled shaft designs

The variations of Figure 5.9 (fixed-length design with L_p = 15 m and Profile 1) with respect to the variability of means of (i) ϕ_c, (ii) D_R, (iii) γ_{soil}, (iv) K_0, (v) M_β, (vi) M_{qb}, and (vii) LL/DL are investigated and shown in Figure 5.10. The red line indicates the designs when the above variables are fixed to the means (see Figure 3.2 and Table 5.1). The ranges of p_f for which the GWP values stay constant are slightly different compared to the reference red line. For example, for a fixed-length design with mean ϕ_c = 33°, the constant ranges of GWP are $10^{-5} \leq p_f \leq 6.0\times10^{-5}$, 7.0×10^{-5}

$\leq p_f \leq 4.0\times10^{-4}$, and $5.0\times10^{-4} \leq p_f \leq 10^{-3}$, which implies that using the upper bounds of target p_f are beneficial when optimizing designs for both reliability and global warming impact. Therefore, for a soil with mean $\phi_c = 28°$ in Profile 1, the recommended target p_f values are $\{2.0\times10^{-5}, 10^{-4}$, and $10^{-3}\}$.

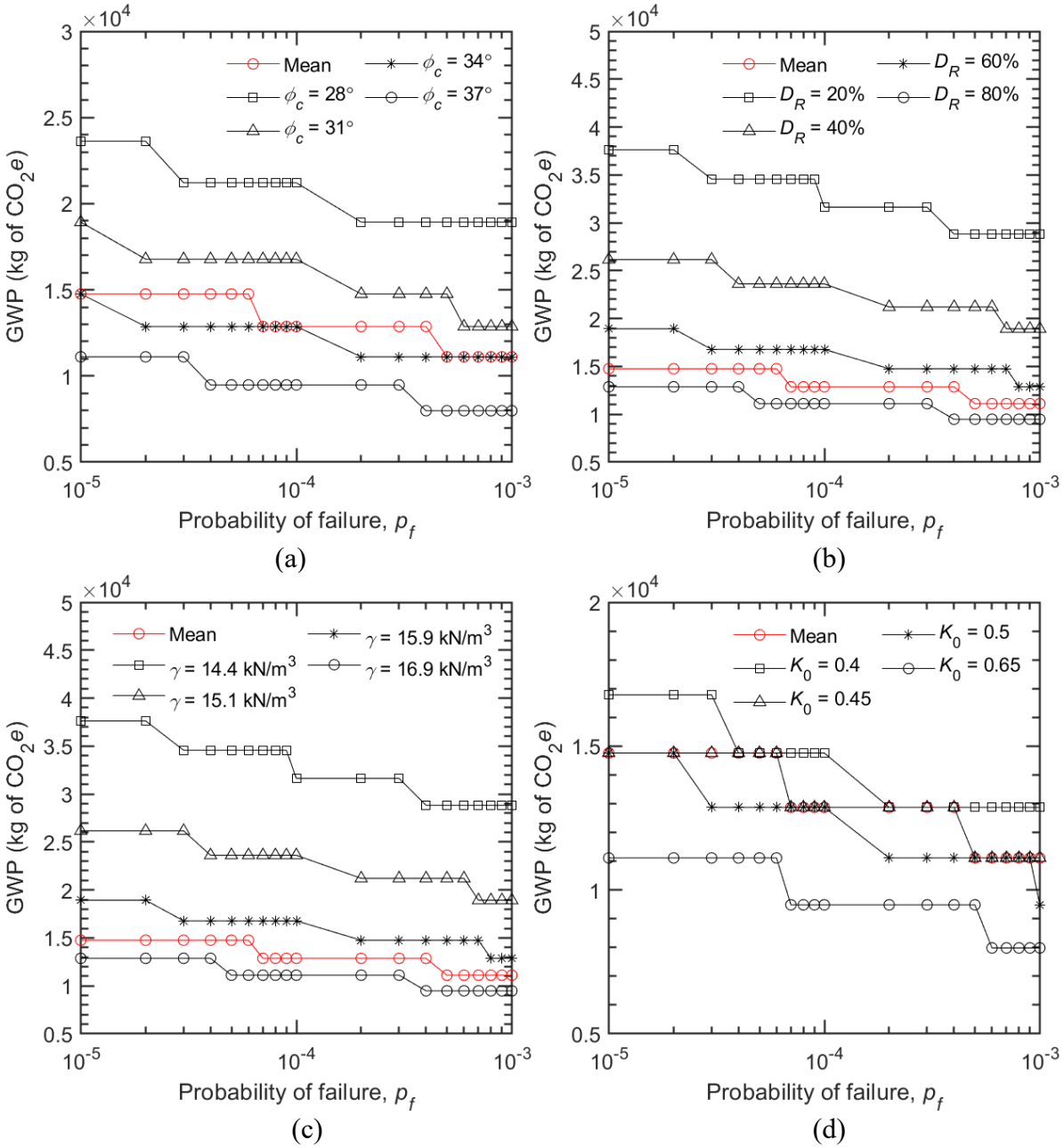

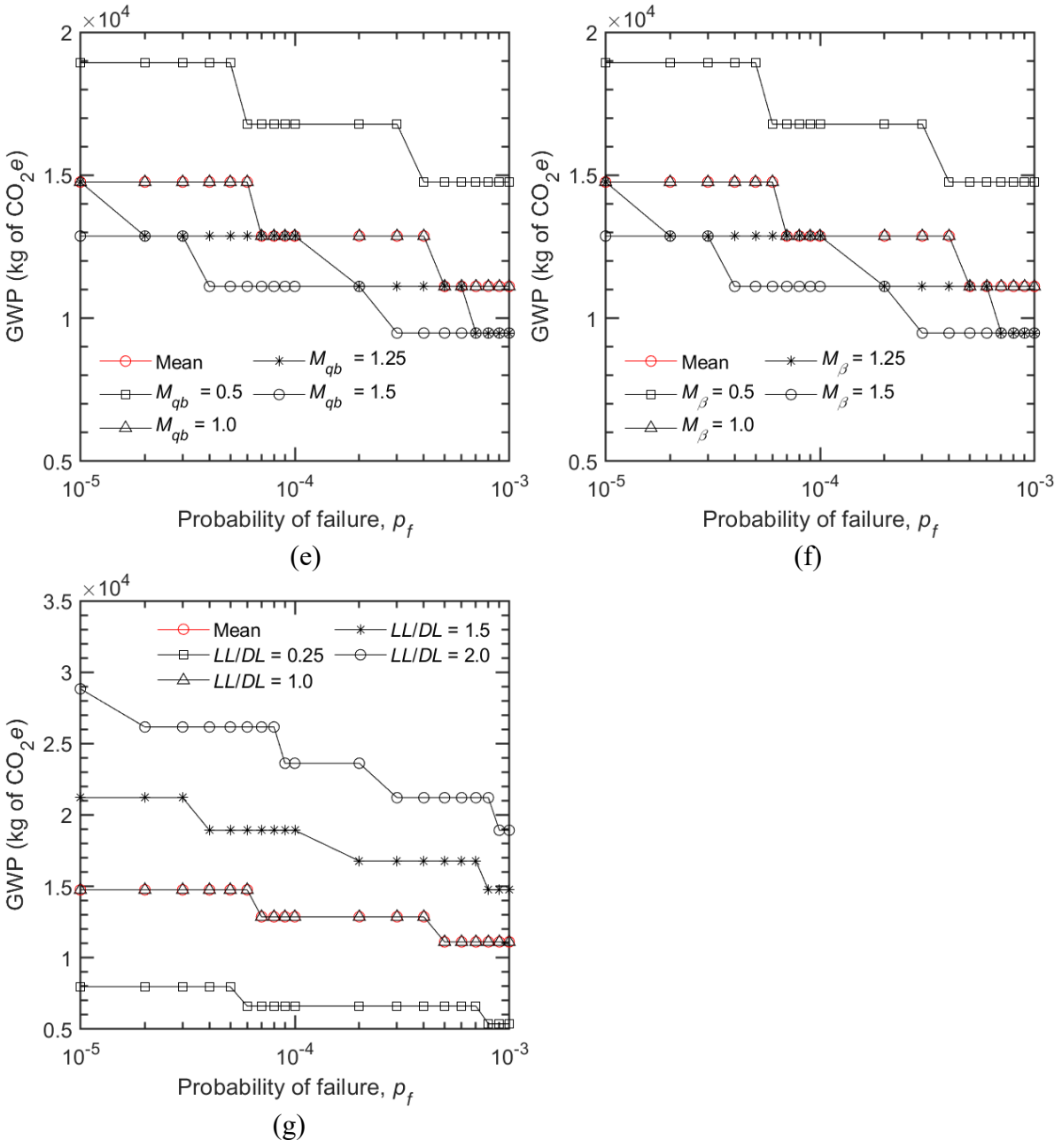

Figure 5.10. Variation of global warming impact at different probabilities of failure for soil profile 1 and for different means of (a) critical state friction angle, (b) relative density of soil, (c) unit weight of soil, (d) coefficient of lateral earth pressure at rest, (e) model uncertainty associated with unit base resistance, (f) model uncertainty associated with unit shaft resistance, and (g) ratio of live load to dead load

5.9.3 Global Warming Impact of LRFD Designs

With the increased adaptation of LRFD design methodology in geotechnical engineering, the relationship of GWP with the resistance and load factors and were also examined, as shown in Figure 5.11. The ultimate base capacity is reduced by the resistance factor $(RF)_b$, the limit shaft capacity of drilled shaft is reduced by the resistance factor $(RF)_s$, the dead load applied to the drilled shaft is factored by the load factor $(LF)_{DL}$, and the live load is increased by $(LF)_{LL}$. In this study, the mean resistance factors from Basu and Salgado (2012) (see Table 5.7) were used to perform the LRFD of drilled shafts. According to Figure 5.11(a), it is observed that GWPs of drilled shaft designed using LRFD do not vary significantly across different soil profiles. The GWPs in Figure 5.11(b) is approximately the same or lower than the GWP values shown in Figure 5.9. Therefore, use of LRFD for design of drilled shaft appears to be adequate as an effort to reduce global warming impact.

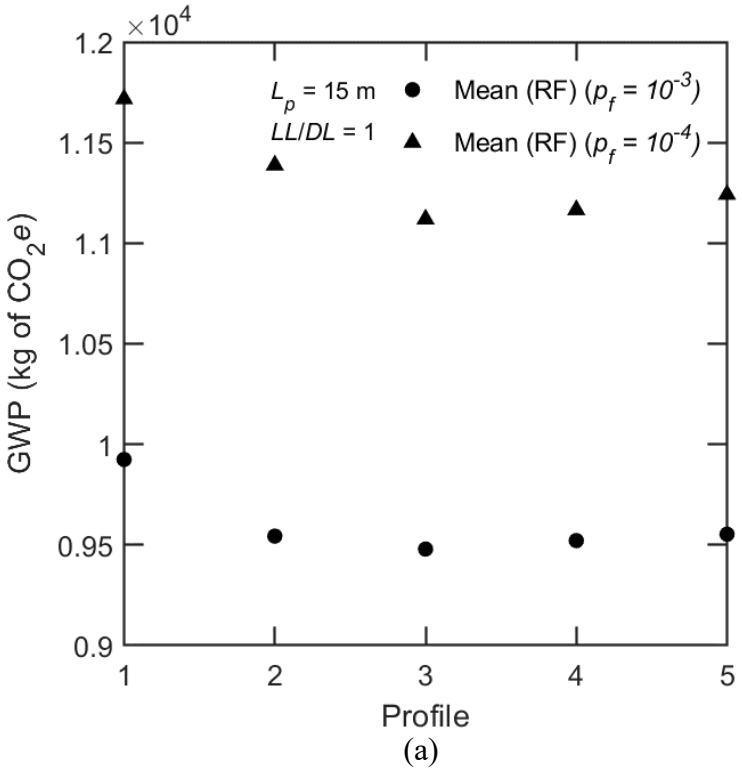

(a)

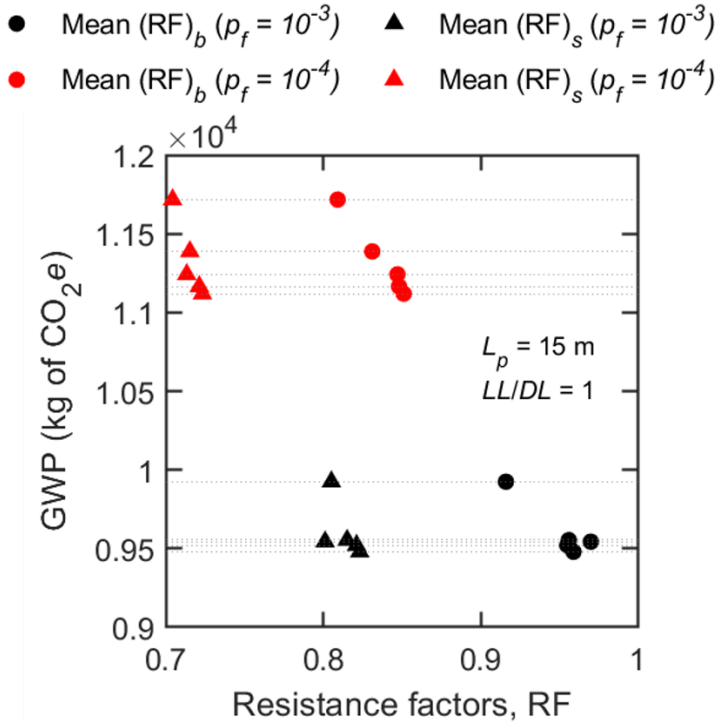

(b)

Figure 5.11. Global warming impact of drilled shaft using LRFD method assuming resistance factors from Basu and Salgado (2012) and $(LF)_{DL}$ = 1.25 and $(LF)_{LL}$ = 1.75 (a) different soil profiles and (b) with relation to resistance factors for all profiles

5.9.4 GWP Estimation Charts

LCA can be a complex and time-consuming analysis to conduct on a daily basis, especially for practitioners who have limited experience with LCA and who do not have access to LCA software programs. Therefore, design charts can be used alternatively to estimate global warming impact of typical drilled shaft designs for given soil and loading conditions. Figure 5.12 shows different drilled shaft design configurations that meet different target reliability indices and under different load ratios for Profile 1. Figure 5.13 shows the projected view of Figure 5.12 along with contours of global warming impact obtained using regression analysis and presented in Figure 5.7(b). For example, a drilled shaft design with 5 m of length and 2.5 m of diameter with $p_f = 5.5 \times 10^{-5}$ is expected to result in approximately 22,500 GWP or kg of CO_2e. Figure 5.13(b) can be used to estimate drilled shaft designs for different load ratios and $p_f = 10^{-3}$. Figure 5.13 can be

recreated for different soil profiles, load conditions, target probability of failures and other variables as necessary.

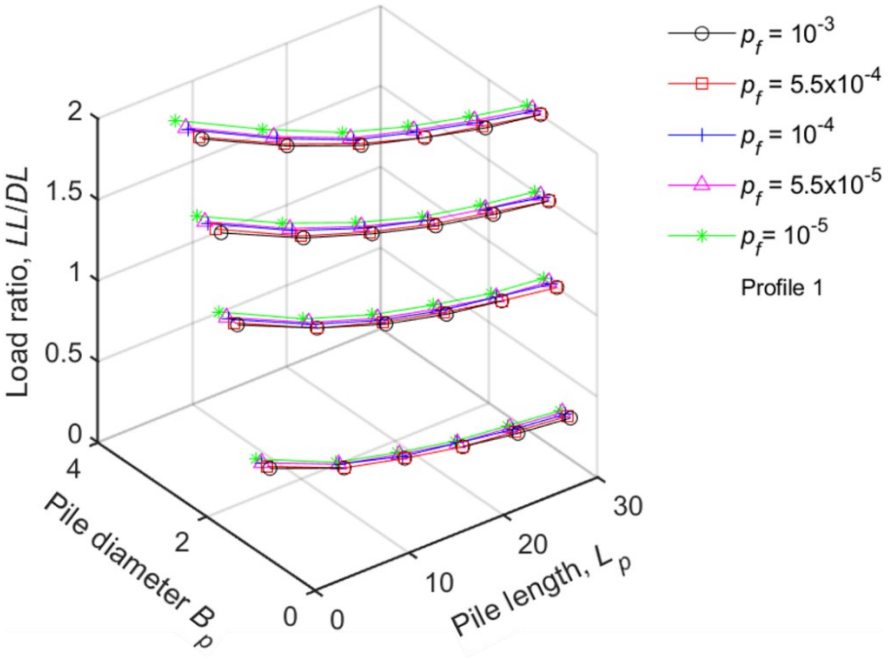

Figure 5.12. Relationship of pile diameter, pile length, load ratio, and probability of failure

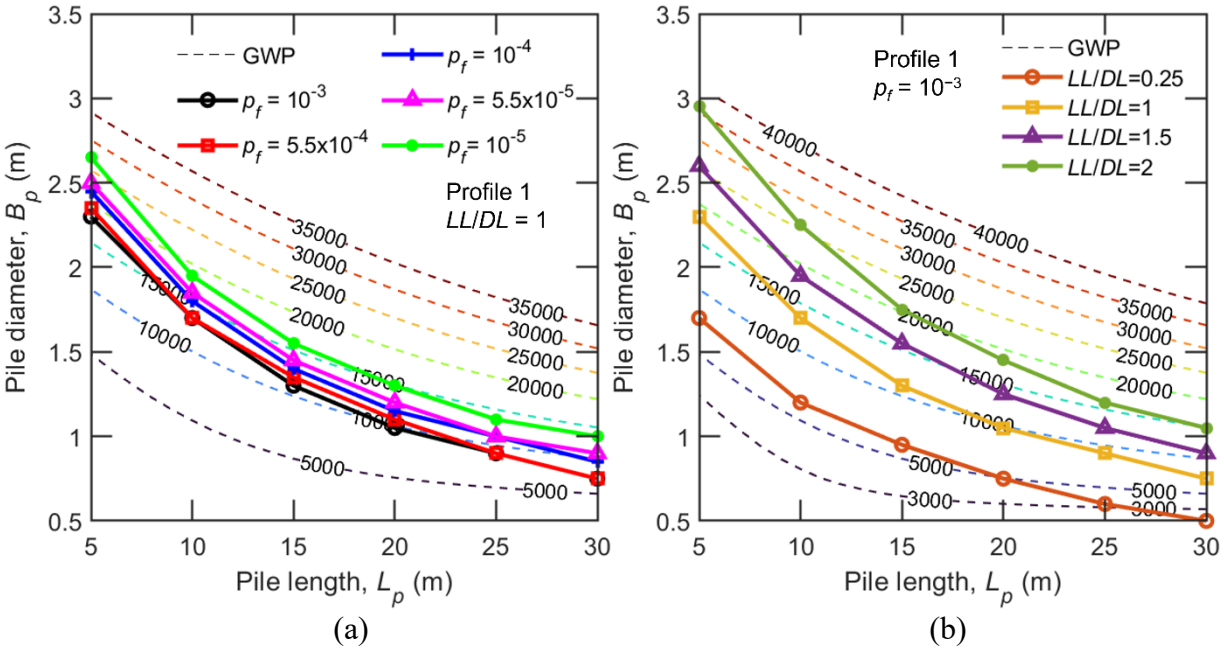

Figure 5.13. 2D projection of Figure 5.12 with GWP contour lines (a) for different target probability of failure and (b) for different load ratios

To validate the results of MCS, two types of goodness-of-fit tests – Chi-square test and Kolmogorov-Smirnov test – were conducted to evaluate if the input random variables (ϕ_c, D_R, γ_{soil}, M_β, M_{qb}, DL, and LL) and output variables ($Q_{b,ult}$ and Q_{sL}) in MCS follow the prescribed probability distributions (i.e., normal and log-normal distributions). The test results initially indicated that the random variables do not follow the prescribed probability distributions; however, it is found that goodness-of-fit tests can provide misleading results if the sample size is very large because small discrepancies accumulate significantly (Fenton and Griffiths, 2008). With the reduction of sample size N from 271000 to 100, the goodness-of-fit test indicated that the random variables follow the prescribed probability distributions. The probabilities of failure obtained from FORM were then validated by comparing with those obtained from MCS. The percent differences in probability of failure between the two methods ranged from 3 to 34%. However, the higher percent differences were observed for target $p_f \leq 10^{-5}$ which makes sense because the lower the target p_f is the results of MCS become more sensitive to the number of failures counted in the MCS. Further, target $p_f \leq 10^{-5}$ is considered very low for practical cases. Hence, the results of FORM are considered adequate.

5.10 Summary

In this chapter, the relationship between the reliability and environmental sustainability of drilled shaft was investigated. First-order reliability method (FORM) was used to perform reliability-based design of drilled shaft assuming uncertainties in the (i) soil properties, (ii) design equations for ultimate and serviceability limit states, (iii) applied loads, and (iv) pile diameter. Five target probabilities of failure, ranging from 10^{-3} to 10^{-5}, were considered in the reliability-based design of drilled shafts. To facilitate the investigation on the relationship between the reliability and environmental impact, multiple regression analysis was used to develop regression models for

estimating the global warming impact of drilled shafts which are particularly useful for conducting the parametric study. Decreasing trends in global warming impact were observed as (i) stronger soil was assumed (e.g., increased relative density, friction angle, and unit weight of soil), (ii) higher uncertainties in design equations were applied, and (iii) the ratios of live load to dead load were decreased. Based on the parametric study, the global warming impact of drilled shaft is the most sensitive to the change in critical-state friction angle and unit weight of soil. The relationship between global warming impact of drilled shaft and target probabilities of failure (used in FORM) was plotted, and a decreasing step-like trend was observed. LRFD was also used to further understand the relationship between global warming impact of drilled shaft and resistance factors. As the resistance factors for the ultimate base capacity and limit shaft capacity of drilled shaft increased, the global warming impact of drilled shaft decreased because higher resistances are assumed in the design. Hence, less quantities of materials (e.g., concrete and steel) are used in construction. The results reported in this chapter can be used as a basis for optimizing reliability-based designs of drilled shaft with global warming impact considerations. Charts for estimating the global warming impact of drilled shaft are developed in which the GWP of drilled shaft is obtained as a function of (i) pile dimensions, (ii) target probabilities of failure, and (iii) ratio of live load to dead load. The charts are intended for practitioners for quick estimation of global warming impact without conducting complex LCA calculations.

5.11 List Of Symbols

Notation	Description
$\hat{y}$	Predicted value
$(LF)_{DL}$ and $(LF)_{LL}$	load factors for dead load and live load, respectively
$(RF)_s$ and $(RF)_b$	Resistance factors for shaft resistance and base resistance, respectively
A_b	Cross-sectional area of pile base

List of Symbols (continued).

Notation	Description
A_s	Surface area of pile foundation
B_p	Pile diameter
c_i	Coded variable
CO_2e	Equivalent mass of carbon dioxide
d	Standardized residual
DL	Applied dead load
D_R	Relative density of soil
D_β	Minimum distance between the origin and most probable failure point in the standard normal space
e	residual
F_0	F statistic value that follows the $F_{k,\, n-k-1}$ distribution
$F_X(x)$	Cumulative distribution function of random variable X
$f_X(x)$	Probability density function of random variable X
$F_{\alpha,k,n-k-1}$	F critical value at preselected significance level α_s
$g(-)$	Performance function
H_0 and H_1	Hypothesis
h_{ii}	Diagonal element of H matrix which maps the vector of observed values into a vector of fitted values
k	Total number of variables in regression analysis
K_0	Coefficient of lateral earth pressure at rest
LL	Applied live load
L_L	Langrage function
L_p	Pile length
L_s	Least square function
M_{qb}	Random part associated with $q_{b,10\%}$ equation
M_{qb}^{bias}	Deterministic bias associated with $q_{b,10\%}$ equation
MS_E	Mean square caused by error
MS_R	Mean square caused by regression
M_β	Random error of the uncertainty in modeling β in the q_{sL} equation
M_β^{bias}	Deterministic bias of β model in the q_{sL} equation
n	Total number of observations
N	Number of observations or realizations
p_A	Atmospheric pressure
p_f	Probability of failure
$p_{f,\text{target}}$	Target probability of failure
Q	Load applied to the system
$q_{b,10\%}$	Ultimate unit base resistance for 10% relative settlement criterion
$Q_{b,ult}$	Ultimate base resistance
$q_{b,ult}$	Ultimate unit base resistance
Q_{sL}	Limit shaft resistance
q_{sL}	Limit unit shaft resistance
Q_{ult}	Total ultimate capacity

List of Symbols (continued).

Notation	Description
r	Externally studentized residual
R	Resistance (capacity) of the system
R^2	Coefficient of multiple determination
R^2_{adj}	Adjusted coefficient of multiple determination
R^2_{pred}	Coefficient of multiple determination for prediction
S	Safety margin
SS_E	Sum of squares of error
SS_R	Sum of squares of regression
SS_T	Total sum of squares
t_s	Studentized residual
X	Random variable
Y	Random variable in standard normal space
y_r	Response surface
$z_{\alpha/2}$	The point on standard normal distribution satisfying P [Z > $z_{\alpha/2}$]
α_s	Significance level
β_{HL}	Hasofer-Lind reliability index
β_i	Regression coefficient
γ_{soil}	Unit weight of soil
ε	Error
ε_{max}	Maximum error on probability of failure at preselected confidence level
ζ	Shape parameter of lognormal distribution
λ	Scale parameter of lognormal distribution
λ_L	Lagrange's multiplier
μ	Mean of probability distribution
μ^N	Equivalent normal mean of non-normal random variable X
ξ	Controllable input variable in natural variable
$\xi_{\max}$ and $\xi_{\min}$	Upper and lower bounds of the natural variable ξ_i
σ	Standard deviation of probability distribution
σ^2	Variance of probability distribution
σ'_h	Horizontal effective stress
σ^N	Equivalent normal standard deviation of non-normal random variable X
σ'_v	Vertical effective stress
$\Phi(-)$	Cumulative distribution function of standard normal distribution
$\phi(-)$	Probability density function of standard normal distribution
ϕ_c	Critical-state friction angle of soil

CHAPTER 6: RELIABILITY AND SUSTAINABILITY OF MSE WALLS

6.1 MSE Wall Considered

MSE wall reinforced by steel strips (inextensible reinforcement) or geogrids (extensible reinforcement) are considered in this study (see Figure 4.1). The MSE wall is subjected to traffic load represented by a uniformly distributed live load and applied on the surface of backfill soil.

6.2 Probabilistic Characterization and Quantification

6.2.1 Soil Variables

Friction angles and unit weights of (i) backfill, (ii) retained, and (iii) foundation soil are treated as random variables to account for the variability in soil properties. The coefficient of active lateral earth pressure K_A is indirectly considered as a random variable because it is calculated based on the friction angles of retained soil (for external stabilities) and backfill soil (for internal stabilities) (see Table 4.2).

Table 6.1 lists the characteristics of random variables and values of deterministic values used in the design of MSE walls. According to Baecher and Christian (2003), the unit weight of soil follows a normal distribution with a COV of 0.05. The means of the unit weight of backfill, retained, and foundation soil (γ_b, γ_r, γ_f) are 19, 19, and 16 kN/m^3, respectively. The friction angle of soil follows a normal distribution with a COV of 0.025 (Verdugo and Ishihara, 1996). The means of the critical-state friction angle of backfill, retained, and foundation soil (ϕ_b, ϕ_r, ϕ_f) are 36, 32, and 30°, respectively. For conducting the parametric study, to understand the effects of random variables to the GWP of MSE walls, the unit weights and friction angles of soil are varied within the ranges 16 – 22 kN/m^3 and 28 – 37°, respectively (Chalermyanont and Benson, 2004).

Table 6.1. Characteristics of deterministic and random variables for MSE walls

Deterministic variable	Value or range			
Height of wall, H	7 or 5 – 15			
Thickness of geogrid, t (mm)	2.5 (Strata, 2014)			
Thickness of steel strip, t_n (mm)	4 (FHWA, 2009b)			
Width of steel strip, b (mm)	50 (FHWA, 2009b)			
Corrosion rate of steel, c_r (m/year)	12×10^{-6} for each side (FHWA, 2009a)			
Service life of Zinc coating, SL_c (year)	16 (Kim and Salgado, 2012b)			
Service life of MSE wall, SL_{MSE} (year)	75 (Kim and Salgado, 2012b)			
Length of reinforcement, L_R	$0.7H$ – $1.1H$ (FHWA, 2009b)			
Vertical spacing of reinforcement, s_v (m)	0.3, 0.45, 0.6 (Fratta and Kim, 2015; Salgado, 2008)			
Horizontal spacing of reinforcement, s_h (m)	0.6, 0.7, 0.8, 0.9, 1.0			
Random variable	**Probability distribution**	**Mean**	**Range**	**Coefficient of variation (COV)**
Unit weight of backfill soil, γ_b (kN/m^3)	Normal	19 (Salgado, 2008)	16 – 22 (Chalermyanont and Benson, 2004)	0.05 (Baecher and Christian, 2003)
Unit weight of retained soil, γ_r (kN/m^3)	Normal	19 (Salgado, 2008)	16 – 22 (Chalermyanont and Benson, 2004)	0.05 (Baecher and Christian, 2003)
Unit weight of foundation soil, γ_f (kN/m^3)	Normal	16 (Salgado, 2008)	16 – 22 (Chalermyanont and Benson, 2004)	0.05 (Baecher and Christian, 2003)
Friction angle of backfill soil, ϕ_b (°)	Normal	30 (Salgado, 2008)	28 – 37 (Chalermyanont and Benson, 2004)	0.025 (Verdugo and Ishihara, 1996)
Friction angle of retained soil, ϕ_r (°)	Normal	32 (Salgado, 2008)	28 – 37 (Chalermyanont and Benson, 2004)	0.025 (Verdugo and Ishihara, 1996)

Table 6.1 (continued).

Random variable	Probability distribution	Mean	Range	Coefficient of variation (COV)
Friction angle of foundation soil, ϕ_f(°)	Normal	36 (Salgado, 2008)	28 – 37 (Chalermyanont and Benson, 2004)	0.025 (Verdugo and Ishihara, 1996)
Tensile strength of geogrid, T (kN/m)	Normal	30 (Strata, 2014)	20 – 200 (Strata, 2014)	0.1 (Low and Tang, 1997; Sayed *et al*. 2008)
Yield strength of steel strip, f_y (MPa)	Normal	448 (Kim and Salgado, 2012b)	450 – 600 (Kim and Salgado, 2012b)	0.05 (Kim and Salgado, 2012b)
Live load surcharge, q (kN/m^2)	Log-normal	[1] $= \gamma_b h_{eq}$ or 11.4 AASHTO (2017)	0 – 21 (Chalermyanont and Benson, 2004)	0.205 (Kim and Salgado, 2012a)

[1] h_{eq}: the equivalent height of soil for vehicular load

6.2.2 Reinforcement Material Properties

The strength of reinforcement material is an important characteristic that enhances the resistances against tension and pullout failures. Two types of reinforcement are considered in this study – steel strip (representing an inextensible reinforcement material) and geogrid (representing an extensible material). The tensile strength of geogrid T and yield strength of steel strip f_y are assumed to be random variables because variations in them will have a significant influence on the stability of the wall structure (Chalermyanont and Benson, 2004; 2005; Sayed *et al*., 2008). The tensile strength of geogrid is assumed to follow a normal distribution with COV of 0.1 (Low and Tang, 1997; Sayed *et al*. 2008), and the yield strength of steel strip is assumed to follow a normal distribution with a COV of 0.05 (Kim and Salgado, 2012b). A mean T = 30 kN/m and

mean f_y = 448 MPa are assumed, and ranges of T = [20, 200] kN/m (Strata, 2014) and f_y = [450, 600] MPa (Kim and Salgado, 2012b) are assumed for the parametric study.

6.2.3 Design Equations

The MSE wall is designed against five failure modes (limit states), out of which three modes are related to external stabilities (e.g., sliding, overturning, and bearing capacity) and two modes are internal stabilities (e.g., tension and pullout) (Clayton *et al*. 1993). It is assumed that if failure occurs in any of the modes mentioned above, the entire system (MSE wall) fails. Table 4.2 summarizes the resisting and driving forces/moments (denoted by R and D, respectively) for the five failure modes. Soil properties (i.e., γ_b, γ_b, γ_b, ϕ_b, ϕ_r, ϕ_f), reinforcement material properties (T and f_y), and applied load (i.e., q) in R and D of Table 4.2 are represented as random variables with specified probability distributions, means, and COVs.

6.2.4 Applied Loads

The live load surcharge q is estimated based on the unit weight of backfill soil and h_{eq} which is the equivalent height of soil for vehicular load (see Equation (4.1)). If the mean γ_b = 19 kN/m^3, the mean q is estimated to be 11.4 kN/m^2. Based on Kim and Salgado (2012a), the live load surcharge is assumed to follow a log-normal distribution with a COV of 0.205. For conducting the parametric study, the mean q is varied from 0 to 21 kN/m^2 (Chalermyanont and Benson, 2004).

6.3 Reliability Analysis of MSE Walls

In this study, reliability analysis of MSE wall is conducted using FORM (Bathurst *et al*., 2019; Chalermyanont and Benson, 2004; 2005; Kim and Salgado, 2012a; 2012b; Low, 2005; Sayed *et al*., 2008). In FORM, the limit state equation $g_i(X)$ for failure mode i are formulated as the difference of associated resistance and driving forces/moments:

$$g(X) = R - D \tag{6.1}$$

where X is the set of random variables $\{x_1, x_2, \ldots, x_n\}$ discussed in Section 6.2. To be conservative, the contribution of live load surcharge q to the resistance forces is neglected for all stability limit states (AASHTO, 2017). Critical-state friction angles are used to calculate the coefficient of lateral earth pressure at active state K_A because the use of peak friction angle leads to lower K_A values and underestimate driving forces (Kim and Salgado 2012a; Salgado 2008).

FORM for each failure mode is performed sequentially, and the minimum reliability index β_{HL} for all failure modes are computed following the procedures in Ang and Tang (1984). For a normally distributed random variable, the standard normal variate Y is computed using Equation (5.7). For the live load surcharge, which follows a log-normal distribution, its standard normal variate Y_q is computed as:

$$Y_q = \frac{\ln x_q - \lambda_q}{\zeta_q} \tag{6.2}$$

in which

$$\zeta = \sqrt{\ln(1 + \mathrm{COV}^2)} \tag{6.3}$$

$$\lambda = \ln(\mu) - \frac{1}{2}\zeta^2 \tag{6.4}$$

where COV is the coefficient of variation, λ and ζ are the scale and shape parameters, respectively, of lognormal distribution. The probability of failure p_f is then calculated using $p_f = 1 - \Phi(\beta_{HL})$.

6.4 Reliability-based MSE Wall Design

For an MSE wall (Figure 4.1) with a given wall height H, soil properties and live load surcharge applied on top of the backfill soil (see Table 6.1), the goal of reliability-based design is to determine the configurations of (i) the length of reinforcement L_R (or ratio of L_R to H), (ii)

vertical spacing of reinforcement s_v, and (iii) horizontal spacing of reinforcement s_h, which meet the target reliability requirements. In this study, the target probabilities of failure are $p_f = \{10^{-3}, 5.5 \times 10^{-4}, 10^{-4}, 5.5 \times 10^{-5}, 10^{-5}\}$. To simplify the design process, the s_h of steel strip is assumed to be 750 mm (FHWA, 2009b) and geogrid is assumed to be continuous throughout the length of wall (s_h = 1000 mm used). Given the typical thickness of compaction lift is 150 mm, the s_v of reinforcement is assumed to be discrete at 300, 450, or 600 mm (Fratta and Kim, 2015; Salgado, 2008). Assuming L_R typically ranges from 0.7H to 1.1H (FHWA, 2009b) and for given s_v and s_h, L_R is increased until the system p_f (i.e., minimum p_f considering all failure modes) is equal to or exceeds the target p_f.

Once the design dimensions are determined, the masses of (i) reinforcement material, (ii) excavated soil, and (iii) backfill soil are estimated which are used as inputs in LCA of MSE walls. The total mass of reinforcement material is estimated assuming ρ_{steel} = 7850 kg/m^3 (CEN, 2002) and ρ_{HDPE} = 950 kg/m^3 (Thinkstep, 2022). Further, the masses of excavated soil and backfill soil are estimated based on the bank volume and loose volume of soil, respectively. Table 4.4 shows the procedure for calculating the masses mentioned above.

6.5 Response Surfaces for Estimating GWP

To reduce the computation times for obtaining GWP of multiple MSE wall designs, selected results of LCA and (e.g., 15 to 25 results depending on the type of reinforcement) are used to formulate regression models using which the GWP of MSE wall designs can be estimated relatively faster and easier.

In this study, a second-order regression model (see Equation (5.27)) for calculating GWP is developed as functions of the three or four variables (i.e., L_R, s_v, s_h, H) depending on the type of

reinforcement. Since the geogrid is assumed to be continuous throughout the wall, three variables (i.e., L_R, s_v, and H) are used. The height of wall is included in the regression model to develop a generic regression model that can be used with variable H. The c_i in Equation (5.27) are the design variables, L_R, s_v, s_h, H, expressed in coded variables. In response surface methodology, it is convenient to transform the natural variables to coded variables (Myers *et al*., 2009). It should be noted these regression coefficients βs are with respect to the coded variables c, which are calculated using Equation (12). For example, $\xi_{\min}$ and $\xi_{\max}$ of s_h are 0.6 and 1.0 m in natural variables and their corresponding coded variables can be expressed as −1 and +1, respectively; therefore, the coded variable corresponding to s_h = 0.7 m is −0.5 according to Equation (5.26). Table 6.2 summarizes the design variables of MSE wall (L_R, s_v, s_h, H) in coded variable format.

Table 6.2. Coded and natural variables of the design variables

Design variable	**Coded variable, *c***				
	−2	**−1**	**0**	**+1**	**+2**
L_R (m)	0.5H	0.7H	0.9H	1.1H	1.3H
s_v (m)	0.15	0.3	0.45	0.6	0.75
s_h (m)	0.4	0.6	0.8	1.0	1.2
H (m)	3	6	9	12	15

To develop the regression model in Equation (5.27), data that captures the relationships between the response y_r and the design variables c_i need to be collected. To do this in a controlled manner, experimental design is performed in which the values of design variables (factors) are varied with control (e.g., maximum, minimum, average, and other significant values) and the corresponding response y_r is obtained. Central composite design (CCD) is an experimental design that is widely used for fitting a second-order regression model (Myers *et al*., 2009). A CCD with 3 factors (k = 3) requires performing 15 trials of experiments in which design variables are set to the following standard coordinates (see Figure 6.1(a)): $2^k = 2^3 = 8$ factorial points (blue points in

Figure 6.1), $2k = 2(3) = 6$ axial points (red points in Figure 6.1(a)), and at least one center point (green point in Figure 6.1(a)). To better understand the relevance of these points, the projected top view of Figure 6.1(a) is shown in Figure 6.1(b) in which the relationships between c_1 and c_2 variables are explored. In Figure 6.1(b), assuming c_1 represents L_R and c_2 represents s_v, respectively, the factorial points examine the combinations of low and high levels of L_R and s_v. In the axial points, the levels of L_R and s_v are examined one at a time, and the center point is at the average levels of L_R and s_v. Data at these points provide important information related to the effect of each design variable c_i to the response surface y_r; hence, the regression coefficients βs define the shape of the response surface. For example, the first-order term (i.e., 2nd term in Equation (5.27)) defines the direction and steepness of y_r in a plane form, and the associated β_is are obtained based on the data at the factorial points. The interaction term (i.e., 4th term in Equation (5.27)) provides information related to the curvature (e.g., twisted plane), and β_{ij}s are also obtained from the factorial points. The axial points lie on the c_1, c_2, or c_3 axis (see Figure 6.1); therefore, they examine the effect of design variables one at a time and are used for estimation of β_{ii}s for the quadratic terms (i.e., 3rd term in Equation (5.27)). The quadratic terms are used to better characterize the curvature of response surface which may not be sufficiently modeled by the interaction terms alone. The center point is useful for testing if there exists excessive curvature in the response surface and is also useful for estimating the pure error based on the variability in the replicated responses obtained at the center point (i.e., L_R, s_v, s_h, H fixed to averages). In this study, replications at the center point are not made because it is assumed that constant GWP values are obtained for every replicated LCA. For example, the coordinate (values) of design variables at the center point expressed in natural variables is (L_R, s_v, s_h, H) = (0.9H, 0.45, 0.8, 9) according to Table 6.2. The

LCA and FORM results obtained for the given design variables are assumed to be the same; hence, replications are not necessary in this study.

The distance from the center to an axial point α defines the region of interest. For example, if one is interested in predicting y_r beyond $c_i = \pm 1$ (see Figure 6.1), $\alpha > \sqrt{1}$ is used. In this study, $\alpha = \sqrt{k}$ is assumed (Myers *et al*., 2009).

The method of least squares is used for estimating the regression coefficients in Equation (5.27). Based on the results of response surface methodology, the regression models for GWP are obtained and summarized in Table 6.3. If the regression coefficients βs are close to zero, it indicates that the corresponding terms have negligible effect on the response. A sample of response surface for estimating GWP of MSE walls with steel strips is shown in Figure 6.2. For visualization purpose, the response surfaces for GWP are plotted as functions of L_R/H and s_v (Figure 6.2(a)), L_R/H and s_h (Figure 6.2(b)), and L_R/H and H (Figure 6.2(c)). Figure 6.3 shows the corresponding contour plot of the response surface in Figure 6.2. GWP of MSE walls can be quickly estimated based on Figure 6.3. For example, an MSE wall reinforced by steel strips with $L_R/H = 0.9$ and $s_v = 0.45$ m (assuming $s_h = 0.75$ m and $H = 7$ m) will result in approximately 1500 GWP (in between 1400 and 1600 GWP contour lines in Figure 6.3(a)).

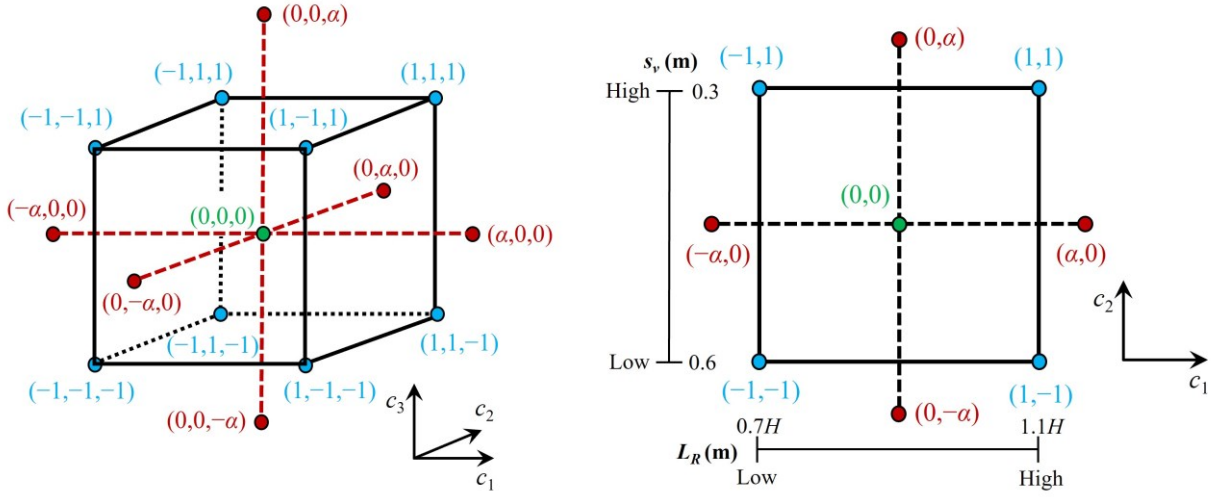

(a) (b)

Figure 6.1. Central composite design used for construction of regression models for calculating global warming potential (GWP) and reliability index β_{HL} of MSE wall (adapted from Myers *et al*. 2009) (a) 3D view (k = 3) and (b) top projected view (k = 2)

Table 6.3. Regression models for global warming impact of MSE Wall

Steel strip	Geogrid
$y_{GWP} = 2425 + 526c_1 - 570c_2$	$y_{GWP} = 1635 + 397c_1 - 275c_2 + 1113c_4$
$-402c_3 + 1516c_4$	$-2c_1^2 + 95c_2^2 + 175c_4^2$
$-65c_1^2 + 190c_2^2 - 89c_3^2 + 173c_4^2$	$-57c_1c_2 + 255c_1c_4 - 151c_2c_4$
$-98c_1c_2 - 96c_1c_3 + 329c_1c_4$	
$+143c_2c_3 - 263c_2c_4 - 259c_3c_4$	

c_1, c_2, c_3, and c_4 are the coded variables of L_R, s_v, s_h, and H, respectively (see Table 6.2)

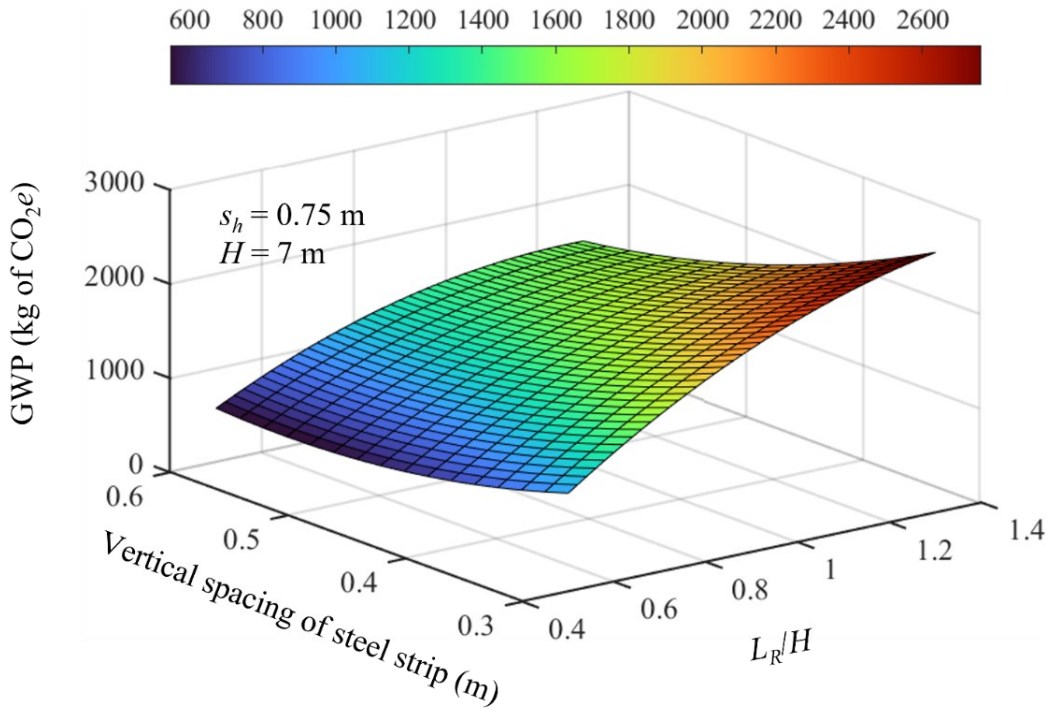
600 800 1000 1200 1400 1600 1800 2000 2200 2400 2600
GWP (kg of CO_2e)
3000
2000
1000
0
s_h = 0.75 m
H = 7 m
0.6
0.5
0.4
0.3
Vertical spacing of steel strip (m)
0.4
0.6
0.8
1
1.2
1.4
L_R/H

(a)

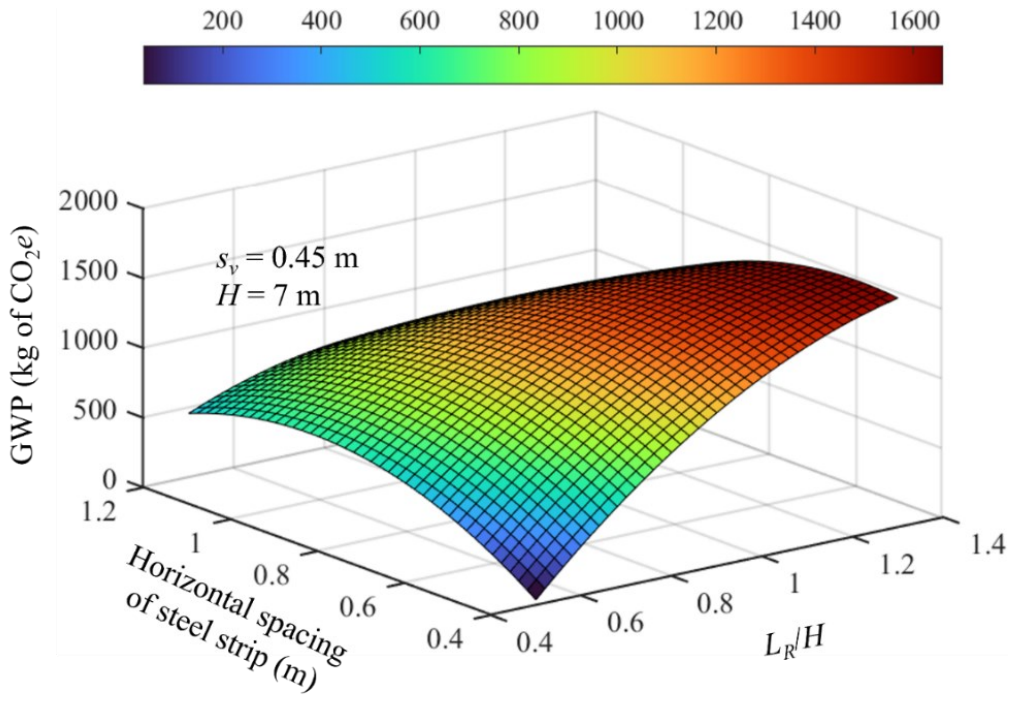
200 400 600 800 1000 1200 1400 1600
GWP (kg of CO_2e)
2000
1500
1000
500
0
s_v = 0.45 m
H = 7 m
1.2
1
0.8
0.6
0.4
Horizontal spacing of steel strip (m)
0.4
0.6
0.8
1
1.2
1.4
L_R/H

(b)

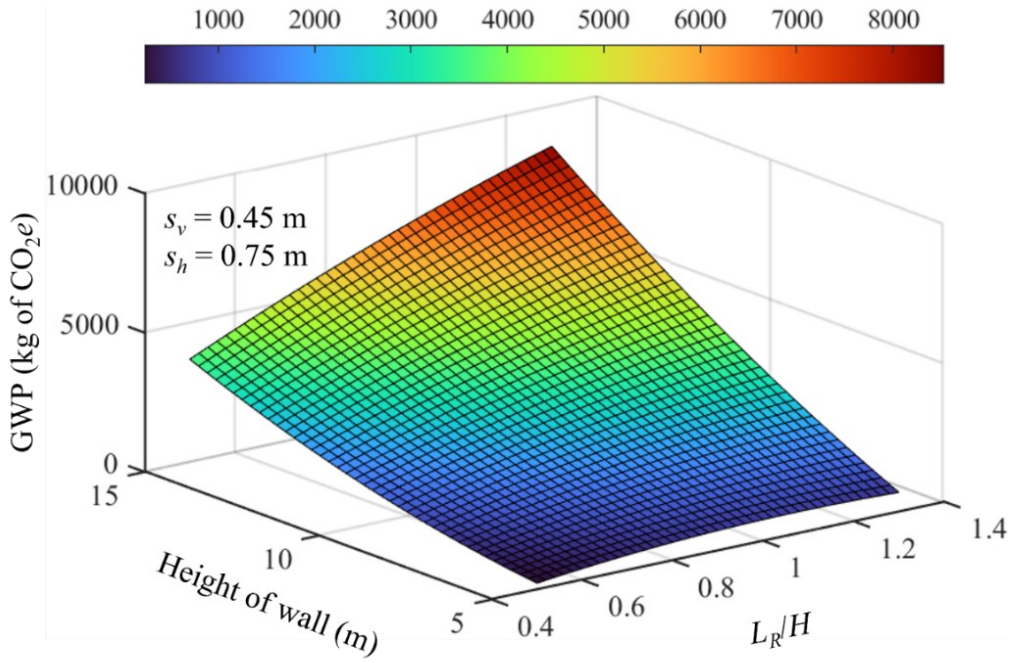

(c)

Figure 6.2. GWP response surfaces as function of (a) L_R/H and s_v, (b) L_R/H and s_h, and (c) L_R/H and H

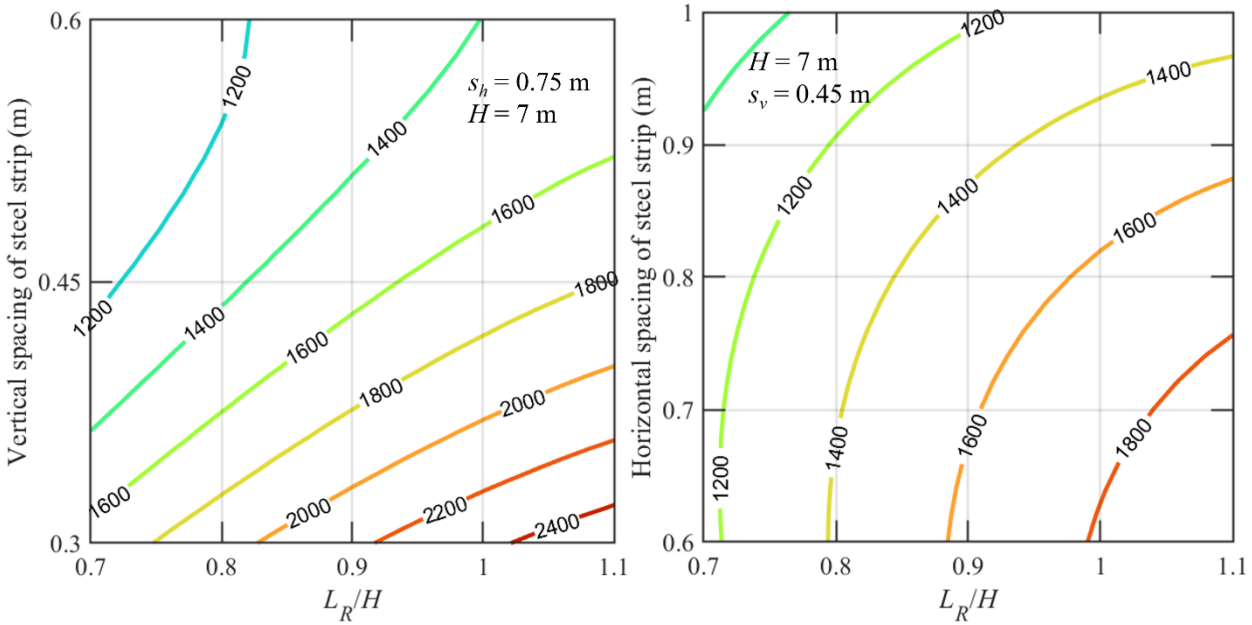

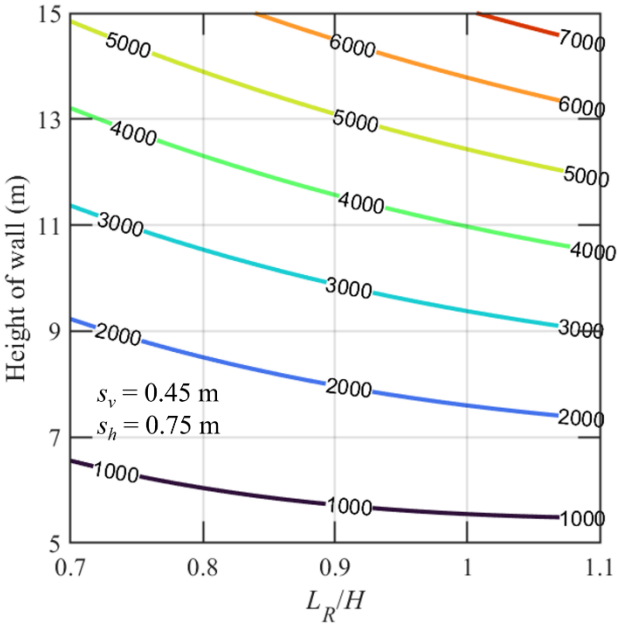

(c)

Figure 6.3. Contours for GWP response surfaces (a) L_R/H and s_v, (b) L_R/H and s_h, and (c) L_R/H and H

6.6 Results

The relationship between the reliability and global warming impact of MSE walls, reinforced by steel strips or geogrids, are investigated. The effects of random variables (i.e., soil properties, tensile strength of reinforcement, and live load surcharge) to the global warming impact of MSE walls are investigated through a parametric study. Since the design of MSE walls is complex because it involves (i) multiple failure modes of external and internal stabilities and (ii) determining multiple dimensions (i.e., length of reinforcement, vertical and horizontal spacings of reinforcement), the change in reliability index of the significant failure modes with respect to the change in design dimensions are examined. Charts for estimating the GWP of MSE walls for different (i) target probabilities of failure and (ii) live load surcharges are provided.

6.6.1 Parametric Study

Figure 6.4 shows the variations in GWP of MSE walls (reinforced by steel strips) with the change in the mean of soil properties, material properties, and surcharge load. Assuming a target $p_f = 10^{-3}$, FORM was performed to obtain the L_R/H for different values of s_v and assuming $H = 7$ m and $s_h = 0.75$ m. The means of other random variables are fixed to the values specified in Table 6.1. Based on the parametric study completed for working stress design in Section 4.3.2, it was found that the GWP of MSE walls is almost unaffected by the change in unit weights and friction angles of retained soil and foundation soil. Hence, in this study, the mean unit weight and friction angle of backfill soil are varied to study the effects of soil properties to the GWP of MSE walls. Decreasing GWPs were observed as the means of γ_b and ϕ_b increased, which implies that having stronger backfill soil reduces the volume of backfill soil to be reinforced. According to Figure 6.4(a), approximately 17.5 kg of CO_2e is decreased per unit mean of γ_b, whereas GWP is more sensitive to the change in ϕ_b (approximately 33.4 kg of CO_2e decreased per unit mean of ϕ_b according to Figure 6.4(b)). It was observed that the MSE wall designs in this study are mostly governed by the internal stabilities (i.e., tension and pullout failures) for which the driving forces are influenced by the coefficient of active lateral earth pressure K_A (computed based on ϕ_b). Hence, selection of backfill material with high ϕ_b can possibly an effective strategy for reducing the global warming impact caused by MSE walls. For MSE walls with geogrids, no changes in GWP were observed with respect to the soil properties.

Increasing the mean of yield strength of steel f_y did not cause changes to GWP of MSE walls because the designs for the cases shown in Figure 6.4(c) are governed by the pullout failure. The GWPs of MSE wall with geogrids were also constant with varied tensile strength of geogrids.

Figure 6.4(d) shows the variations in GWP with respect to the live load surcharge q, and an increasing trend in GWP is observed as the live load surcharge increases.

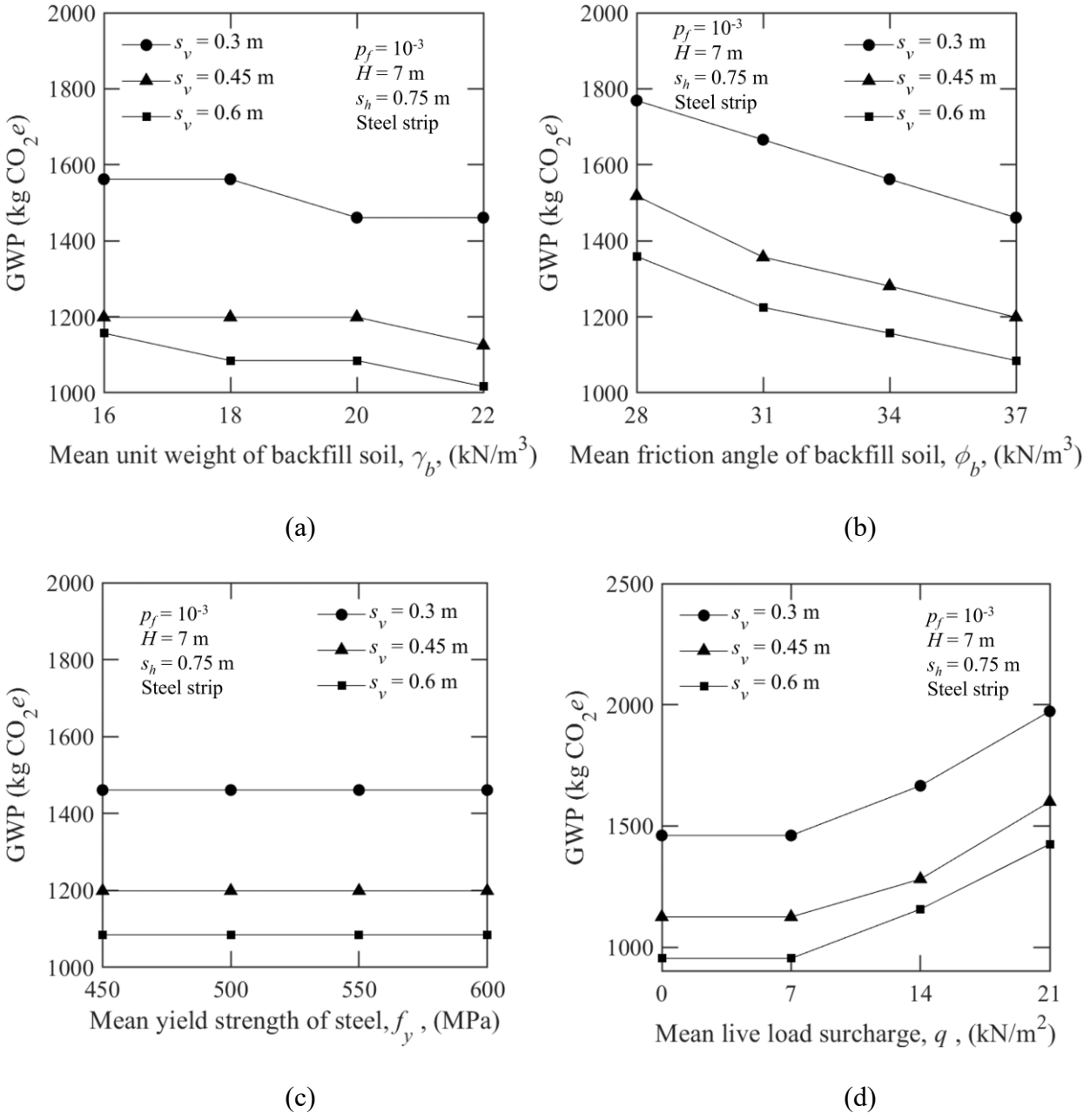

Figure 6.4. Variations of global warming impact for different means of (a) unit weight of backfill soil, (b) friction angle of backfill soil, (c) yield strength of steel, and (d) live load surcharge

6.6.2 Relationship Between Reliability and Global Warming Impact

Figure 6.5 shows the relationship between global warming impact and target probability of failure for the design of MSE walls. No changes in GWP were observed for MSE walls with geogrids with changes in the target probability of failure because the safety requirements were already met at the minimum L_R/H = 0.7. Hence, it can be concluded that the vertical spacing of geogrid is the most important design dimension for reducing the global warming impact of MSE walls with geogrids. On the other hand, some variations in GWP for MSE walls with steel strips were observed. GWP is reduced by approximately 100 or less GWP at certain levels of p_f (e.g., 3×10^{-5}, 4×10^{-5}, 4×10^{-4}, 5×10^{-4}). However, increasing the vertical spacing of steel strip is still the most effective method for reducing the GWP of MSE walls. When comparing the two reinforcement options in terms of GWP, using geogrid is preferred over steel strip.

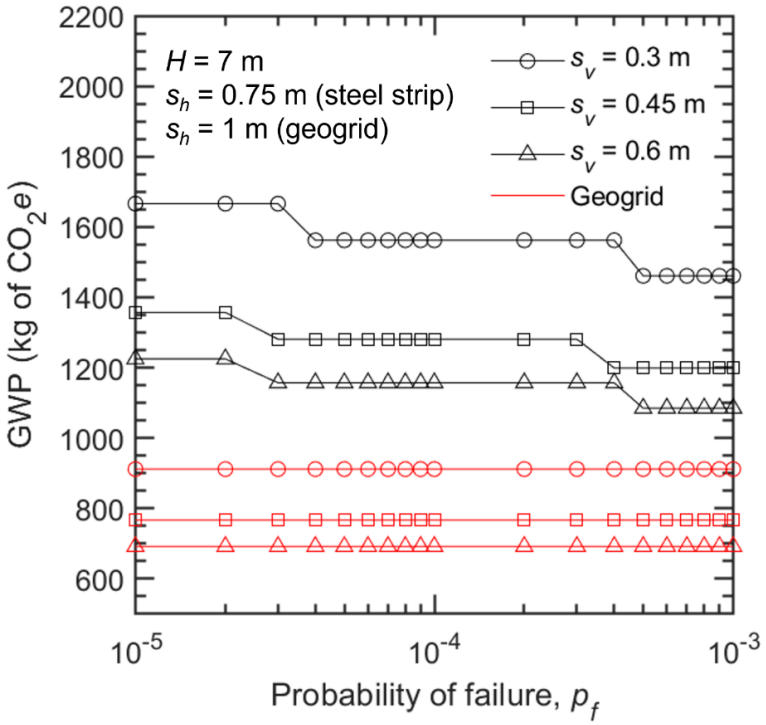

Figure 6.5. Relationship between global warming impact and probability of failure of MSE wall designs

6.6.3 Relationship Between Reliability and Design Variables

Since MSE walls are designed for multiple failure modes, the relationships between reliability index and the three design variables of MSE walls (i.e., L_R/H, s_v, and s_h) are investigated in Figure 6.6. In this study, the designs of MSE walls are governed by the internal stabilities. The reliability index of bearing capacity failure was the lowest amongst the external failure modes. According to Figure 6.6, it is observed that design of MSE walls with steel strips are governed by pullout failure and the designs with geogrids are governed by tension failure. Therefore, the design dimensions of steel strips (L_R, s_v, and s_h) need to be optimized and the friction between steel strip and soil can be improved such that the pullout resistance of steel strips is enhanced and the GWP of MSE walls is reduced at the same time. Using geogrids with higher tensile strength and adjusting the vertical spacing of geogrid are the methods for improving the stability against tension failure of geogrids and for possibly reducing the GWP of MSE walls.

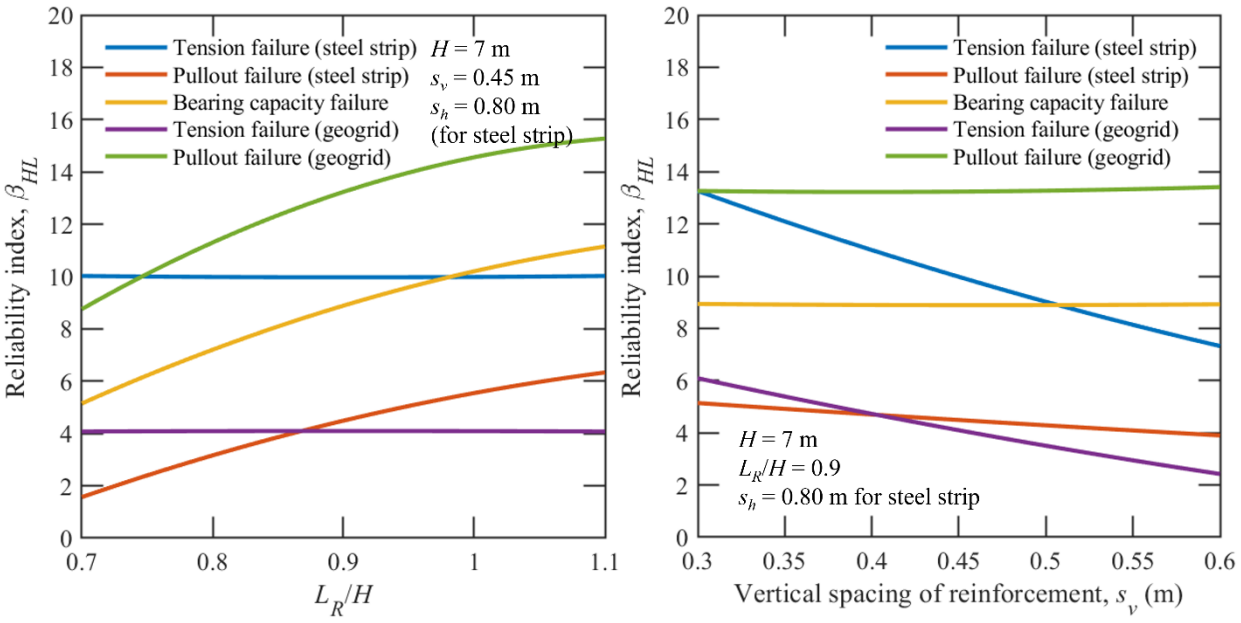

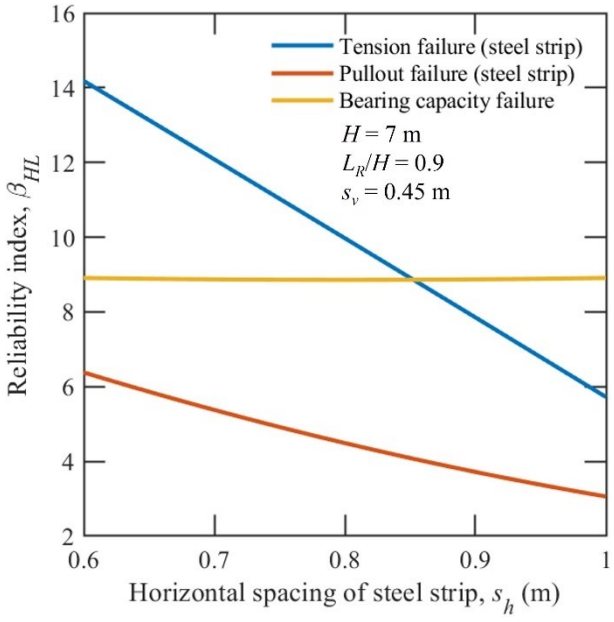

(c)

Figure 6.6. Relationship between reliability index and (a) L_R/H, (b) s_v, and (c) s_h of MSE walls

6.6.4 GWP Estimation Charts

To facilitate the process of incorporating environmental impact considerations in the design of MSE wall, samples of GWP estimation charts, shown in Figure 6.7, are developed. These charts are specifically developed for MSE walls with steel strips because the use of geogrids did not show meaningful variations in GWP in this study. The estimation charts include GWP contours (coloured dashed lines in Figure 6.7) which indicate the different values of GWP at different values of design dimensions (e.g., L_R/H, s_v, s_h, and H). In Figure 6.7(a) and (b), the possible designs of MSE walls (i.e., combinations of design dimensions) for different target p_fs are shown. Compared to the GWP values shown in Figure 6.5, the estimated GWP based on Figure 6.7 is generally overestimated by roughly 100 to 200 kg of CO_2e. In Figure 6.7(c), the live load surcharge q is varied assuming a target $p_f = 10^{-3}$. Figure 6.7(d) is useful for estimating the GWP of MSE walls for different heights of wall.

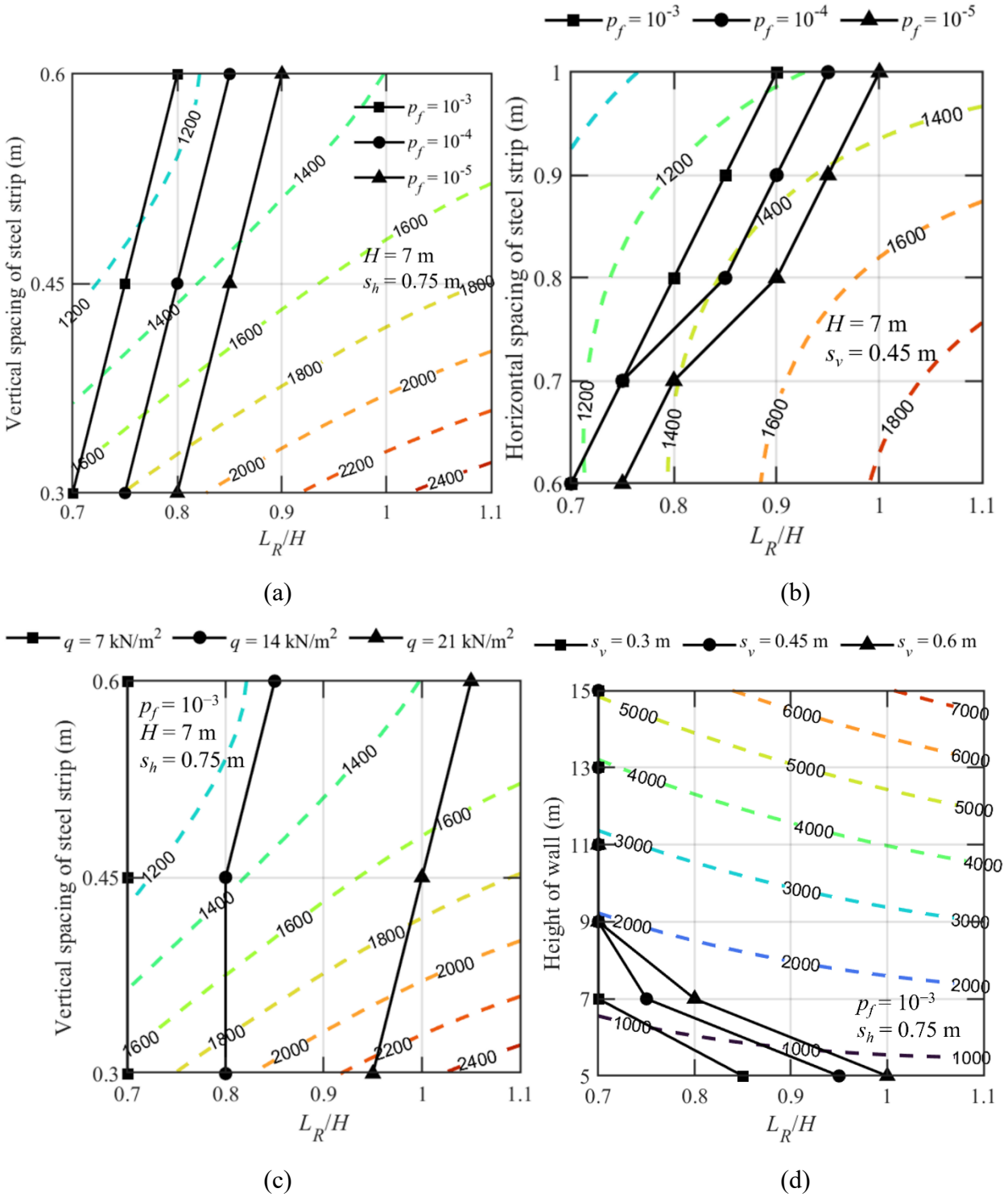

Figure 6.7. GWP estimation charts for MSE walls with steel strips (a) s_v versus L_R/H for different p_f, (b) s_h versus L_R/H for different p_f, (c) s_v versus L_R/H for different q, and (d) H versus L_R/H for different s_v

6.7 Summary

In this chapter, the relationship between reliability and sustainability of MSE walls were examined. FORM was used to perform reliability-based design of MSE walls. In FORM, the followings were characterized as random variables: (i) soil properties (i.e., unit weights and critical-state friction angles of backfill, retained, and foundation soil), (ii) tensile strength of steel strips and geogrids, and (iii) live load surcharge applied on top of backfill soil. Multiple regression analysis was used to generate response surfaces of global warming impact of MSE walls as functions of height of wall, length of reinforcement, and spacings of reinforcement. The response surfaces were used to facilitate the process of connecting reliability and environmental impacts of MSE walls.

Parametric study was conducted to understand the effects of the random variables mentioned above to the global warming impact of MSE walls. Minimal changes in the GWPs of MSE walls with geogrids were observed as the parameters were varied. In contrast, the GWPs of MSE walls with steel strips were found to be the most sensitive to the changes in the unit weight and critical-state friction angle of backfill soil. Decrease in global warming impact was observed as the reliability of MSE walls increased (i.e., target probability of failure decreased); however, no changes were observed for MSE walls with geogrids because they were already overdesigned at the minimum dimensions of length of reinforcement and spacings in this study. The MSE walls in this study were governed by the internal stabilities. Specifically, MSE walls with steel strips were governed by pullout failure, and MSE walls with geogrids were governed by tension failure. It was determined that spacings of reinforcement affected the tension failures while the length of reinforcement influenced the pullout failure. Sample GWP estimation charts were developed for MSE walls with steel strips using which the global warming impact of MSE walls can be estimated

based on the different combinations of design dimensions, target probabilities of failure, and live load surcharges.

6.8 List of Symbols

Notation	Description
b	Width of steel strip
c_i	Coded variable
CO_2e	Equivalent mass of CO_2 of emissions x
c_r	Corrosion rate of steel
D	Summation of all driving forces or moments in an MSE wall
fy	Yield strength of steel strip
$g(–)$	Performance function
H	Height of wall
k	Total number of variables in regression analysis
K_A	Coefficient of lateral earth-pressure at active state
L_R	Length of reinforcement
p_f	Probability of failure
q	Live load surcharge
R	Summation of all resisting forces in an MSE wall
s_h	Horizontal spacing of reinforcement
SL_c	Service life of Zinc coating on the strips
SL_{MSE}	Service life of retaining wall
s_v	Vertical spacing of reinforcement
T	Tensile strength of reinforcement
t_n	Thickness of steel strip
X	Random variable
Y	Random variable in standard normal space
y_r	Response surface
z	Depth below top of the wall
α	Distance from the center to an axial point in a central composite design
β_{HL}	Hasofer-Lind reliability index
β_i	Regression coefficient
γ_b, γ_r, γ_f	Unit weight of backfill, retained, and foundation soils, respectively
ζ	Shape parameter of lognormal distribution
λ	Scale parameter of lognormal distribution
ξ	Controllable input variable in natural variable
ρ_{HDPE}	Density of high density polyethylene (geogrid)
ρ_{steel}	Density of steel
$\Phi(–)$	Cumulative distribution function of standard normal distribution
$\phi(–)$	Probability density function of standard normal distribution
ϕ_b, ϕ_r, ϕ_f	Critical-state friction angle of backfill, retained, and foundation soil, respectively

PART III: OPTIMIZATION FOR SUSTAINABLE GEOTECHNICAL DESIGN

CHAPTER 7: MULTI-OBJECTIVE OPTIMIZATION FRAMEWORK

7.1 Need for an Optimization Framework in Geotechnical Engineering

A sustainable geotechnical design needs to be reliable, cost effective, environmentally friendly, and socially acceptable. Designing sustainable geotechnical structures is a complex problem involving quantification and optimization of design implications and outputs such that the four Es of sustainability — engineering, economy, environment, and equity — are balanced (Basu *et al*., 2015). The current design practice primarily aims at minimizing the cost while ensuring adequate engineering performance, and environmental considerations are usually not taken into account (Juang and Wang, 2013; Saribas and Erbatur, 1996; Wang and Kulhawy, 2008). Bringing in sustainability considerations in design introduces complexities because there can be multiple aspects of sustainability that has to be taken into account with trade-offs between them. For example, constructing a highly reliable structure leads to overconsumption of materials and energy which implies higher cost and emissions. Each aspect of sustainability can be affected by several variables such as soil properties, loading conditions, safety requirements, unit costs, project-specific parameters, construction methods, and so on, which further adds to the complexity. To systematically consider sustainability aspects in geotechnical design with the trade-offs, multi-objective optimization (MOO) techniques can be used by which design dimensions optimized with respect to different aspects of sustainability are determined based on practical ranges of design variables.

The objectives of this study are (i) to develop a multi-objective optimization framework for achieving sustainable designs of geotechnical structures (e.g., retaining wall and pile foundation) with simultaneous consideration of reliability, cost, and environmental impact, (ii) to

study the trade-offs between the three objectives (e.g., reliability, cost, and environmental impact) considered in MOO, and (iii) to develop design charts based on the results of MOO so that designers can quickly determine the optimized dimensions of geotechnical structures in practice.

The methodologies used in the MOO framework include NSGA-II, life cycle assessment (LCA), first-order reliability method (FORM), cost estimation, and response surface method. The procedures of the proposed framework are explained in the next sections.

7.2 Multi-Objective Optimization Methods and Problems

The developed multi-objective optimization framework aims for sustainable geotechnical design by concurrently evaluating the engineering reliability, environmental impact, and cost of geotechnical designs to determine optimized designs based on given ranges of design variables. Figure 7.1 illustrates the proposed framework. A fast and elitist NSGA-II by Deb *et al*. (2002), a well-known and credible algorithm (Konak *et al*., 2006), is used to conduct the MOO in this study. In the framework, the following are defined (Figure 7.1): (i) design variables for geotechnical design and their bounds, (i) objective functions to evaluate the sustainability of geotechnical structure (e.g., MSE wall and drilled shaft), and (iii) constraints. Figure 7.2 illustrates the general process of MOO with two objective functions f_1 and f_2. The goal of optimization in Figure 7.2 is to find the Pareto front which consists of non-dominated solutions at minimum f_1 and f_2. The design variables and their bounds define the search space in the MOO, which is the bounded region (area surrounded by the grey dash line in Figure 7.2) within which the optimization algorithm is allowed to search for the optimum solutions. For example, the design variables of an MSE wall are the length of reinforcement L_R, vertical spacing of reinforcement s_v, and horizontal spacing of reinforcement s_h. If the bounds of length of reinforcement L_R of an MSE wall is 5 m $\leq L_R \leq$ 10 m, the algorithm is only allowed to generate solutions within the specified bounds. The set of solutions

(grey circles in Figure 7.2) generated within the bounds of design variables is called a population P, and it is expressed in terms of design variables (e.g., values of L_R, s_v, and s_h of the grey circles in Figure 7.2). This population is then evaluated with respect to the defined objectives f_1 and f_2 (i.e., $f_i(L_R,s_v,s_h)$ values are assigned to each solution) to identify if the solutions are fit for the Pareto front (minimum f_1 and f_2 values). Through iterations, the population is gradually evolved to converge towards the Pareto front while maintaining the diversity in the solutions as shown in Figure 7.2. The diversity indicates the trade-off between the objective functions; thus, a diverse Pareto front extends in all directions of objective space (e.g., in both f_1 and f_2 directions in Figure 7.2). In this study, the objective functions of MOO are related to the environmental impact, engineering reliability, and cost of the geotechnical structure. LCA and FORM are used for quantifying global warming impact (environmental impact) and reliability of geotechnical structure, respectively. Since it is extremely time consuming to perform LCA and FORM multiple times to evaluate a large-size population, the response surface methodology is used to construct the objective functions for global warming impact and reliability of the geotechnical structure. The objective function for the cost is formulated based on unit costs obtained from a cost estimation handbook and the literature. The outcome of the MOO framework is a set of geotechnical designs that are optimized based on the three objectives and satisfy the defined constraints.

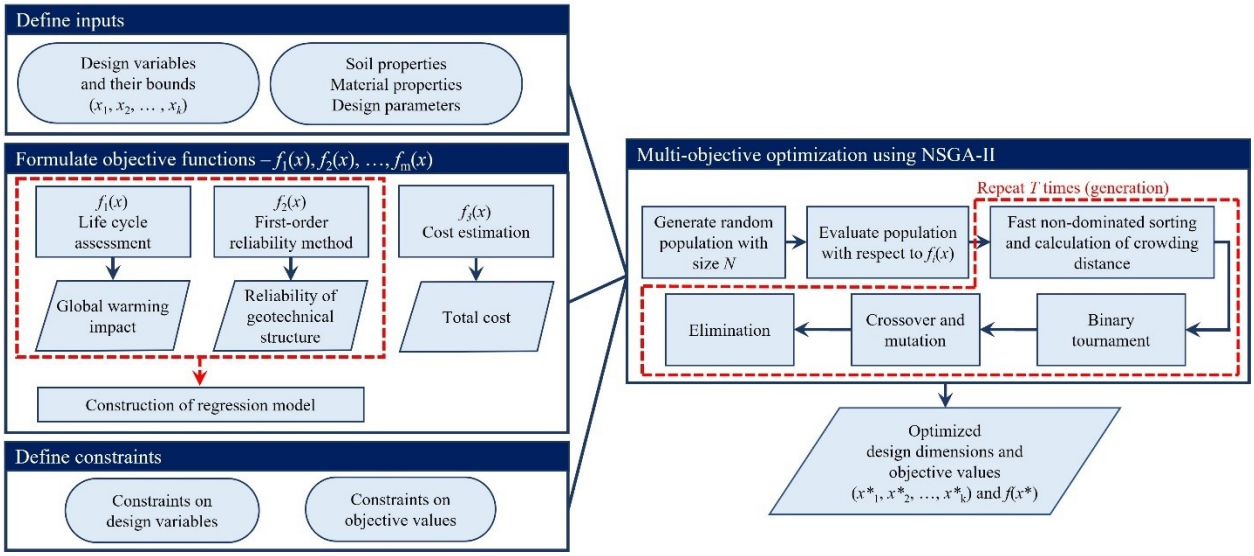

Figure 7.1. Multi-objective optimization framework for sustainable geotechnical design

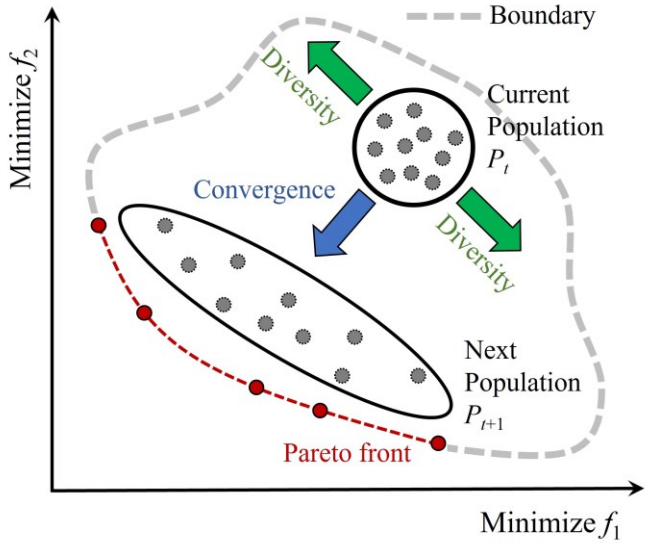

Figure 7.2. General process of multi-objective optimization

7.3 Defining Input Variables and Objective Functions

The input variables needed for the MOO-based framework in this study are (i) design variables (e.g., L_R, s_v, and s_h of MSE wall), (ii) soil properties (e.g., unit weight, friction angle, relative density, coefficient of lateral earth pressure, and other soil parameters important in the

design), (iii) material properties (e.g., tensile strength of soil reinforcement, width and thickness of soil reinforcement, compressive strength of concrete, density of materials, and other properties important in both design and LCA calculations), and (iv) design parameters (e.g., loading conditions, height of wall, target probability of failure, and etc.).

The objective functions related to environmental impact, engineering reliability, and cost of geotechnical structure can be represented by a relevant metric for each. For example, the global warming potential, obtained from LCA, can represent the environmental impact of an MSE wall, the system reliability, expressed in the minimum reliability index β_{HL}, can represent the engineering reliability, and the total cost of materials and construction is adequate to measure cost associated with a geotechnical structure.

7.4 Constraints

Constraints are used to ensure that the optimization results are within a feasible region. The constraints presented in this paper can be freely modified to meet preferences of designers. In this study, the constraints are applied on the following parameters: (i) reliability index β_{HL} of geotechnical structure, (ii) design increments for certain design variables, and (iii) cost differences between optimized solutions.

The reliability index is constrained to ensure that the optimized designs are feasible and practical. For example, a minimum $\beta_{HL} \geq 2$ may be set to ensure that all geotechnical designs are sufficiently safe (i.e., the designs are feasible), and a constraint on the maximum value of β_{HL} ($\beta_{HL} \leq 6$) ensures that the designs are not extremely conservative (i.e., the designs are practical).

To keep the designs practical from a construction point of view, increments for some design variables (e.g., L_p and B_p of drilled shaft, s_v and s_h of soil reinforcement in an MSE wall) are defined.

For example, the length of drilled shaft can be defined in increment of 1 m. The increments can be modified to ensure standardized dimensions are used.

A constraint on cost differences between optimized solutions is used to eliminate designs that have trivial cost differences. For example, based on the result of MOO, two designs may have only $1 difference which make at least one of the designs redundant. To keep the MOO results practical in the decision-making process, the results are refined using the cost constraint such that the important discrete designs are recommended as opposed to a continuous Pareto front.

7.5 NSGA-II

NSGA-II is a multi-objective optimization algorithm developed based on genetic algorithm (GA), which is inspired by the theory of natural selection. NSGA-II connects the theory that fittest species will adapt better to the environment, survive, and reproduce for the next generation, with the process of reaching convergence in optimization. In other words, the solutions are evolved every iteration (generation) toward the best solutions, as illustrated in Figure 7.2. Figure 7.3 shows the flowchart of conducting the NSGA-II for geotechnical structures following five major steps – (i) initialization, (ii) evaluation, (iii) selection, (iv) reproduction, and (v) elimination.

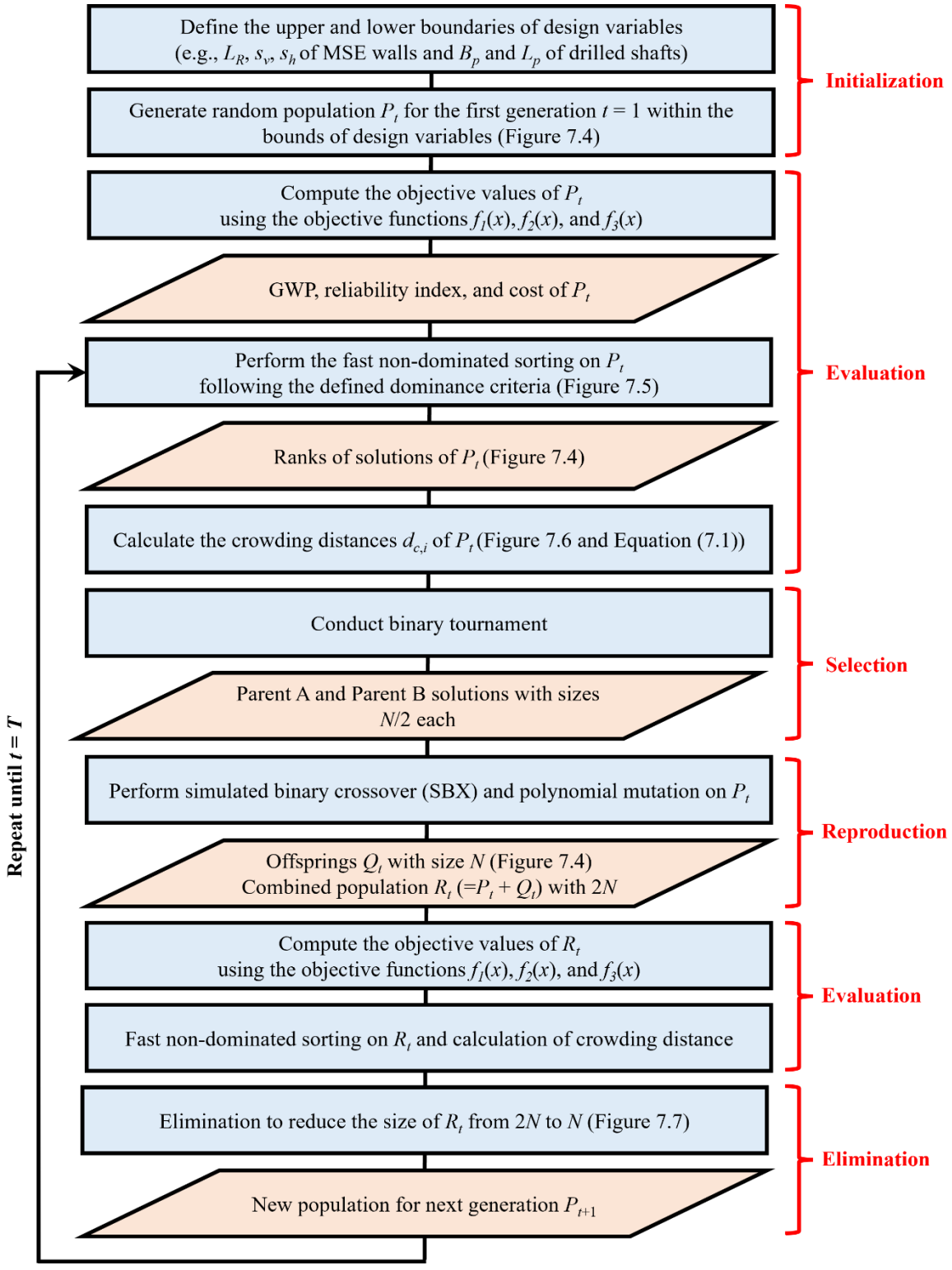

Figure 7.3. Flowchart of NSGA-II

The first step in NSGA-II is to generate a random population P_t with a size N within a defined boundary, as shown in Figure 7.4 by the grey circles and dashed boundary. The ranges of design variables (e.g., L_R, s_v, and s_h of MSE wall) define the boundary. The initial population represents the first generation $t = 1$, and this population will evolve through series of the evaluation, selection, reproduction, and elimination stages of NSGA-II until the number of iteration t reaches the total number of generations T. The goal of MOO is to find the Pareto Front (e.g., red line in Figure 7.4 for minimization of two objective functions) which is the set of optimal solutions, also called as the non-dominated solutions.

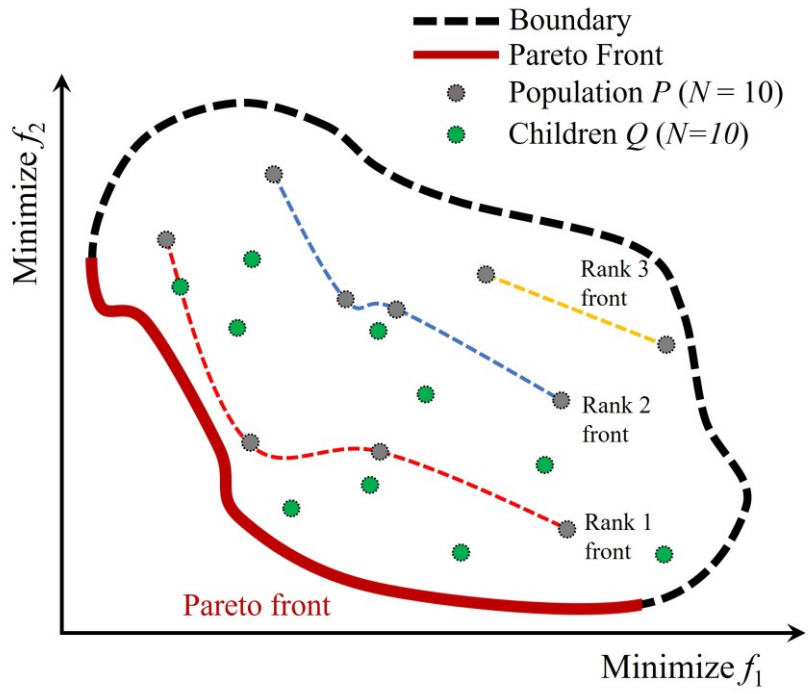

Figure 7.4. Initialization, evaluation, and reproduction of NSGA-II

The objective values of the initial population are computed based on the objective functions $f(x)$ (e.g., GWP, reliability, and cost in this study). The population is then evaluated using the fast non-dominated sorting (Deb *et al*., 2002), which is a technique to sort and assign ranks to the solutions of population based on the defined dominance criteria. In the fast non-dominated sorting,

a solution is considered to have dominance and better rank compared to other solutions if it (i) has better objective values for meeting the goal of MOO (e.g., lower f_1 and f_2 values in Figure 7.4) and (ii) is within the feasible region defined by the constraints. Therefore, the dominance criteria is defined as: solution *i* is said to constrained-dominate a solution *j*, if any of the following conditions is true (Deb *et al*., 2002): (a) solution *i* is feasible and solution *j* is not, (b) solutions *i* and *j* are both infeasible, but solution *i* has a smaller overall constraint violation, and (c) solutions *i* and *j* are feasible and solution *i* dominates solution *j*. NSGA-II handles the constraints based on the dominance criteria described above. If a solution violates the constraint excessively, it will likely not survive after the selection and elimination stages. Figure 7.5 shows examples of the three cases (a)-(c) defined in the dominance criteria. The red dash lines in Figure 7.5 indicate the constraint on the reliability index of MSE wall (i.e., $2 \leq \beta_{HL} \leq 6$). Any solution outside the constraint is considered infeasible and its constraint violation is calculated based on the distance from the solution to the bounds of constraint (see points A and C in Figure 7.5). Solution B in Figure 7.5 dominates solution A (case (a)), solution A dominates solution C because solution A has smaller constraint violation (case (b)), and solution B dominates solution D because they are both feasible, but solution B has higher β_{HL} and lower GWP (case (c)). Figure 7.4 shows an example of sorted solutions. Rank 1 solutions are essentially non-dominated solutions, and rank 2 solutions are dominated by rank 1 but not dominated by rank 3 solutions. Fronts are formed by the solutions with the same rank.

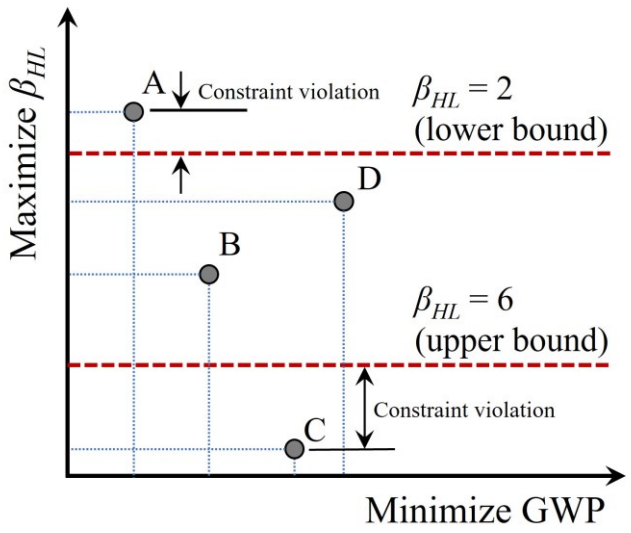

Figure 7.5. Dominance criteria

Once the fronts are determined, the crowding distances of solutions can be computed. Crowding distance is the average distance of neighbour solutions ($i-1$) and ($i+1$) from a solution i in the objective space (Figure 7.6), and it is calculated as below:

$$d_{c,i} = \frac{d_1}{f_1^{\max} - f_1^{\min}} + \frac{d_2}{f_2^{\max} - f_2^{\min}} + \cdots + \frac{d_m}{f_m^{\max} - f_m^{\min}} \tag{7.1}$$

where $d_{c,i}$ is the crowding distance of solution i, d_1 and d_2 are the distances between ($i-1$) and ($i+1$) with respect to objective function f_1 and f_2, respectively (see Figure 7.6), $f^{\max}$ and $f^{\min}$ are the maximum and minimum values of the corresponding objective function in the same rank, and m is the total number of objective functions. Crowding distance $d_{c,i}$ provides information related to the density around the solution i. In other words, a lower crowding distance indicates that the neighbour solutions are close to solution i; therefore, it is more crowded. In multi-objective optimization, diversity along the fronts is preferred because it gives information on the trade-off between the conflicting objectives. In other words, a set of solutions spread along the Pareto Front (red circles in Figure 7.6) is desired than a set of solutions clustered close to a single solution i.

Crowding distance is an important metric used in the binary tournament and elimination stages in NSGA-II.

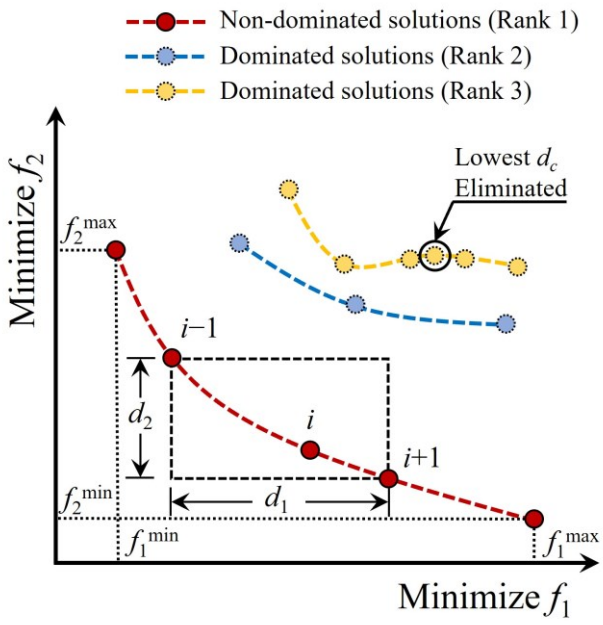

Figure 7.6. Crowding distance of solution *i*

A binary tournament is conducted to select the 'fittest' solutions that will be used for the 'reproduction' for the next generation. The outcome of binary tournament is a set of solutions representing 'Parent A' and 'Parent B' pools. In the tournament, two solutions are randomly selected from the population and first compared in terms of their rank. A solution with lower rank is selected as the winner of tournament. In case of a tie (same ranks), the solution with higher crowding distance is selected as the winner. This is to ensure the diversity of solutions is preserved. The binary tournament is iterated until the total size of parents is equal to N (i.e., Parents A and B with a size of $N/2$ each).

The winners of binary tournament (i.e., Parent A and Parent B solutions) undergo the reproduction schemes called crossover and mutation. In optimization, it is understood that crossover of two parents, that are considered optimal in a population, will produce solutions

(termed as 'offsprings') that are also deemed optimal. Iteration of crossover will result in good solutions appearing more frequently in the population, eventually leading to convergence in the optimization. Figure 7.4 shows examples of offsprings (green circles), and visually it can be concluded they are generally better solutions than their parents (grey circles) because they are mostly situated closer to the Pareto Front. In this study, simulated binary crossover (SBX) (Deb and Jain, 2011) is used to obtain the offsprings Q_t with a size of N. Mutation is used to modify the offsprings so that new solutions can be explored. The concept of mutation is used in GA to add diversity in the population so that the solutions can escape from local optima (Konak *et al*., 2006). However, mutations should not be applied excessively that will cause hindrance to reaching convergence to best solutions. In this study, polynomial mutation (Deb and Deb, 2014) is used. After crossover and mutation, the total size of population ($R_t = P_t + Q_t$) becomes $2N$.

The combined population R_t is evaluated using the fast non-dominated sorting and crowding distance based on which N solutions are eliminated. The goal of elimination is to select the best N solutions that will be carried on as the population for the next generation P_{t+1}. Figure 7.7 illustrates the process of elimination. Solutions with higher ranks are eliminated first, and in case solutions with the same rank need to be eliminated, the solutions with higher crowding distance are favoured to preserve the diversity.

The new population P_{t+1} undergoes the evaluation, selection, reproduction, and elimination stages again, and it is expected the population at the termination condition ($t = T$) represents the non-dominated solutions or Pareto front.

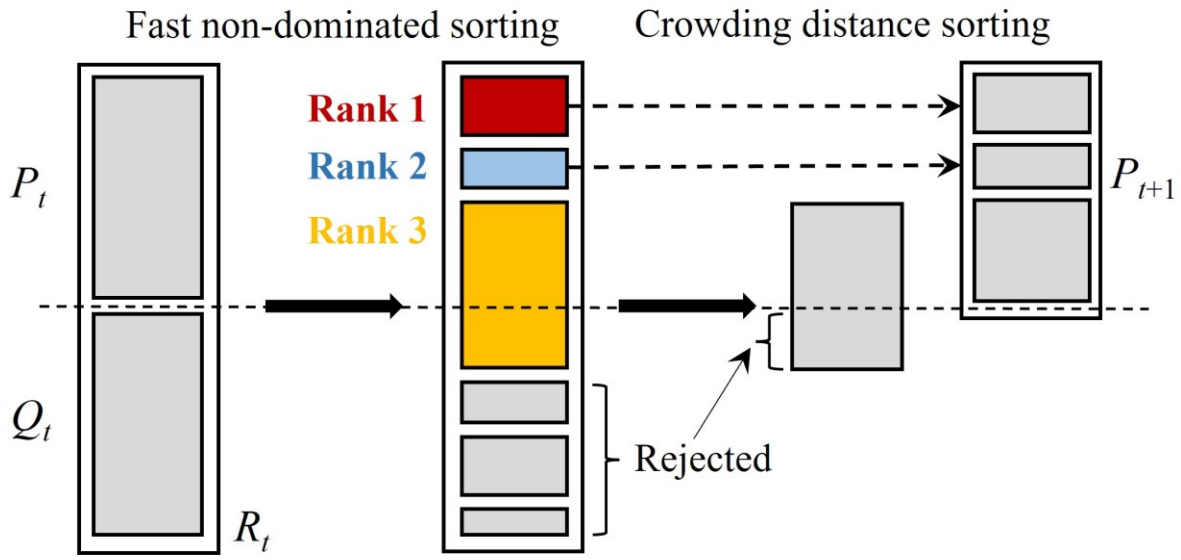

Figure 7.7. Elimination procedure in NSGA-II (adapted from Deb *et al*., 2002)

In this study, NSGA-II is conducted using a MATLAB program based on the following:

$$\begin{aligned}
&\text{Minimize } f_1 : \text{GWP} \\
&\text{Minimize } f_2 : \text{Cost} \\
&\text{Maximize } f_3 : \beta_{HL} \\
&\text{subjected to : design variables } \in [\text{min, max}] \\
&\qquad 2 \le \beta_{HL} \le 6
\end{aligned} \tag{7.2}$$

A population size N =100 and generation size T = 200 are chosen. The probabilities and indices related to crossover and mutation schemes are obtained from Zitzler *et al*. (2000). In this study, the probability of crossover is 0.9, and the distribution index for crossover is 20. The probability of mutation is 1/k, and the index parameter for mutation is 20. The MATLAB script is verified based on five benchmark problems so called the ZDT1, ZDT2, ZDT3, DTLZ1, and DTLZ2 defined by Zitzler *et al*. (2000) and Deb *et al*. (2001). ZDT problems are MOO problems with two objective functions, and DTLZ problems involve at least three objective functions. The script is verified for various types of Pareto front; for example, ZDT1 involves a convex Pareto front, ZDT2

has a concave Pareto front, ZDT3 has a disconnected Pareto front, DTLZ1 has a hyperplane Pareto front, and DTLZ2 has a sphere Pareto front.

In this study, the optimized results are further refined in terms of cost because non-dominated solutions with only a small cost difference may not be meaningful. Further, reducing the number of optimized solutions simplifies the decision-making process as designers choosing the final design from a large-size population with $N = 100$ does not seem practical. A constraint on cost difference between competing designs can be applied to eliminate designs that have small cost differences from their 'neighboring' solutions, as shown in Figure 7.8. In this study, a threshold of $100 is chosen. The first set of elimination starts from the minimum cost of all solutions (see Figure 7.8), then the next elimination is completed with respect to the next reference solution that is at least $100 higher than the minimum cost of all solutions. This process is continued until all non-dominated solutions are checked. This constraint is applied after the optimization results are obtained because NSGA-II already has an elimination function, as shown in Figure 7.3 and Figure 7.7, which can be conflicting to this constraint. If the elimination related to cost is forced into the NSGA-II, there is a possibility that solutions that have less than the cost threshold (e.g., $100) will be eliminated irrespective of their rank. For example, if most solutions in rank 1 have cost difference less than the $100 threshold and are eliminated, the next population will have less 'elite' solutions that will interrupt reaching convergence toward the optimal solutions.

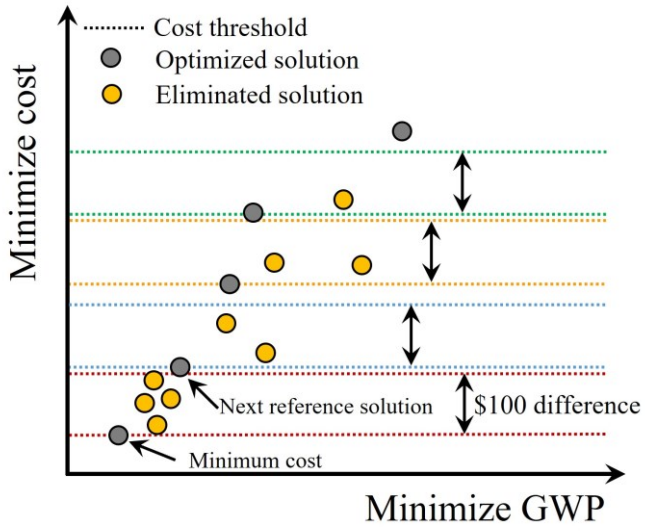

Figure 7.8. Constraint on the cost difference between solutions

7.6 Summary

In this chapter, a multi-objective optimization based framework is proposed. The main purpose of the framework is to determine the optimized design dimensions of geotechnical structures that result in balanced environmental impact, cost, and engineering reliability of the geotechnical structures. The framework uses several robust methodologies for quantifying the different aspect of sustainability: LCA and FORM. To reduce the computation times, response surface methodology is used to estimate the global warming impact and reliability of the geotechnical structures. Non-dominated sorting genetic algorithm (NSGA-II) was used to perform the multi-objective optimization in which the objective functions are defined for the engineering reliability, cost, and global warming impact of geotechnical structures. The lower and upper bounds of the design variables (dimensions) are defined to constrain the objective space of optimization for practicality. Constraints are also used to ensure (i) the engineering reliability of geotechnical structures exceed the minimum requirement and (ii) the cost difference between optimized solutions is at least a certain amount.

7.7 List Of Symbols

Notation	Description
B_p	Pile diameter
$d_{c,i}$	Crowding distance of solution i
f_i	Objective function
f^{max} and f^{min}	Maximum and minimum values of the corresponding objective function in the same rank
H	Height of wall
L_p	Pile length
L_R	Length of reinforcement
m	Total number of objective functions
N	Total number of solutions in a population
P_t	Population at generation t
Q_t	Offsprings at generation t
R_t	Combined population of parents and offsprings at generation t
s_h	Horizontal spacing of reinforcement
s_v	Vertical spacing of reinforcement
T	Total number of generations
t	Current generation
β_{HL}	Hasofer-Lind reliability index

CHAPTER 8: OPTIMIZED MSE WALL DESIGNS

In this chapter, the designs of MSE walls are optimized for engineering reliability, environmental impact, and cost using the MOO framework introduced in Chapter 7. The MSE walls are reinforced by steel strips or geogrids (see Figure 4.1). The input variables, objective functions, and constraints used in the MOO framework for MSE walls are discussed here.

8.1 Selection of Design Variables and Bounds

The design variables of MSE wall are (i) the length of reinforcement L_R, (ii) vertical spacing of reinforcement s_v, and (iii) horizontal spacing of reinforcement s_h. The steel strips are placed with vertical and horizontal spacings (s_v and s_h), and the geogrids are spaced only vertically because geogrids are assumed to be continuous in the horizontal direction (i.e., throughout the length of wall). A practical range is selected to define the lower and upper bounds of the design variables. According to FHWA (2009b), the length of reinforcement can vary from $0.7H$ to $1.1H$. The vertical spacing of reinforcement is dependent on the thickness of compaction layers; therefore, it typically ranges between 300 mm and 600 mm (Fratta and Kim, 2015; Salgado, 2008). The horizontal spacing of steel strips is assumed to range from 600 mm to 1000 mm based on the information that a typical horizontal spacing for steel strip is 762 mm (30 in) (FHWA, 2009b).

8.2 Formulation of Objective Functions

Three objective functions related to engineering reliability, environmental impact, and cost are considered to evaluate the sustainability of the MSE wall. The engineering reliability of MSE wall is expressed in terms of the reliability index β_{HL} (Hasofer and Lind, 1974) computed using FORM (Ang and Tang, 1984). The environmental impact associated with the MSE wall is quantified in terms of the global warming potential (GWP) using LCA (ISO 2006a; 2006b). GWP

is a measure that collectively represent the impacts of greenhouse gases on global warming effect, and it is expressed in mass of carbon dioxide (CO_2) equivalent (IPCC, 1990). The costs of material, labour, and equipment for the construction of MSE wall are estimated based on unit prices provided by cost estimation handbook and literature (Basudhar *et al*., 2008; FHWA, 2009c; RSMeans, 2015). The environmental impact and total cost are estimated per 1 m length of wall. How these objectives, i.e., β_{HL}, GWP, and cost, are calculated is described separately in the subsequent sections.

In this study, the constraints are applied on the following parameters: (i) reliability index β_{HL} of MSE wall, (ii) design increments for vertical and horizontal reinforcement spacings s_v and s_h, and (iii) cost differences between optimized solutions. For vertical spacing, it is assumed that the thickness of compaction layer is in multiples of 150 mm; therefore, the optimized designs are expected to range within the bounds of 300 to 600 mm with 150 mm increment. Similarly, it is assumed 100 mm is adequate as the design increment for horizontal spacing.

8.2.1 Estimation of Environmental Impact

In this study, LCA is used to quantify the global warming impact of MSE walls, and the databases, parameters, and assumptions used in the LCA are described in Section 4.2. The functional unit defined in this LCA is an assembled MSE wall that is safely designed against external and internal stabilities with at least probability of failure of 2.3×10^{-2} or reliability index of 2.0. It should be noted that the values of probability of failure and reliability index will differ case by case because the purpose of this study is to evaluate MSE wall designs with different reliabilities.

8.2.2 Estimation of Cost

The costs of material, labour, and equipment associated with the construction of MSE walls are estimated using the cost estimation handbook by RSMeans (2015) and the literature (FHWA 2009c; Basudhar *et al*., 2008). Table 8.1 lists the unit costs used in the cost estimation.

Table 8.1. Unit costs of material, construction work, and transportation activity for MSE wall

Material	**Unit cost**	**Reference**
Backfill soil from borrow pit	$ 24 per bank volume of soil	RSMeans (2015)
Steel strip	$ 1.25 per m length of reinforcement per 1 m wall	FHWA (2009c)
Geogrid	$ 2.90 per m length of reinforcement per 1 m wall	Basudhar *et al*. (2008)
Construction work or transportation	**Unit cost**	**Reference**
Excavation of soil	$ 2.48 per bank volume of soil	RSMeans (2015)
Transportation of excavated or backfill soil	$ 8.65 per loose volume of soil	RSMeans (2015)
Spreading backfill soil	Included in the material cost for backfill soil	
Compaction of soil	$ 1.37 per compacted volume of soil	RSMeans (2015)
Placement of reinforcement	$ 25 per m length of reinforcement per 1 m wall	FHWA (2009c)

8.2.3 Estimation of Engineering Reliability

The reliability indices of MSE wall against the five failure modes (i.e., sliding, overturning, bearing capacity, tension, and pullout failures) are computed using FORM following the procedures described in Sections 6.2.3 and 6.3. The characteristics of random variables are summarized in Table 6.1.

8.2.4 Construction of Regression Models

In the multi-objective optimization process (Figure 7.1), a design needs to be evaluated with respect to the objective functions related to β_{HL}, GWP, and total cost of the designed MSE wall. Therefore, LCA, FORM, and cost estimation need to be performed for every design the optimization program considers as a possible solution for the Pareto front (i.e., minimized GWP and total cost, and maximized reliability index). However, it is extremely time-consuming to perform LCAs and FORMs for a large population size N and a large number of generations T. For example, if $N = 100$ and $T = 200$, which are the typical sizes required for reaching convergence and diversity in the optimized solutions (Deb *et al*., 2001; Zitzler *et al*., 2000), the LCA and FORM should be performed $N \times T = (100)(200) = 20{,}000$ times. To reduce the computation times, the response surface methodology is used to formulate regression models so that GWP and β_{HL} of MSE wall designs can be estimated using the regression model without a large number of calculations.

The second-order regression models in Table 6.3 are used as the objective functions for GWP of MSE walls. Following the same procedures described in Section 6.5, the second-order regression models for reliability index of MSE walls are developed and summarized in Table 8.2.

Table 8.2. Regression models for reliability index of MSE wall

Failure mode	Steel strip	Geogrid
Sliding	$y_{\beta_s} = 11.67 + 1.95c_1 + 0.87c_4 - 0.37c_1^2 + 0.01c_2^2 + 0.01c_3^2 - 0.04c_4^2 + 0.05c_1c_4$	$y_{\beta_s} = 11.67 + 1.96c_1 + 0.85c_4 - 0.37c_1^2 + 0.01c_2^2 - 0.39c_4^2 + 0.05c_1c_4$
Overturning	$y_{\beta_o} = 16.58 + 2.45c_1 + 0.91c_4 - 0.82c_1^2 + 0.01c_2^2 + 0.01c_3^2 - 0.45c_4^2 - 0.62c_1c_4$	$y_{\beta_o} = 16.58 + 2.42c_1 + 1.02c_4 - 0.8c_1^2 + 0.05c_2^2 - 0.59c_4^2 - 0.61c_1c_4$

Table 8.2 (continued).

Failure mode	Steel strip	Geogrid
Bearing capacity	$y_{\beta_{BC}} = 9.17 + 3c_1 + 0.38c_4$ $-0.8c_1^2 + 0.05c_2^2 + 0.05c_3^2 - 0.13c_4^2$ $-0.06c_1c_4$	$y_{\beta_{BC}} = 9.17 + 2.96c_1 + 0.35c_4$ $-0.74c_1^2 + 0.04c_2^2 - 0.11c_4^2$ $-0.01c_1c_2 - 0.06c_1c_4 + 0.01c_2c_4$
Tension	$y_{\beta_T} = 7.97 - 3.29c_2 - 4.75c_3 - 2.93c_4$ $+0.05c_1^2 + 0.32c_2^2 - 0.02c_3^2 + 0.11c_4^2$ $-0.84c_2c_3 - 0.48c_2c_4 - 0.78c_3c_4$	$y_{\beta_T} = 2.65 - 2.18c_2 - 2.09c_4$ $-0.02c_1^2 + 0.16c_2^2 + 0.12c_4^2$ $-0.52c_2c_4$
Pullout	$y_{\beta_P} = 6.23 + 2.25c_1 - 0.48c_2$ $-1.56c_3 + 2.25c_4$ $-0.54c_1^2 + 0.03c_2^2$ $+0.23c_3^2 - 0.54c_4^2$ $+0.21c_1c_2 + 0.15c_1c_3 - 0.20c_1c_4$ $-0.16c_2c_3 + 0.21c_2c_4 + 0.15c_3c_4$	$y_{\beta_P} = 14.26 + 3.34c_1 + 0.06c_2 + 1.43c_4$ $-1.22c_1^2 + 0.1c_2^2 - 0.16c_4^2$ $-0.04c_1c_2 + 0.12c_1c_4 - 0.02c_2c_4$

c_1, c_2, c_3, and c_4 are the coded variables of L_R, s_v, s_h, and H, respectively (see Table 6.2)

8.3 Formulation Of MOO Program

In MATLAB, the MOO program for obtaining sustainable designs of MSE walls is formulated as follows:

$$
\begin{aligned}
&\text{Minimize } f_1 \text{ : GWP} \\
&\text{Minimize } f_2 \text{ : Cost} \\
&\text{Maximize } f_3 \text{ : } \min \beta_{HL} \text{ of the five failure modes} \\
&\text{subjected to : } 0.7H \le L_R \le 1.1H \\
&\qquad s_v = \{0.3, 0.45, 0.6\} \\
&\qquad s_h = \{0.6, 0.7, 0.8, 0.9, 1.0\} \text{ for steel strip} \\
&\qquad 2 \le \beta_{HL} \le 6
\end{aligned}
\tag{8.1}
$$

It should be noted that the MOO in this study is conducted with respect to the minimum of the reliability indices (i.e., governing β_{HL}) corresponding to all failure modes. Parameters used for conducting the NSGA-II in this study are described in Section 7.5.

8.4 Results

In this section, sample results obtained from using the multi-objective optimization framework are provided for MSE walls. Progressive results of the optimization process are also provided to facilitate the understanding of the role of NSGA-II algorithm in the MOO framework. Based on the optimization results, design charts are created in which the optimized dimensions of MSE walls for different heights of wall are recommended.

8.4.1 Evolutions of MOO Results Over NSGA-II Stages and Generations

The results presented in this section are for 1 m length of the wall. Figure 8.1(a)-(d) show the MOO results after the initialization and evaluation, selection, reproduction, and elimination of NSGA-II (see Figure 7.3). The solutions are plotted with the total cost and GWP on the x and y axis, respectively, and the colours in Figure 8.1(a)-(d) represent the different ranges of reliability index. Figure 8.1(a) shows the evaluated initial population P_t in which some of the solutions are considered infeasible (i.e., $\beta_{HL} < 2.0$ and red circles in Figure 8.1(a)). Figure 8.1(b) shows the winners of binary tournament which are the selected parents for the reproduction. The infeasible designs are significantly reduced because better solutions are likely to win the tournament. Figure 8.1(c) shows the offsprings created after the crossover and mutation operators. Some infeasible designs are created, but the number of green circles is significantly increased which indicates maximization of reliability of MSE wall. In Figure 8.1(d), the infeasible designs are completely eliminated, and the solutions are slowly converging to the optimum (following the arrow direction

in Figure 8.1(d) while maximizing the number of green circles). The results shown in Figure 8.1(d) represent an iteration for one generation. The stages shown in Figure 8.1 are repeated T times to reach convergence to Pareto Front and improve diversity of solutions.

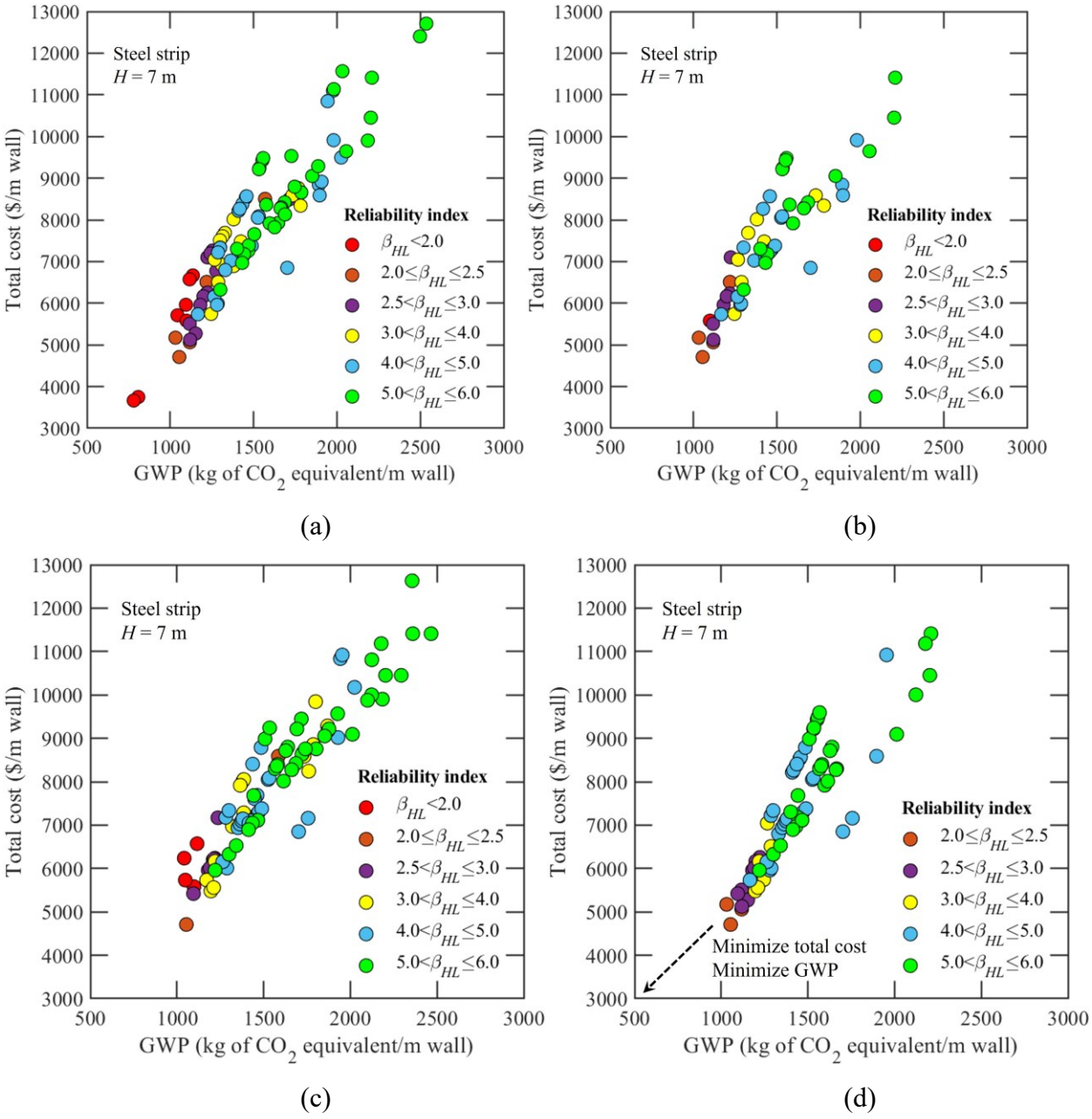

Figure 8.1. MOO results after (a) initialization, (b) binary tournament, (c) reproduction, and (d) elimination of NSGA-II

Figure 8.2(a)-(f) show the progress of reaching convergence and diversity over generations. At t = 1 (Figure 8.2(a)), the population is scattered and includes some infeasible designs. As the population evolves (the generation increases), solutions appear to gradually move towards the Pareto front (i.e., towards the origin of plot and increasing the number of circles in higher β_{HL} ranges). At the same time, the diversity of solutions is maintained as manifested by the wide spread of solutions having different values of cost, GWP, and reliability of MSE wall (Figure 8.2(d)-(f)).

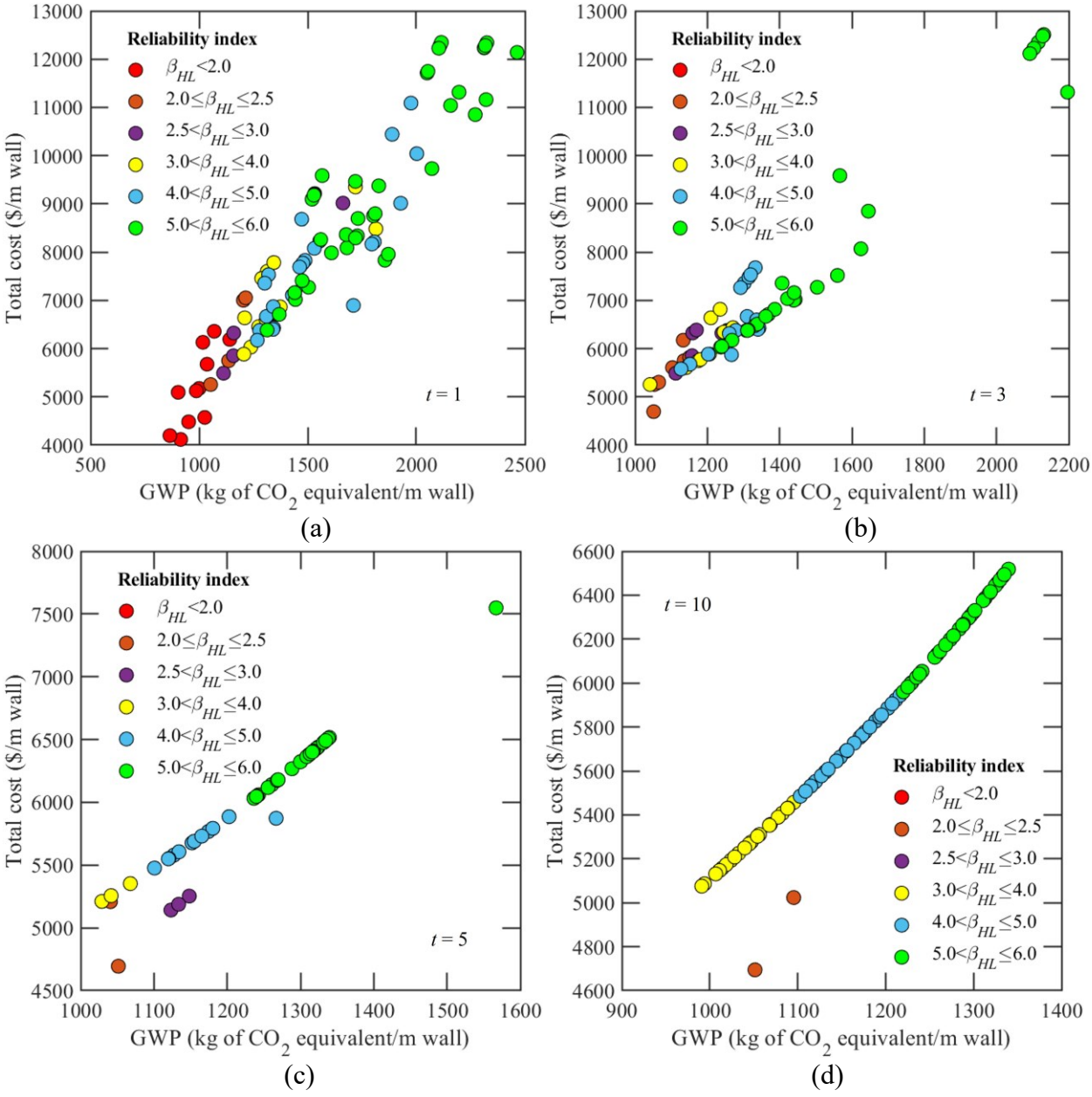

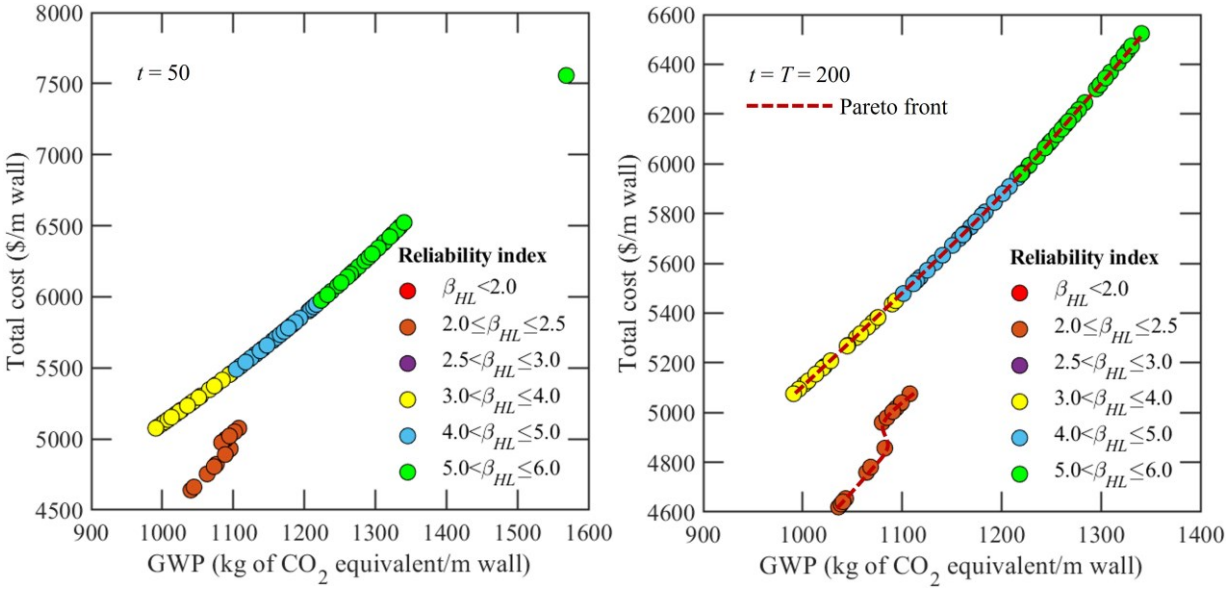

Figure 8.2. Evolution of population at (a) $t = 1$, (b) $t = 3$, (c) $t = 5$, (d) $t = 10$, (e) $t = 50$, and (f) $t = T = 200$

8.4.2 Relationships Between Objective Functions

The Pareto fronts for optimized MSE wall designs are shown in Figure 8.3, considering the three objective functions (i.e., GWP, total cost, and reliability index of MSE wall). It is difficult to visually understand the relationships between the three objectives based on a three-dimensional plot; hence, Figure 8.3(a) is projected such that the relationships between two objective functions are examined at a time. Figure 8.4(a) shows the relationship between reliability and GWP of MSE wall with steel strips, and Figure 8.4(b) shows the relationship between reliability and total cost. Conflicting relationships are observed in both the figures, which indicate that an MSE wall design with maximized reliability are likely to result in higher GWP and cost. Similar relationships are observed for MSE wall designed with geogrids. However, MSE walls with steel strips are mostly governed by bearing capacity, pullout, and tension failures, while MSE walls with geogrids are mostly governed by tension and bearing capacity failures. In contrast, conflicting relationship between the cost and GWP of MSE wall is not observed, as shown in Figure 8.4(c). Minimizing

the GWP will most likely result in minimizing the total cost of MSE wall. Some designs have different reliability and cost while having more or less the same GWP value as pointed with the blue dash lines in Figure 8.4(a) and (c). This is caused by the disconnection in the Pareto front. The designs have different values of s_h to meet the constraint of $\beta_{HL} \geq 2.0$. As s_h is decreased, there exists a capacity to decrease L_R/H, which result in the designs having the same GWP but higher cost and reliability. Although the costs of excavation, filling, and compaction are reduced as L_R/H is decreased, the cost pertaining to reinforcement is significantly increased as s_h is decreased.

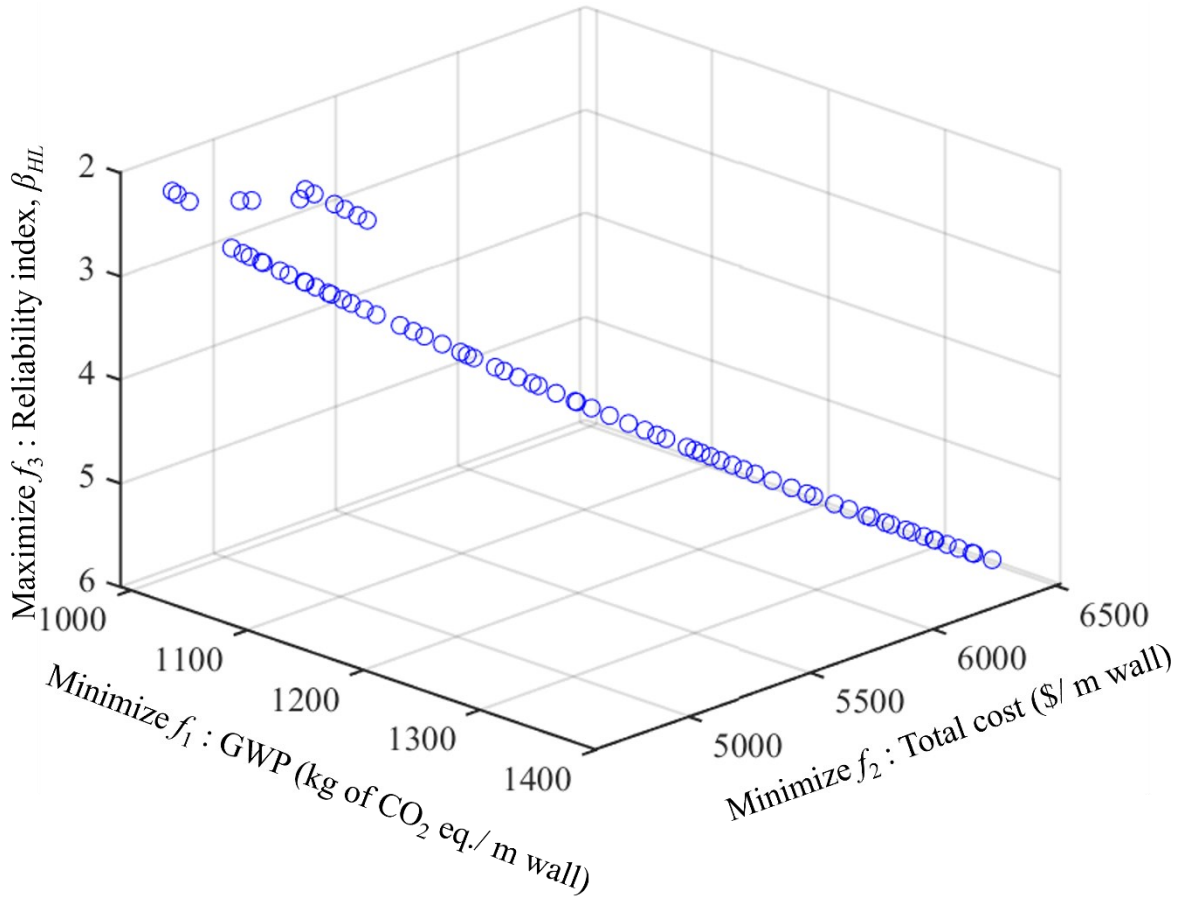

(a)

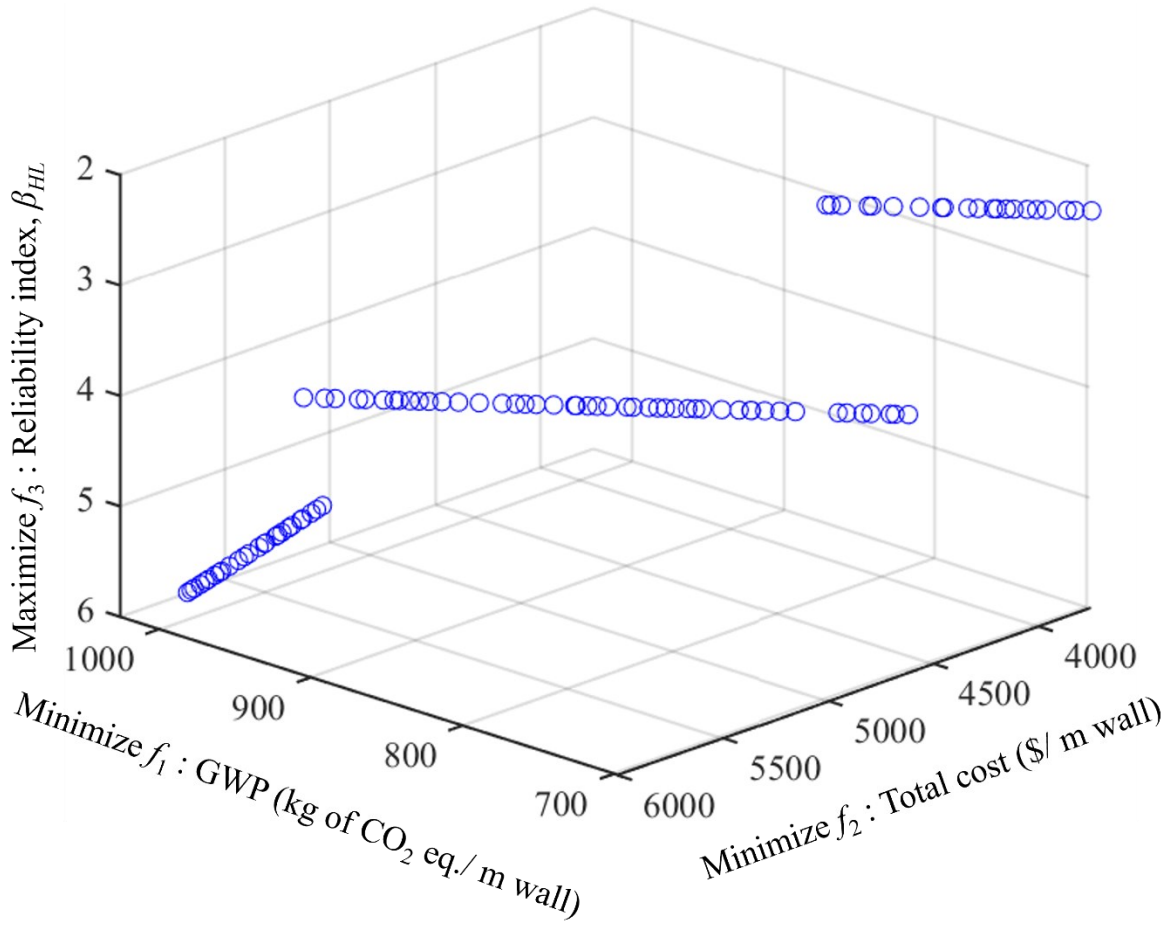

(b)

Figure 8.3. Sustainable solutions of MSE wall reinforced with (a) steel strips and (b) geogrids

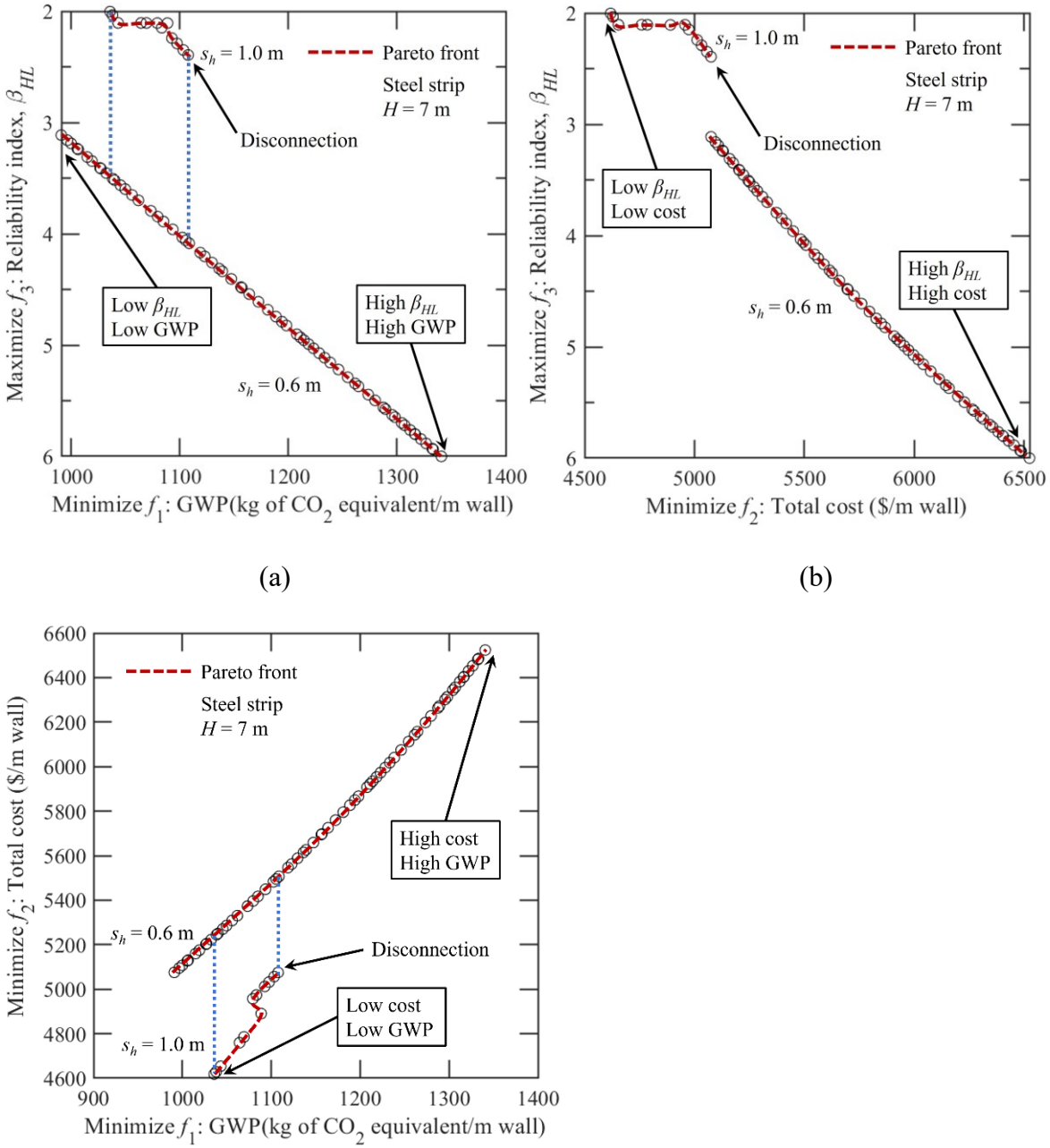

Figure 8.4. Relationship between reliability and (a) global warming impact, (b) total cost of MSE wall reinforced with steel strips, and (c) between total cost and global warming impact

8.4.3 MOO Results with Ranges of β_{HL}

Figure 8.5(a) and (b) show the Pareto front for MSE wall with steel strip and geogrid, respectively, with solutions categorized into different ranges of β_{HL}. A total of $N = 100$ solutions is shown in Figure 8.5. In both Figure 8.5(a) and (b), linearly increasing and disconnected Pareto fronts are observed. Solutions that are closer to the origin are deemed optimal given their reliabilities are acceptable to the designer. For example, the designs indicated by the orange circles in Figure 8.5 have lower GWP and total cost; however, its reliability is less than 2.5 which may not be sufficient. Hence, it is recommended that the designer selects the optimal design that meets the reliability requirements.

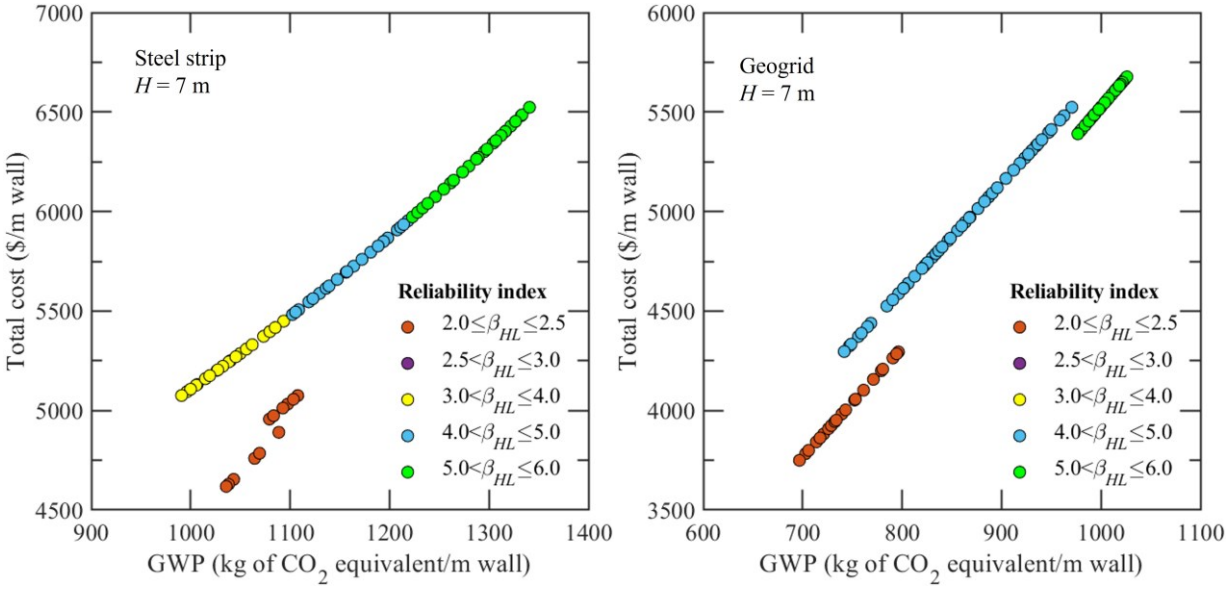

(a) (b)

Figure 8.5. Optimized solutions of MSE wall reinforced with (a) steel strips and (b) geogrids

8.4.4 MOO Results After Applying Cost Constraint

As for the final selection of optimized MSE wall design, it can be uncertain which design to choose from Figure 8.5 as a large pool of optimal designs ($N = 100$) is available. To reduce the

number of solutions and for practical reason, the constraint on cost difference is applied to the final MOO result to eliminate solutions that are too close to each other (i.e., solutions that have insignificant differences in terms of cost). Assuming a threshold of $100 cost difference, the results of MOO in Figure 8.5(a) and (b) are refined into Figure 8.6(a) and (b) for steel strip and geogrid, respectively. There are five steel strip designs (i.e., A, B, C, D, and E in Figure 8.6(a)) and four geogrid designs (i.e., F, G, H, and I in Figure 8.6(b)) that appear optimal in each range of β_{HL}. The selection of final design is dependent on the importance the designer places on each objective function. For example, the solution denoted as design 'A' has the lowest cost, but has higher GWP and lower β_{HL} than design 'C'. Given the total cost and GWP are estimated for 1 m length of wall, the $515 difference in cost and 28 kg of CO_2 equivalent difference in GWP between designs 'A' and 'C' can be significant for the entire wall. For example, these designs for a 20 m long wall will have differences of $515/m × 20 m = $10,300 and 28/m × 20 m = 560 kg of CO_2 equivalent in total. In this case, it is recommended that the trade-off between the cost and GWP is considered if $2.0 \leq \beta_{HL} \leq 2.5$ is acceptable. Figure 8.7(a) and (b) show the corresponding dimensions of designs shown in Figure 8.6(a) and (b), respectively. The reason why designs in $2.0 \leq \beta_{HL} \leq 2.5$ (i.e., orange circles in Figure 8.6(a) and Figure 8.7(a)) and in $3.0 < \beta_{HL} \leq 4.0$ (i.e., yellow circles in Figure 8.6(a) and Figure 8.7(a)) have more or less the same GWP values is because they have different horizontal spacing of steel strip. According to Figure 8.7(b), it is observed that solutions in different ranges of β_{HL} are caused by the different vertical spacing of geogrid. It is recommended the designer choose any of the design in Figure 8.7(a) and (b) that meet the reliability requirements specified by the jurisdiction.

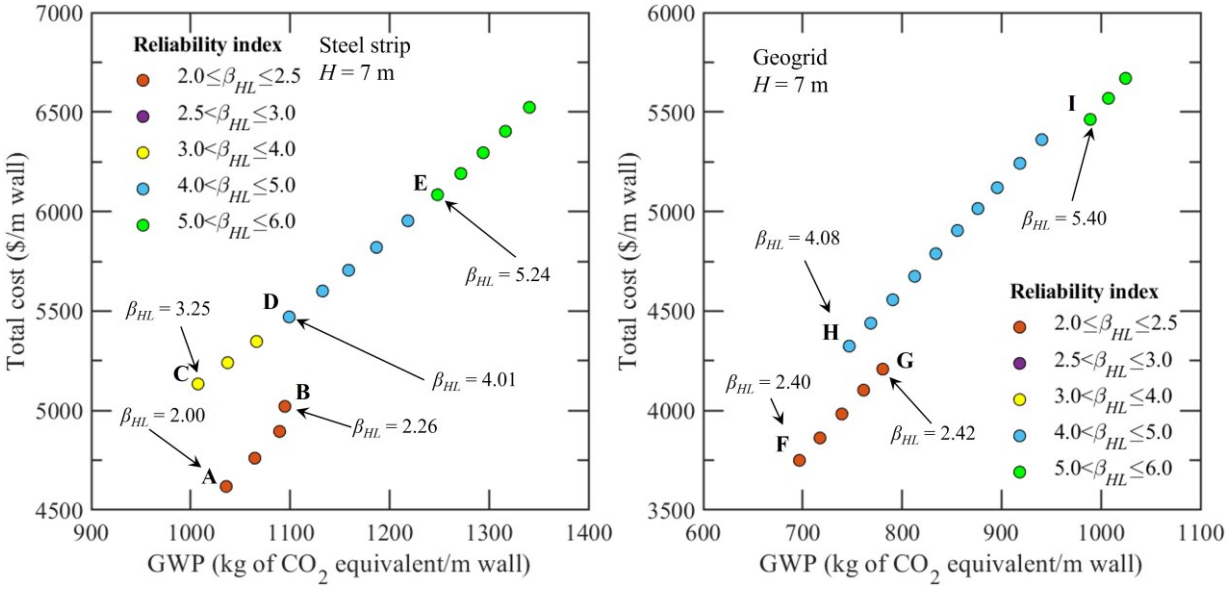

(a) (b)

Figure 8.6. Optimized solutions after application of constraint on cost difference: (a) steel strip and (b) geogrid

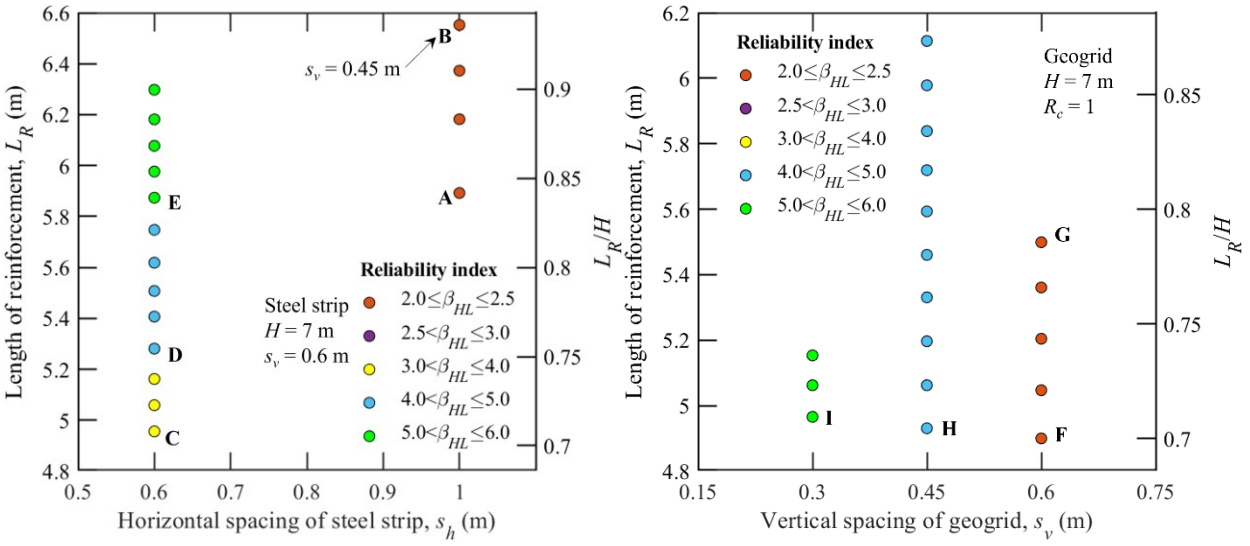

(a) (b)

Figure 8.7. Optimized design dimensions after application of constraint on cost difference: (a) steel strip and (b) geogrid

8.4.5 Other Parameters that Affect the MOO results

It should be noted that the results of MOO are influenced by the (i) bounds of design variables, (ii) site-specific parameters like soil properties and loading conditions, (iii) design increments for spacings of reinforcement, (iv) material properties of reinforcement, (v) unit costs for material, labour, and equipment, (vi) specifications of construction equipment, (vii) threshold for cost differences, and (viii) project-specific parameter like transportation distances. The bounds of design variables define the search space of MOO, which will expand or shrink accordingly. The regression models for GWP and reliability of MSE wall, provided in Table 6.3 and Table 8.2, respectively, are dependent on the soil properties, loading conditions, characteristics of random variables, and material properties of reinforcement. Specifications of construction equipment will affect the GWP and cost. Similarly, changing the unit costs will change the objective function for cost. The design increments for spacings of reinforcement and threshold for cost differences will change the spread between non-dominated solutions. Smaller increments and cost thresholds will have non-dominated solutions in closer ranges. All of these parameters can be freely modified in the framework to obtain results that are specific to the site and project.

8.4.6 Design Charts with Variable H

Figure 8.8(a) and (b) are the design charts for MSE walls with steel strip and geogrid, respectively, developed based on the results of MOO. In the design charts, the most optimal designs at different heights of wall are reported. For example, if the MSE wall is to be designed for H = 9 m and reinforced with steel strips, and given the minimum β_{HL} in the range of $2.0 \leq \beta_{HL} \leq 2.5$ is acceptable, the most optimal design configuration is L_R/H = 1.06, s_v = 0.6 m, s_h = 1.0 m according to Figure 8.8(a). The constraint on the cost difference of $100 is already applied to the design charts. Table 8.3 and Table 8.4 summarize the corresponding design dimensions of optimal

designs for each height of wall and range of β_{HL}. It should be noted that some designs are absent for certain ranges of β_{HL} because of several factors. In some cases, it may not be possible to obtain designs that fall within certain ranges of β_{HL}; for example, an MSE wall with H = 15 m cannot have $2.5 < \beta_{HL} \leq 5.0$ for the given bounds of design variables and increments of s_v and s_h. In other cases, the designs may be extremely limited for some ranges of β_{HL}; therefore, there is a high chance that those designs are eliminated because of the constraint on cost difference. For example, there are practically only one design possible (i.e., $L_R/H = 0.7$, s_v = 0.6 m, and s_h = 0.6 m) for $4.0 \leq \beta_{HL} \leq 5.0$ and for H = 9 m, and this design was eliminated after the constraint on cost difference was applied. For this specific design, the governing β_{HL} is 4.96 and given the L_R/H and s_v are already at extreme values, increasing s_h is the only possible scenario that will likely reduce β_{HL}. However, if s_h is increased to 0.7 m (the next increment), β_{HL} is dramatically reduced 3.8, which explains the lack of diversity in solutions within $4.0 \leq \beta_{HL} \leq 5.0$. Hence, choices on the design increment also affect the diversity in solutions. In some rare cases, after applying the constraint on cost difference, designs that have the same cost but different GWP and β_{HL} will be eliminated even thought they are both non-dominant solutions. Hence, Table 8.3 and Table 8.4 are adjusted such that the designs eliminated, because of the above reasons, are not excluded.

In the design charts, designs with H = 3 m are not considered because of the limitations of the regression models. The GWP values obtained from the regression model were significantly inaccurate. Adjusting the regression model by using inscribed or face-centered CCD, or by adjusting α value of the axial points may increase the accuracy of response surface for GWP; however, improving the response surface in this regard is beyond the scope of study.

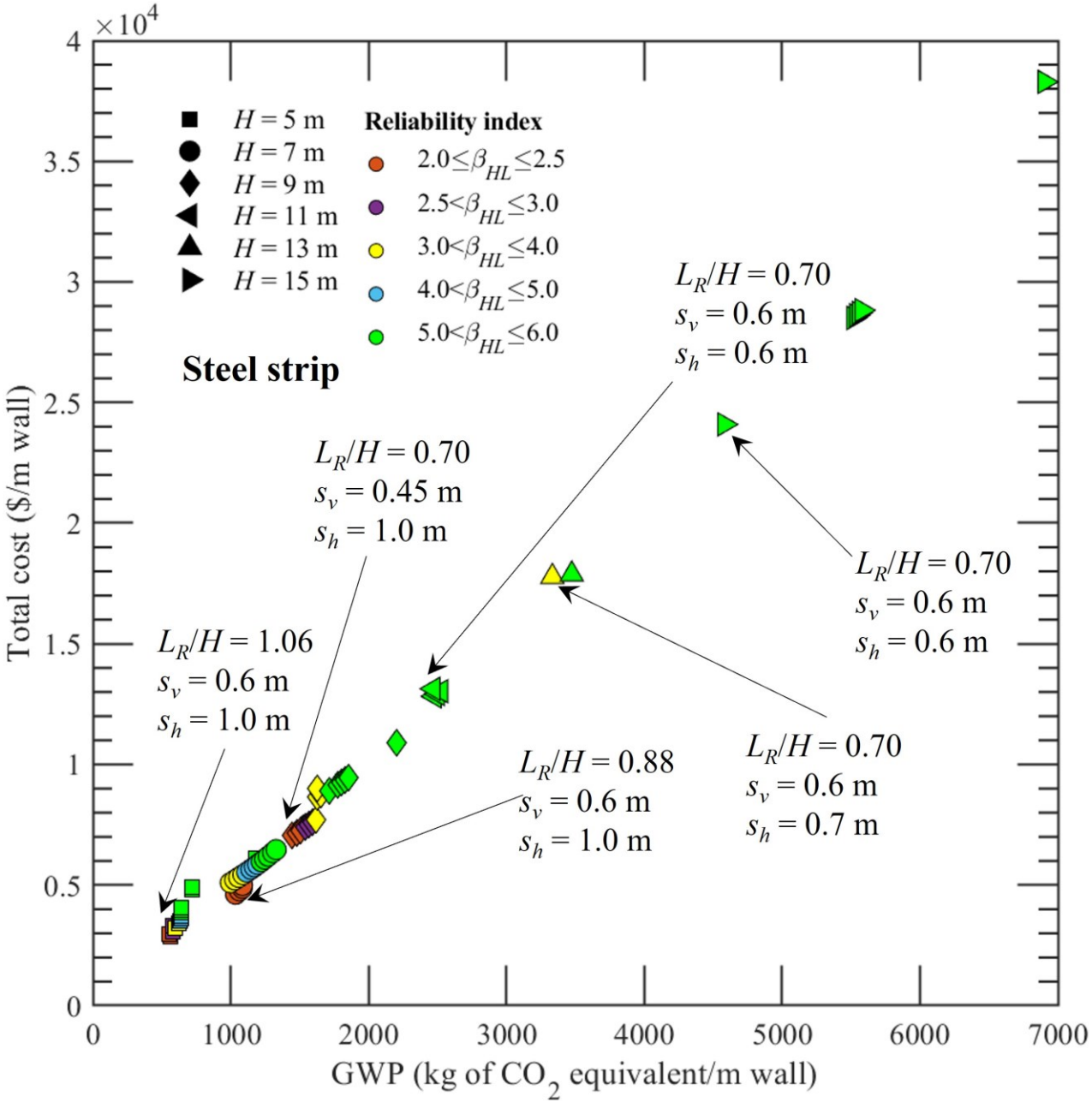
×10^4
4
3.5
3
2.5
2
1.5
1
0.5
0
Total cost ($/m wall)
0
1000
2000
3000
4000
5000
6000
7000
GWP (kg of CO2 equivalent/m wall)
H = 5 m
H = 7 m
H = 9 m
H = 11 m
H = 13 m
H = 15 m
Reliability index
2.0≤β_HL≤2.5
2.5<β_HL≤3.0
3.0<β_HL≤4.0
4.0<β_HL≤5.0
5.0<β_HL≤6.0
Steel strip
L_R/H = 0.70
s_v = 0.6 m
s_h = 0.6 m
L_R/H = 0.70
s_v = 0.45 m
s_h = 1.0 m
L_R/H = 0.70
s_v = 0.6 m
s_h = 0.6 m
L_R/H = 1.06
s_v = 0.6 m
s_h = 1.0 m
L_R/H = 0.88
s_v = 0.6 m
s_h = 1.0 m
L_R/H = 0.70
s_v = 0.6 m
s_h = 0.7 m

(a)

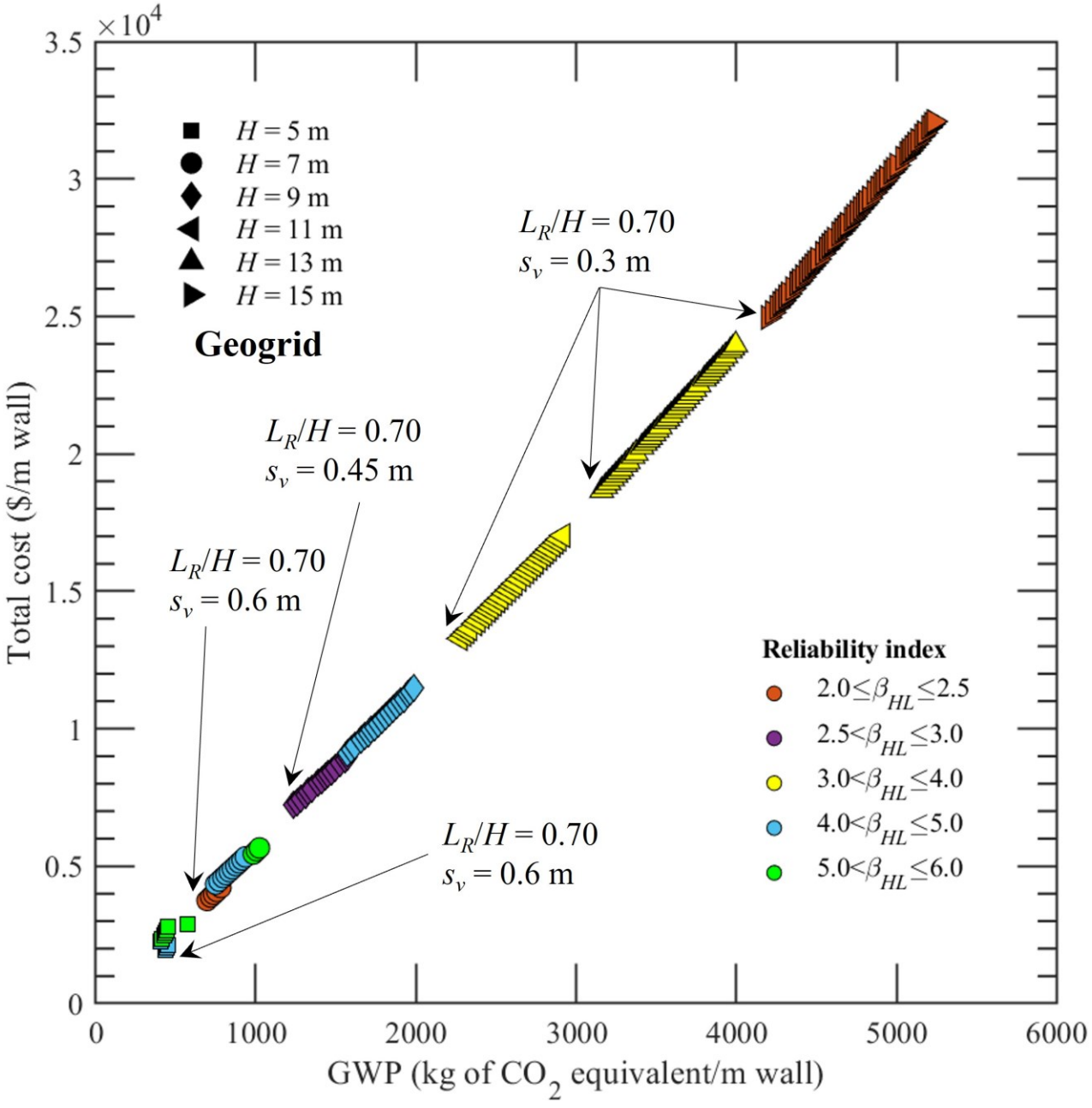

(b)

Figure 8.8. Optimization design charts of MSE wall reinforced by (a) steel strips and (b) geogrids

Table 8.3. Optimized design dimensions of MSE wall with steel strips

Reliability index	Height of wall, H (m)								
	5			7			9		
	L_R/H	s_v (m)	s_h (m)	L_R/H	s_v (m)	s_h (m)	L_R/H	s_v (m)	s_h (m)
$2.0 \leq \beta_{HL} \leq 2.5$	1.06	0.6	1.0	0.88	0.6	1.0	0.70	0.45	1.0
$2.5 < \beta_{HL} \leq 3.0$	0.83	0.6	0.6	–	–	–	0.74	0.45	1.0
$3.0 < \beta_{HL} \leq 4.0$	0.91	0.6	0.6	0.70	0.6	0.6	0.77	0.45	1.0
$4.0 < \beta_{HL} \leq 5.0$	0.94	0.6	0.6	0.76	0.6	0.6	0.70*	0.6*	0.6*
$5.0 < \beta_{HL} \leq 6.0$	1.03	0.6	0.6	0.82	0.6	0.6	0.74	0.6	0.6

Reliability index	Height of wall, H (m)								
	11			13			15		
	L_R/H	s_v (m)	s_h (m)	L_R/H	s_v (m)	s_h (m)	L_R/H	s_v (m)	s_h (m)
$2.0 \leq \beta_{HL} \leq 2.5$	–	–	–	–	–	–	0.70*	0.6*	0.7*
$2.5 < \beta_{HL} \leq 3.0$	0.70*	0.6*	0.8*	–	–	–	–	–	–
$3.0 < \beta_{HL} \leq 4.0$	–	–	–	0.70	0.6	0.7	–	–	–
$4.0 < \beta_{HL} \leq 5.0$	–	–	–	–	–	–	–	–	–
$5.0 < \beta_{HL} \leq 6.0$	0.70	0.6	0.6	0.70	0.6	0.6	0.70	0.6	0.6

*design eliminated by the cost constraint

Table 8.4. Optimized design dimensions of MSE wall with geogrids

Reliability index	Height of wall, H (m)					
	5		7		9	
	L_R/H	s_v (m)	L_R/H	s_v (m)	L_R/H	s_v (m)
$2.0 \leq \beta_{HL} \leq 2.5$	–	–	0.7	0.6	–	–
$2.5 < \beta_{HL} \leq 3.0$	–	–	–	–	0.7	0.45
$3.0 < \beta_{HL} \leq 4.0$	–	–	–	–	–	–
$4.0 < \beta_{HL} \leq 5.0$	0.70	0.6	0.71	0.45	0.71	0.3
$5.0 < \beta_{HL} \leq 6.0$	0.74	0.45	0.71	0.3	–	–

Reliability index	Height of wall, H (m)					
	11		13		15	
	L_R/H	s_v (m)	L_R/H	s_v (m)	L_R/H	s_v (m)
$2.0 \leq \beta_{HL} \leq 2.5$	–	–	–	–	0.7	0.3
$2.5 < \beta_{HL} \leq 3.0$	–	–	–	–	–	–
$3.0 < \beta_{HL} \leq 4.0$	0.7	0.3	0.7	0.3	–	–
$4.0 < \beta_{HL} \leq 5.0$	–	–	–	–	–	–
$5.0 < \beta_{HL} \leq 6.0$	–	–	–	–	–	–

8.5 Summary

The multi-objective optimization framework proposed in Chapter 7 is demonstrated using examples of MSE walls. Using the framework, the design dimensions of MSE walls (i.e., length of reinforcement, vertical and horizontal spacings of reinforcement), which result in (i) minimized environmental impact, (ii) minimized cost, and (iii) maximized engineering reliability of MSE walls, are determined. Since five failure modes of MSE walls were assumed, the optimization was

performed based on the minimum system reliability of MSE walls, assuming failure in any of the mode will result in failure in the MSE walls (system). Two types of reinforcement were considered in this study – steel strips and geogrids. The optimized solutions (i.e., designs that are most optimized with respect to the three objective functions of engineering reliability, cost, and global warming impact) were categorized into different ranges of reliability index so that the designer can select the design dimensions that suit the project requirements. Design charts that provide optimized design dimensions of MSE walls, reinforced by steel strips or geogrids, were developed so that practitioners can easily determine the dimensions of MSE wall which resulted in balance of environmental impact, cost, and engineering reliability.

8.6 List Of Symbols

Notation	Description
c_i	Coded variable
f_i	Objective function
H	Height of wall
L_R	Length of reinforcement
m	Total number of objective functions
N	Total number of solutions in a population
P_t	Population at generation t
s_h	Horizontal spacing of reinforcement
s_v	Vertical spacing of reinforcement
T	Total number of generations
t	Current generation
y_{β_S}, y_{β_O}, $y_{\beta_{BC}}$, y_{β_T}, y_{β_P}	Regression models for estimating reliability index of MSE walls for sliding, overturning, bearing capacity, tension, and pullout failures, respectively
β_{HL}	Hasofer-Lind reliability index

CHAPTER 9: OPTIMIZED PILE FOUNDATION DESIGNS

In this chapter, the multi-objective optimization is performed to determine sustainable designs of drilled shaft and pile group. Reinforced concrete shaft is used for the single drilled shaft, and group piles consist of multiple drilled shafts with a pile cap. The drilled shafts are designed for the soil profile 1 shown in Figure 3.2(a), and the ratio of live load to dead load $LL/DL = 1$ is assumed. The parameters used in the MOO framework (see Figure 7.2) for the pile foundation designs are discussed in the next sections.

9.1 Selection of Design Variables and Bounds

The design variables of single drilled shafts are the pile diameter B_p and pile length L_p, and the design variables of drilled shafts in groups are (i) B_p, (ii) L_p, (iii) center-to-center spacing between the single drilled shafts or its factor f_{sp}, and (iv) number of single piles in row N_r and N_c column direction. The pile diameter is assumed to range from 0.3 to 2.0 m with a 100 mm increment, and the pile length is ranged from 5 to 30 m (for single drilled shafts) and 10 to 30 m (for pile group) with a 1 m increment.

For pile group designs, the center-to-center spacing s_p between the single piles is assumed to range from $2B_p$ to $5B_p$ (Salgado, 2008) (i.e., $f_{sp} = 2$ to 5), and the number of piles in each row and column can range from 2 to 6 piles. The thickness of pile cap T_c is determined based on the diameter of individual drilled shafts as follows (Magade and Ingle, 2020):

$$\left\{\begin{array}{l} T_c = 2B_p + 0.1 \text{ for } B_p \le 0.55 \\ T_c = \dfrac{8(B_p - 0.1)}{3} \text{ for } B_p > 0.55 \end{array}\right\} \tag{9.1}$$

The clear edge distance of pile cap is assumed to be half of B_p as per recommendations by ACI (2011) and Magade and Ingle (2020). Hence, the pile cap length and width can be estimated as follows:

$$\begin{aligned} l_c &= \left(N_r - 1\right) f_{sp} + B_p + 2d_{ce} \\ w_c &= \left(N_c - 1\right) f_{sp} + B_p + 2d_{ce} \end{aligned} \tag{9.2}$$

where l_c and w_c are the length and width of pile cap, respectively, N_r and N_c are the number of piles in row and column direction, respectively, f_{sp} is the factor for pile spacing (2 to 5), and d_{ce} is the clear edge distance of pile cap.

9.2 Formulation of Objective Functions

9.2.1 Estimation of Environmental Impact

LCA is used to estimate the global warming impact of single drilled shafts and pile group. The functional unit used for the LCA of singled drilled shaft is 'the mass of drilled shaft to sufficiently support the applied load without bearing capacity failure (assuming a specified target probability of failure) and settlement exceeding 30 mm'. For pile group, the functional unit is defined as 'the mass of pile group (with the pile cap included) to support the applied load without individual pile and block failures given a specified target p_f. The assumptions and parameters used in the LCA calculations are provided in Section 3.2.

9.2.2 Estimation of Cost

The cost estimation handbook for construction by RSMeans (2015) is used for estimating the material and construction cost of single drilled shafts and pile groups. The total cost of a single drilled shaft is calculated based on the pile diameter size, length of pile, and amount of steel reinforcement, as summarized in Table 9.1. If the mass of steel reinforcement exceeds 50 pounds

per cubic yard (29.66 kg per volume) of drilled shaft, $1.28 is added per pound (lb) of steel reinforcement. If the length of pile diameter ranges between 15.24 to 30.48 m (50 to 100 feet), 7% of the unit cost in Table 9.1 is added per the additional linear foot of drilled shaft. For pile group, the total cost is the summation of (i) the cost for individual piles (i.e., the cost calculated using Table 9.1 is multiplied by the total number of piles) and (ii) cost for the pile cap. Table 9.2 summarizes the unit costs related to the excavation, formwork, concrete, and steel reinforcement for the construction of pile cap.

Table 9.1. Unit cost of single drilled shaft

Range of pile diameter, B_p (m)	Unit cost[1] ($/linear foot of drilled shaft)
$B_p \leq 0.46$	38
$0.46 < B_p < 0.61$	47
$0.61 < B_p < 0.76$	64
$0.76 < B_p < 0.91$	83
$0.91 < B_p < 1.22$	123
$1.22 < B_p < 1.52$	166
$1.52 < B_p < 1.83$	218
$1.83 < B_p < 2.13$	276

[1]includes cost of excavation, concrete, and steel reinforcing for 50 feet long (15.24 m) drilled shaft; no ground water

Table 9.2. Unit costs of pile cap

Material or construction work	Unit cost
Excavation using hydraulic excavator	$2.48 per bank cubic yard[1]
Loading excavated soil onto trucks	$1.24 per bank cubic yard
Hauling and dumping excavated soil	$8.65 per loose cubic yard[2]
Concrete formwork	$10.75 per square foot contact area[3] (perimeter surfaces of pile cap)
Concrete ready mix	$112 per cubic yard
Concrete pouring using direct chute	$33 per cubic yard for under 5 cubic yards $16.8 per cubic yard for 5 to 10 cubic yards $13.65 per cubic yard for over 10 cubic yards
Steel reinforcement for pile cap	2325 per ton of steel

[1]The bank volume is calculated as $l_c \times w_c \times T_c$
[2]The loose volume is calculated as $l_c \times w_c \times T_c \times (1+b_f)$ in which the bulk factor $b_f = 0.25$ is assumed
[3]The square foot contact area is estimated as $2 \times T_c(l_c+w_c)$

9.2.3 Estimation of Engineering Reliability

Using FORM, the reliability indices β_{HL}s of single drilled shafts and pile group are obtained following the procedures described in Section 5.3.2 and 5.4. The characteristics of random variables used in the FORM are summarized in Table 5.1.

For pile group in sand, block failure is unlikely to occur; therefore, the reliability against bearing capacity failure of individual piles in the group is computed in this study (Salgado, 2008). The reliability analysis is conducted based on the maximum compression load obtained from the distribution of applied load, calculated using Equation (3.10).

9.2.4 Construction of Regression Models

Response surface methodology is used to construct regression models for GWP and β_{HL} of drilled shafts. The second-order regression model (with interaction effect) for GWP in Table 5.3 is used for estimating the GWP of single drilled shafts. The same procedure described in Section 5.7 is used for developing second-order regression models for β_{HL} of single drilled shaft:

$$y_{ULS} = -17.35 + 13.59B_p + 0.72L_p - 2.90B_p^{\,2} - 0.008L_p^{\,2} - 0.15B_pL_p \tag{9.3}$$

$$y_{SLS} = 5.87 + 16.40B_p - 0.49L_p - 4.87B_p^{\,2} + 0.005L_p^{\,2} + 0.11B_pL_p \tag{9.4}$$

where y_{ULS} is the estimated β_{HL} for bearing capacity failure and y_{SLS} is the estimated β_{HL} for settlement. The minimum of (y_{ULS}, y_{SLS}) is used to represent the objective value of engineering reliability.

For pile group, a central composite design (CCD) with k = 5 variables (i.e., B_p, L_p, f_{sp}, N_r, and N_c) is conducted to develop second-order regression model for β_{HL}. Hence, 33 results of FORM are used out of which 10 results correspond to the factorial points, 32 results are the axial points, and 1 result is for the center point of CCD. Table 9.3 summarizes the coded variables c used in

conducting the CCD of pile groups. The second-order regression model for β_{HL} of pile groups is expressed as:

$$\begin{aligned} y_{\beta_{\text{GROUP}}} &= 7.2665 + 1.24c_1 - 0.324c_2 + 0.076c_3 + 0.239c_4 + 0.239c_5 \\ &-0.343{c_1}^2 + 0.045{c_2}^2 + 0.039{c_3}^2 - 0.003{c_4}^2 - 0.003{c_5}^2 \\ &-0.356c_1c_2 - 0.064c_1c_3 - 0.155c_1c_4 - 0.155c_1c_5 \\ &-0.042c_2c_3 - 0.121c_2c_4 - 0.121c_2c_5 \\ &-0.032c_3c_4 - 0.032c_3c_5 - 0.081c_4c_5 \end{aligned} \tag{9.5}$$

where $y_{\beta_{\text{GROUP}}}$ is the estimated β_{HL} for bearing capacity failure of pile group and c_1, c_2, c_3, c_4, and c_5 are the coded variables for B_p, L_p, f_{sp}, N_r, and N_c, respectively.

To reduce the number of variables, the regression model for GWP is developed based on (i) mass of concrete, (ii) mass of steel, and (iii) volume of diesel. Thus, a CCD with k = 3 variables is conducted, and their coded variables are obtained based on the maximum and minimum values ($\xi_{\max}$ and $\xi_{\min}$) listed in Table 9.4 and Equation (5.26). The second-order regression model for estimating the GWP of group piles is expressed as:

$$\begin{aligned} y_{GWP_{\text{GROUP}}} &= 31928244 + 1379748c_1 + 214271c_2 + 4075c_3 \\ &+0.49c_1^2 + 0.49c_2^2 + 0.49c_3^2 + 0.25c_1c_3 \end{aligned} \tag{9.6}$$

where $y_{GWP_{\text{GROUP}}}$ is the estimated GWP of pile group and c_1, c_2, and c_3 are the coded variables for mass of concrete, mass of steel, and volume of diesel, respectively.

Table 9.3. Coded variables used in CCD of pile group (for β_{HL})

Design variable	Coded variable, c				
	−2	**−1**	**0**	**+1**	**+2**
B_p (m)	0.3	0.725	1.15	1.575	2
L_p (m)	10	15	20	25	30
f_{sp}	2	2.75	3.5	4.25	5
N_r	2	3	4	5	6
N_c	2	3	4	5	6

Table 9.4. Maximum and minimum values of natural variables used in CCD of pile group (for GWP)

Natural variables	Maximum value, ξ_{max}	Minimum value, ξ_{min}
Mass of concrete (kg)	43,610,000	9,200
Mass of steel (kg)	674,500	580
Volume of diesel (L)	6,000	30

9.3 Formulation of MOO Programs

The NSGA-II for single drilled shaft is formulated as follows in MATLAB:

$$\begin{aligned}
&\text{Minimize } f_1 : \text{GWP} \\
&\text{Minimize } f_2 : \text{Cost} \\
&\text{Maximize } f_3 : \text{ min of } \beta_{HL} \text{ for ULS and SLS} \\
&\text{subjected to : } B_p \in [0.3, 2.0] \text{ with 100 mm increment} \\
&\qquad\qquad L_p \in [5, 30] \text{ with 1 m increment} \\
&\qquad\qquad 2 \le \beta_{HL} \le 6
\end{aligned} \tag{9.7}$$

For pile group, the following formulation is used in MATLAB:

$$\begin{aligned}
&\text{Minimize } f_1 : \text{GWP} \\
&\text{Minimize } f_2 : \text{Cost} \\
&\text{Maximize } f_3 : \beta_{HL} \\
&\text{subjected to : } B_p \in [0.3, 2.0] \text{ with 100 mm increment} \\
&\qquad\qquad L_p \in [10, 30] \text{ with 1 m increment} \\
&\qquad\qquad f_{sp} \in [2, 5] \\
&\qquad\qquad N_r = \{2, 3, 4, 5, 6\} \\
&\qquad\qquad N_c = \{2, 3, 4, 5, 6\} \\
&\qquad\qquad 2 \le \beta_{HL} \le 6
\end{aligned} \tag{9.8}$$

9.4 Results

Sample optimization results for single and group drilled shafts are provided in this section. The relationships between the three objective functions (i.e., engineering reliability, cost, and

global warming impact) used in the optimization program are discussed. Based on the optimization results, design charts for selecting the optimized design dimensions of single and group drilled shafts are developed.

9.4.1 Optimization of Single Drilled Shaft Designs

Figure 9.1 shows the results of multi-objective optimization for single drilled shafts. To better visualize the Pareto front, Figure 9.1 is projected such that the relationship between two objective functions are shown one at a time in Figure 9.2. A convex Pareto front is observed when Figure 9.1 is projected for the objective functions of reliability index and GWP, as shown in Figure 9.2(a). The convex Pareto front indicates a conflicting relationship between reliability index and GWP of drilled shafts. Disconnected Pareto fronts are observed in both Figure 9.2(b) and (c); however, the directions to which the Pareto fronts are extended differ. For example, the Pareto fronts in Figure 9.2(b) extend in vertical direction which indicates optimized designs can vary in the engineering reliability of drilled shaft but have very small changes in the cost. In Figure 9.2(c), the Pareto fronts are extended horizontally which indicates optimized drilled shaft designs can have some variations in GWP but have more or less the same cost. This constant trend in terms of cost occurs because the designs with higher GWP also have higher reliability index for which the optimization program aims to maximize. The disconnection in the Pareto fronts is mainly caused because of the changes in the unit costs of drilled shafts, as shown in Table 9.1.

Figure 9.3 shows the final results of MOO with the designs categorized into different ranges of reliability index. The cost constraint with $100 difference threshold is also applied in Figure 9.3 which mean designs that have less than $100 cost difference in Figure 9.2(c) are eliminated. For each range of reliability index, the most optimized designs are determined (see A, B, C, D in Figure 9.3). For example, if a drilled shaft design with a reliability index between 2 to

3 is acceptable for the project, a drilled shaft with B_p = 0.8 m and L_p = 25 m is the most optimized design considering the GWP, cost, and reliability of drilled shaft. It is recommended that a design, from A, B, C, and D in Figure 9.3, that meets the safety requirements of the project is chosen. Figure 9.3 is a sample MOO result specifically developed for drilled shafts designed for soil profile 1 (Figure 3.2); hence modifications to the input variables (see Figure 7.1) will change the MOO results. For example, the optimization results are likely to change if the followings are changed: (i) design increments in and bounds of diameter and length, (ii) soil profile, (iii) loading conditions, (iv) cost threshold, and (v) unit costs for material and construction work.

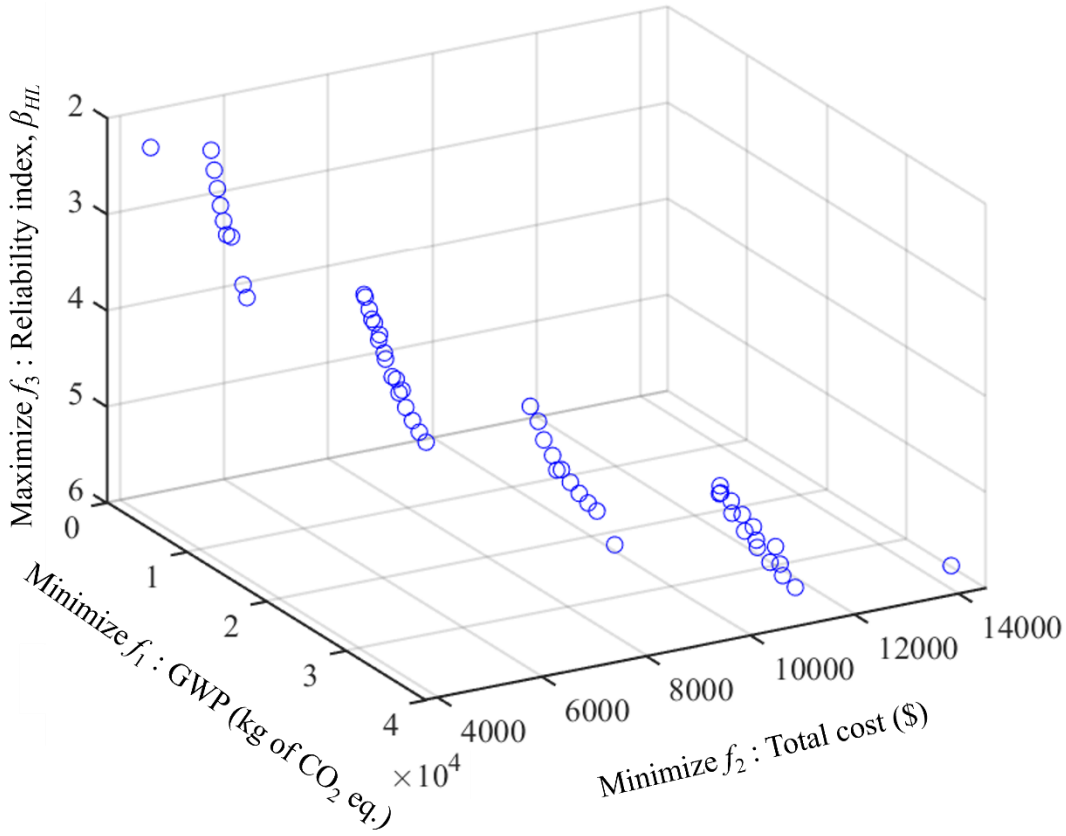

Figure 9.1. Sustainable solutions for single drilled shaft designs

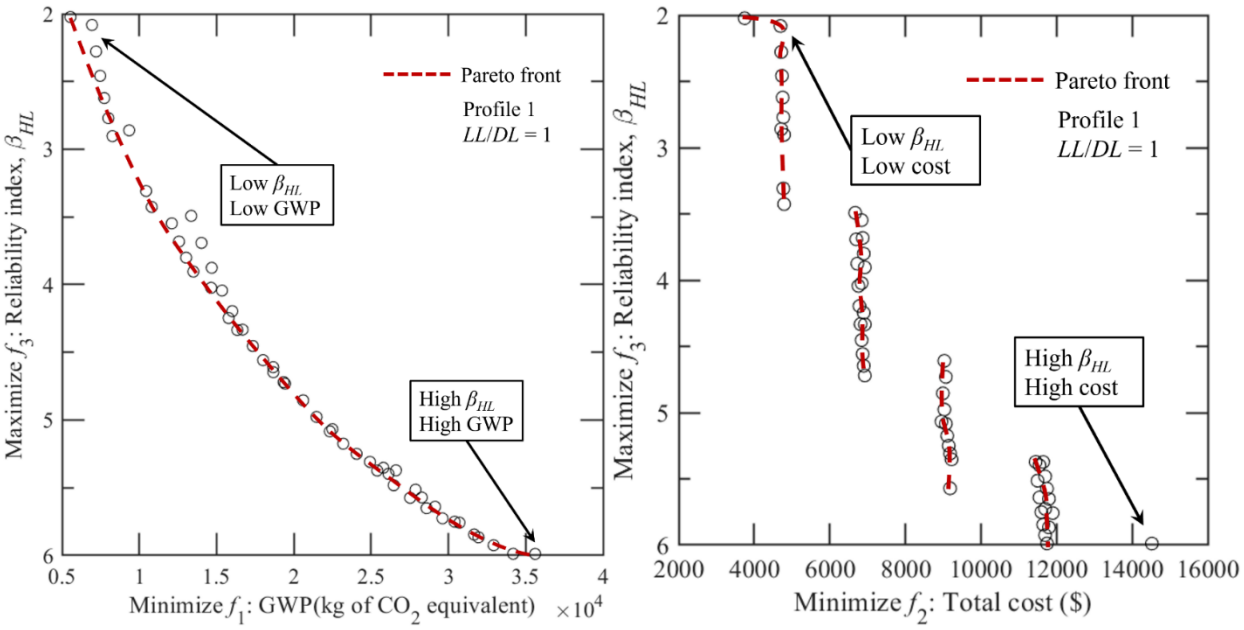

(a) (b)

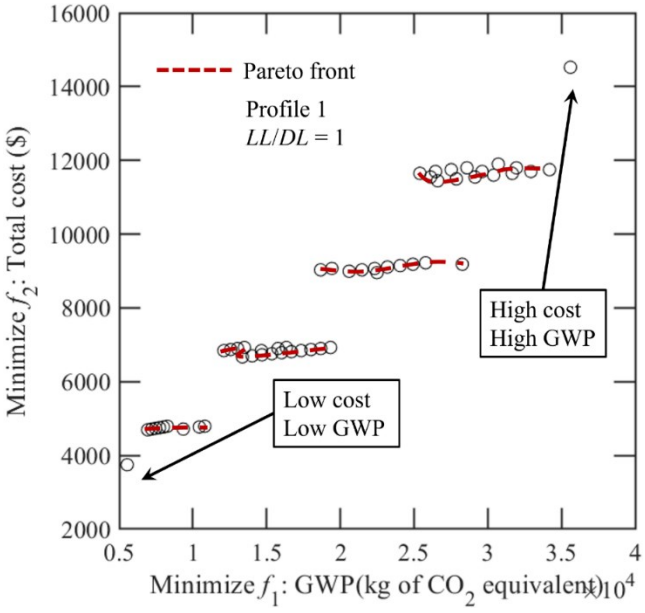

(c)

Figure 9.2. Relationship between reliability and (a) global warming impact, (b) total cost, and (c) between global warming impact and total cost of single drilled shafts

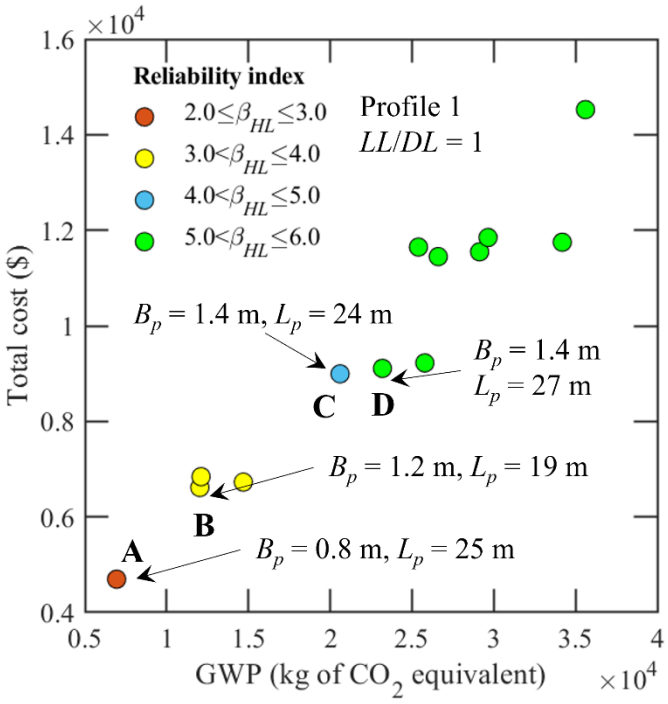

Figure 9.3. Design charts for optimized single drilled shaft designs

9.4.2 Optimization of Pile Group Designs

Figure 9.4 shows the Pareto front which consists of the optimized designs of pile group, considering engineering reliability, cost, and global warming impact. Figure 9.5 shows the projected Pareto fronts of optimized solutions for pile group. Convex Pareto fronts are observed in Figure 9.5(a) and (b) which indicates conflicting relationship between (a) reliability index and GWP and (b) reliability index and total cost of pile group. Disconnected and nearly linear Pareto fronts are observed in Figure 9.5(c), indicating an increase in GWP of pile group also results in increase in the total cost. The disconnection in the Pareto front, as observed in Figure 9.5 (c), is caused by the differences in the length of pile and the total number of individual piles. For example, in the optimization, pile group designs with longer piles and fewer number of individual piles are considered equivalent with designs that have shorter piles but more number of individual piles. Figure 9.6 shows the design chart developed for pile groups. The optimized solutions are clustered

for low cost and GWP (i.e., the left corner of Figure 9.6(a)); hence Figure 9.6(b) shows the design chart for the red area indicated in Figure 9.6(a). The optimum design in each range of reliability index is annotated by A, B, C, and D in Figure 9.6. It is observed that the MOO program generally favors designs of pile group that consists of long piles ($L_p \geq 24$ m) with small diameter ($B_p = 0.3$ m) and smallest number of piles (i.e., 2 by 2 configuration).

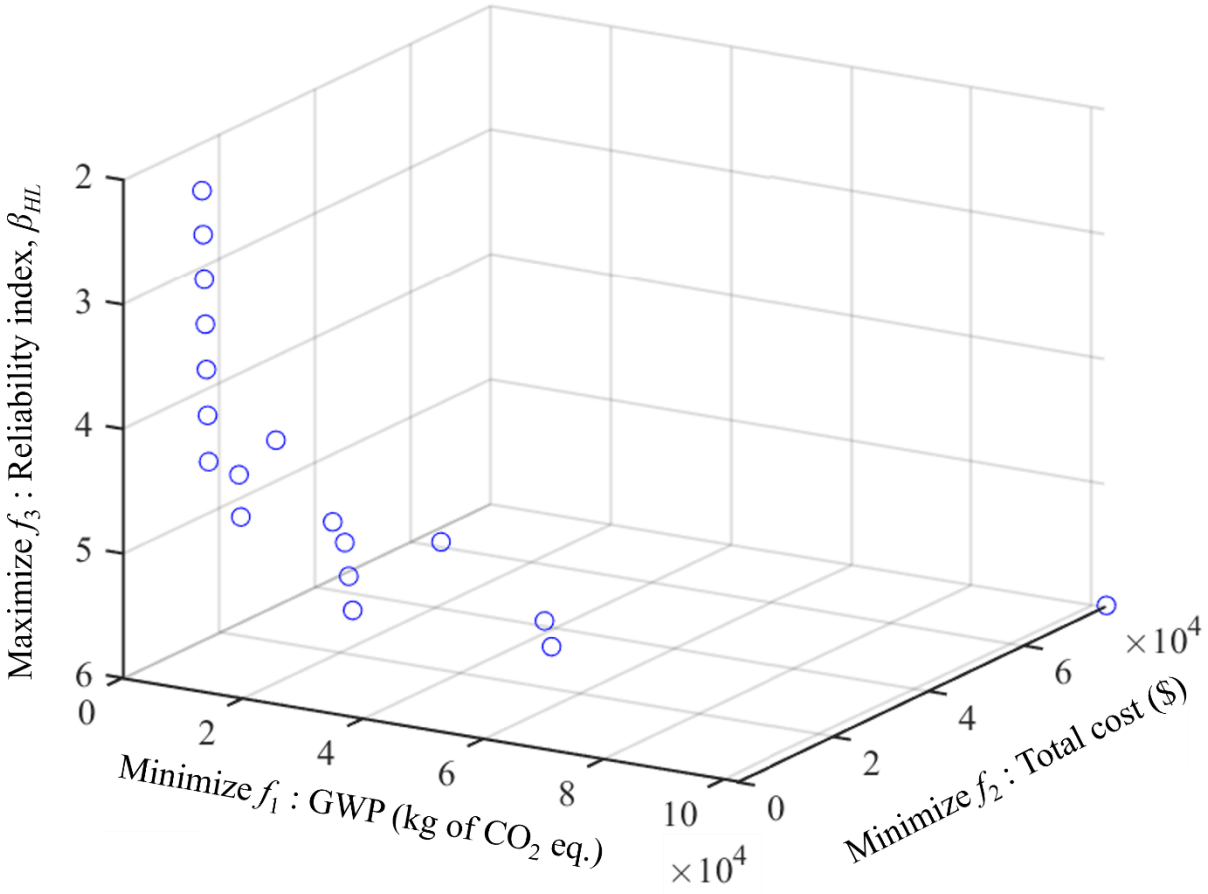

Figure 9.4. Sustainable solutions for pile group designs

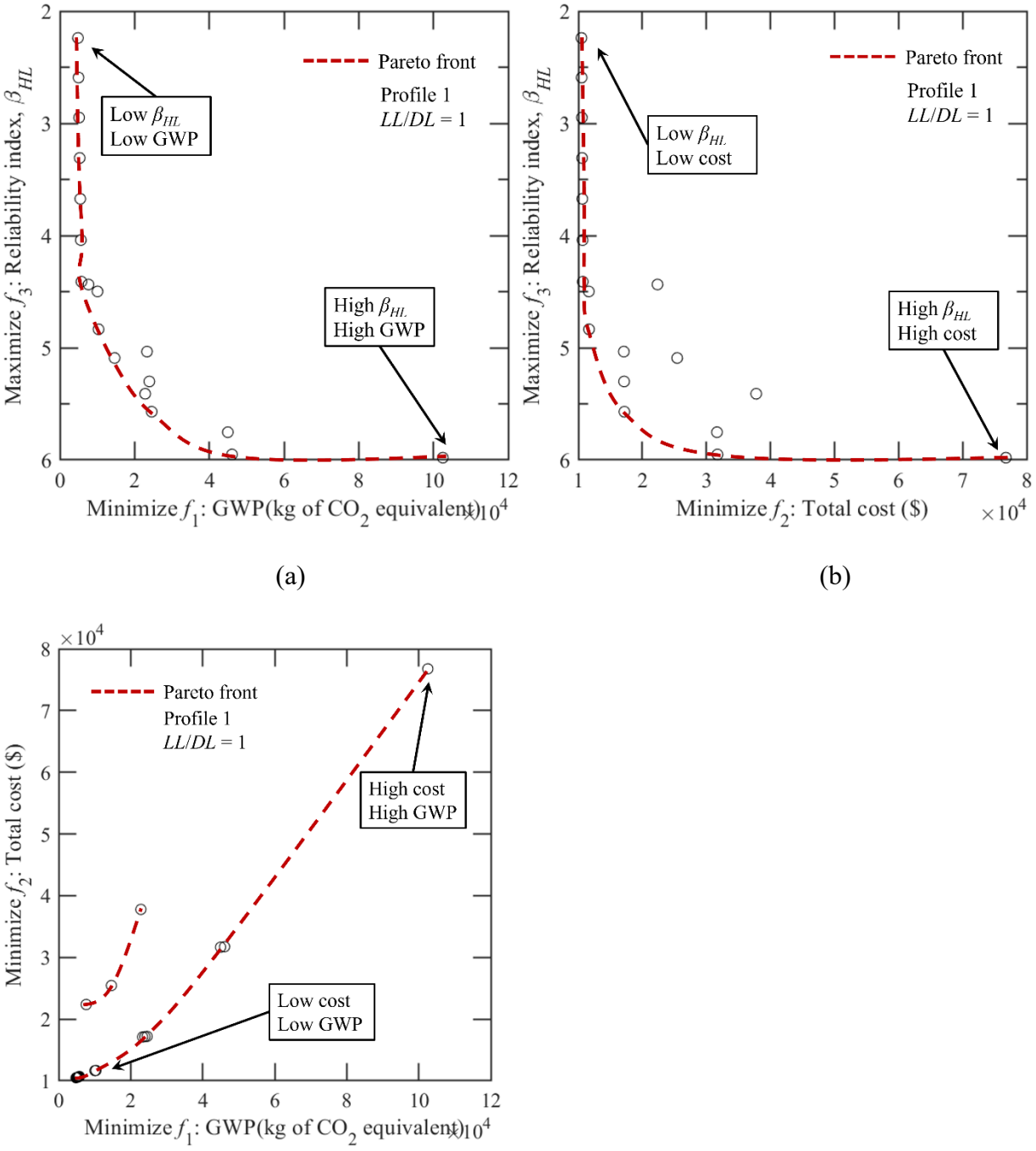

Figure 9.5. Relationship between reliability and (a) global warming impact, (b) total cost, and (c) between global warming impact and total cost for pile group

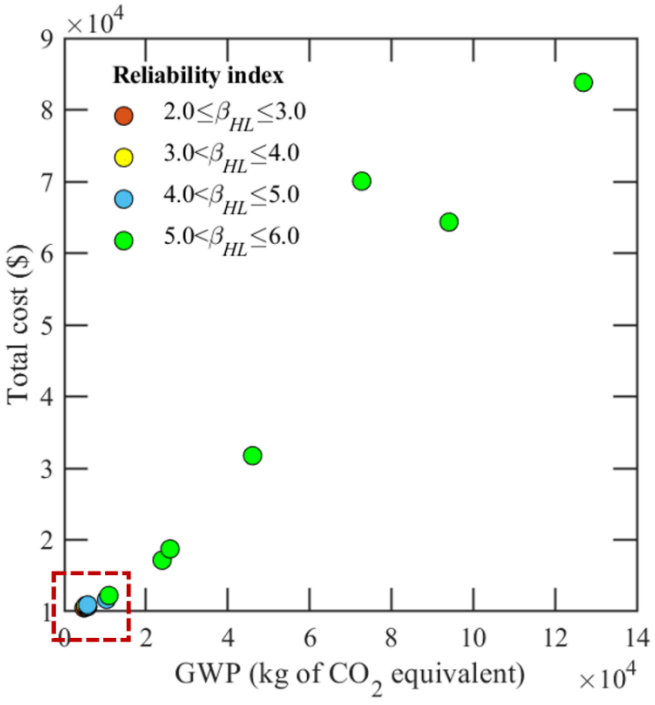

(a)

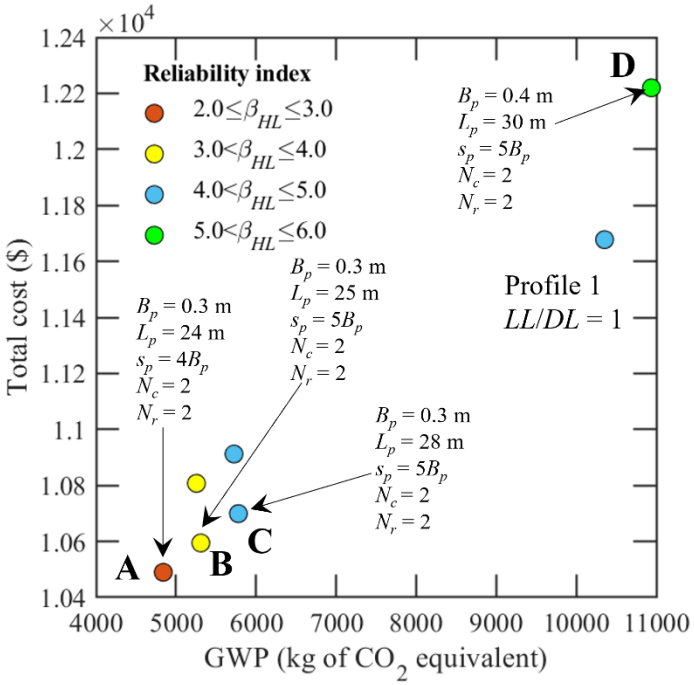

(b)

Figure 9.6. Design charts for optimized pile group designs

9.5 Summary

In this chapter, the multi-objective optimization framework proposed in Chapter 7 is applied to single and group drilled shafts. The goal of the multi-objective optimization is to determine dimensions of drilled shafts (i.e., pile diameter and length for single drilled shafts and pile diameter and length, center-to-center spacing between the piles and number of piles for group drilled shafts) that result in minimized global warming impact, minimized cost, and maximized engineering reliability of drilled shafts. Conflicting relationships were observed between (i) reliability and cost and (ii) reliability and global warming impact of drilled shafts. Considering the three objectives simultaneously, disconnected Pareto front was observed for both single and group drilled shafts. As for the case of single drilled shaft, the disconnection is caused by the cost estimation of drilled shaft which is modeled as a step-like function of the pile diameter. The Pareto front for group piles was caused by the differences in the pile length and number of individual piles. Optimized designs of single and group drilled shafts were provided, in a form of design charts, which recommend the optimum design dimensions for different ranges of reliability index. Designers can select any of the optimized designs that best suit the project requirements (e.g., budget and safety requirements).

9.6 List Of Symbols

Notation	Description
B_p	Pile diameter
c_i	Coded variable
d_{ce}	Clear edge distance of pile cap
f_{sp}	Factor for center-to-center pile spacing
k	Number of design variables in central composite design
l_c	Length of pile cap
L_p	Pile length
N_c	Number of piles in a column
N_r	Number of piles in a row

List of Symbols (continued).

Notation	Description
s_p	Center-to-center pile spacing in group piles
T_c	Pile cap thickness
w_c	Width of pile cap
$y_{GWP_{\text{GROUP}}}$	Regression model for estimating global warming potential of group drilled shafts
y_{SLS}	Regression model for estimating β_{HL} for settlement of single drilled shafts
y_{ULS}	Regression model for estimating β_{HL} for bearing capacity failure of single drilled shafts
$y_{\beta_{\text{GROUP}}}$	Regression model for estimating β_{HL} for bearing capacity failure of group drilled shafts
β_{HL}	Hasofer-Lind reliability index
$\xi_{\max}$ and $\xi_{\min}$	Upper and lower bounds of the natural variable ξ_i

CHAPTER 10: CONCLUSIONS, LIMITATIONS, AND FUTURE STUDIES

Geotechnical constructions generate substantial amount of carbon emissions and other pollutants that impact the environment. Cement and steel – the two most used materials in geotechnical constructions – are energy- and carbon-intensive because a large amount of fossil fuel is usually consumed in the production phase, and the direct carbon emissions from operation of construction equipment are substantial. Minimization of environmental impacts, caused by geotechnical structures, is highly desirable, and it can be practiced as early as in the design phase. Using a quantitative environmental impact assessment, such as life cycle assessment (LCA), can bring better understanding on which life cycle stage of geo-structures contributes the most to environmental impacts and which design parameter can be adjusted to minimize the environmental impacts. Hence, LCA can help geotechnical engineers optimize their designs not only for safety and cost, but also for environmental sustainability.

Reliability based design (RBD) of geo-structures can be used to produce lean designs that correlate well with the principles of sustainability. Lean designs can have lower cost and result in lower environmental impact because less construction materials and energy are consumed. However, the impacts of design decisions made in RBD of geo-structures to environmental impacts have not been rigorously studied. Understanding the relationship between the reliability and environmental impact of geo-structures can help make informed decisions. For example, selecting a certain reliability requirement can be a crucial decision that leads to high environmental impacts. Continuous efforts are made to improve the conventional geotechnical design methodologies from being extremely conservative to being able to make informed decisions based on quantified risk. It is important that environmental impacts of geotechnical structures are not overlooked when making such design decisions. Hence, understanding the relationship between

reliability and environmental sustainability of geotechnical structures can be useful when optimizing the geotechnical designs with respect to acceptable risk and environmental impact (e.g., acceptable amount of carbon dioxide released to reach the net-zero carbon target).

Designing for sustainability is a complex process because different parameters that affect multiple dimensions of sustainability (i.e., environment, economy, engineering, and equity) need to be thoroughly studied, and the trade-offs between the dimensions need to be understood to achieve a well-balanced design. Hence, it is important to integrate the methodologies, used for quantifying the multiple dimensions of sustainability, into a unified framework, and multi-objective optimization needs to be performed to determine geotechnical designs that are balanced with sustainability considerations.

In this thesis, the principles and framework of LCA are explained, and the application of LCA is demonstrated with examples of drilled shafts, pile group, and mechanically stabilized earth (MSE) walls. A parametric study was conducted to study the effects of (i) soil properties, (ii) design parameters, (iii) material properties, and (iv) transportation distances for hauling construction materials and equipment, on the global warming impact. Based on the LCA results, it was found that the environmental impacts of drilled shafts are heavily dependent on the life cycle processes of concrete and steel (especially the extraction and refining of raw materials and manufacturing), whereas the environmental impacts of MSE walls are mostly influenced by the earth works such as excavation, backfilling, and compaction. Furthermore, it was found that marine eutrophication and photochemical oxidant formation are some of the most important environmental impacts for both drilled shafts and MSE walls. Global warming impact was also one of the highest environmental impacts caused by drilled shafts. Ultimately, charts that can be used for quick and preliminary estimation of global warming impacts of drilled shafts and MSE

walls are developed. The main advantage of these charts is the ease of estimating global warming impacts of drilled shafts and MSE walls without the use of sophisticated and costly LCA software packages. Similar project-specific charts can be developed for ready reference. LCA is applicable to any type of geo-structures as long as the life cycle stages and processes are defined properly and relevant databases are used. Finding the inventory databases for unique materials (e.g., bentonite slurry) can be challenging and can potentially degrade the reliability of LCA study if the unique materials comprise most of the geo-structure of interest. The same challenge applies to construction equipment. Continued research on developing the inventory databases for construction materials and equipment that are widely used in geotechnical construction may help geotechnical engineers conduct accurate LCAs with less complexity. It is expected that the LCA procedure and application of LCA to geotechnical structures described in this thesis will encourage geotechnical engineers to incorporate LCA in their design and collectively contribute to sustainable development.

The relationship between the reliability and environmental sustainability of geotechnical structures (e.g., drilled shaft and MSE wall) is discussed in this thesis. Reliability based design of geotechnical structures is performed using Monte Carlo simulations (MCS) and first-order reliability method (FORM). Uncertainties in soil property, applied load, design equation, and design dimension are taken into account in the reliability based design. The global warming impacts of reliability based designs, at different levels of target probability of failure, are quantified using LCA to investigate the impacts of design decisions to environmental impacts of geotechnical structures. As the target probability of failure in the RBD of drilled shaft and MSE wall is decreased, an increase in the global warming impact (measured in global warming potential (GWP)) was observed; however, GWP stayed constant for certain ranges of target probability of

failure. Understanding these ranges can help in optimizing geotechnical designs with respect to reliability and environmental sustainability. The effect of resistance factors in the load and resistance factor design (LRFD) to the global warming impact of drilled shafts was also examined. As higher values of resistance factors are assumed, higher base and shaft resistances against bearing capacity failure are assumed; hence, a decrease in GWP of drilled shafts were observed accordingly. GWP estimation charts were developed for drilled shafts and MSE walls using which designers can determine the global warming impact of the said geo-structures solely based on their design dimensions, target probability of failure, and applied loads.

A multi-objective optimization-based framework for designing geotechnical structures with sustainability considerations is proposed in this thesis. NSGA-II algorithm is used to conduct the multi-objective optimization in which the objectives are minimization of global warming impact and cost and maximization of reliability of geotechnical structures. The objective functions were formulated as functions of the design variables (e.g., pile length and diameter for drilled shafts and length and spacings of reinforcement for MSE walls). The framework involves conducting the followings: (i) quantification of global warming impact using life cycle assessment, (ii) estimation of costs related to material, labour, and equipment use in the construction phase, (iii) performing first-order reliability method to calculate the reliabilities of geotechnical structures, and (iv) conducting response surface methodology to construct the regression models for estimating the objective values (i.e., global warming impact, cost, and engineering reliability associated with drilled shafts and MSE walls). The framework determines a set of optimal designs, and the final selection of which design to use depends on the safety requirements specified by the jurisdiction and the budget of the project. Designs charts were developed which can be used to quickly determine the designs of (i) single drilled shaft, (ii) pile group, and (iii) MSE walls

reinforced by steel strips and geogrids, optimized for global warming impact, cost, and engineering reliability. The framework can be applied to other types of geotechnical structures if relevant objective functions and design variables are used. It should be noted that the regression models for estimating GWP and reliability of drilled shaft and MSE wall, provided in this thesis, are specific to the soil properties, loading conditions, characteristics of random variables, material properties, specifications of construction equipment, and unit costs assumed in this study.

This research study has several limitations that need to be addressed. The optimization-based framework presented in this study considers multiple dimensions of sustainability; however, the social aspect of sustainability is not explicitly considered in this study. For a comprehensive sustainability assessment, social indicators relevant to the geotechnical project of interest need to be identified and quantified. The designs of drilled shaft and MSE wall are specific to the soil profiles, loading conditions, design equations used, and safety requirements specified in this study. Hence, adjustments to the inputs mentioned above may be necessary based on the specifics of the project and jurisdictions to obtain accurate and applicable results. Further, there are uncertainties related to the LCA and cost data because there can be variations with geographical location and time. For example, the values of GWP may change over time because of the evolving science involved in estimating the radiative efficiency and lifetime of greenhouse gases. Given the results presented in this study are dependent on the quality of database used (e.g., life cycle inventory database and cost estimation handbook), these variations need to be addressed.

To expand the understanding of environmental impacts in geotechnical engineering, life cycle assessment can be applied to other geotechnical structures such as slopes, driven piles, reinforced concrete retaining walls, and geothermal piles. A comprehensive sustainability assessment requires quantification of indicators that represent the four E's of sustainability (i.e.,

environment, economy, equity, and engineering). In this research study, the social aspect of sustainability was not considered because of limited data and challenges with characterizing qualitative data into quantitative value. Hence, research on the social aspects of sustainability that are directly or indirectly relevant to geotechnical projects needs to be continued. A multi-criteria decision making method can be used to evaluate geotechnical solutions and compare different alternatives with sustainability points of view.

REFERENCES

AASHTO (American Association of State Highway and Transportation Officials). (2007). *AASHTO LRFD bridge design specifications*. AASHTO, Washington, DC, USA.

AASHTO. (2017). *AASHTO LRFD Bridge Design Specifications*. 8th Ed. LRFD-8. AASHTO, Washington, DC, USA.

Abolhasani, S., & Frey, H. C. (2013). Engine and duty cycle variability in diesel construction equipment emissions. *Journal of Environmental Engineering*, *139*(2), 261-268.

Abolhasani, S., Frey, H. C., Kim, K., Rasdorf, W., Lewis, P., & Pang, S. (2008). Real-world in-use activity, fuel use, and emissions for nonroad construction vehicles: A case study for excavators. *Journal of the Air & Waste Management Association*, *58*(8), 1033-1046.

Abreu, D. G., Jefferson, I., Braithwaite, P. A., & Chapman, D. N. (2008). Why is sustainability important in geotechnical engineering?, *Proceedings of GeoCongress 2008*: *Geosustainability and Geohazard Mitigation*, New Orleans, Louisiana, USA, 812-828.

ACI (American Concrete Institute). (2011). *ACI 318-11: Building code requirements for structural concrete and commentary*. American Concrete Institute, Farmington Hills, MI, USA.

Ang, A. H., & Tang, W. H. (1984). *Probability Concepts in Engineering Planning and Design Volume II: Decision, Risk, and Reliability*. John Wiley & Sons Inc., United States.

Arena, A., & de Rosa, C. (2003). Life cycle assessment of energy and environmental implications of the implementation of conservation technologies in school buildings in Mendoza – Argentina. *Building and Environment*, *38*(2), 359-368.

Ay-Eldeen, M., & Negm, A. (2011). Global warming potential impact due to pile foundation construction using life cycle assessment. *Electronic Journal of Geotechnical Engineering*, *20*(1), 4413-4421.

Baecher, G., & Christian, J. (2003). *Reliability and statistics in geotechnical engineering*. John Wiley and Sons, West Sussex, England.

Basu, D., & Salgado, R. (2012). Load and resistance factor design of drilled shaft in sand. *Journal of Geotechnical and Geoenvironmental Engineering, 138*(12), 1455-1469.

Basu, D., Misra, A., & Puppala, A. J. (2015). Sustainability and geotechnical engineering: perspectives and review. *Canadian Geotechnical Journal, 52*(1)*,* 96-113.

Basu, P., Basu, S. B., & Ghasemi-Fare, O. (2020). Fragility analysis of drilled shafts in sand – an analytical correspondence between reliability index and factor of safety. *Soils and Foundations*, *60*(1), 1112-1130.

Basudhar, P. K., Vashistha, A., Deb, K., & Dey, A. (2008). Cost optimization of reinforced earth walls. *Geotechnical and Geological Engineering*, *26*(1), 1-12.

Bathurst, R.J., Lin, P., & Allen, T. (2019). Reliability-based design of internal limit states for mechanically stabilized earth walls using geosynthetic reinforcement. *Canadian Geotechnical Journal*, *56*(6), 774-788.

Bauer Maschinen GmbH. (2021). *Bauer BH 15 H. Bauer*. Retrieved from https://www.bauer.de/export/shared/documents/pdf/bma/datenblatter/BG_valueline/BG_15_H_BT_50_EN_905_786_2.pdf (accessed June 24, 2022).

Bowles, J. E. (1997). *Foundation analysis and design* (5th Ed.). McGraw-Hill, Singapore.

CAC (Cement Association of Canada). (2006). *Concrete design handbook* (3rd Ed.). CAC, Ottawa, Canada.

Carpenter, A. C., Gardner, K. H., Fopiano, J., Benson, C. H., & Edil, T. B. (2007). Life cycle based risk assessment of recycled materials in roadway construction. *Waste Management*, *27*(1), 1458-1464.

Caterpillar. (2014). *Caterpillar Performance Handbook*. Caterpillar, Peoria, IL, USA.

Caterpillar. (2022). *330 GC Hydraulic Excavator*. Retrieved from https://s7d2.scene7.com/is/content/Caterpillar/CM20181002-69369-07070 (accessed October 7, 2022)

CEN (European Committee for Standardization). (2002). *Eurocode 1: Actions on structures – Part 1-1: General actions – Densities, self-weight, imposed loads for buildings*. EN 1991-1-1:2002 E. European Committee for Standardization.

CEN. (2004). *Eurocode 2: Design of concrete structures – Part 1-1: General rules and rules for buildings*. EN 1992-1-1. European Committee for Standardization.

CEN. (2011). *Sustainability of construction works – Assessment of environmental performance of buildings – Calculation method*. EN 15978:2011. European Committee for Standardization.

Chalermyanont, T., & Benson, C. H. (2004). Reliability-based design for internal stability of mechanically stabilized earth walls. *Journal of Geotechnical and Geoenvironmental Engineering*., *130*(2), 163-173.

Chalermyanont, T., & Benson, C. H. (2005). Reliability-based design for external stability of mechanically stabilized earth walls. *International Journal of Geomechanics*, *5*(3), 196-205.

Chan, P., & Tighe, S. (2010). Quantifying pavement sustainability in economic and environmental perspective. *Proceedings of the Transportation Research Board 89th Annual Meeting*, Washington, DC, 1-15.

Chau, C., Soga, K., & Nicholson, D. (2006). Comparison of embodied energy of four different retaining wall systems. In A. P. Butcher, J.J.M. Powell & H.D. Skinner (Eds.), *Proceedings of International Conference on Reuse of Foundations for Urban Sites* (pp. 277-286). Watford, United Kingdom: BRE Press.

Chau, C., Soga, K., Nicholson, D., O'Riordan, N., & Inui, T. (2008). Embodied energy as environmental impact indicator for basement wall construction. *Proceedings of Geo Congress 2008: Geosustainability and Geohazard Mitigation*, New Orleans, Louisiana, USA, 867-874.

Chau, C., Soga, K., O'Riordan, N., & Nicholson, D. (2012). Embodied energy evaluation for section of the UK Channel Tunnel rail link. *Geotechnical Engineering*, *165*(GE2), 65-81.

Clayton, C., Milititsky, J., & Woods, R. (1993). *Earth Pressure and Earth-Retaining Structures*. Taylor and Francis, Oxford, UK.

Coduto, D. P. (2001). *Foundation design: Principles and practices* (2nd Ed.). Prentice-Hall, Upper Saddle River, NJ.

Colombi, A. (2005). *Physical modeling of an isolated pile in coarse grained soils* [Doctoral dissertation, University of Ferrara].

Crawford, R. H. (2011). *Life cycle assessment in the built environment.* Spon Press, New York, NY.

Crooks, A.R. (2013). *Applications of shrinkage and swelling factors on state highway construction* [Master's thesis, Auburn University].

Curran, M. A. (2008). Life-Cycle Assessment. *Encyclopedia of Ecology*, 2168-2174.

Curran, M. A. (2017). Goal and scope definition in life cycle assessment. In W. Klöpffer & M. A. Curran, *LCA compendium - The complete world of life cycle assessment*. Springer. https://doi.org/10.1007/978-94-024-0855-3

da S Trentin, A. W., Reddy, K. R., Kumar, G., Chetri, J. K., & Thome, A. (2019). Quantitative assessment of life cycle sustainability (QUALICS): Framework and its application to assess electrokinetic remediation. *Chemosphere*, *230*(1), 92-106.

Dam, T. V., & Taylor P. C. (2011). Seven principles of sustainable concrete pavements. *Concrete International*, *33*(11), 49-52.

Damians, I. P., Bathurst, R. J., Adroguer, E. G., Josa, A., & Lloret, A. (2017). Environmental assessment of earth retaining wall structures. *Environmental Geotechnics, 4*(6), 415-431.

Damians, I. P., Bathurst, R. J., Adroguer, E. G., Josa, A., & Lloret, A. (2018). Sustainability assessment of earth-retaining wall structures, *Environmental Geotechnics, 5*(4), 187-203.

Das, J. T., Puppala, A. J., Bheemasetti, T. V., Walshire, L., & Corcoran, M. K. (2018). Sustainability and resilience analyses in slope stabilization. *Engineering Sustainability*, *171*(ES1), 25-36.

Deb, K., & Deb, D. (2014). Analysing mutation schemes for real-parameter genetic algorithms. *International Journal of Artificial Intelligence and Soft Computing*, *4*(1), 1-28.

Deb, K., & Jain, H. (2011). *Parent to mean-centric self-adaptation in single and multi-objective real-parameter genetic algorithms with SBX operator*. KanGAL Report No. 2011017. Indian Institute of Technology Kanpur.

Deb, K., Pratap, A., Agarwal, S., & Meyarivan, T. (2002). A fast and elitist multiobjective genetic algorithm: NSGA-II. *IEEE Transactions on Evolutionary Computation*, *6*(2), 182-197.

Deb, K., Thiele, L., Laumanns, M., & Zitzler, E. (2001). *Scalable test problems for evolutionary multi-objective optimization.* TIK Report No. 112. ETH Zürich – Computer Engineering and Networks Laboratory, Switzerland.

Djadouni, H., Trouzine, H., Correia, A., & Filipe da Silva Miranda T. (2019). Life cycle assessment of retaining wall backfilled with shredded tires. *International Journal of Life Cycle Assessment*, *24*(1), 581-589.

Dodigović, F., Ivandić, K., Jug, J., & Agnezović, K. (2021). Multi-objective optimization of retaining wall using genetic algorithm. *Environmental Engineering*, *8*(1-2), 58-65.

Egan, D., & Slocombe, B.C. (2010). Demonstrating environmental benefits of ground improvement. *Ground Improvement*, *163*(1), 63-69.

Ellingwood, B., & Tekie, P. (1999). Wind load statistics for probability-based structural design. *Journal of Structural Engineering*, *125*(4), 453-463.

Entwisle, D., Lee, K. A., & Lawley, R. S. (2015). *User Guide for BGS Civils – A Suit of Engineering Properties*. British Geological Survey, Nottingham, UK, Report OR/15/065. http://nora.nerc.ac.uk/id/eprint/513379/1/OR15065.pdf (accessed June 6, 2021).

EPA (Environmental Protection Agency). (2004). *Exhaust and crankcase emission factors for nonroad engine modeling – Compression-ignition*. United States. NR-009c. Office of Transportation and Air Quality. Washington, DC, USA.

EPA. (2010). *Median life, annual activity, and load factor values for nonroad engine emissions modeling*. NR-005d. Office of Transportation and Air Quality. Washington, DC, USA.

EPA. (2012). *Tool for the reduction and assessment of chemical and other environmental impacts (TRACI): user's guide*. Retrieved from https://nepis.epa.gov/Adobe/PDF/P100HN53.pdf (accessed September 7, 2021).

European Commission. (2008). *Environmental improvement of passenger cars (IMPRO-car)*. Report EUR 23038 EN. Official Publications of the European Communities, Luxembourg.

European Commission. (2018). *European reference life cycle database*. Retrieved from https://data.jrc.ec.europa.eu/collection/EPLCA#datasets (accessed September 7, 2021).

Fenton, G. A., & Griffiths, D. V. (2007). Reliability-based deep foundation design. *Proceedings of Geotechnical Special Publications: Probabilistic Applications in Geotechnical Engineering,* 1-12.

Fenton, G. A., & Griffiths, D. V. (2008). *Risk Assessment in Geotechnical Engineering*, Wiley, New York, USA.

Fenton, G. A., Griffiths, D. V., & Zhang, X. (2008). Load and resistance factor design of shallow foundations against bearing failure. *Canadian Geotechnical Journal*, *45*(11), 1556-1571.

Fenton, G. A., Naghibi, F., Dundas, D., Bathurst, R. J., & Griffiths, D. V. (2016). Reliability-based geotechnical design in 2014 Canadian Highway Bridge Design Code. *Canadian Geotechnical Journal*, *53*(2), 236-251.

FHWA (Federal Highway Administration). (2000). *Comprehensive Truck Size and Weight Study*. FHWA-PL-00-029. Retrieved from https://www.fhwa.dot.gov/reports/tswstudy/Vol2-Chapter3.pdf (accessed June 6, 2021).

FHWA. (2009a). *Corrosion/degradation of soil reinforcements for mechanically stabilized earth walls and reinforced soil slopes*. FHWA-NHI-09-087. Washington, DC: FHWA.

FHWA. (2009b). *Design and construction of mechanically stabilized earth walls and reinforced soil slopes – Volume I*. FHWA-NHI-10-024. Washington, DC: FHWA.

FHWA. (2009c). *Design and construction of mechanically stabilized earth walls and reinforced soil slopes – Volume II*. FHWA-NHI-10-025. Washington, DC: FHWA.

FHWA. (2010a). *Drilled Shafts: Construction Procedures and LRFD Design Methods.* FHWA-NHI-10-016. Washington, DC: FHWA.

FHWA. (2010b). *Implementation of LRFD Geotechnical Design for Bridge Foundations*. Report FHWA-NHI-10-039. Washington, DC: FHWA.

Fioravante, V. (2002). On the shaft friction modeling of non-displacement piles in sand. *Soils Foundation*, *42*(2), 23-33.

Foye, K., Scott, B., & Salgado, R. (2006). Assessment of variable uncertainties for reliability-based design of foundations. *Journal of Geotechnical and Geoenvironmental Engineering*, *132*(9), 1197-1207.

Fratta, D., & Kim, K. (2015). *Effective depth of soil compaction in relation to applied compactive energy*. WisDOT No. 0092-08-11. Wisconsin Department of Transportation. Retrieved from https://wisconsindot.gov/documents2/research/WisDOT-WHRP-project-0092-08-11-final-report.pdf (accessed March 29, 2023).

GaBi. (2021). *GaBi life cycle inventory data documentation*. Retrieved from https://gabi.sphera.com/canada/support/gabi/gabi-database-2020-lci-documentation/ (accessed September 7, 2021).

Giri, R., & Reddy, K. (2014). LCA and sustainability assessment for selecting deep foundation system for high-rise buildings. In *Proceedings of International Conference on Sustainable Infrastructure 2014* (Crittenden J, Hendrickson C and Wallace B (eds)). American Society of Civil Engineers, Long Beach, CA, USA, pp. 621-630.

Goedkoop, M., Heijungs, R., Huijbregts, M., Schryver, A., Struijs, J., & Zelm, R. (2013). *Recipe 2008: A life cycle impact assessment method which comprises harmonised category indicators at the midpoint and endpoint Level (version 1.08)*. Retrieved from https://www.rivm.nl/documenten/a-lcia-method-which-comprises-harmonised-category-indicators-at-midpoint-and-endpoint (accessed May 4, 2020)

Goedkoop, M., Heijungs, R., Huijbregts, M., Schryver, A., Struijs, J., & Zelm, R. (2014). *Characterisation and normalisation factors*, Retrieved from https://www.rivm.nl/documenten/6recipe111 (accessed May 4, 2020).

Guo, X., Pham, T. A., & Dias, D. (2023). Multi-objective optimization of geosynthetic-reinforced and pile-supported embankments. *Acta Geotechnica*, DOI: https://doi.org/10.1007/s11440-022-01782-4.

Haldar, S., & Basu, D. (2013). Load and resistance factor design of laterally loaded piles. *Proceedings of the International Symposium on Advances in Foundation Engineering*, Singapore, 351-357.

Hammond, G., & Jones, C. (2008). *Inventory of carbon and energy (ICE) Version 1.6a*. Bath, United Kingdom: University of Bath.

Hasofer, A. M., & Lind, N. C. (1974). Exact and invariant second-moment code format. *Journal of the Engineering Mechanics Division*, *100*(1), 111-121.

HBEFA (Handbook Emission Factors for Road Transport). (2010). *HBEFA 4.1*. Environmental Protection Agencies of Germany, Switzerland and Austria, Switzerland. Retrieved from http://www.hbefa.net (accessed May 4, 2020).

Heerten, G. (2012). Reduction of climate-damaging gases in geotechnical engineering practice using geosynthetics. *Geotextiles and Geomembranes*, *30*(1), 43-49.

Hojjati, A., Jefferson, I., Metje, N., & Rogers, C. D. F. (2017). Embedding sustainability criteria into pre-appraisal of underground utility for future cities. *Urban Design and Planning*, *170*(DP6), 258-271.

Holt, D.G.A, Jefferson, I., Braithwaite, P.A., & Chapman, D.N. (2010). Embedding sustainability into geotechnics. Part A: Methodology. *Engineering Sustainability*, *163*(ES3), 127-135.

Holt, D.G.A. (2011). *Sustainable assessment for geotechnical projects* [Doctoral dissertation, University of Birmingham].

Honda. (2020). *GX160: Horizontal Shaft Gasoline (Petrol) Engine*. Honda Motor Europe Logistics, Bracknell, UK. https://www.honda-engines-eu.com/documents/10912/15973/TS_GX160 (accessed June 6, 2021).

Hong, B., & Lu, L. (2022). Assessment of emissions and energy consumption for construction machinery in earthwork activities by incorporating real-world measurement and discrete-event simulation. *Sustainability*, *14*(9), 5326.

Huang, L., Krigsvoll, G., Johansen, F., Liu, Y., & Zhang, X. (2018). Carbon emission of global construction sector. *Renewable and Sustainable Energy Reviews*, *81*(2), 1906-1916.

Huijbredgts, M., Steinmann, Z., Elshout, P., Stam, G., Verones, F., Vieira, M., Hollander, A., Zijp, M., & van Zelm, R. (2017). ReCiPe 2016: A harmonized life cycle impact assessment method at midpoint and endpoint level. *International Journal of Life Cycle Assessment*, *22*(2), 138-147.

Huijbregts, M., Steinmann, Z., & Elshout, P. *et al*. (2016). *Normalization scores ReCiPe 2016*. Ministry of Housing, Spatial Planning and Environment, Den Haag, Netherlands. See https://www.rivm.nl/en/documenten/normalization-scores-recipe-2016 (accessed June 21, 2021).

Huijbregts, M., Steinmann, Z., Elshout, P., Stam, G., Verones, F., Vieira, M., … & van Zelm, R. (2017). ReCiPe2016: A harmonized life cycle impact assessment method at midpoint and endpoint level. *International Journal of Life Cycle Assessment*, *22*(2), 138-147.

Humbert, S., De Schryver, A., Bengoa, X., Margni, M., & Jolliet, O. (2012). *IMPACT 2002+: User guide*. Retrieved from https://www.quantis-intl.com/pdf/IMPACT2002_UserGuide_for_vQ2.21.pdf (accessed September 8, 2021).

Inui, T., Chau, C., Soga, K., Nicolson, D., & O'Riordan, N. (2011). Embodied Energy and Gas Emissions of Retaining Wall Structures. *Journal of Geotechnical and Geoenvironmental Engineering*, *137*(10), 958-697.

IPCC (Intergovernmental Panel on Climate Change). (1990). *Climate change: The IPCC scientific assessment*, Cambridge: Press Syndicate of the University of Cambridge.

IRP (International Resource Panel). (2019). *Global resources outlook 2019: Natural resources for the future we want*. Nairobi, Kenya: United Nations Environment Programme.

ISO (International Organization for Standardization). (2006a). *ISO 14040: Environmental management – life cycle assessment – Principles and framework* (ISO 14040: 2006). ISO.

ISO. (2006b). *ISO 14044: Environmental management - life cycle assessment - Requirements and guidelines*. (ISO 14044:2006). ISO.

Jefferis, S. A. (2008). Moving towards sustainability in geotechnical engineering. *Proceedings of GeoCongress 2008*: *Geosustainability and Geohazard Mitigation*, New Orleans, Louisiana, USA, 844-851.

Jefferson, I., Hunt, D. V. L., Birchall, C. A., & Rogers, C. D. F. (2007). Sustainability indicators for environmental geotechnics. *Engineering Sustainability*, *160*(2), 57-78.

Jensen, A. A., Hoffman, L. Møller, B. T., & Schmidt, A. (1997). *Life cycle assessment (LCA): A guide to approaches, experiences and information sources*. European Environmental Agency.

Jimenez, M. (2004). *Assessment of geotechnical process on the basis of sustainability principles* [Master's thesis, University of Birmingham].

Juang, C. H., & Wang, L. (2013). Reliability-based robust geotechnical design of spread foundations using multi-objective genetic algorithm. *Computers and Geotechnics*, *48*(1), 96-106.

Juang, C. H., Wang, L., Liu, Z., Ravichandran, N., Huang, H., & Zhang, J. (2013). Robust geotechnical design of drilled shafts in sand: New design perspective. *Journal of Geotechnical and Geoenvironmental Engineering*, *139*(12): 2007-2019.

Kashani, A. R., Camp, C. V., Azizi, K., & Rostamian, M. (2022a). Multi-objective optimization of mechanically stabilized earth wall using evolutionary algorithms. *International Journal for Numerical Analytical Methods in Geomechanics*, *46*(8): 1433-1465.

Kashani, A. R., Gandomi, A. H., Azizi, K., & Camp, C. V. (2022b). Multi-objective optimization of reinforced concrete cantilever retaining wall: a comparative study. *Structural and Multidisciplinary Optimization*, *65*(1), 262.

Kayabekir, A. E., Arama, Z. A., Bekdaş, G., Nigdeli, S. M., & Geem, Z. (2020). Eco-friendly design of reinforced concrete retaining walls: Multi-objective optimization with harmony search applications. *Sustainability*, *12*(15), 6087.

Khajehzadeh, M., Taha, M.R., & Eslami, M. (2014). Multi-objective optimization of foundation using global-local gravitational search algorithm. *Structural Engineering and Mechanics*, *50*(3), 257-273.

Khoshnevisan, S., Gong, W., Juang, C. H., & Atamturktur, S. (2014). Efficient robust geotechnical design of drilled shafts in clay using a spreadsheet. *Journal of Geotechnical and Geoenvironmental Engineering*, *141*(2): 0401492.

Kim, D., & Salgado, R. (2012a). Load and resistance factors for external stability checks of mechanically stabilized earth walls. *Journal of Geotechnical and Geoenvironmental Engineering*, *138*(3), 241-251.

Kim, D., & Salgado, R. (2012b). Load and resistance factors for internal stability checks of mechanically stabilized earth walls. *Journal of Geotechnical and Geoenvironmental Engineering*, *138*(8), 910-921.

Kim, D. W. (2008). *Load and resistance factor design of slopes and MSE walls* [Doctoral dissertation, Purdue University].

Knuth, D., & Fortmann, J. (2010). The development of I-LAST™ Illinois - Livable and sustainable transportation. *Proceedings of the Green Streets and Highways 2010 Conference*, Denver, CO, 495-503.

Konak, A., Coit, D, W., & Smith, A. E. (2006). Multi-objective optimization using genetic algorithms: A tutorial. *Reliability Engineering and System Safety*, *91*(9), 992-1007.

Kulhawy, F. H. (1991). Drilled shaft foundations. In *Foundation Engineering Handbook* (Fang H (ed.)). Springer, Boston, MA, USA, pp. 537-552.

Kulhawy, F. H., Phoon, K. K., & Wang, Y. (2012). Reliability-based design of foundations – a modern view. *Proceedings of Geotechnical Engineering State of the Art and Practice, GeoCongress 2012,* 102-22.

Lacasse, S., & Nadim, F. (1996). Uncertainties in characterising soil properties. *Uncertainty in the geologic environment: from theory to practice*. 49-75.

Lacasse, S., & Nadim, F. (1998). Risk and reliability in geotechnical engineering. *Proceedings of International Conference on Case Histories in Geotechnical Engineering*, St. Louis, MO, 1172-1192.

Laefer, D. F (2011). Quantitative support for a qualitative foundation reuse assessment tool, *Proceedings of the GeoFrontiers 2011*, Dallas, TX, 113-121.

Lam, C. (2016). Evaluation of density-measurement methods for construction slurries. *Geotechnical Testing Journal*, *39*(3), 507-514.

Lee, J.H., & Salgado, R. (1999). Determination of pile base resistance in sands. *Journal of Geotechnical and Geoenvironmental Engineering*, *135*(8), 673-683.

Lee, M., & Basu, D. (2018). An integrated approach for resilience and sustainability in geotechnical engineering. *Indian Geotechnical Journal*, *48*(2), 207-234.

Lee, J., Edil T. B., Tinjum J. M., & Benson C. H. (2010b). Quantitative assessment of environmental and economic benefits of using recycled construction materials in highway construction. *Transportation Research Record: Journal of the Transportation Research Board, 2158*(1), 138-142.

Lee, J., Edil T. B., Benson C. H., & Tinjum J. M. (2010a). Use of BE^{2}ST In-Highways for green highway construction rating in Wisconsin. *Proceedings of the Green Streets and Highways 2010 Conference*, Denver, CO, 480-494.

Leiden University. (2016). *CML-IA characterization factors*. Retrieved from https://www.universiteitleiden.nl/en/research/research-output/science/cml-ia-characterisation-factors#downloads (accessed September 8, 2021).

Lewis, W.A. (1961). Recent research into the compaction of soil by vibratory compaction equipment. In *Proceedings of the 5th International Conference of Soil Mechanics and Foundation Engineering*, Dunod, Paris, France, pp. 261-268.

Lewis, H., & Demmers, M. (1996). Life cycle assessment and environmental management. *Australian Journal of Environmental Management*, *3*(2), 110-123.

Lewis, P., Leming, M., Christopher, F. H., & Rasdorf, W. (2011). Assessing effects of operational efficiency on pollutant emissions of nonroad diesel construction equipment. *Transportation Research Record*, *2233*(1), 11-18.

Loukidis, D., & Salgado, R. (2008). Analysis of the shaft resistance of non-displacement piles in sand. *Géotechnique*, *58*(4), 283-296.

Low, B. K. (2005). Reliability-based design applied to retaining walls. *Geotechnique*, *55*(1), 63-75.

Low, B. K., & Tang, W. H. (1997). Reliability analysis of reinforced embankments on soft ground. *Canadian Geotechnical Journal*, *34*(5), 672-685.

Luo, W., Sandanayake, M., & Zhang, G. (2019). Direct and indirect carbon emissions in foundation construction – Two case studies of driven precast and cast-in-situ piles. *Journal of Cleaner Production*, *211*(1), 1517-1526.

Magade, S., & Ingle, R. (2020). Effect of clear edge distance on failure of pile cap. *American Concrete Institute Structural Journal*, *117*(3), 131-140.

Matthews, H. S., Hendrickson, C. T., & Matthews, D. H. (2014). *Life Cycle Assessment: Quantitative Approaches for Decisions that Matter*. Retrieved from https://www.lcatext book.com/ (accessed September 8, 2021).

McVoy, G. R., Nelson, D. A, Krekeler, P., Kolb, E., & Gritsavage, J. S. (2010). Moving towards sustainability: New York State Department of Transportation's GreenLITES story. *Proceedings of the Green Streets and Highways 2010 Conference*, Denver, CO, 461-479.

Measurement Canada. (2018). Volume correction factors – diesel fuel. Innovation, Science and Economic Development Canada. Retrieved from https://www.ic.gc.ca/eic/site/mc-mc.nsf/vwapj/VCF_Diesel.pdf/$file/VCF_Diesel.pdf (accessed July 28, 2021).

Mikasa Sangyo (2019). Construction equipment. Mikasa Sangyo, Tokyo, Japan. See https://www.mikasas.com/english/products/catalog/new/download.pdf (accessed May 4, 2020).

Misra, A., & Basu, D. (2012). A quantitative sustainability indicator system for pile foundations. In *Proceedings of Geocongress 2012: State of the Art and Practice in Geotechnical Engineering* (Hryciw RD, Athanasopoulos-Zekkos A and Yesiller N (eds)). Geotechnical Special Publication No. 225. ASCE, Oakland, California, USA, pp. 4252-4261.

Misra, A. (2010). *A multicriteria based quantitative framework for assessing sustainability of pile foundations* [Master's Thesis, University of Connecticut - Storrs]. Retrieved from http://digitalcommons.uconn.edu/gs_theses/27/

Montgomery, D. C. Peck, E. A., & Vining, G. G. (2012). *Introduction to Linear Regression Analysis*, 5th Ed., John Wiley & Sons. Hoboken:NJ, USA.

Muench, T. S., & Anderson, J. L. (2009). Greenroads: A Sustainability Performance Metric for Roadway Design and Construction. Final Technical Report TNW 2009-13, WA-RD 725.1 Transportation Northwest (TransNow), University of Washington, Seattle, Washington, USA.

Myers, R. H., Montgomery, D. C., & Anderson-Cook, C. M. (2009). *Response Surface Methodology: Process and Product Optimization Using Designed Experiments,* 3rd Ed. John Wiley & Sons. Hoboken:NJ, USA.

Myhre, G., Shindell, D., Bréon, F. M., Collins, W., Fuglestvedt, J., Huang, J., Koch, D., Lamarque, J.F., Lee, D., Mendoza, B., Nakajima, T., Robock, A., Stephens, G., Takemura, T., & Zhang, H. (2013). Anthropogenic and natural radiative forcing. In T. F. Stocker, D. Qin, G. K. Plattner, M. Tignor, S. K. Allen, J. Boschung, A. Nauels, Y. Xia, V. Bex & P. M. Midgley

(Eds.), *Climate Change 2013: The Physical Science Basis. Contribution of Working Group I to the Fifth Assessment Report of the Intergovernmental Panel on Climate Change* (pp. 659-740). Cambridge University Press.

NCHRP (National Cooperative Highway Research Program). (2013). *Fuel usage factors in highway and bridge construction*. Report No. 744, Washington, DC: Transportation Research Board.

Negussey, D., Wijewickreme, W. K. D., & Vaid, Y. P. (1988). Constant volume friction angle of granular materials. *Canadian Geotechnical Journal*, *25*(1), 50-55.

Nicholson, D., Smith, P., Bowers, G. A., Cuceoglu, F., Olgun, C. G., McCartney, J. S., Henry, K., Meyer, L. L., & Loveridge, F. A. (2014). Environmental impact calculations, life cycle cost analysis. *DFI Journal – The Journal of the Deep Foundations Institute*, *8*(2), 130-143

NREL (National Renewable Energy Laboratory). (2012). *U.S. life cycle inventory database*. Retrieved from https://www.lcacommons.gov/nrel/search (accessed May 4, 2020).

Pantelidou, H., Nicholson, D., & Gaba, A. (2012). Sustainable geotechnics. In B. John, C. Tim, S. Hilary & B. Michael (Eds.), *ICE manual of geotechnical engineering: Volume I* (pp. 125-136). Institution of civil Engineers.

Phoon, K. (2008). *Reliability-Based Design in Geotechnical Engineering: Computations and Applications*. Taylor & Francis, Oxon, UK.

Phoon, K., & Kulhawy, F.H. (1999). Characterization of geotechnical variability. *Canadian Geotechnical Journal*, 36(4), 612-624.

Phoon, K., Kulhawy, F. H., & Grigoriu, M. D. (1995). Reliability-based design of foundations for transmission line structures, Electric Power Research Institute, TR-105000, Pleasant Hill, CA, USA.

Pittenger, D. M. (2011). Evaluating sustainability of selected airport pavement treatments with life-cycle cost, raw material consumption, and greenroads standards. *Transportation Research Record: Journal of the Transportation Research Board, 2206*, 61-68.

Praticò F., Saride S., & Puppala A. (2011). Comprehensive life cycle cost analysis for the selection of stabilization alternative for better performance of low volume roads. *Transportation Research Record: Journal of the Transportation Research Board, 2204*(1), 120-129.

Purdy, C. M., Raymond, A. J., DeJong, J. T., Kendall, A., Krage, C., & Sharp, J. (2022). Life-cycle sustainability assessment of geotechnical site investigation. *Canadian Geotechnical Journal*, *59*(6), 863-877.

Ravichandran, N., & Shrestha, S. (2020). Performance- and cost-based robust design optimization procedure for typical foundations for wind turbine. *International Journal of Geotechnical Engineering*, *14*(4): 395-408.

Raymond, A. J., Dejong, J. T., Kendall, A., Blackburn, J. T., & Deschamps, R. (2021). Life cycle sustainability assessment of geotechnical ground improvement methods. *Journal of Geotechnical and Geoenvironmental Engineering*, *147*(12), 04021161.

Raza, F., Alshameri, B., & Jamil, M.S. (2020). Engineering aspect of sustainability assessment for geotechnical projects, *Environment, Development, and Sustainability, 23*(3), 6359-6394

Raza, F., Alshameri, B., & Jamil, M.S. (2021). Assessment of triple bottom line of sustainability for geotechnical projects. *Environment, Development, and Sustainability, 23*(4), 4521-4558.

Reese, L. C., Isenhower, W. M., & Wang S. (2006). *Analysis and design of shallow and deep foundations*. John Wiley and Sons, Hoboken, NJ.

Reigle, J. A., & Zaniewski, J. P. (2002). Risk-based life-cycle cost analysis for project-level pavement management. *Transportation Research Record: Journal of the Transportation Research Board*, *1816*(1), 34-42.

RIVM (National Institute for Public Health and the Environment). (2016). *Normalization scores ReCiPe 2016*. Retrieved from https://www.rivm.nl/en/documenten/normalization-scores-recipe-2016 (accessed May 4, 2020).

Robbins, T. A., & Chittoori, B. (2021). A practical framework to assess the sustainability and resiliency of civil infrastructure. *Engineering Sustainability*, *174*(3), 145-158.

Roberts, L. A., & Misra, A. (2009). Reliablity-based design of deep foundations based on differential settlement criterion. *Canadian Geotechnical Journal, 46*(2)*,* 168-176.

RSMeans. (2015). *Heavy Construction Cost Data*. 29th Ed. RSMeans, Massachusetts, USA.

Salgado, R. (2008). *The Engineering of Foundations.* McGraw Hill, Boston, MA, USA.

Sandanayake, M., Zhang, G., Setunge, S., & Thomas, C.M. (2015). Environmental Emissions of Construction Equipment Usage in Pile Foundation Construction Process – A Case Study. *Proceedings of the 19th International Symposium on Advancement of Construction Management and Real Estate*, 327-339.

Sandanayake, M., Zhang, G., Setunge, S., Luo, W., & Li, Ch. (2017). Estimation and comparison of environmental emissions and impacts at foundation and structure construction stages of a building – A case study. *Journal of Cleaner Production*, *151*(1), 319-329.

Saribas, A., & Erbatur, F. (1996). Optimization and sensitivity of retaining structures. *Journal of Geotechnical Engineering*, *122*(8): 649-656.

Sayed, S., Dodagoudar, G. R., & Rajagopal, K. (2008). Reliability analysis of reinforced soil walls under static and seismic forces. *Geosynthetics International*, *15*(4): 246-257.

Seager, T., Selinger, E., & Wiek, A. (2012). Sustainable engineering science for resolving wicked problems. *Journal of Agricultural and Environmental Ethics, 25*(1), 467-484.

Shillaber, C., Mitchell, J. K., & Dove, J. E. (2014). Assessing environmental impacts in geotechnical construction: Insights from the fuel cycle. *Proceedings of GeoCongress 2014: Geo-characterization and Modeling for Sustainability*, Atlanta, Georgia, 3516-3525.

Shillaber, C. M., Mitchell, J. K., & Dove, J. E. (2016a). Energy and carbon assessment of ground improvement works. I: Definitions and background. *Journal of Geotechnical and Geoenvironmental Engineering*, *142*(3), 04015083.

Shillaber, C. M., Mitchell, J. K., & Dove, J. E. (2016b). Energy and carbon assessment of ground improvement works. II: Working model and Example. *Journal of Geotechnical and Geoenvironmental Engineering*, *142*(3), 04015084.

Soga, K. (2011). Infrastructure: Embodied energy and gas Emission of geotechnical infrastructure. In S. Iai (Ed.), *Geotechnics and Earthquake Geotechnics Towards Global Sustainability* (pp. 59-74). Springer.

Song, X., Carlsson, C., Killsgaard, R., Bendz, D., & Kennedy, H. (2020). Life cycle assessment of geotechnical works in building construction: A review and recommendations. *Sustainability*, *12*(20), 1-17.

Spaulding, C., Massey, F., & LaBrozzi, J. (2008). Ground improvement technologies for a sustainable world. In *Proceedings of GeoCongress 2008: Sustainability and Geohazard Mitigation* (Reddy KR, Khire MV and Alshawabkeh AN (eds)). Geotechnical Special Publication No. 178, ASCE, New Orleans, Louisiana, USA, pp. 891-898.

Steedman, R. S. (2011). Geotechnics and society: Carbon, a new focus for delivering sustainable geotechnical engineering. In S. Iai (Ed.), *Geotechnics and Earthquake Geotechnics Towards Global Sustainability* (pp. 75-88). Netherlands: Springer.

Storesund, R., Messe, J., & Kim, Y. (2008). Life cycle impacts for concrete retaining walls vs. bioengineered slopes. In *Proceedings of GeoCongress 2008: Sustainability and Geohazard Mitigation* (Reddy KR, Khire MV and Alshawabkeh AN (eds)). Geotechnical Special Publication No. 178, ASCE, New Orleans, Louisiana, USA, pp. 875-882.

Strata. (2014). *Stratagrid Product Data Sheet*. Strata Systems. Retrieved from https://terrafixgeo.com/wp-content/uploads/2021/03/ProductData_Stratagrid.pdf (accessed June 6, 2021).

Tadano. (2018). *GR-150XL*. Retrieved from https://www.tadano.com/businesses/service/upload/docs/GR-150-1-00101_US-01.pdf (accessed June 26, 2022).

Tang, H., Gong, W., Wang, L., Juang, C.H., Martin, J.R., & Li, C. (2019). Multiobjective optimization-based design of stabilizing piles in earth slopes. *International Journal for Numerical and Analytical Methods in Geomechanics*, *43*(7): 1516-1536.

Thinkstep. (2019). *Documentation for duty vehicle processes*. Retrieved from https://gabi.sphera.com/fileadmin/gabi/Documentation_GaBi_Transport_Processes_-_Duty_Vehicles_2019.pdf (accessed May 4, 2020).

Thinkstep. (2022). *GaBi database & modelling principles.* Retrieved from https://sphera.com/wp-content/uploads/2022/02/MODELING-PRINCIPLES-GaBi-Databases-2022.pdf (accessed June 29, 2022)

Tomlinson, M., & Woodward, J. (2008). *Pile Design and Construction Practice*, 5th ed., Taylor and Francis, Oxon, United Kingdom.

Torres, V. N., & da Gama, C. D. (2006). Quantifying the environmental sustainability in underground mining. *Proceedings of the 15th International Symposium on Mine Planning and Equipment Selection*, Torino, Italy, 1-7.

U.S. Army Corps of Engineers. (1997). *Engineering and design: Introduction to probability and reliability methods for use in geotechnical engineering*. Engineer Technical Letter 1110–2–547, Department of the Army, Washington, D.C.

UN (United Nations). (2015). *Transforming Our World: The 2030 Agenda for Sustainable Development*. Retrieved from https://sustainabledevelopment.un.org/content/documents/21252030%20Agenda%20for%20Sustainable%20Development%20web.pdf (accessed November 16, 2020).

UNEP (United Nations Environment Programme). (2015). *Global waste management outlook*. United Nations Environment Programme. Retrieved from https://www.unep.org/resources/report/global-waste-management-outlook (accessed February 28, 2021).

UNEP. (2016). *Global material flows and resources productivity: Assessment study of the UNEP International Resource Panel*. Paris: United Nations Environment Programme.

UNEP. (2020). *2020 Global status report for buildings and construction: Towards a zero-emission, efficient and resilient buildings and construction sector*. United Nations Environment Programme, Nairobi, Kenya. Retrieved from https://wedocs.unep.org/bitstream/handle/20.500.11822/34572/GSR_ES.pdf?sequence=3&isAllowed=y (accessed February 28, 2021).

Verdugo, R., & Ishihara, K. (1996). The steady state of sandy soils. *Soils and Foundations*, *36*(2), 81-91.

Vieira, M. (2015). Concrete. In *Materials for construction and Civil Engineering: Science, Processing, and Design* (Gonçalves MC and Margarido F (eds)). Springer, Cham, Switzerland, 185-236.

Wang, Y., & Kulhawy, F. H. (2008). Economic design optimization of foundations. *Journal of Geotechnical and Geoenvironmental Engineering*, *134*(8), 1097-1105.

Wang, Y., Au, S., & Kulhawy, F. H. (2011). Expanded reliability-based design approach for drilled shafts. *Journal of Geotechnical and Geoenvironmental Engineering, 137*(2), 140-149.

Wernet, G., Bauer, C., Steubing, B., Reinhard, J., Moreno-Ruiz, E., & Weidema, B. (2016). The ecoinvent database version 3 (part I): overview and methodology. *The International Journal of Life Cycle Assessment*, *21*(9), 1218-1230.

Wilmotte, J., & Borie, S. (2020). *EFFC DFI Carbon Calculator*. Retrieved from https://www.effc.org/how-we-operate/eco$_2$-foundations/ (accessed June 20, 2022).

Zagula, M., Hinkle, J. Mobley, B. Williams, D., & Mullings, G. M. (2012). *2012 National ready mixed concrete association fleet benchmarking and costs survey*. Silver Spring, MD: National Ready Mixed Concrete Association.

Zayed, T. M., & Halpin, D. W. (2005). Pile Construction Productivity Assessment. *Journal of Construction Engineering and Management, 131*(6), 705-714.

Zhang, H., Keoleian, G. A, & Lepech, M. D. (2008). An integrated life cycle assessment and life cycle analysis model for pavement overlay systems. In F. Biondini, & D. Frangopol (Eds.), *Life-Cycle Civil Engineering* (pp. 907-912). London, United Kingdom: Taylor and Francis Group.

Zitzler, E., Deb, K., & Thiele, L. (2000). Comparison of multiobjective evolutionary algorithms: Empirical results. *Evolutionary Computation*, *8*(2): 173-195.